INVESTIGATION OF ELASTIC DISTORTIONAL WAVE BIREFRINGENCE DUE TO CRYSTALLITE PREFERRED ORIENTATION AND STRESS IN ANISOTROPIC POLYCRYSTALLINE ALUMINUM

By

RAYMOND LEON GAUSE

Bachelor of Science

Southwestern State College

Weatherford, Oklahoma

1957

Submitted to the faculty of the Graduate School of
the Oklahoma State University
in partial fulfillment of the requirements
for the degree of
DOCTOR OF PHILOSOPHY
May, 1967

OKLAHOMA
STATE UNIVERSITY
LIBRARY
JAN 10 1968

INVESTIGATION OF ELASTIC DISTORTIONAL WAVE BIREFRINGENCE DUE TO CRYSTALLITE PREFERRED ORIENTATION AND STRESS IN ANISOTROPIC POLYCRYSTALLINE ALUMINUM

Thesis Approved:

Thesis Adviser

Dean of the Graduate School

658750

ACKNOWLEDGMENTS

The author wishes to express his gratitude and to acknowledge his indebtedness to several people for their roles in the completion of this study.

Particular appreciation is expressed to the thesis advisor, Dr. R. L. Lowery, for his encouragement, interest, and guidance during the preparation of the thesis. In addition, especial thanks are due Dr. J. R. Norton for his many helpful suggestions, continuing advice, and friendship during the course of the author's graduate study. Appreciation for their assistance and guidance in formulating the author's graduate program is extended to Dr. Leroy Folks and Dr. Clark Dunn.

To Dr. W. R. Lucas and The National Aeronautics and Space Administration, the author wishes to express his sincere and lasting appreciation for providing him the opportunity to pursue this final phase of his graduate study and the support required for the research program. Indebtedness also is due J. E. Kingsbury and E. C. McKannan for their motivation and their interest in the author's academic endeavors. Gratefully, the author acknowledges the Lawrence Radiation Laboratory and Donald Frazer for their support in the preparation of the pole figures which appear in this study. Recognition also is due the Aluminum Company of America for providing the test materials. Finally, thanks are extended to Cleo Peterson for his assistance in the construction of some of the

experimental apparatus and to Mrs. Mary Ann McDonald for the typing of the final manuscript.

The author is forever indebted to his wife, Janell, for her patience, interest, and motivation during these years of graduate study, and to Randy and Shari, who endured much inattention and a few harsh words during the writing of this dissertation.

TABLE OF CONTENTS

Chapter		Page
I.	INTRODUCTION	1
	Definition of the Problem	1
	The Purpose and Scope of the Study	2
	Previous Work	4
II.	THEORETICAL CONSIDERATIONS	6
	Wave Propagation in Anisotropic Media	7
	Birefringence Due to Preferred Orientation	16
	Stress-Induced Birefringence	20
III.	EXPERIMENTAL PROGRAM	27
	Theory of Birefringence Measurement	27
	Experimental Technique	34
	Test Material Characterization	37
	Determination of Preferred Orientation	38
	Preparation of Birefringence Test Specimens	43
	Experimental Apparatus	47
IV.	EXPERIMENTAL PROCEDURE AND RESULTS	55
	Experimental Procedure	56
	Analysis of Preferred Orientation	59
	Results of Birefringence Measurements	69
	The Effect of Applied Stress	86
V.	CONCLUSIONS AND RECOMMENDATIONS	91
	Recommendations for Further Study	93
	SELECTED BIBLIOGRAPHY	94

APPENDIX 96

A. Pole Figure Data 96
B. List of Symbols 181
C. List of Major Equipment 185

LIST OF TABLES

Table		Page
I.	Elastic Constants of Aluminum	15
II.	Pole Figure Specimen Numbering System	42
III.	Preferred Orientation in Cold-Rolled 1100-0 Aluminum	64
IV.	Preferred Orientation in Cold-Rolled 6061-T6 Aluminum	68
V.	Birefringence Data for 1100-0 Aluminum	70
VI.	Birefringence Data for 6061-T6 Aluminum	72
VII.	Analysis of Variance Table and Calculations	75
VIII.	AOV for 1100-0 Aluminum with Zero Cold Work	77
IX.	AOV for 1100-0 Aluminum with 40% Cold Work	77
X.	AOV for 1100-0 Aluminum with 60% Cold Work	78
XI.	AOV for 1100-0 Aluminum with 80% Cold Work	78
XII.	AOV for 6061-T6 Aluminum with Zero Cold Work	79
XIII.	AOV for 6061-T6 Aluminum with 20% Cold Work	79
XIV.	AOV for 6061-T6 Aluminum with 36% Cold Work	80
XV.	AOV for 6061-T6 Aluminum with 50% Cold Work	80
XVI.	Significance of the Variation in $\frac{\Delta V}{V}$ with Direction for Cold-Rolled 1100-0 and 6061-T6 Aluminum	81
XVII.	Summary of the Birefringence Data for Cold-Rolled 1100-0 and 6061-T6 Aluminum	83

Table		Page
XVIII.	Comparison of Birefringence and Preferred Orientation Data	85
XIX.	Calculated Stress in Cold-Rolled 6061-T6 Sheet Aluminum	89
XX.	Pole Figure Data for Specimen II-A-1	99
XXI.	Pole Figure Data for Specimen II-B-1	105
XXII.	Pole Figure Data for Specimen II-C-1	111
XXIII.	Pole Figure Data for Specimen II-D-1	117
XXIV.	Pole Figure Data for Specimen II-B-2	123
XXV.	Pole Figure Data for Specimen II-C-2	129
XXVI.	Pole Figure Data for Specimen II-D-2	135
XXVII.	Pole Figure Data for Specimen 2A	141
XXVIII.	Pole Figure Data for Specimen 3A	147
XXIX.	Pole Figure Data for Specimen 4A	153
XXX.	Pole Figure Data for Specimen 1B	159
XXXI.	Pole Figure Data for Specimen 2B	165
XXXII.	Pole Figure Data for Specimen 3B	171
XXXIII.	Pole Figure Data for Specimen 4B	177

LIST OF FIGURES

Figure		Page
1.	The Components of Stress for a Rectangular Cartesian Coordinate System	8
2.	Schematic Representation of Crystallite Preferred Orientation in a Sheet of Rolled Metal	17
3.	Wave Birefringence Due to Preferred Orientation in Rolled Metal Sheet	19
4.	Force Versus Interatomic Separation for Two Atoms in Free Space	21
5.	Coordinate System for Distortional Wave Propagation in Stressed Solids	24
6.	Schematic Representation of (a) Distortional Wave Propagation in an Anisotropic Medium and (b) the Resulting Particle Motion	29
7.	Pulse Echo Pattern Showing (a) No Birefringence and (b) Modulation Produced by the Anisotropy of the Medium	36
8.	X-ray Diffraction Determination of Preferred Orientation	40
9.	Polar Stereographic Net	41
10.	Birefringence Specimen Lay-out for Rolled Metal Sheet	44
11.	Schematic Representation of Non-Parallel Specimen Faces	46
12.	Experimental Apparatus	48
13.	Simplified Block Diagram of Birefringence Measuring System	50
14.	Specimen Holder	53

Figure Page

15. Typical Photomicrographs (100X) of 6061-T6 Aluminum (a) Prior and (b) Subsequent to Heat Treatment 58

16. Ideal (111) Pole Figure for Orientation Near (123)[$1\bar{2}1$]. 61

17. Preferred Orientation Versus Percent Cold Work for 1100-0 Aluminum 65

18. Theoretical (111) Pole Figure for the (001)[100] Orientation . . 66

19. Preferred Orientation Versus Percent Cold Work for 6061-T6 Aluminum 69

20. Birefringence Versus Percent Cold Work for 1100-0 Aluminum 82

21. Birefringence Versus Percent Cold Work for 6061-T6 Aluminum 82

22. Stress-Induced Birefringence in Cold-Rolled 6061-T6 Aluminum 88

23. (111) Pole Figure for Specimen II-A-1 98

24. (111) Pole Figure for Specimen II-B-1 104

25. (111) Pole Figure for Specimen II-C-1 110

26. (111) Pole Figure for Specimen II-D-1 116

27. (111) Pole Figure for Specimen II-B-2 122

28. (111) Pole Figure for Specimen II-C-2 128

29. (111) Pole Figure for Specimen II-D-2 134

30. (111) Pole Figure for Specimen 2A 140

31. (111) Pole Figure for Specimen 3A 146

32. (111) Pole Figure for Specimen 4A 152

33. (111) Pole Figure for Specimen 1B 158

34. (111) Pole Figure for Specimen 2B 164

Figure Page

35. (111) Pole Figure for Specimen 3B 170

36. (111) Pole Figure for Specimen 4B 176

CHAPTER I

INTRODUCTION

In the last several years, attention has been given by several investigators to the analysis of stress using ultrasonic techniques based on the "acoustoelastic effect" (1)[1]. The general theory of acoustoelasticity predicts a simple relationship between the velocity of ultrasonic distortional waves and the state of stress in an elastically anisotropic material. In an isotropic material, the wave velocity is independent of the direction of particle motion. If, however, a stress is applied, the material becomes slightly anisotropic and the velocity is found to vary with the direction of particle motion. Thus, according to the acoustoelasticity theory, the experimental measurement of the fractional velocity difference between elastic distortional waves propagated normal to, and polarized normal and parallel to, a principal stress axis should be sufficient to determine this stress.

Definition of the Problem

A major complication of this method of stress analysis is that the fractional velocity difference is simply a measure of the elastic anisotropy averaged

---

[1] The numbers in parentheses refer to references of the selected bibliography.

over the total distance the waves travel, and as a result, is independent of the origin of the anisotropy which could be stress, crystallite preferred orientation, or a combination of the two. The method apparently gives satisfactory results when an external stress is applied to a body which is known to be initially isotropic. However, very few materials of engineering importance are naturally elastically isotropic. On the contrary, most metals possess varying degrees of anisotropy depending on their basic crystallographic structure and their metallurgical and stress histories. Thus, the application of the acoustoelastic method to the analysis of stress in these materials requires a knowledge of the influence of other sources of anisotropy, in addition to stress, on the velocity of elastic stress waves. Because this information generally is not available, a common practice is to ignore some of these complications and assume that the major contribution to the velocity change is stress. For this reason, a study is needed to evaluate the influence of nonstress-produced anisotropy on distortional wave velocity.

The Purpose and Scope of the Study

This study was undertaken to determine the relative magnitudes of the birefringence[2] of elastic distortional waves due to stress and crystallite preferred orientation in polycrystalline aluminum. Aluminum was chosen as the test material because it is one of the most important metals used in the aerospace

---

[2] Anisotropic bodies have the property of resolving a plane polarized wave into two components and transmitting them on planes at right angles. This phenomenon is referred to as birefringence or double refraction.

industry. In its role as a structural material for rockets and spacecraft, it commonly appears in the form of sheet or plate. To achieve the high strength needed, the metal often is subjected to some type of cold work which is defined as the reduction in cross-sectional area of a metal which occurs as a result of rolling, forging, drawing, or extrusion at temperatures in the neighborhood of room temperature (2). In the case of sheet or plate stock, the cold work generally is introduced by cold-rolling. Metals which have been cold-worked by cold rolling are characterized by mechanical property directionality due to the alignment of crystallographic axes and planes in certain preferred directions and to internal or residual stresses resulting from directionality and inhomogeneity in plastic flow. Thus, cold-rolled sheet or plate aluminum is elastically anisotropic because of non-random crystallite orientation and internal stresses. The analysis of these internal stresses by acoustoelastic methods requires a knowledge of the influence of the crystallite orientation on the velocity of distortional waves. This study provides this information and also determines, through comparison of the stress effect with the orientation effect, the suitability of the acoustoelastic method to the analysis of stress in aggregates of non-randomly oriented metal crystallites.

The study consists of two phases; theoretical and experimental. In the theoretical phase, consideration was given to the propagation of an elastic wave in an anisotropic medium. The results then were applied to the case of cold rolled polycrystalline aluminum sheet in which a certain crystallographic axis and plane is aligned with the rolling direction and plane, respectively. Next, the birefringence of a distortional elastic wave propagating through the thickness of

the sheet was considered. The effect of stress was shown by applying the results of non-linear elasticity theory to the problem of the finite deformation of an initially isotropic medium.

The scope of the experimental phase included the design and construction of a goniometer-type ultrasonic specimen holder; the fabrication of necessary distortional wave transducers; machining and lapping of the test specimens; the determination of preferred orientation by the preparation of pole figures; an investigation to determine the proper annealing conditions for cold rolled aluminum; and the testing of the specimens for birefringence before and after heat treatment and at various applied stresses.

Because of the anticipated variation in the elastic properties across the test material, the experiments were designed so that the data could be statistically analyzed. In this way, statements could be made concerning the significance of any observed variations in birefringence.

Previous Work

There is no known previous work in which an effort has been made to relate quantitatively distortional wave birefringence to measurements of crystallite orientation in aluminum. Double refraction (birefringence) of distortional waves has been observed in hot rolled 4150 steel plate (3), cold rolled steel plate, and forged aluminum blocks (4). But since no metallurgical evaluations of crystallite orientation were made, no quantitative correlation between orientation and birefringence was shown. However, preferred orientation was suggested as the possible cause of the observed velocity changes.

The stress dependence of elastic wave double refraction has been demonstrated by several investigators. The effect of simple uniaxial stress on the velocities of longitudinal and distortional waves in polystyrene, iron, and glass has been measured (5). Appreciable changes in the velocity of distortional waves polarized normal and parallel to the direction of an applied uniaxial stress in an aluminum specimen have been reported (1, 6, 7). Recent work with an annealed sample of nickel-steel has given the variation in velocity for distortional and longitudinal waves as a function of stress (8).

In most of the work reported, it was assumed that the specimens were isotropic in the stress free state and that the effects observed were due primarily to stress. It is surprising that in many cases sufficient information concerning the metallurgical history or the microstructure of the test material was not available to corroborate this assumption.

Several theories based on second order elasticity have been formulated to explain the experimental data for stress-induced birefringence. Based on the finite strain formulation of Murnaghan (9), expressions for the stress dependence of the velocities of principal elastic waves in initially isotropic materials have been derived by Hughes and Kelly (5) in which third order elastic constants have been introduced. Another more general theory of wave propagation, also based on finite deformation considerations, has been developed by Toupin and Bernstein (10). This theory includes third order constants which have been shown by Smith (11) to be proportional to those introduced by Hughes and Kelly. It should be emphasized, however, that these theories pertain only to materials which are isotropic in the initial state and not to materials possessing preferential crystallite orientation.

CHAPTER II

THEORETICAL CONSIDERATIONS

A polycrystalline metal is composed of many small crystals called crystallites or grains which are separated by boundaries that generally have different elastic properties than the rest of the material. When a wave propagates through the solid, it encounters these intercrystalline boundaries and is subjected to reflection and refraction. The resulting mode conversion and beam deviation is a function of several parameters, the most important being the inherent anisotropy of the individual crystallites composing the solid; the degree of orientation of these crystallites; the average crystallite size; and the wavelength of the propagating wave. If the solid is a random array of crystallites, the beam deviations will be averaged to zero, but if some preferred orientation is present, the net deviation of the beam may not be averaged to zero. The solid then exhibits a directionality effect and is said to be anisotropic with respect to its wave propagation characteristics. If a sufficient number of the crystallites are oriented in a preferred direction, the properties of the aggregate may approach those of the single crystal of the metal. Therefore, a knowledge of wave propagation in naturally anisotropic single crystals is necessary for the interpretation of propagation in bulk, non-randomly oriented, polycrystalline aggregates. Thus, the mathematical treatment of the propagation of an elastic wave in an anisotropic

medium will be given. Since the continuum theory is used, it is assumed that the wavelength is large with respect to the interatomic spacing of the crystal lattice.

Wave Propagation in Anisotropic Media

If a force is applied to a continuous, homogeneous, elastic medium and then released, the medium will be disturbed from its equilibrium position and will assume a motion which is due to the internal stresses produced by the disturbance. This motion then will be propagated through the medium as an elastic wave. The resulting component equations of motion for small deformations are, in general form (12),

$$\begin{aligned} \rho\ddot{\xi} &= \frac{\partial T_{11}}{\partial X_1} + \frac{\partial T_{21}}{\partial X_2} + \frac{\partial T_{31}}{\partial X_3} \\ \rho\ddot{\eta} &= \frac{\partial T_{12}}{\partial X_1} + \frac{\partial T_{22}}{\partial X_2} + \frac{\partial T_{32}}{\partial X_3} \\ \rho\ddot{\zeta} &= \frac{\partial T_{13}}{\partial X_1} + \frac{\partial T_{23}}{\partial X_2} + \frac{\partial T_{33}}{\partial X_3} \quad , \end{aligned} \tag{2.1}$$

where ξ, η, and ζ are the displacements in the X_1, X_2, and X_3 directions, respectively; ρ is the density of the undeformed medium; and the T_{ij} are the components of the stress tensor $\hat{T}$ as shown in Figure 1. The double dot, e g., $\ddot{\xi}$, denotes the second derivative with respect to time, i.e., $\frac{d\xi^2}{dt^2}$.

For anisotropic media, each stress component is directly proportional to each strain component, or

$$T_{ij} = c_{ijkl}\, e_{kl} \, , \tag{2.2}$$

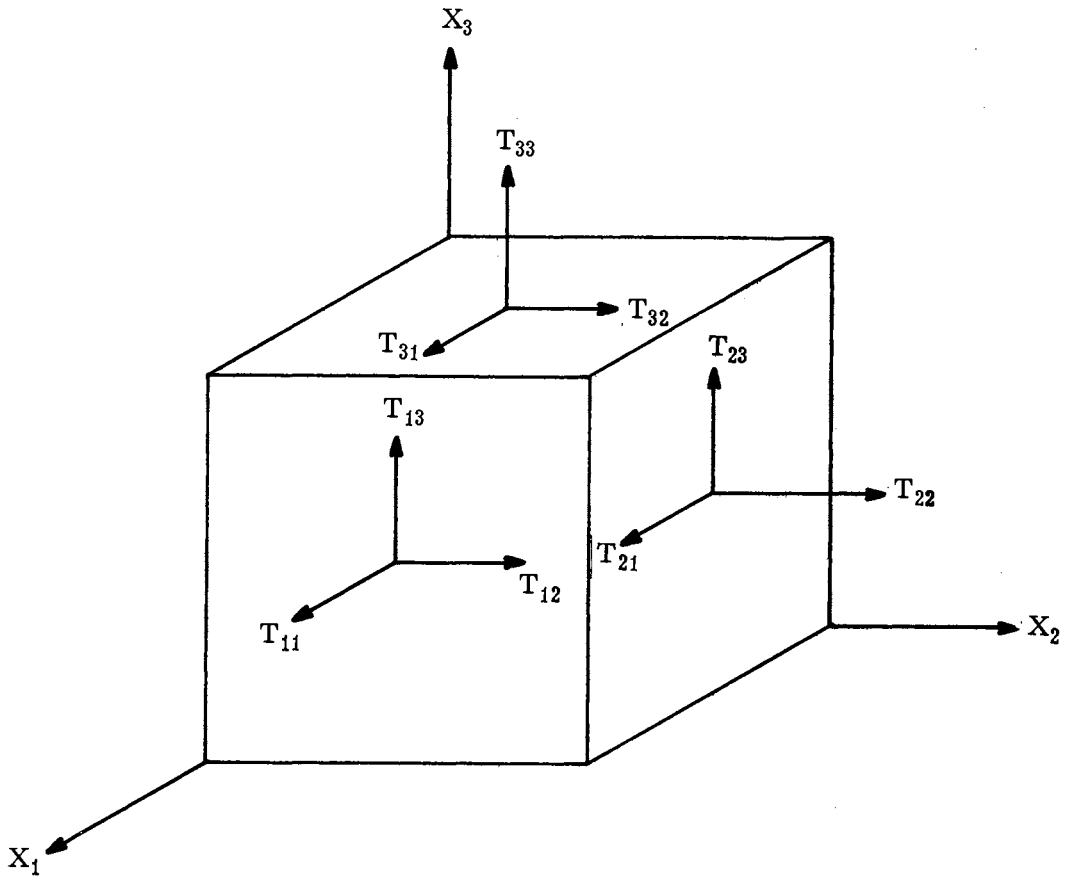

Figure 1. The Components of Stress for a Rectangular Cartesian Coordinate System

where i, j, k, l = 1, 2, or 3. The c_{ijkl} are termed the elastic constants of the anisotropic medium and the e_{kl} are the strains. Note that the summation convention of tensor notation has been employed; i.e., the expression is summed over any repeated indices. By using this same convention, the expressions (2.1) may be written as

$$\rho \ddot{U}_j = \frac{\partial T_{ij}}{\partial X_i} \; ; \; i, j = 1, 2, 3, \qquad (2.3)$$

where

$$U_1 = \xi ; \qquad U_2 = \eta ; \qquad U_3 = \zeta .$$

The relation between the displacements U_i and the strains e_{kl} can be written (13) as

$$e_{kl} = \tfrac{1}{2}\left[\frac{\partial U_k}{\partial X_l} + \frac{\partial U_l}{\partial X_k} \right] . \tag{2.4}$$

The strain tensor $\hat{e}$ may be written in matrix form as

$$\hat{e} = \begin{bmatrix} \dfrac{\partial U_1}{\partial X_1} & \tfrac{1}{2}\left[\dfrac{\partial U_1}{\partial X_2} + \dfrac{\partial U_2}{\partial X_1}\right] & \tfrac{1}{2}\left[\dfrac{\partial U_1}{\partial X_3} + \dfrac{\partial U_3}{\partial X_1}\right] \\ \tfrac{1}{2}\left[\dfrac{\partial U_2}{\partial X_1} + \dfrac{\partial U_1}{\partial X_2}\right] & \dfrac{\partial U_2}{\partial X_2} & \tfrac{1}{2}\left[\dfrac{\partial U_2}{\partial X_3} + \dfrac{\partial U_3}{\partial X_2}\right] \\ \tfrac{1}{2}\left[\dfrac{\partial U_3}{\partial X_1} + \dfrac{\partial U_1}{\partial X_3}\right] & \tfrac{1}{2}\left[\dfrac{\partial U_3}{\partial X_2} + \dfrac{\partial U_2}{\partial X_3}\right] & \dfrac{\partial U_3}{\partial X_3} \end{bmatrix} \tag{2.5}$$

In order to simplify the above equations and others yet to be developed, the following change in notation will be adopted:

$$\begin{gathered} T_{11} = T_1 ; \qquad T_{22} = T_2 ; \qquad T_{33} = T_3 ; \\ T_{23} = T_{32} = T_4 ; \quad T_{13} = T_{31} = T_5 ; \quad T_{12} = T_{21} = T_6 . \end{gathered} \tag{2.6}$$

Similarly, the strain components can be expressed in the form:

$$\begin{gathered} e_{11} = e_1 ; \qquad e_{22} = e_2 ; \qquad e_{33} = e_3 ; \\ e_{23} = e_{32} = \frac{e_4}{2} ; \quad e_{13} = e_{31} = \frac{e_5}{2} ; \quad e_{12} = e_{21} = \frac{e_6}{2} . \end{gathered} \tag{2.7}$$

By employing the relations of (2.6) and (2.7), equation (2.2) may be rewritten as

$$T_i = c_{ik}\, e_k;\ i, k = 1, \ldots 6 . \tag{2.8}$$

Assume the case of a plane harmonic wave propagating through the medium. For this (14)

$$U_j = U_{jo}\ \exp\left[i(\omega t - Kl_n X_n)\right];\ j, n = 1, 2, 3 \tag{2.9}$$

where the U_{jo} are the components of the displacement amplitude, ω is the angular frequency, K is the ratio of the angular frequency to the wave velocity, i.e., $(K = \frac{\omega}{v})$, and the l_n are the direction cosines of the normal to the wavefront; i.e., $\sum_{i=1}^{3} l_n^{\,2} = 1$.

From equations (2.9) and (2.4), the strains associated with the passage of the wave through the medium may be obtained. The stresses then may be obtained by employing equation (2.8), using the notation of (2.7).

The strains are:

$$\begin{aligned}
e_1 = \frac{\partial U_1}{\partial X_1} &= -\,i K l_1 U_{10}\ \exp\left[i(\omega t - Kl_n X_n)\right] \\
&= -\,i K l_1 U_1 \\
e_2 = \frac{\partial U_2}{\partial X_2} &= -\,i K l_2 U_2 \\
e_3 = \frac{\partial U_3}{\partial X_3} &= -\,i K l_3 U_3 \\
e_4 = \frac{\partial U_2}{\partial X_3} &= \frac{\partial U_3}{\partial X_2} \qquad -\,i K(l_2 U_3 + l_3 U_2)
\end{aligned} \tag{2.10}$$

$$e_5 = \frac{\partial U_1}{\partial X_3} + \frac{\partial U_3}{\partial X_1} = -i K(l_1 U_3 + l_3 U_1)$$

$$e_6 = \frac{\partial U_1}{\partial X_2} + \frac{\partial U_2}{\partial X_1} = -i K(l_1 U_2 + l_2 U_1).$$

From (2.8), the stress T_{11} is

$$T_1 = T_{11} = c_{11} e_1 + c_{12} e_2 + c_{13} e_3 + c_{14} e_4 + c_{15} e_5 + c_{16} e_6, \tag{2.11}$$

or

$$T_1 = -iK[c_{11} l_1 U_1 + c_{12} l_2 U_2 + c_{13} l_3 U_3 + c_{14} (l_2 U_3 + l_3 U_2) + c_{15} (l_1 U_3 + l_3 U_1) + c_{16} (l_1 U_2 + l_2 U_1)] . \tag{2.12}$$

By differentiating (12) and again using (2.9),

$$\frac{\partial T_{11}}{\partial X_1} = -i K l_1 T_{11} . \tag{2.13}$$

Similar analysis yields

$$T_{12} = T_{21} = -iK [U_1(c_{61} l_1 + c_{66} l_2 + c_{65} l_3) + U_2 (c_{66} l_1 + c_{62} l_2 + c_{64} l_3) + U_3 (c_{65} l_1 + c_{64} l_2 + c_{63} l_3)] , \tag{2.14}$$

and

$$\frac{\partial T_{12}}{\partial X_2} = -i K l_2 T_{12} . \tag{2.15}$$

Also,

$$T_{13} = T_{31} = -iK[U_1(c_{51}l_1 + c_{56}l_2 + c_{55}l_3) + U_2(c_{56}l_1 + c_{52}l_2 + c_{54}l_3) + U_3(c_{55}l_1 + c_{54}l_2 + c_{55}l_3)] \tag{2.16}$$

and

$$\frac{\partial T_{13}}{\partial X_3} = -iKl_3T_{13}. \tag{2.17}$$

The first equation of (2.3) can be written as

$$\begin{aligned}\rho\ddot{U}_1 &= \frac{\partial T_{11}}{\partial X_1} + \frac{\partial T_{12}}{\partial X_2} + \frac{\partial T_{13}}{\partial X_3} \\ &= -iK[l_1T_{11} + l_2T_{12} + l_3T_{13}] \\ &= -K^2\Big\{U_1[c_{11}l_1^2 + c_{66}l_2^2 + c_{55}l_3^2 + 2c_{16}l_1l_2 + 2c_{56}l_2l_3 + 2c_{15}l_1l_2] + U_2[c_{16}l_1^2 + c_{26}l_2^2 + c_{45}l_3^2 + (c_{12}+c_{66})l_1l_2 + (c_{25}+c_{46})l_2l_3 + (c_{14}+c_{56})l_1l_3] + U_3[c_{15}l_1^2 + c_{46}l_2^2 + c_{35}l_3^2 + (c_{14}+c_{56})l_1l_2 + (c_{36}+c_{45})l_2l_3 + (c_{13}+c_{55})l_1l_3]\Big\},\end{aligned} \tag{2.18}$$

where the symmetry of the elastic constants has been utilized (3), i.e.,

$c_{ij} = c_{ji}$.

To simplify (2.18) let

$$D_{11} = c_{11}l_1^2 + c_{66}l_2^2 + c_{55}l_3^2 + 2c_{16}l_1l_2 + 2c_{56}l_2l_3 + 2c_{15}l_1l_2 \ ;$$

$$D_{12} = c_{16}\, l_1^2 + c_{26}\, l_2^2 + c_{45}\, l_3^2 + (c_{12} + c_{66})\, l_1 l_2 + (c_{25} + c_{46})\, l_2 l_3 + (c_{14} + c_{56})\, l_1 l_3 ;$$

$$D_{13} = c_{15}\, l_1^2 + c_{46}\, l_2^2 + c_{35}\, l_3^2 + (c_{14} + c_{56})\, l_1 l_2 + (c_{36} + c_{45})\, l_2 l_3 + (c_{13} + c_{55})\, l_1 l_3. \qquad (2.19)$$

From (2.9)

$$\dot{U}_1 = \frac{\partial U_1}{\partial t} = i\omega U_1 , \qquad (2.20)$$

and

$$\ddot{U}_1 = i^2 \omega^2 U_1 = -\omega^2 U_1 . \qquad (2.21)$$

If the relations (2.19) and (2.21) are used in (2.18), the result is

$$\rho\omega^2 U_1 = K^2 [\, D_{11} U_1 + D_{12} U_2 + D_{13} U_3] . \qquad (2.22)$$

But

$$K^2 = \frac{\omega^2}{v^2} ;$$

therefore

$$\rho v^2 U_1 = D_{11} U_1 + D_{12} U_2 + D_{13} U_3. \qquad (2.23)$$

Similarly,

$$\rho v^2 U_2 = D_{12} U_1 + D_{22} U_2 + D_{23} U_3 \qquad (2.24)$$

$$\rho v^2 U_3 = D_{13} U_1 + D_{23} U_2 + D_{33} U_3, \qquad (2.25)$$

where

$$
\begin{aligned}
D_{22} &= c_{66}\, l_1^2 + c_{22}\, l_2^2 + c_{44}\, l_3^2 + 2c_{26}\, l_1\, l_2 \\
&\quad + 2c_{24}\, l_2\, l_3 + 2c_{46}\, l_1\, l_3; \\
D_{33} &= c_{55}\, l_1^2 + c_{44}\, l_2^2 + c_{33}\, l_3^2 + 2c_{45}\, l_1\, l_2 \\
&\quad + 2c_{34}\, l_2\, l_3 + 2c_{35}\, l_1\, l_3; \\
D_{23} &= c_{56}\, l_1^2 + c_{24}\, l_2^2 + c_{34}\, l_3^2 + (c_{25} + c_{46})\, l_1\, l_2 \\
&\quad + (c_{23} + c_{44})\, l_2\, l_3 + (c_{36} + c_{45})\, l_1\, l_3 .
\end{aligned}
\tag{2.26}
$$

The condition that the three homogeneous equations (2.23), (2.24), and (2.25) have a non-vanishing solution is that the determinant of the coefficients be zero; that is,

$$
\begin{vmatrix}
(D_{11} - \rho v^2) & D_{12} & D_{13} \\
D_{12} & (D_{22} - \rho v^2) & D_{23} \\
D_{13} & D_{23} & (D_{33} - \rho v^2)
\end{vmatrix} = 0. \tag{2.27}
$$

The resulting equation is a cubic in v^2 which has three positive roots for any real elastic solid. In general, these roots will be different, and will correspond to three distinct velocities of propagation. The values of these velocities will depend on the specific elastic constants of the medium and on the direction of propagation as defined by l_1, l_2, and l_3.

To apply the above analysis to the problem being investigated, it is necessary to know the elastic constants for the test material, i.e., aluminum. The structure of aluminum is face-centered cubic and, because of the symmetry of the unit cell, has only three non-zero independent elastic constants which are c_{11},

c_{12}, and c_{44}. The values of these constants, according to Taylor (15), are given in Table I.

TABLE I

ELASTIC CONSTANTS OF ALUMINUM

Constant	Value (10^{11} dyne - cm^{-2})
c_{11}	10.82
c_{12}	6.13
c_{44}	2.85

Therefore, the D_{ij} coefficients become

$$D_{11} = c_{11} l_1^2, \quad D_{12} = c_{12} l_1 l_2, \quad D_{13} = 0,$$

$$D_{22} = c_{44} l_3^2, \quad D_{23} = c_{44} l_2 l_3, \quad D_{33} = c_{44} l_2^2 ,$$

and (2.27) can be written for the special case of aluminum as

$$\begin{vmatrix} (D_{11} - \rho v^2) & D_{12} & 0 \\ D_{12} & (D_{22} - \rho v^2) & D_{23} \\ 0 & D_{23} & (D_{33} - \rho v^2) \end{vmatrix} = 0. \qquad (2.28)$$

The application of (2.28) requires a knowledge of the wave propagation direction with respect to the crystal axes since the D_{ij} are functions of the direction cosines. Hence, the calculation of the velocities depends on the experimental determination of the orientation of the crystallites with respect to the wave propagation direction.

Birefringence Due to Preferred Orientation

By using the results of the preceding analysis, the birefringence of a distortional wave due to preferred orientation now can be treated. Consider a specimen of rolled aluminum which is composed of a number of crystallites oriented in the most preferential way embedded in a matrix of crystallites oriented in a completely random fashion. Assume the geometry shown in Figure 2 in which the X_1 axis is the rolling direction of the specimen, the X_3 axis is the wave propagation direction, and the X_2 axis is perpendicular to both X_1 and X_3. Now, if a distortional wave is sent through the specimen along the X_3 axis, it will be doubly refracted or resolved into two components such that there is particle motion in both the X_1 and X_2 directions. This division of the wave is significant only in the fraction of the crystallites which are preferentially oriented because of the assumption that its effect averages to zero among the randomly oriented crystallites. To predict the velocity difference between the two components produced by the oriented crystallites, the transit times through the specimen have to be known.

Let V be the distortional wave velocity in an isotropic specimen of polycrystalline aluminum; V_1 and V_2, the velocities of a distortional wave in the oriented crystallites when the particle motion is along X_1 and X_2 axes, respectively; h, the thickness of the specimen along the X_3 axis; F, the fraction of the crystallites oriented in the most preferential way; t_1 and t_2, the transit times of a distortional wave polarized along the X_1 and X_2 axes, respectively, for a path length h.

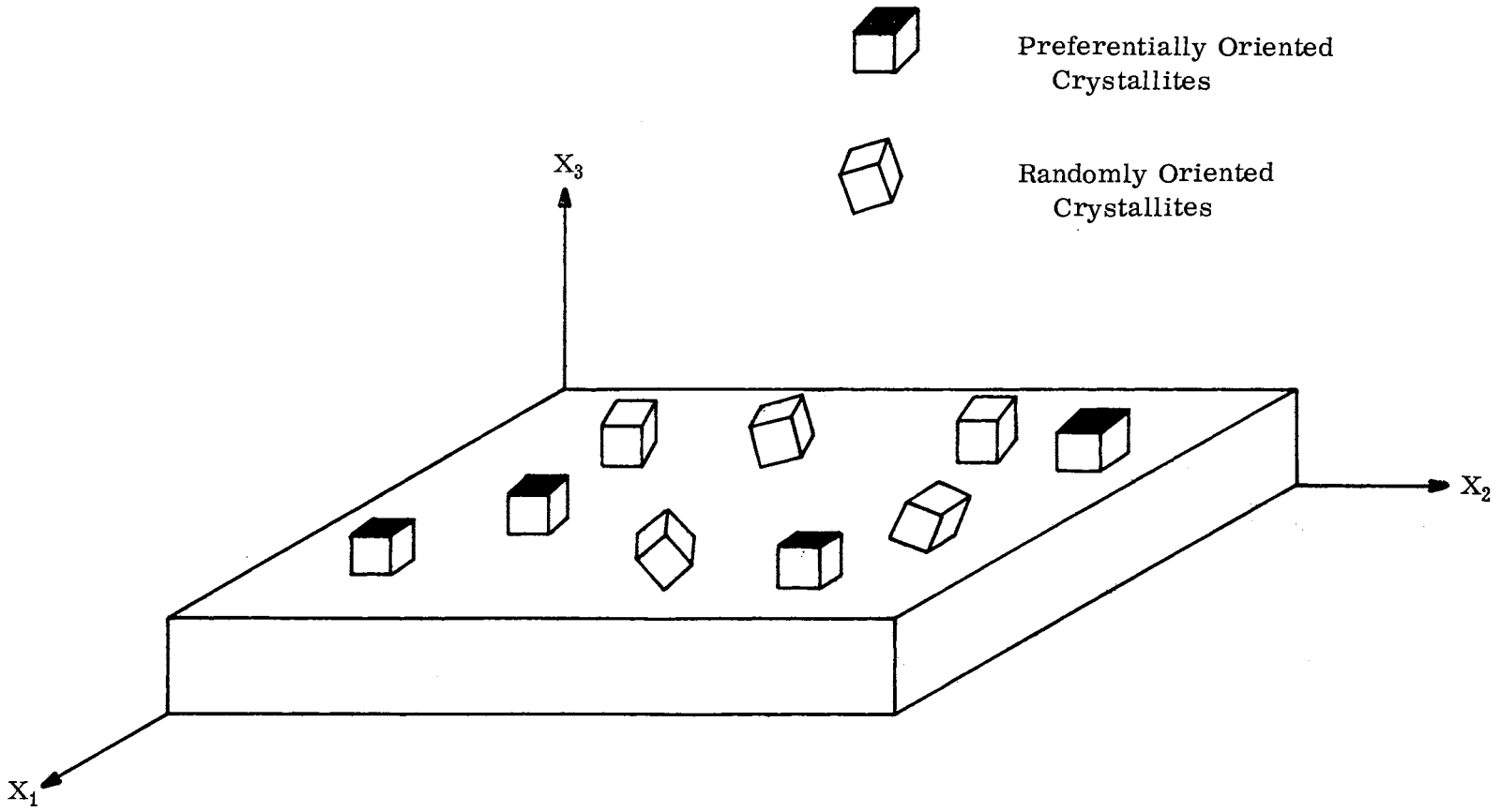

Figure 2. Schematic Representation of Crystallite Preferred Orientation in a Sheet of Rolled Metal

If it is assumed that the path length in the oriented crystallites is proportional to the number of oriented crystallites, the equations for the transit times can be written as

$$t_1 = \frac{h(1 - F)}{V + \frac{hF}{V_1}} \tag{2.29}$$

and

$$t_2 = \frac{h(1 - F)}{V + \frac{hF}{V_2}} \tag{2.30}$$

whose difference is

$$t_1 - t_2 = \frac{hF(V_2 - V_1)}{V_1 V_2} \quad . \tag{2.31}$$

The velocities V_1 and V_2 can be approximated by the two distortional wave velocities in aluminum single crystals for propagation along the crystal axis which is parallel to the specimen short transverse direction (Figure 3).

Since the fractional velocity difference $\frac{\Delta V}{V}$ generally is the quantity which is of most interest in this investigation, equation (2.31) is rewritten below in terms of the velocities $\dot{X}_1$ and $\dot{X}_2$ which are the velocities associated with a distortional wave polarized along the X_1 and X_2 axes, respectively:

$$\frac{h}{\dot{X}_1} - \frac{h}{\dot{X}_2} = \frac{hF(V_2 - V_1)}{V_1 V_2} . \tag{2.32}$$

Hence,

$$\left(\frac{1}{\dot{X}_1} - \frac{1}{\dot{X}_2}\right) = \frac{F(V_2 - V_1)}{V_1 V_2} \tag{2.33}$$

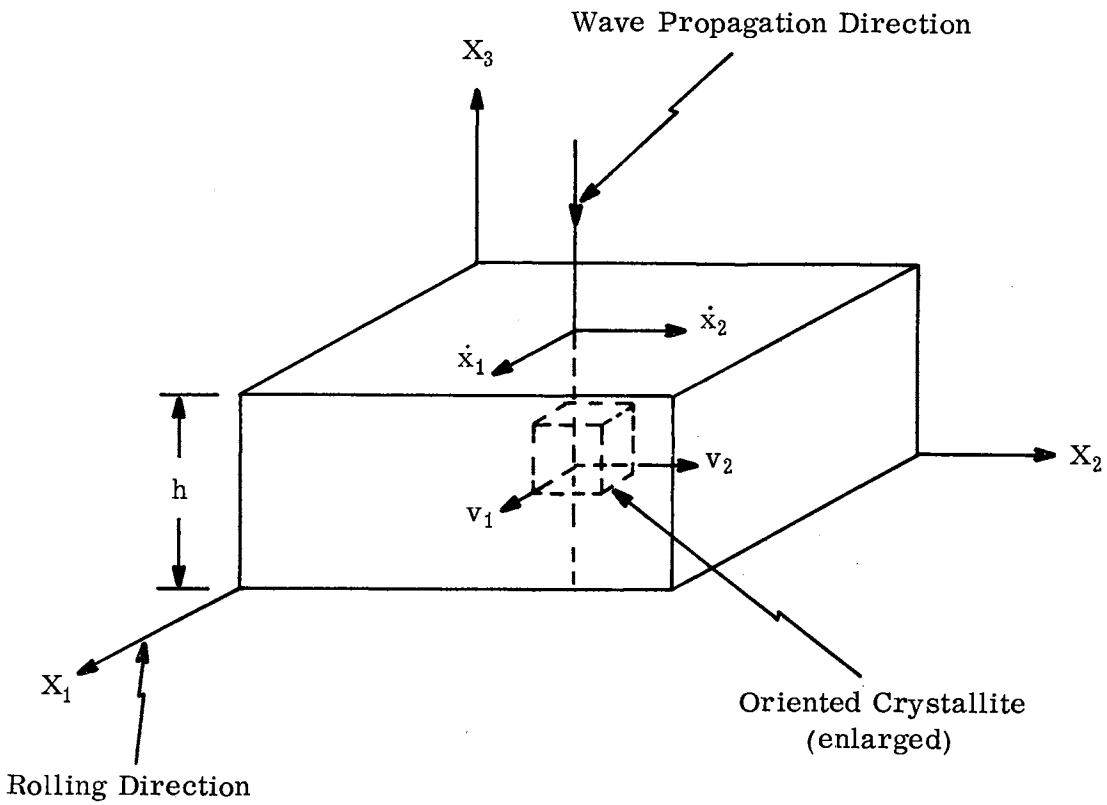

Figure 3. Wave Birefringence Due to Preferred Orientation in Rolled Metal Sheet

and

$$\frac{\dot{X}_2 - \dot{X}_1}{\dot{X}_1 \dot{X}_2} = \frac{F(V_2 - V_1)}{V_1 V_2} \quad . \tag{2.34}$$

Because the difference between $\dot{X}_1$ and $\dot{X}_2$ is usually small, the product can be approximated by the square of the average velocity V in an isotropic body. Thus,

$$\frac{\dot{X}_2 - \dot{X}_1}{V^2} = \frac{F(V_2 - V_1)}{V_1 V_2} \quad . \tag{2.35}$$

If

$$\dot{X}_2 - \dot{X}_1 = \Delta V, \tag{2.36}$$

then

$$\frac{\Delta V}{V}(p) = \frac{VF(V_2 - V_1)}{V_1 V_2} \qquad (2.37)$$

where $\frac{\Delta V}{V}(p)$ denotes the fractional velocity change due to the crystallite preferred orientation.

The significance of equation (2.37) is that the birefringence ($\frac{\Delta V}{V}$) can be approximated theoretically if the preferred orientation is known in terms of the number of crystallites which are aligned with a specified crystallographic axis and plane parallel to the rolling axis and plane, respectively. It is realized that the preceding analysis gives approximate results only since it ignores the wave interaction with the boundaries of the oriented crystallites. However, a detailed theoretical analysis of mode conversion, beam deviation, etc., associated with wave interaction at intercrystalline boundaries in polycrystalline solids is exceedingly complex, if not intractable, and is considered to be beyond the scope of this study.

Stress-Induced Birefringence

An elastically isotropic material is known to become anisotropic with respect to its elastic properties when subjected to a state of stress other than a hydrostatic pressure or tension (9). Thus, when an elastic stress wave is propagated through the material, its velocity will depend on the propagation direction. This stress dependence of the velocity occurs because the modulus of elasticity changes very slightly with the distance between the atoms of a solid. The effect of the stress field is to increase or decrease slightly the spacing of the atoms at

their lattice sites and thereby alter the modulus of elasticity. Figure 4 shows qualitatively how the force between a pair of atoms varies in free space. The slope of the curve at any point is a measure of the modulus of elasticity of the two atoms at that point. It can be seen that the slope is different at every point along the line. The calculation of the force versus distance relationship between the atoms in a real solid becomes very complicated because the interaction of many atoms, not just two, must be considered. The principle is the same, however.

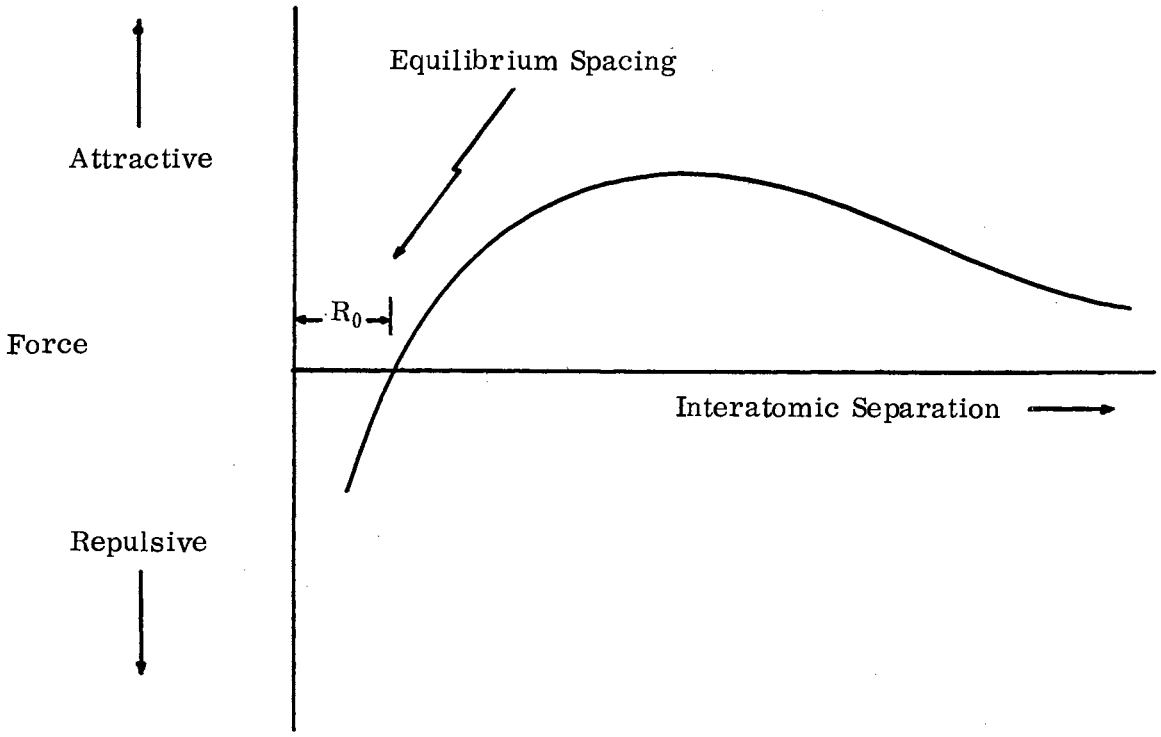

Figure 4. Force Versus Interatomic Separation for Two Atoms in Free Space

As was discussed in Chapter I, the problem of the propagation of elastic waves in stressed solids has been considered by several authors. The theories that evolved are based on the existence of a strain energy function of the type

expressed below in tensor notation:

$$\theta(S) = \frac{1}{2} c_{ijkl} S_{ij} S_{kl} + \frac{1}{6} c_{ijklmn} S_{ij} S_{kl} S_{mn} + \ldots \tag{2.38}$$

where the constant coefficients c_{ijkl}, c_{ijklmn}, ... are called the second order, third order, etc., elastic constants since they are coefficients of terms containing strain products of the second, third, ... degree. The S_{ij}, S_{kl}, ... are the elastic strains, the i, j, k, l, m, and n = 1, 2, or 3, and the summation notation of tensor analysis is used. If only the first term in the expression for the strain energy function θ is included, the theory is called first order or linear elasticity theory and the stresses obtained by the differentiation of θ with respect to strain are linearly related to the strains. When the second term in the expansion for θ is included, the theory is referred to as second order elasticity theory and the stresses are quadratically related to the strains. The application of first order elasticity theory to the propagation of elastic waves in homogeneous, isotropic media results in the following familiar expressions for the longitudinal (V_L) and distortional (V_D) wave velocities:

$$V_L = \sqrt{\frac{\lambda + 2\mu}{\rho}} \quad ; \quad V_D = \sqrt{\frac{\mu}{\rho}} \quad . \tag{2.39}$$

Here, λ and μ are the second order or Lamé elastic constants and ρ is the density of the media. Note that these velocities are not stress dependent if the bulk density remains constant. Also, because linear elasticity was used in their derivation, they are valid only for infinitesimal deformations. Therefore, when an

isotropic body is strained appreciably, the linear theory is no longer adequate and finite deformation theory has to be applied to obtain stress dependent wave velocities.

A theory of finite deformation involves two departures from the infinitesimal theory (5). First, since the deformations are large, the final coordinates of a point are not interchangeable with the original coordinates as in the infinitesimal theory, and second, the strain energy function must include strain products of higher degree than two, as in the second-order elasticity theory. Perhaps the most widely applied theory of finite deformation is that of Murnaghan (9). Based on Murnaghan's theory, Hughes and Kelly (5) derived the following seven expressions relating the velocities of elastic waves in stressed solids to the magnitude of the prevailing stresses:

$$\rho V_{LO}^2 = \lambda + 2\mu - \frac{P}{3K_O}\,[6l + 4m + 7\lambda + 10\mu] \tag{2.40}$$

$$\rho V_{DO}^2 = \mu - \frac{P}{3K_O}\,[3m - \tfrac{1}{2}n + 3\lambda + 6\mu] \tag{2.41}$$

$$\rho V_{LX}^2 = \lambda + 2\mu - \frac{T}{3K_O}\,[2l + \lambda + \frac{\lambda}{\mu}(4m + 4\lambda + 10\mu)] \tag{2.42}$$

$$\rho V_{DX}^2 = \mu - \frac{T}{3K_O}\,[m + \frac{\lambda n}{4\mu} + 4\lambda + 4\mu] \tag{2.43}$$

$$\rho V_{LY}^2 = \lambda + 2\mu - \frac{T}{3K_O}\,[2l - \frac{2\lambda}{\mu}(m + \lambda + 2\mu)] \tag{2.44}$$

$$\rho V_{DY}^2 = \mu - \frac{T}{3K_O}\,[m + \frac{\lambda n}{4\mu} + \lambda + 2\mu] \tag{2.45}$$

$$\rho V_{DZ}^2 = \mu + \frac{T}{3K_O}\,[2\lambda - m + \frac{n}{2} + \frac{\lambda}{\mu}\,\frac{n}{2}]\,. \tag{2.46}$$

In the above equations, the first subscript to the velocity-squared terms denotes the type of wave motion, i.e., longitudinal (L) or distortional (D). The

second subscript indicates the type and direction of the applied stress: O for the applied hydrostatic pressure P and X, Y, Z for an axial compressive stress T in the X, Y, or Z direction. The density of the material in the unstrained state is ρ; λ and μ again are the Lamé constants; l, m, and n are the third order or Murnaghan elastic constants; and K_O is the bulk modulus for an isotropic material in the unstrained state, i.e.,

$$K_O = \frac{1}{3} (3\lambda + 2\mu). \tag{2.47}$$

The coordinate system relevant to the propagation direction, wave polarizations, and applied stress directions is shown in Figure 5.

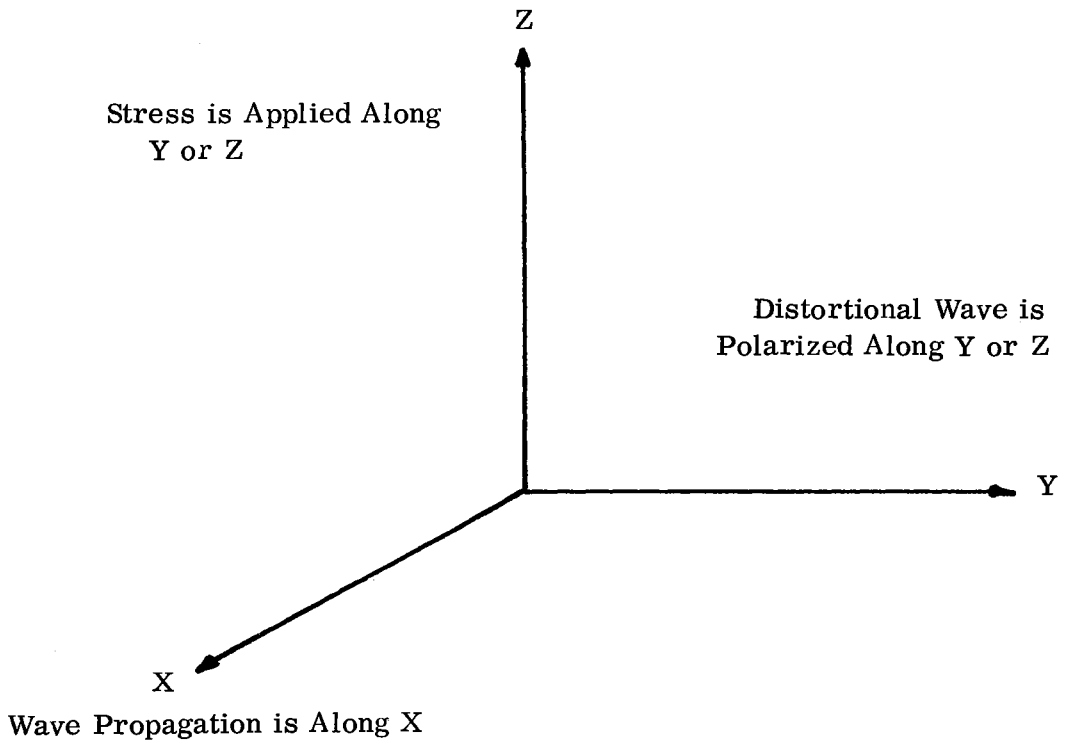

Figure 5. Coordinate System for Distortional Wave Propagation in Stressed Solids

As stated earlier, Toupin and Bernstein (10) derived expressions similar to those of Hughes and Kelly (5). However, Smith (11) analyzed both sets of equations and showed that they are equivalent if the third order constants of Toupin and Bernstein are redefined in terms of those used by Hughes and Kelly. Therefore, for the purposes of this study, these Hughes and Kelly expressions will be used to relate the wave velocities to the applied stresses.

The fractional velocity difference ($\frac{\Delta V}{V}$) between two principal distortional waves propagated normal to an applied uniaxial stress and polarized normal and parallel to this stress is the quantity of interest in this investigation. Subtracting equation (2.46) from (2.45) shows that

$$\rho(V_{DY}^2 - V_{DZ}^2) = -\frac{T}{3K_O}\left[3\lambda + 2\mu + \frac{n}{4}\frac{(3\lambda + 2\mu)}{\mu}\right]. \qquad (2.48)$$

Now if equation (2.47) is substituted into equation (2.48), the result is

$$\rho(V_{DY}^2 - V_{DZ}^2) = \frac{-T(4\mu + n)}{4\mu}. \qquad (2.49)$$

Since V_{DY} and V_{DZ} differ from the distortional wave velocity (V) in the unstressed material by only a fraction of a percent for large stresses, the quantity $(V_{DY} + V_{DZ})$ can be approximated by 2V so that equation (2.49) becomes:

$$(V_{DY} - V_{DZ}) = \frac{-T(4\mu + n)}{8\mu V\rho}. \qquad (2.50)$$

If

$$V_{DY} - V_{DZ} = \Delta V, \qquad (2.51)$$

then equation (2.50) can be rewritten as

$$\frac{\Delta V(S)}{V} = \frac{-T(4\mu + n)}{8\mu V^2 \rho} \quad , \tag{2.52}$$

where $\frac{\Delta V(S)}{V}$ denotes the fractional velocity difference produced by the compressive uniaxial stress T.

The significance of equation (2.52) is that it can be used to predict the stress-induced fractional velocity difference between two distortional waves polarized normal and parallel to the applied stress and propagating in a direction normal to the stress axis providing the third order constant n is known. Conversely, the value of n may be calculated from equation (2.52) if a known uniaxial stress is applied to the material and the resulting $\frac{\Delta V}{V}$ is measured.

CHAPTER III

EXPERIMENTAL PROGRAM

The following chapter describes in detail the theory and technique of birefringence measurement, the characterization of the test material, the preparation of the test specimens, and the experimental apparatus used in this study.

Theory of Birefringence Measurement

The double refraction of a plane polarized wave incident on an anisotropic body was treated theoretically in Chapter II. In this section, a departure from the previous treatment will be made to provide the theoretical foundation for the experimental measurement of birefringence. Although a few pertinent facts concerning the measuring technique were introduced in earlier sections to illuminate specific points of interest at the time, no detailed discussion has as yet been presented. This section and those to follow repeat some of the previous information, but do so only in the interest of completeness and unity.

Recall that when a plane polarized wave is incident on an anisotropic body, double refraction occurs and the wave is resolved into two components which are transmitted through the body on planes at right angles. Now, since the body is anisotropic the wave propagation characteristics of the body along the two planes will, in general, be different so that the two components will be transmitted with

different velocities. Therefore, as they propagate through the body, their phase difference will increase progressively from the initial in-phase condition at generation. It will be shown that the fractional difference in velocity ($\frac{\Delta V}{V}$) between the two components is related to this phase difference, and that the fractional velocity difference can be calculated if the phase difference is determined experimentally. It is desirable to determine the $\frac{\Delta V}{V}$ in this manner rather than by directly measuring the individual velocities absolutely since a differential measurement can be made more precisely, requires less sophisticated experimental apparatus, and is not affected by changes in specimen temperature and density.

Consider the situation shown in Figure 6a where a plane polarized distortional wave of the form

$$\phi = \phi_0 \cos \omega t \tag{3.1}$$

enters an initially isotropic body which for purposes of illustration has been made anisotropic by the application of a tensile force T. The direction of propagation is parallel to the Z axis and the plane of vibration is at an angle ν to the X axis. Upon entering the body, the original wave is resolved immediately into two components which travel through the thickness h with different velocities. The component parallel to the XZ plane of transmission will be

$$\phi_x = \phi_0 \cos \nu \cos \omega t, \tag{3.2}$$

whereas the component parallel to the YZ plane of transmission will be

$$\phi_y = \phi_0 \sin \nu \cos \omega t. \tag{3.3}$$

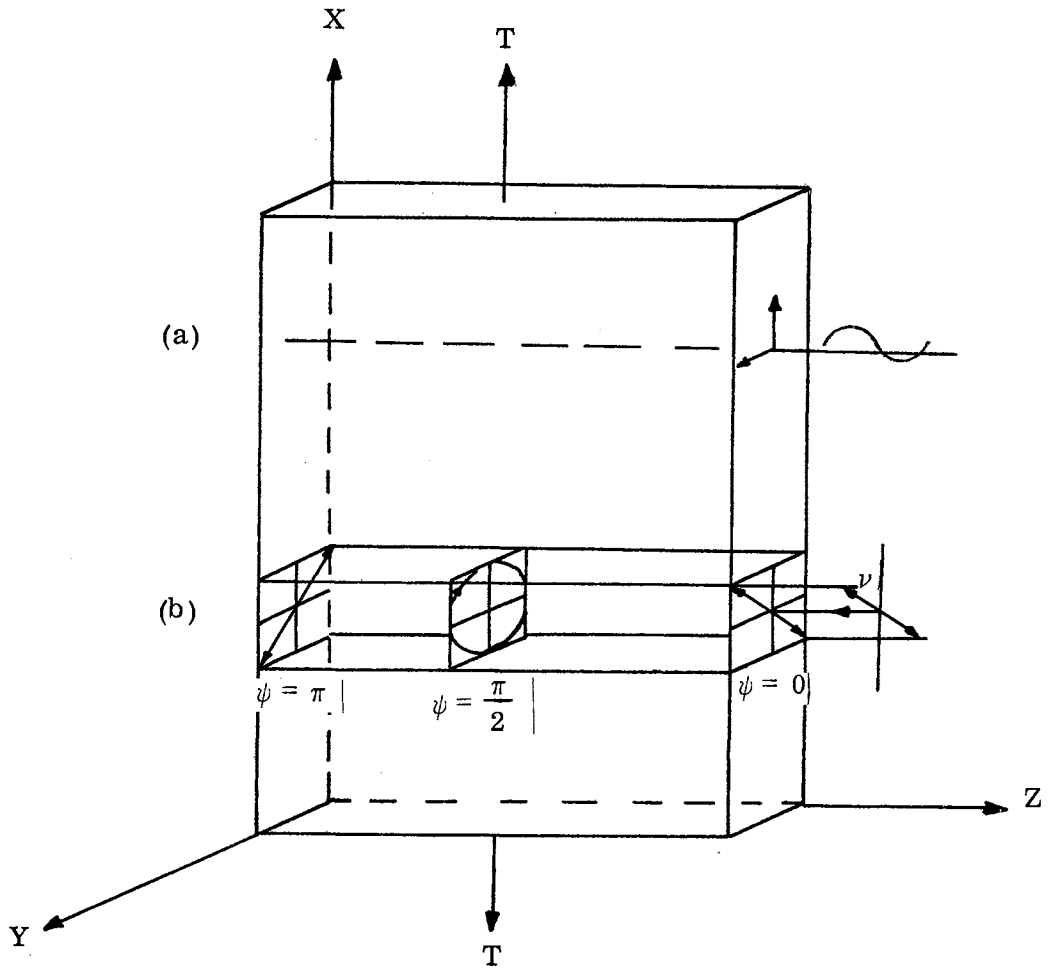

Figure 6. Schematic Representation of (a) Distortional Wave Propagation in an Anisotropic Medium and (b) the Resulting Particle Motion

Assume that the wave with particle motion normal to the direction of the applied stress has the greater velocity and therefore lags in phase behind the other wave at points away from the source. Thus, after propagating a distance Z in the body, the two component vibrations will be represented by the following equations:

$$\phi_x = \phi_0 \cos \nu \cos \omega t \tag{3.4}$$

$$\phi_y = \phi_0 \sin \nu \cos (\omega t + \psi). \tag{3.5}$$

To determine the resultant disturbance corresponding to the superposition of ϕ_x and ϕ_y, the following substitutions are made:

$$A_1 = \phi_0 \cos \nu \tag{3.6}$$

$$A_2 = \phi_0 \sin \nu \, . \tag{3.7}$$

By using (3.6) and (3.7), equations (3.4) and (3.5) can be written as

$$\phi_x = A_1 \cos \omega t, \tag{3.8}$$

$$\phi_y = A_2 \cos (\omega t + \psi). \tag{3.9}$$

If ωt is eliminated between ϕ_x and ϕ_y, the result is

$$\frac{\phi_x^2}{A_1^2 \sin^2 \psi} - \frac{2 \phi_x \phi_y}{A_1 A_2 \sin \psi \tan \psi} + \frac{\phi_y^2}{A_2^2 \sin^2 \psi} = 1. \tag{3.10}$$

This is an equation of second degree in ϕ_x and ϕ_y and is of the form

$$AX^2 + BXY + CY^2 + DX + EY + F = O, \tag{3.11}$$

where

$$A = \frac{1}{A_1^2 \sin^2 \psi}; \qquad B = \frac{-2}{A_1 A_2 \sin \psi \tan \psi};$$

$$C = \frac{1}{A_2^2 \sin^2 \psi}; \qquad D = E = O; \quad F = -1. \tag{3.12}$$

Equation (3.11) is the general equation of a conic and has as a locus a circle (if $A = C$, $B = O$), an ellipse (if $B^2 - 4AC < O$), a hyperbola (if $B^2 - 4AC > O$),

or a parabola (if $B^2 - 4AC = O$). To determine the form of equation (3.10), it is necessary to evaluate $B^2 - 4AC$ using the relations of (3.12). The result is

$$B^2 - 4AC = \frac{-4}{A_1^2 A_2^2 \sin\psi}, \tag{3.13}$$

which is less than zero. Therefore, the locus of the conic is an ellipse. This means that the particles of the medium, whose disturbance from equilibrium is propagated as a harmonic wave, move in such a way that the projection of their motion on any plane perpendicular to the direction of propagation is an ellipse with semiaxes $A_1 \sin\psi$ and $A_2 \sin\psi$. The result is termed an elliptically polarized harmonic wave. Since the disturbance of ϕ_x is in the X direction and confined to the XZ plane, it is called a plane polarized wave; the same is true for ϕ_y.

It has been shown that the superposition of two plane polarized harmonic waves proceeding in a common direction with the same angular frequency but with different amplitudes and velocities leads to an elliptically polarized wave. Certain special cases are of interest. If the amplitudes A_1 and A_2 are equal and $\psi = \frac{\pi}{2}$, the ellipse reduces to a circle and the resultant wave is termed circularly polarized. However, if $\psi = O$, and $\psi = \pi$, the resultant disturbances lie in the plane through the Z axis given by the respective equations

$$\frac{\phi_x}{A_1} = \frac{\phi_y}{A_2}; \quad \frac{\phi_x}{A_1} = -\frac{\phi_y}{A_2}. \tag{3.14}$$

Thus, for a phase difference of 180 degrees, the particle motion is perpendicular to the initial in-phase motion, a relationship which provides the basis for the experimental technique described in Chapter III.

These disturbances are still plane polarized waves, but the plane of polarization oscillates between two fixed orientations, i.e., through angle θ on either side of the stress direction defined by

$$\theta = \arctan\left(\frac{A_2}{A_1}\right). \tag{3.15}$$

It is obvious that as the two waves propagate through the anisotropic body, their phase difference will change and the particle motion will vary as illustrated in Figure 6b.

For the purposes of this investigation, it is necessary to determine the envelope of the resultant motion when the two waves have the same amplitude, i.e., when ν is 45 degrees and $A_1 = A_2$. If ϕ_R represents the resultant of ϕ_x and ϕ_y, then

$$\phi_R = \phi_x + \phi_y = \frac{\phi_0}{2}\left[\cos \omega t + \cos (\omega t + \psi)\right]. \tag{3.16}$$

By applying the following trigonometric identities:

$$\cos (x + y) = \cos x \cos y - \sin x \sin y, \tag{3.17}$$

$$\cos \left(\frac{x}{2}\right) = \left(\frac{1 + \cos x}{2}\right)^{\frac{1}{2}}, \tag{3.18}$$

$$\sin x = 2 \sin \frac{x}{2} \cos \frac{x}{2}, \tag{3.19}$$

the above equation for ϕ_R simplifies to

$$\phi_R = \phi_0 \cos \frac{\psi}{2} \cos \left(t + \frac{\psi}{2}\right), \tag{3.20}$$

whose envelope is $\left|\phi_0 \cos \frac{\psi}{2}\right|$ which has nodes for

$$\psi = (2n - 1)\,\pi\,; \quad n = 1, 2, 3, \ldots \quad . \tag{3.21}$$

If t_1 and t_2 represent the times required for transmission on planes parallel to the X and Y axes, respectively, the phase difference will be

$$\psi = \omega\ (t_1 - t_2). \tag{3.22}$$

Let Z be the distance propagated by ϕ_x with velocity V_x and by ϕ_y with velocity V_y in the time t_1 and t_2 respectively. Then

$$t_1 = \frac{Z}{V_x} \quad \text{and} \quad t_2 = \frac{Z}{V_y}\ , \tag{3.23}$$

whence

$$t_1 - t_2 = Z\left(\frac{1}{V_x} - \frac{1}{V_y}\right) = Z\left(\frac{V_y - V_x}{V_x\ V_y}\right), \tag{3.24}$$

and the phase difference ψ is

$$\psi = \omega\left(\frac{V_y - V_x}{V_x\ V_y}\right) Z. \tag{3.25}$$

The angular frequency ω is related to the linear frequency f by

$$\omega = 2\pi f. \tag{3.26}$$

By combining equations (3.25) and (3.26), the phase difference can be expressed as

$$\psi = 2\pi f\left(\frac{V_y - V_x}{V_x\ V_y}\right) Z. \tag{3.27}$$

Since the difference between V_x and V_y is generally small, their product can be approximated by the square of the velocity of propagation in an isotropic body of the same material, i.e.,

$$V_x V_y \cong V^2. \tag{3.28}$$

Therefore, equation (3.27) can be written as

$$\psi = 2\pi f \left(\frac{V_y - V_x}{V^2} \right) Z, \tag{3.29}$$

or alternately as

$$\psi = \frac{2\pi f}{V} \left(\frac{\Delta V}{V} \right) Z, \tag{3.30}$$

where ΔV is the difference between V_x and V_y. Thus, equation (3.30) establishes the functional relationship between the phase difference and the fractional velocity change associated with the propagation of a doubly refracted distortional elastic wave through an anisotropic body.

Experimental Technique

The phase difference can be found by experimentally determining the distance the wave travels for a node to occur. From equation (3.21), it is known that complete interference occurs for $\psi = (2n - 1)\pi$ where n denotes the nodal number. Therefore, the phase difference corresponding to the first node is $\psi = \pi$. From (3.30), the associated fractional velocity change then is

$$\frac{\Delta V}{V} = \frac{V}{2fZ_0} \tag{3.31}$$

where Z_0 denotes the distance the wave travels for a node to occur. In order to determine Z_0, an experimental technique based on the familiar pulse reflection method is used. In this technique, short duration pulses of ultrasonic energy in the form of distortional waves are sent into the specimen. Each pulse is transmitted through the specimen and is reflected from the free surface on the opposite side of the specimen. The reflections or echoes are then monitored on an oscilloscope. If the specimen is isotropic, no birefringence of the wave will occur and the amplitudes of the reflected pulses will decrease exponentially, as shown in Figure 7a, because of energy absorption in the specimen. However, if the specimen is anisotropic, birefringence will occur (providing propagation is not along a principal axis) and the particle motion in general will be "elliptical" as explained earlier. However, when $\psi = \pi$, the particle motion will be at right angles to the incident particle motion. This condition will produce a minimum in the echo pattern as illustrated in Figure 7b. It should be mentioned that the amplitude of vibration is not necessarily zero here but, as will be explained later, the transducer which acts as both a transmitter and a receiver is unresponsive to distortional waves whose plane of vibration is perpendicular to its own. It is now obvious that to determine the distance the wave travels for a node to occur ($\psi = \pi$ condition), it is necessary only to observe the number of echoes to the first minimum in the echo pattern. Since one echo p corresponds to a wave propagation distance of twice the specimen thickness h, the fractional velocity difference $\frac{\Delta V}{V}$ associated with the first minimum, by using equation (3.31), is

$$\frac{\Delta V}{V} = \frac{V}{4fph} . \qquad (3.32)$$

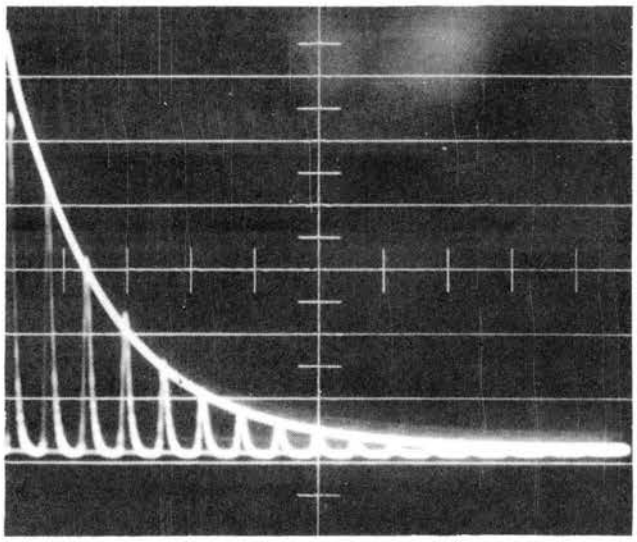

(a)

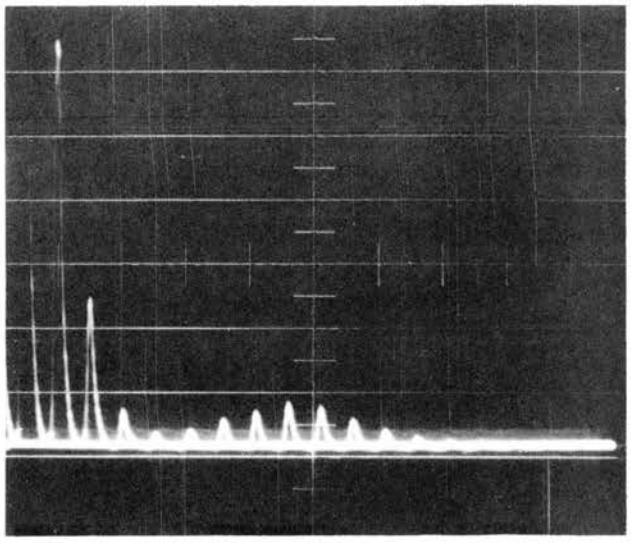

(b)

Figure 7. Pulse Echo Pattern Showing (a) No Birefringence and (b) Modulation Produced by the Anisotropy of the Medium

Thus, this equation establishes the relationship between the experimentally obtainable quantity p and the quantity of interest in this investigation, i.e., $\frac{\Delta V}{V}$.

Test Material Characterization

To obtain meaningful results in an investigation of this nature, the material selected for testing must have a well known work history since this affects both the microstructure and the state of stress of the material. Therefore, the Research Laboratory of the Aluminum Company of America (ALCOA) was contacted and was requested to provide samples of aluminum whose work history was known. After an explanation was given of the objectives of this study, ALCOA agreed to furnish for this investigation specially fabricated 6061-T6 and 1100-0 aluminum alloy stock. The 6061-T6 material was selected because it is a widely used, medium strength alloy and the information obtained would be of general engineering interest. However, because of its strength, it generally is not available with the 80 to 90% cold work required for this study. Thus, a softer aluminum, 1100-0, which could be obtained with the required degree of cold work, was included to enable data to be obtained for the larger reductions in gage.

The material subsequently received from ALCOA was in sheet form and had been fabricated to produce varying degrees of crystallite orientation and states of stress. This was accomplished by carefully unidirectionally rolling the sheets to specific reductions in gage. These were 0%, 20%, 36%, and 50% for the 6061-T6 alloy and 0%, 40%, 60%, and 80% for the 1100-0 material. Theoretically, an increase in the reduction of gage produces an increase in the number of crystallites that are oriented in a specific direction. In addition, residual

stresses are introduced due to the inhomogeneous plastic flow of the material produced by the rolling forces.

Determination of Preferred Orientation

The specific orientations produced in a metal by rolling and the quantitative determination of the relative number of crystallites which are aligned in the rolling direction can be obtained from pole figures[1] based on x-ray diffraction data (16). Consequently, specimens were fabricated from each sheet of aluminum for x-ray diffraction analysis of preferred orientation. The specimens were in the form of a disc approximately 1.125 inches in diameter and 0.015 inch thick. Both surface (outer) and interior (inner) specimens were prepared since it was desired to determine if the surface orientation differed significantly from that in the center of the sheet. The specimens were removed from the sheet by machining and then were etched in an acid bath to remove the effects of the machining operation. The etchant used consisted of 9 parts hydrochloric acid (HCl), 3 parts nitric acid (HNO_3), 2 parts hydrofluoric acid (HF), and 5 parts water (H_2O). A large quantity of etchant was used with respect to the surface of the specimen and care was taken to avoid the heating of the etchant during the etching process.

Since the necessary equipment for obtaining the data required for the construction of the desired pole figures was not available, arrangements were

---

[1] A pole figure is the stereographic projection of the intercepts, called poles, of the normals to one set of crystallographic planes with the reference sphere. The pole figure describes the orientation of these planes with respect to the outside dimensions of the specimen.

made to have this work done in the Chemistry Department of the Lawrence Radiation Laboratory, which is operated for the Atomic Energy Commission by the University of California. It is one of a few laboratories in the country which possesses an automatic pole figure plotting system. A similar system has been described by Eichhorn (17). The advantages of an automatic system are the reduction in time and effort required to prepare a pole figure through the elimination of the hand plotting of data read from films or strip charts and the increase in accuracy which can be obtained.

As an aid in interpreting the pole figures which were obtained for the specimens described previously, a brief explanation will be given concerning the acquisition of preferred orientation information by x-ray diffraction techniques and the plotting of this information in pole figure form (a detailed discussion of pole figures is contained in Reference 16). Consider the experimental arrangement shown in Figure 8. A crystal plane is shown in position to reflect a beam of x-rays to form a spot S on the film. The plane normal intersects the reference sphere, which is inscribed about it, at the point P, which projects stereographically to the point P' in the projection plane. The incident beam, the reflected beam, and the pole of the reflecting plane all lie in the same plane inclined at an angle β from the vertical. Thus, when the film and projection planes are placed normal to the beam as shown, it will be seen that the angle β on the projection will be equal to β on the film. Since the angle of incidence, θ_i, of the beam on an (hkl) plane is determined by the Bragg law, $\eta\Lambda = 2d \sin \theta_i$, whenever reflection occurs, it follows that the poles of all such (hkl) planes capable of reflecting must lie at a constant angle ($\alpha = 90 - \theta_i$) from the incident beam and must intersect

the reference sphere only along the circle known as the "reflection circle," a circle on the projection $90-\theta_i$ from the centrally located beam. Both the azimuthal and radial positions on the pole figures are thus determined. Quantitative information is obtained by fixing a Geiger counter at one position and tilting and rotating the specimen so as to determine intensities diffracted from the selected atomic planes at various angles within the specimen. These intensities, which are proportional to concentrations of poles, are plotted on a polar stereographic

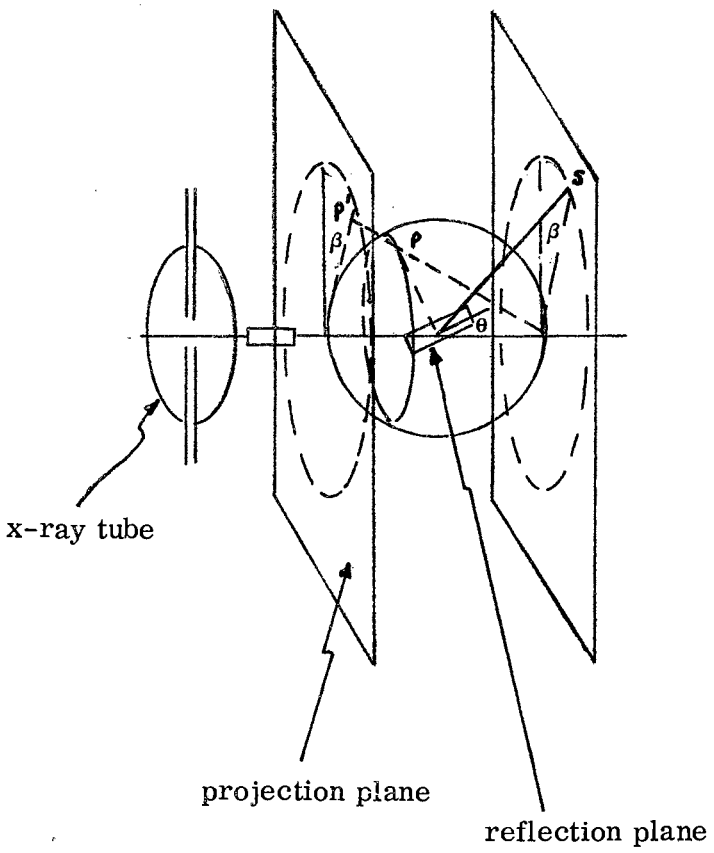

Figure 8. X-ray Diffraction Determination of Preferred Orientation

net shown in Figure 9 to obtain the pole figure. The pole figure is made quantitative by determining the intensity of diffraction (corrected for absorption) by

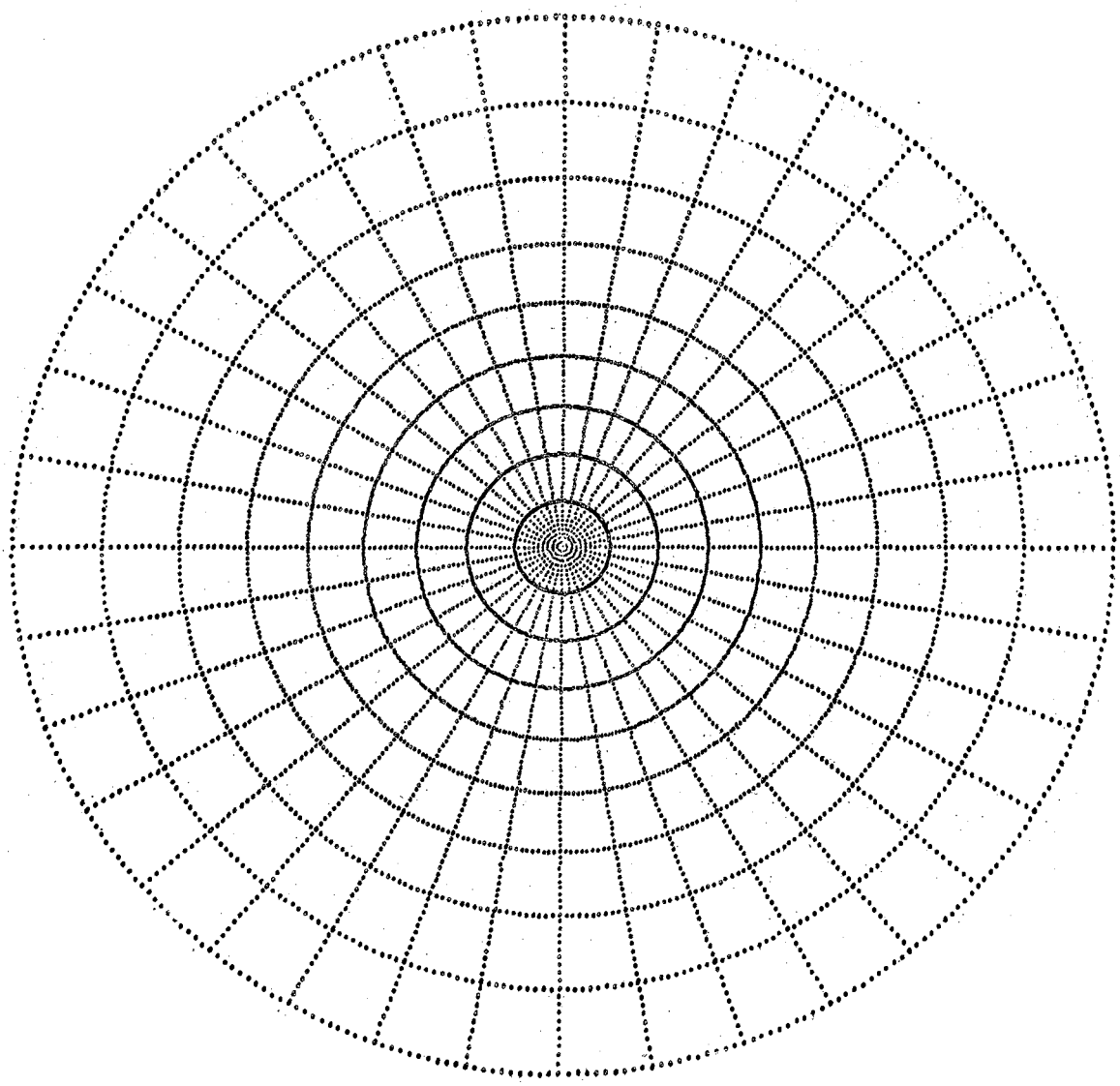

Figure 9. Polar Stereographic Net

comparison with an identical specimen with random orientation of grains or by calculation from readings on a similar specimen. The data then is obtained in terms of the Random Count such as one times Random (1R), two times Random (2R) etc. After this data is obtained, isointensity or contour lines are drawn through points of approximately the same random intensity. In this way, a visual representation of the orientation in the specimen is obtained.

The actual pole figures obtained for the specimens which were extracted from each sheet are given in Appendix A where the specimen numbers bear the relationship shown in Table II to the material from which the specimens were obtained.

TABLE II

POLE FIGURE SPECIMEN NUMBERING SYSTEM

Specimen Number	Type of Specimen	Material	Cold Work (%)
1B	Inner	6061-T6	0
2A	Outer	6061-T6	20
2B	Inner	6061-T6	20
3A	Outer	6061-T6	36
3B	Inner	6061-T6	36
4A	Outer	6061-T6	50
4B	Inner	6061-T6	50
II-A-1	Outer	1100-0	0
II-B-1	Outer	1100-0	40

TABLE II (Continued)

Specimen Number	Type of Specimen	Material	Cold Work (%)
II-B-2	Inner	1100-0	40
II-C-1	Outer	1100-0	60
II-C-2	Inner	1100-0	60
II-D-1	Outer	1100-0	80
II-D-2	Inner	1100-0	80

The supporting data sheets giving the array of intensities in multiples of random intensity at each alpha-beta angular coordinate pair, from which the pole figures were plotted, also are given in Appendix A and are arranged so that each set immediately follows the pole figure to which it pertains. If the intensity for each alpha-beta coordinate pair is examined, it will be observed that the pole figure may be visualized in the tabular data, as indicated for the data array for specimen II-A-1. The interpretation and application of these data will be made in a later section.

Preparation of Birefringence Test Specimens

Birefringence test specimens were fabricated from each sheet of aluminum received from ALCOA. Since it was desirable to determine whether there was any significant difference in birefringence along the rolling and long transverse directions of the rolled sheets, specimens were removed from the sheets according to the scheme shown in Figure 10. Each specimen was approximately

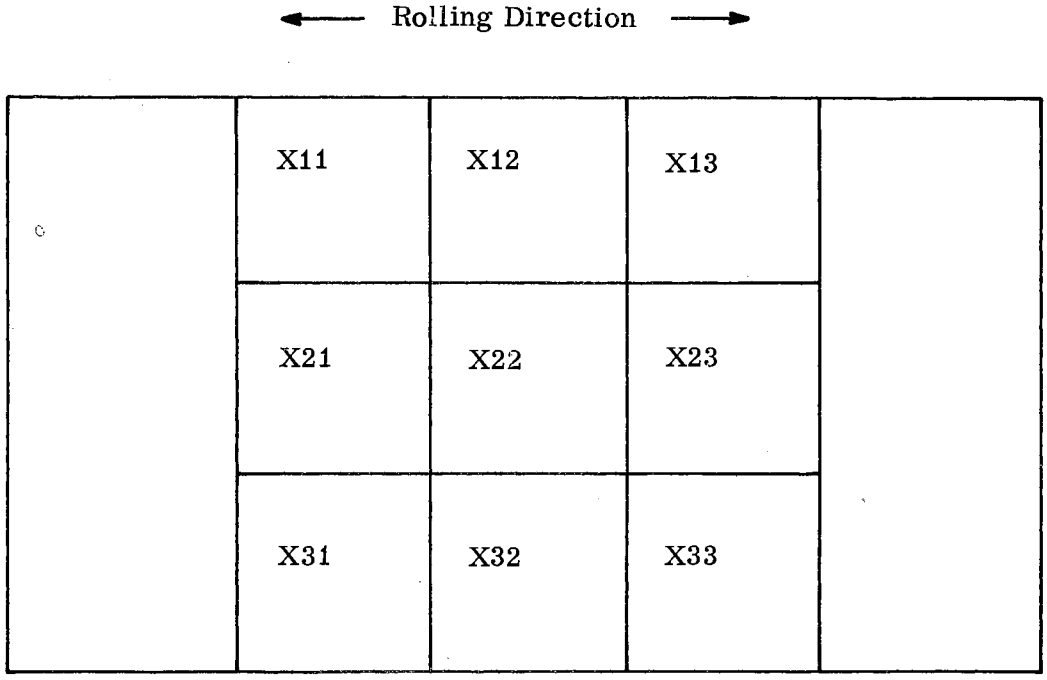

Figure 10. Birefringence Specimen Lay-Out for Rolled Metal Sheet

three inches square with a nominal thickness of 0.125 to 0.250 depending on the particular sheet from which the specimen was obtained. The three-inch dimension was chosen so that the lateral dimension would be large in comparison to the thickness so as to establish a plane stress situation in each specimen. As was illustrated in Figure 10, three digit code numbers were assigned to the 6061-T6 specimens to denote their origin. The first digit denoted the particular sheet, the second digit the position along the rolling direction, and the third digit the location of the specimen with respect to the long transverse direction. The sheet numbers ran from one to four and were related to the particular sheets as follows:

1	zero cold work
2	20% cold work
3	36% cold work
4	50% cold work

A similar scheme was used for the 1100-0 specimens except that letters were used as follows to denote the parent sheets:

A	zero cold work
B	40% cold work
C	60% cold work
D	80% cold work

As mentioned previously, the pulse echo technique was used for the birefringence tests which are described in a later section. The use of this technique imposed rather stringent requirements on the preparation of the test specimens. These were surface condition and parallelism of the major specimen faces. The effect of nonparallelism on the reflected echoes when a common sending and receiving crystal is used (as was the case in this study) has been investigated by Roderick and Truell (18). Their results show that in order to be sure nonparallelism has no effect on the reflected echoes, it is necessary that $\delta << 0.6 \frac{\Lambda}{an}$ where δ is a measure of the lack of parallelism as illustrated in Figure 11, n is the number of usable echoes, a is the radius of the transducer, and Λ is the wavelength of the stress wave. Typical values of a and n for this investigation were 3/8 inch and 8 respectively. The velocity of distortional waves in 6061-T6 aluminum according to measurements made in the laboratory is 1.10×10^5 inches per second or 0.11 inch per microsecond. Since the velocity is equal to the frequency times the wavelength i.e., $V = f\Lambda$, then $\Lambda = \frac{V}{f} = \frac{0.110}{f}$ where f is in

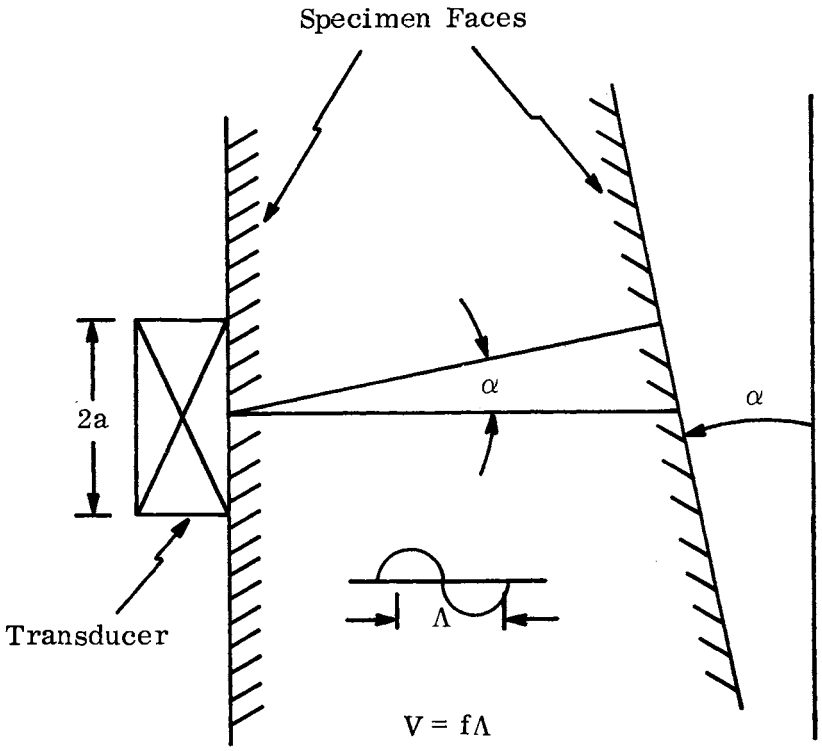

Figure 11. Schematic Representation of Non-Parallel Specimen Faces

megacycles per second (Mc). For f equal to 10 Mc, a equal to 3/8, and n equal to 8, $\delta << 0.0022$. In order to satisfy this relationship and ensure no effect due to nonparallelism of specimen faces, the specimens were fabricated with faces parallel to at least 0.0001 inch per inch. In addition, the faces were lapped after machining to reduce surface effects on the incident stress waves.

For the stress-induced birefringence work, a rectangular rosette strain gage was applied to the test specimens. This provided strain measurements from which principal stresses could be calculated. Even though a uniaxial stress was applied, the possibility of the misalignment of the specimen in the grips of the

tensile machine, which could result in a biaxial stress, made it desirable to determine the principal stresses.

Experimental Apparatus

The experimental technique used in this study to make birefringence measurements was based on the familiar pulse echo technique and included the following basic steps:

a. generation of an electrical pulse of the desired frequency and pulse length;

b. conversion from electrical to ultrasonic energy by means of an appropriate piezoelectric transducer;

c. coupling of the ultrasonic energy into the metal specimen;

d. transmission of the ultrasonic pulses through the metal specimen;

e. reflection and retransmission of the pulses from the opposite face of the specimen;

f. coupling of the reflected ultrasonic energy into the transducer;

g. conversion of the ultrasonic energy to electrical energy;

h. amplification of the electrical energy for display on a cathode ray tube; and finally,

i. interpretation of the electrical pulses to provide a measurement of acoustic birefringence.

The electrical instrumentation used to perform the above steps was in the form of a commercial ultrasonic unit (see Figure 12) called an Ultrasonic Attenuation Comparator manufactured by the Sperry Products Company, Danbury,

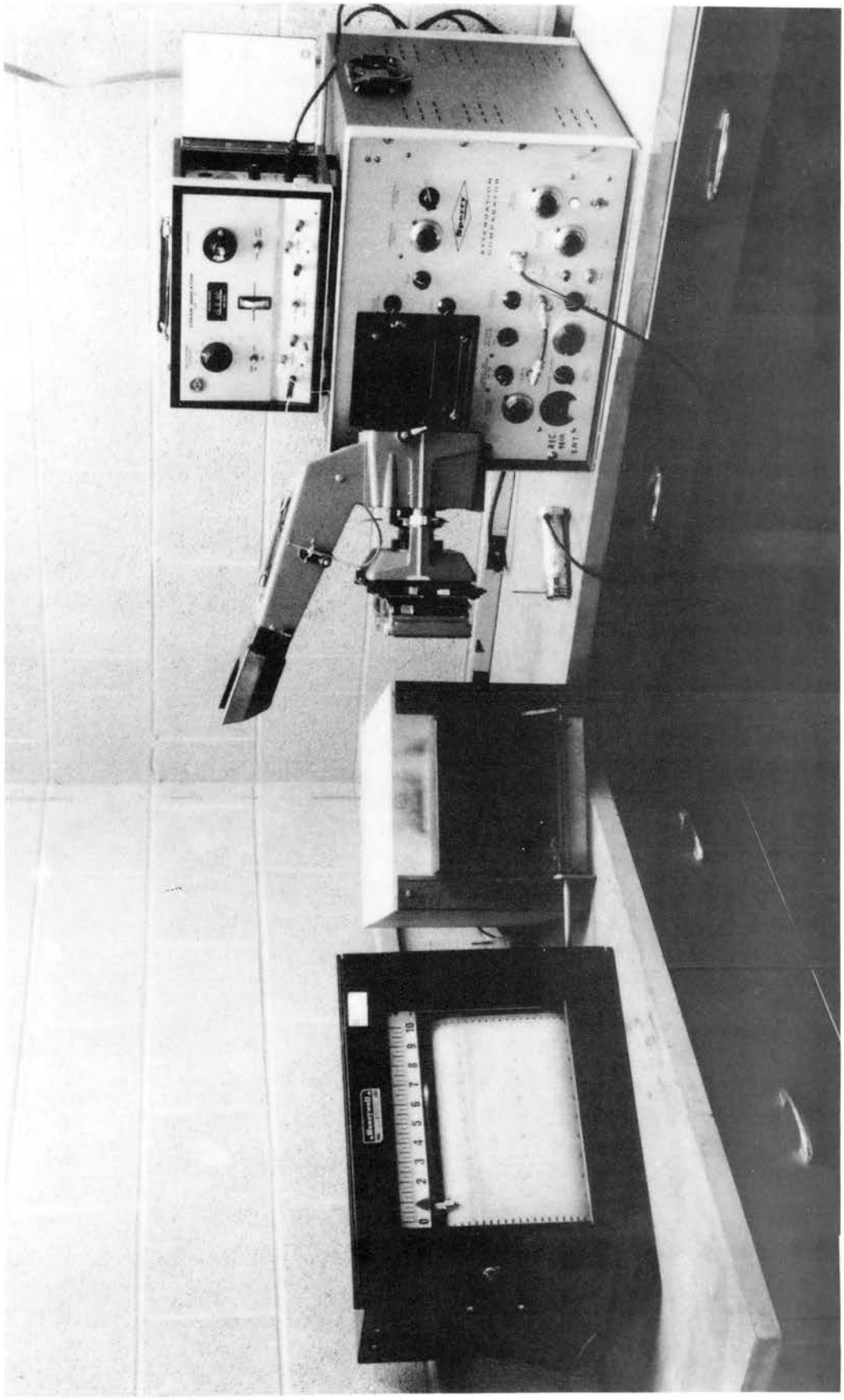

Figure 12. Experimental Apparatus

Connecticut. As the name implies, this unit is built primarily for the measurement of ultrasonic attenuation. However, since it comprises all the electrical apparatus needed to make the desired measurements, it was utilized in this investigation. Basically, the unit consists of a pulsed radio frequency (RF) source of energy (pulsed oscillator), a high gain superheterodyne receiver, a wide range continuously variable exponential wave form generator (required for attenuation measurements), a linear time delay generator, and appropriate trigger and sweep circuits for the built-in cathode ray tube. In operation, the pulsed RF oscillator is used to drive an appropriate transducer whose mechanical output (produced by the piezoelectric effect) is coupled into the material under investigation. The reverberations or echoes in the material are detected by the same transducer, coupled to the receiver where they are amplified and detected, and then displayed on the vertical axis of the cathode ray tube. Figure 13 illustrates in simplified block diagram form how these functions are performed and are interrelated. The system is capable of providing electrical pulses having carrier frequencies of 5 to 200 megacycles per second (Mc) with corresponding pulse widths of 0.5, 1, and 2 microseconds (μs) at a pulse repetition rate of 100 pulses per second.

The piezoelectric transducers used to generate the desired distortional waves were fabricated using Y-cut quartz crystals obtained from the E. B. Lewis Company, East Hartford, Connecticut. The crystals, having a diameter of 3/4 inch, a resonant frequency of 10 Mc, and a silver plated electrode on one side, were bonded with Eastman 910 adhesive to a backing plate of metal-filled phenolic which had a high acoustic attenuation and an impedance close to that of aluminum.

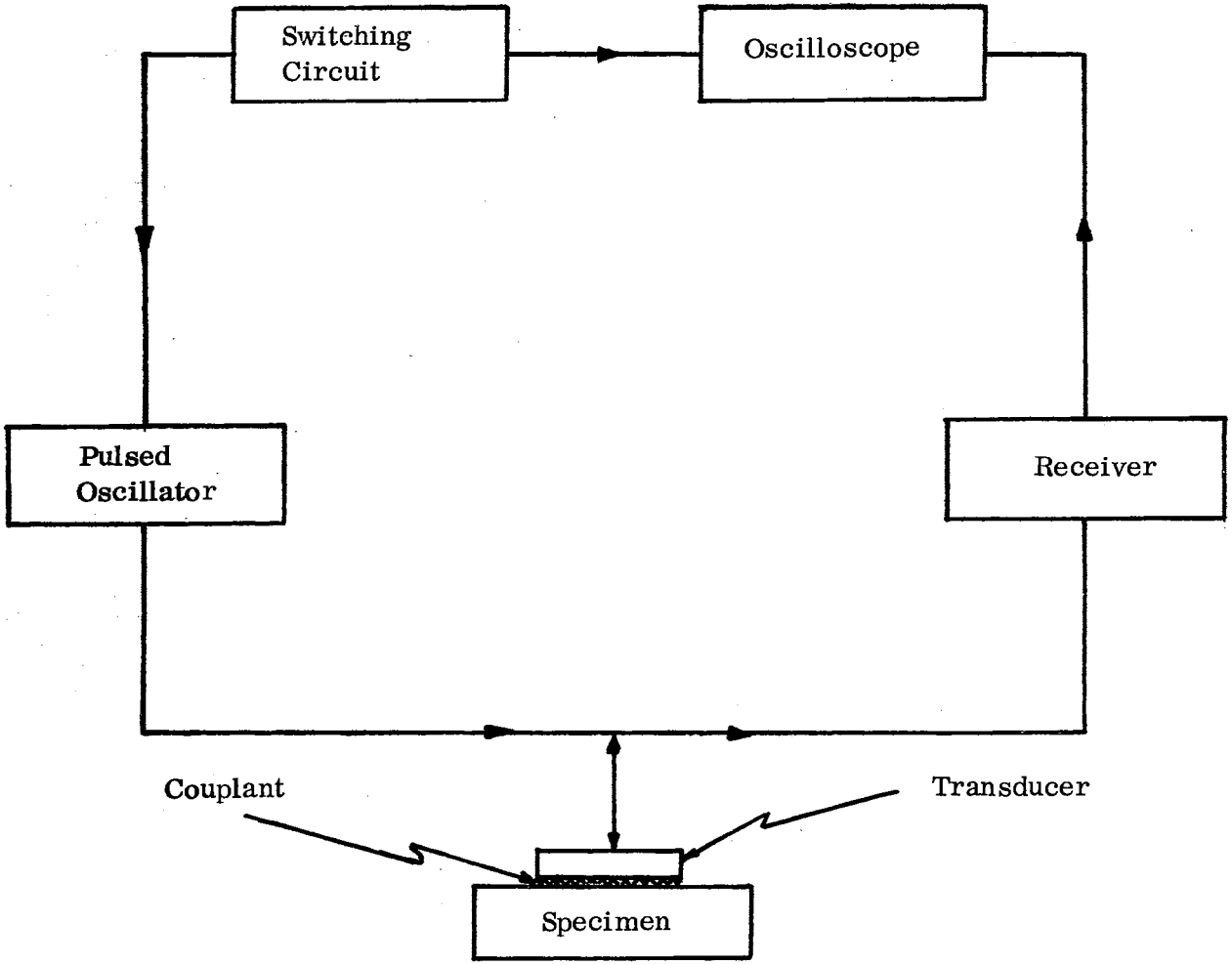

Figure 13. Simplified Block Diagram of Birefringence Measuring System

The phenolic then was cemented to a mechanical energy absorbing silicone rubber disc which was attached to a UGH type electrical connector. The polarization of the transducer was determined by using the shear wedge technique of Crecraft (19).

In order to transmit a distortional wave on an axis normal to the surface of a solid, a suitable couplant must be used. Since distortional waves are characterized by particle oscillations in a plane normal to the direction of propagation, they therefore can propagate only by the transmission of shear stresses from one particle to the next. Because gases do not have a modulus of rigidity, distortional waves can in general be propagated only in extremely viscous liquids and in solids. One viscous liquid which has been used successfully as a couplant for distortional waves is "Nonaq," a grease sold by the Fisher Scientific Company (7). Another couplant which has given satisfactory results for this application is phenyl salicylate, a low melting point solid, which also is available from the Fisher Scientific Company (19). For this study, the liquid couplant Nonaq was used in conjunction with an applied pressure to obtain the desired coupling. The liquid was selected because measurements were to be made on many specimens which required the application and reapplication of the transducer many times. In addition, it was required that the transducer be coupled at different positions on the specimen during the measurement process. It is obvious that a solid couplant requiring the use of heat for application would have been considerably less convenient. Tests were made to check the quality of the coupling obtained with the grease as compared to that obtained with a solid couplant. Aside from slightly larger energy losses, no significant difference was observed.

The application of pressure on the couplant was achieved by the use of the specially designed specimen holder shown in Figure 14. The force was applied by means of the hand screw and was transmitted to the back of the transducer via a 3/4 inch diameter steel ball which allowed the transducer to "sit" squarely on the surface to which it was applied. In order to ensure that the same force was applied each time the transducer was used, a strain gage was mounted on the support arm and connected to a Baldwin-Lima-Hamilton (BLH) strain gage indicator. In the initial test, an increasing force was applied to the transducer, by rotating the hand screw, until a suitable echo pattern was observed on the cathode ray tube which indicated proper coupling. The strain gage reading then was obtained from the strain gage indicator. All subsequent measurements were made at this same strain value.

In addition to applying force to the transducer, the specimen holder provided for the vernier controlled movement of the specimen laterally in the x and y directions and also angularly 360 degrees about the transducer axis. This controlled positioning of the specimen was necessary because of the need for making measurements at known positions on the specimen and for determining the angle at which the minimum occurred in the pulse echo pattern.

In addition to the previously mentioned apparatus, several other items of experimental equipment were used in this investigation. Because of the necessity for heat treating the test specimens, a small laboratory furnace capable of providing temperatures of 1000° F was fabricated. A chromel-alumel thermocouple was connected to a Minneapolis-Honeywell Electronic Recorder which was equipped with a built-in relay system to control the power input to the furnace. Using

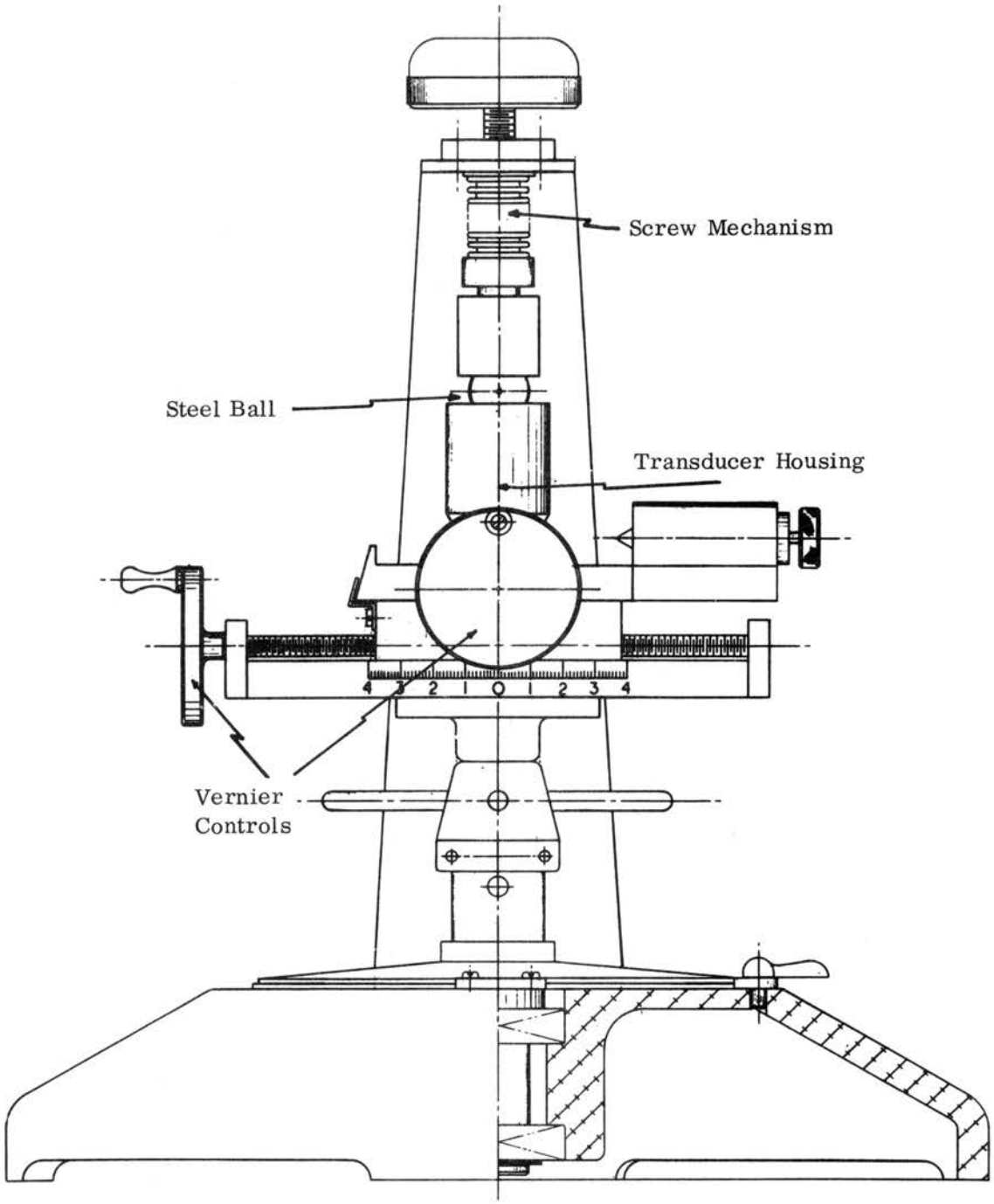

Figure 14. Specimen Holder

this system, the specimen temperature could be maintained to ± 5° F of the desired temperature.

In the stress-induced birefringence portion of the experimental program, a Model TT-C Instron Universal Testing Instrument was used to apply the loads to the specimens. This instrument is capable of providing loads to 10,000 pounds and crosshead speeds of 0.02 to 20.0 inches per minute. A strip chart recorder was used to record the load and crosshead travel information. All the data for this study were obtained using a strain rate of 0.02 inch per minute. The maximum load applied to any specimen was approximately 9,000 pounds.

CHAPTER IV

EXPERIMENTAL PROCEDURE AND RESULTS

It was shown in a preceding chapter that a material may be birefringent to an elastic distortional wave if it contains preferentially oriented crystallites or is subjected to a state of stress. As stated earlier, both of these conditions are present in cold-rolled metal sheet. Since it is desired to evaluate the relative effects due to these two factors, one of the two must be varied or eliminated. It has been stated that the degree of orientation possessed by a rolled sheet is dependent on the amount of cold work it receives, i. e., the greater the reduction in gage the greater the orientation. Thus, preferred orientation can be controlled to some extent by the application of cold work but it cannot be eliminated easily. On the other hand, the residual stresses produced by the cold rolling process can be partially or, in some cases, completely relieved by properly heat treating the material. According to Dieter (20), a light anneal, which accomplishes recovery only and does not produce recrystallization, will not change the size, shape, or orientation of the crystallites. Therefore, any previously existing preferred orientation will persist essentially unchanged after heat treatment as an annealing texture which is simply a preferred orientation in an annealed metal. The procedure then was to determine the birefringence of the specimens initially, subject them to heat treatment, and make a subsequent

measurement to determine the effect of the treatment. To evaluate the effect of stress, birefringence measurements were made while the specimens were subjected to various applied stresses.

Experimental Procedure

The previously described experimental equipment was used to make the necessary measurements. The procedure for initiating a birefringence measurement involved making the necessary electrical connections to the strain gage indicator and to the Ultrasonic Attenuation Comparator, clamping the specimen in the specimen holder, applying a thin film of the liquid couplant to the transducer, and mounting the transducer on the specimen. Hand pressure was applied to the transducer as it was slightly oscillated to remove any excess couplant (wringing-in process). Pressure then was applied by means of the hand screw until the predescribed strain was achieved as evidenced by the reading on the strain gage indicator. The echo pattern on the cathode ray tube of the Ultrasonic Attenuation Comparator (which had been previously tuned to the 10 Mc resonant frequency of the Y-cut crystal) was monitored. If the echoes were returning to the baseline, proper coupling was indicated. If the echoes did not return to the baseline, the pressure was relieved slightly on the transducer and the wringing-in process was repeated. Measurements generally were made with the transducer mounted in the center of the specimen, but in some cases measurements were made at points away from the center to determine the degree of variation (if any) of birefringence across the specimen. In making measurements, the pressure on the transducer was reduced slightly so the specimen mounting platform could be

rotated until a minimum was observed in the pulse echo pattern. The number of echoes to the minimum was counted and the angular position of the specimen with respect to the axis of polarization of the piezoelectric crystal was noted. If the rolling direction of the specimen were a principal axis of anisotropy, a minimum was obtained when the polarization axis was displaced approximately 45° from the rolling direction. The node occurred when the polarization axis was midway between the principal axes (in this case, the rolling axis and the one transverse to it) because of the condition shown earlier by equation (3.14). After the waves (which had equal amplitudes) traveled a distance required to produce a phase difference of 180 degrees, the particle motion was perpendicular to the original motion imparted by the transducer. Since the transducer (which acted also as a receiver) was insensitive to particle motion perpendicular to its axis of polarization, it did not sense the motion, and thus did not transmit an electrical signal.

After the initial measurements were made, the specimens were heat treated and then remeasured. Two separate heat treating times and temperatures were used, namely, 8 hours at 475° F and 2 hours at 650° F. These temperatures and times were selected after a heat treatment program was completed to determine the annealing conditions which would accomplish recovery only and not induce recrystallization or grain growth in the cold worked specimens. Several different conditions of time and temperature were investigated. Photomicrographs were made prior and subsequent to heat treating and were analyzed for any changes in microstructure produced by the heat treating. Typical examples of these photomicrographs are shown in Figure 15.

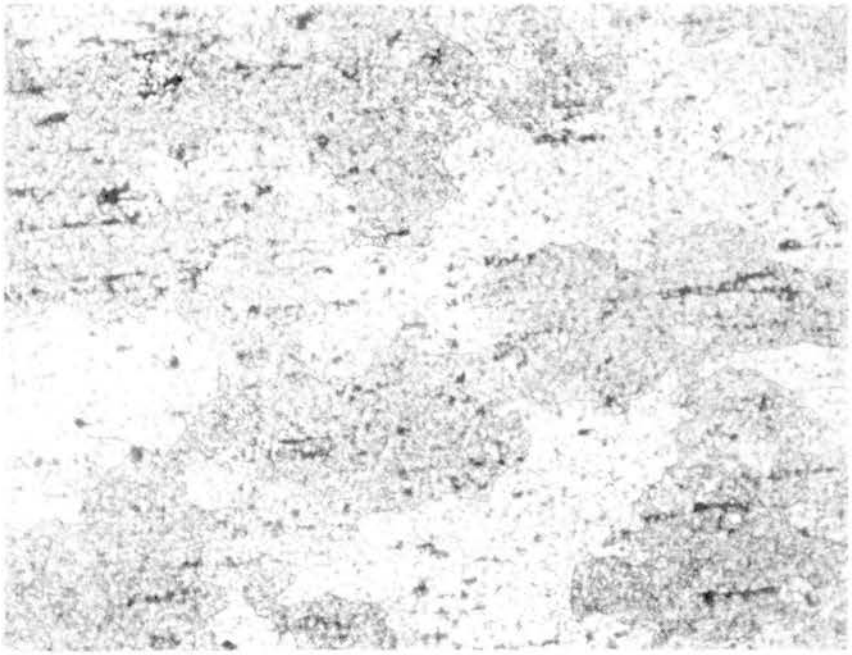

(a)

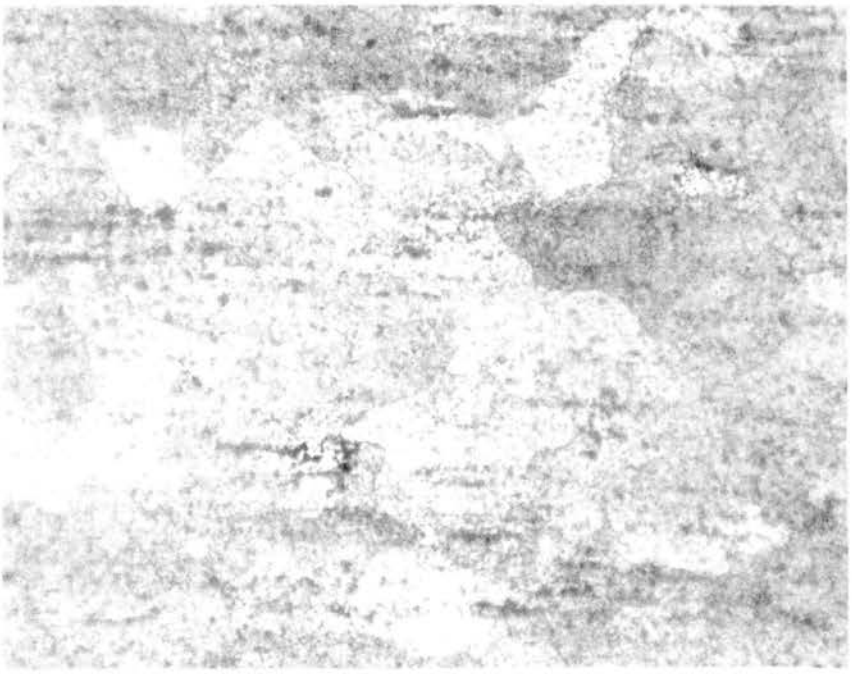

(b)

Figure 15. Typical Photomicrographs (100X) of 6061-T6 Aluminum (a) Prior and (b) Subsequent to Heat Treatment

It was required that the stress-induced birefringence measurements be made with the specimen attached to the pull rods of the Instron machine. This necessitated using a different transducer mounting technique since the specimen holder could not be used in this position. A hand screw type clamping mechanism was made which was similar to the specimen holder except that no provision was made for controlled movement of the specimen beneath the transducer. Instead, the transducer was mounted in the center of the specimen using the liquid couplant with the polarization axis rotated approximately 45 degrees from the specimen rolling direction. The specific mounting angle depended on the particular specimen but never deviated more than ± 6 degrees from the 45° position. Initial strain and birefringence measurements were made using the equipment and method previously described. Measurements were made at constant tensile loads of various magnitudes to determine the functional relationship between birefringence and stress.

Analysis of Preferred Orientation

The pole figures shown in Appendix A were analyzed to determine the type and degree of preferred orientation possessed by the previously described specimens.[1] The analysis of the data for the 1100-0 material will be given first since it was cold worked more than the 6061-T6 alloy and therefore showed a more pronounced orientation.

---

[1] Assistance in the analysis of the pole figures contained herein was graciously provided by Mr. Don Frazer of the General Chemistry Department of the Lawrence Radiation Laboratory.

The data available in the literature on preferred orientation in cold worked aluminum is principally due to a study made by Hu, Sperry, and Beck (21) on preferred orientation in rolled, face-centered, cubic metals. The experimentally determined pole figures obtained for 1100-0 aluminum in this study agree qualitatively with those obtained by Hu, et al., for 2S aluminum but are rotated ninety degrees about the center from the ones they obtained (or vice versa). To determine the source of this discrepancy, the specimens used in this study were checked to ascertain whether the notches denoting the transverse direction were placed correctly. The notches were indeed correctly positioned as evidenced by the grain elongation normal to their direction on the etched surfaces of the specimens. In addition, the specimens were oriented correctly in the x-ray diffraction goniometer, with the fiducial marks at 90° and 270° to the rolling (0°) index. Thus, the difference is not due to the misorientation of the specimens in this study and therefore, the explanation must lie elsewhere, e.g., in the different rolling procedures used in the two studies. It should be noted that Hu, et al., characterized the orientation for their specimens as "(123) [$1\bar{2}1$]" (the $1\bar{2}1$ is exact) which applies to the pole figures in this study but which is rotated ninety degrees in theirs.[2] Thus, the (123) [$1\bar{2}1$] orientation is ascribed to the pole figures obtained in this investigation; the ideal (111) pole figure for this orientation is shown in Figure 16 in which theoretical relative intensities are indicated approximately by the size of the symbols.

---

[1] The numbers in parentheses refer to the Miller indices which define the crystal plane that is aligned parallel to the rolling plane, whereas the numbers in the brackets denote the crystal direction which is aligned parallel to the rolling direction.

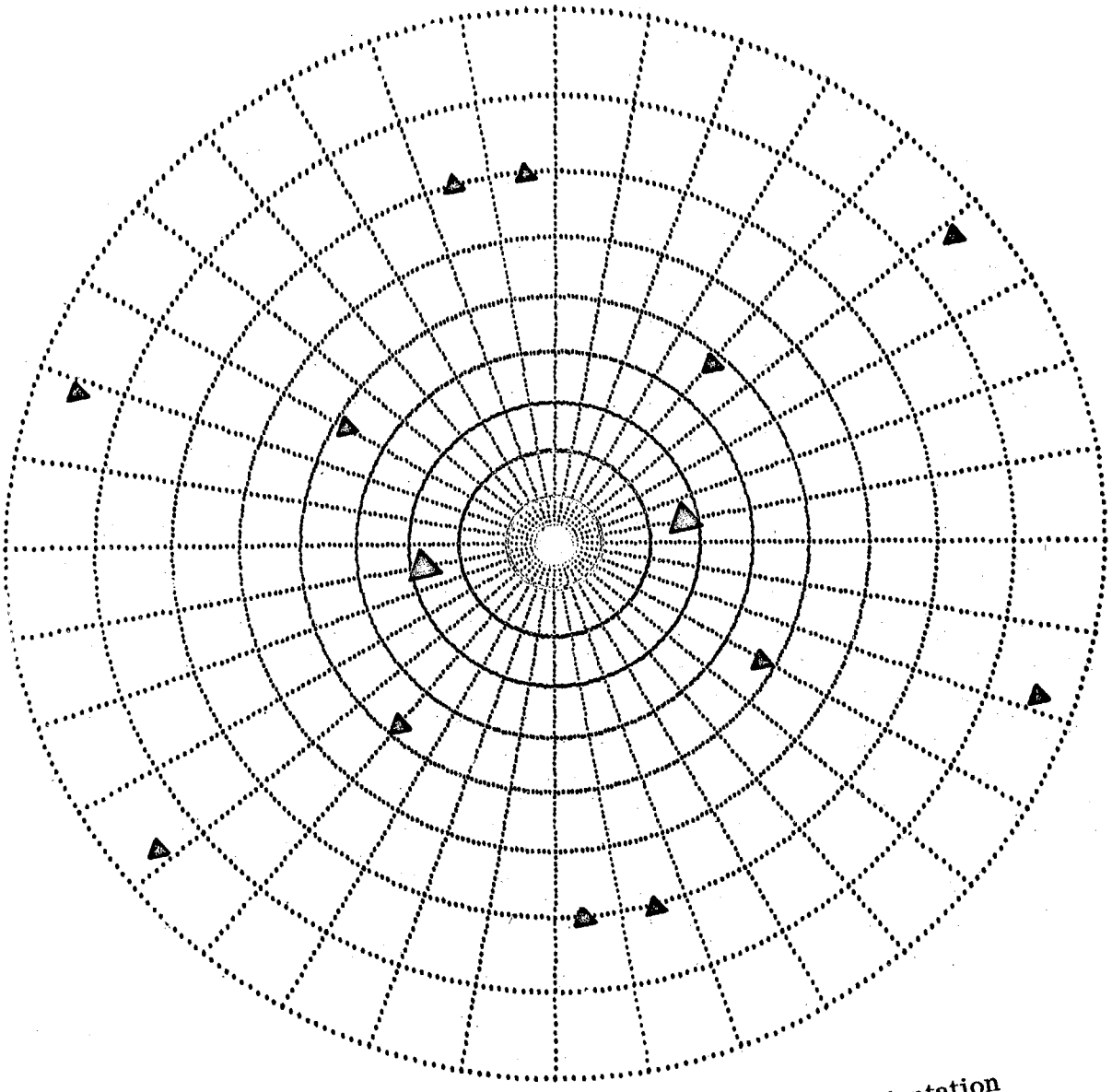

Figure 16. Ideal (111) Pole Figure for Orientation Near (123) [$1\bar{2}1$]

As was mentioned in Chapter III, both outer (surface) and inner (interior) specimens were obtained from each sheet. For convenience, the detailed discussion of the experimental pole figures will deal with the outer specimens first; discussion of the inner specimens will follow. Throughout the discussion of the 1100-0 specimens, the (123)[$1\bar{2}1$] preferred orientation will be referred to as "basic," and the discussion will proceed from least to greatest cold work. The specimen number will be listed first followed by an abbreviated description of the specimen and the figure and table numbers in Appendix A, which contain the pertinent pole figure and the supporting data, respectively.

Specimen II-A-1 (zero cold work, outer, Figure 23, Table XX) shows a very poorly developed but recognizable basic orientation. The maximum pole density of 2.4R and the broad, ill-defined pattern may represent the closest practical approach to random orientation for this material. The asymmetry of the pattern is the result of a slight rotation about [$1\bar{2}1$] (hereafter referred to as RD).

Specimen II-B-1 (40% cold work, outer, Figure 24, Table XXI) shows a well defined basic orientation, with the exception of the small inner arc in the first quadrant. (Other pole figures for the 1100-0 specimens show similar central anomalies. They are the result of a small experimental error in obtaining the central region of the pole figure and, therefore, will be disregarded.) There is a slight intensity asymmetry from the previously mentioned rotation about RD, with the maximum density of 6.6R lying in the left peak.

Specimen II-C-1 (60% cold work, outer, Figure 25, Table XXII) again exhibits the basic orientation, modified by a more marked rotation about RD.

The maximum of 6.3R again lies in the left peak. The origin of the diffuse area on the right is unknown.

Specimen II-D-1 (80% cold work, outer, Figure 26, Table XXIII) is similar to the preceding one, but with an intermediate degree of rotation about RD. The basic orientation may be clearly discerned. The maximum of 6.5R now lies in the right peak, but this is the result of a 180° rotation of the specimen about its center. (This rotation may be observed in some of the other pole figures. Unfortunately, the ends of the transverse direction were not differentiated, so absolute orientation of the specimens was impossible.)

The discussion concerning the inner specimens will be presented now. Specimen II-B-2 (40% cold work, inner, Figure 27, Table XXIV) shows a sharpened version of the orientation found for II-A-1. The maximum of 4.0R is in the right peak, and there is a similar rotation about RD.

Specimen II-C-2 (60% cold work, inner, Figure 28, Table XXV) exhibits a near perfect basic orientation. The maximum (6.2R) happens to be in the left peak, but the quantitative imbalance is very slight (about 0.3R between peaks).

Specimen II-D-2 (80% cold work, inner, Figure 29, Table XXVI) shows a similar, nearly perfect, basic orientation of by far the highest density observed. The maximum of 8.6R cannot be unequivocally placed in either peak because the quantitative differences are so small.

The data given above are summarized in Table III in which the preferred orientation in terms of Random Intensity (R) is presented for the surface and center specimens as a function of the amount of cold work.

TABLE III

PREFERRED ORIENTATION IN COLD-ROLLED
1100-0 ALUMINUM

Percent Cold Work	Preferred Orientation (R)	
	Center Specimens	Surface Specimens
0	--	2.4
40	4.0	6.6
60	6.2	6.3
80	8.6	6.5

In addition, the data are displayed in Figure 17. As can be seen in the graph, the preferred orientation for the specimens removed from the center of the sheet appears to increase linearly with increasing cold work, whereas the surface specimens show no such linear behavior.

In conclusion, it appears that the surface orientation of 1100-0 aluminum is established early in the cold working process at a level in the interval 6.5 ± .2R, is independent of the degree of cold work, and retains the fundamental rotational asymmetry of the unworked metal. The orientation at the center of the sheet, however, is established more slowly, is directly proportional to the degree of cold work, and gradually becomes symmetrical.

The preferred orientation data obtained for the 6061-T6 specimens now will be presented. The cold work given these specimens was considerably less than that given the 1100-0 material. Hence, the orientation obtained was not as pronounced. In addition, the basic orientation was found to be (001)[100] instead

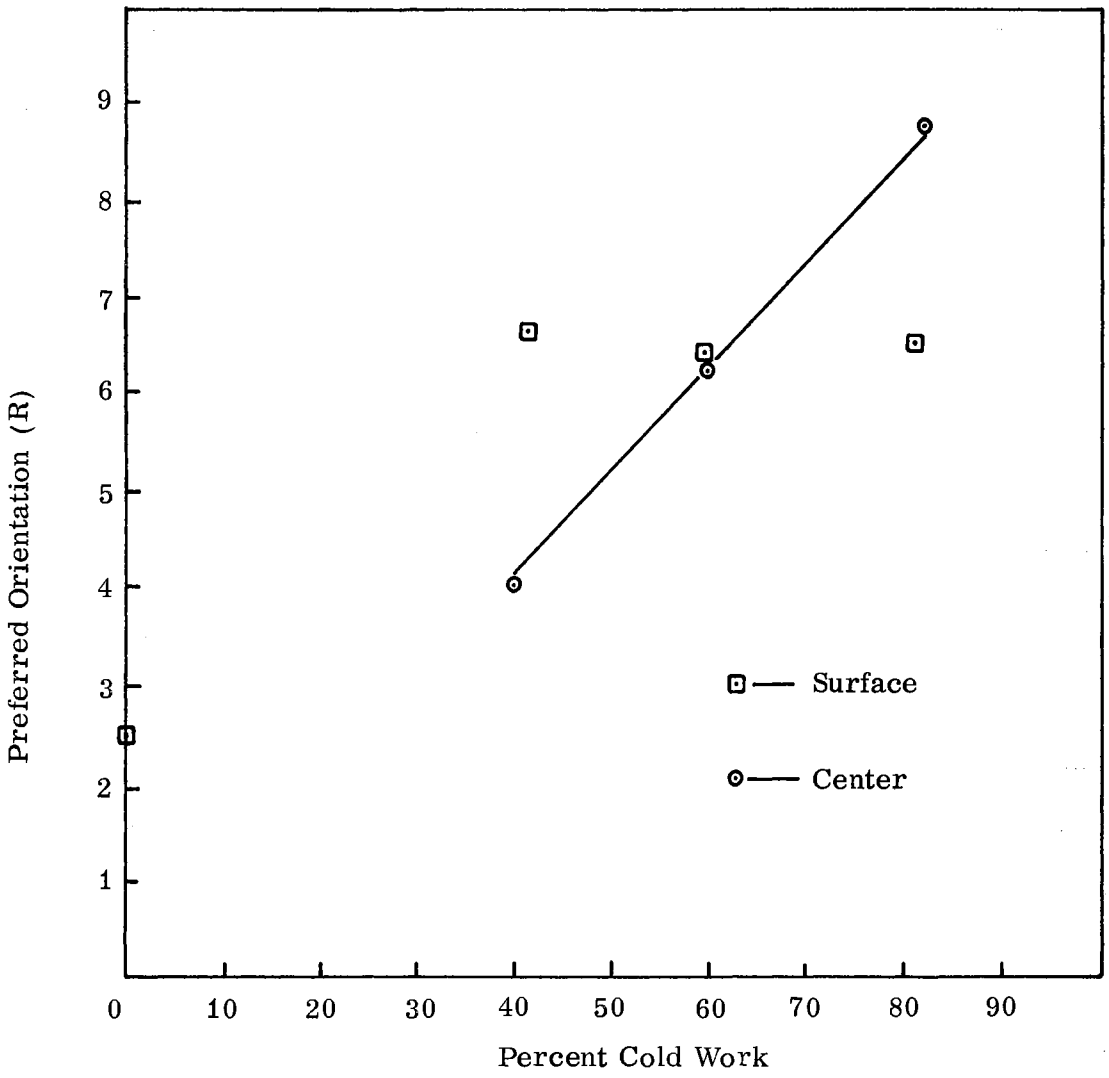

Figure 17. Preferred Orientation Versus Percent Cold Work for 1100-0 Aluminum

of the (123) [$1\bar{2}1$] previously described for the 1100-0 material. This new orientation, whose inverse (111) pole figure is shown in Figure 18, ordinarily is considered to be a metastable compression orientation (16).

As before, the discussion will begin with the outer specimens and will proceed from those with the least to those with the greatest cold work. Specimen 2A (20% cold work, outer, Figure 30, Table XXVII) is slightly asymmetrical

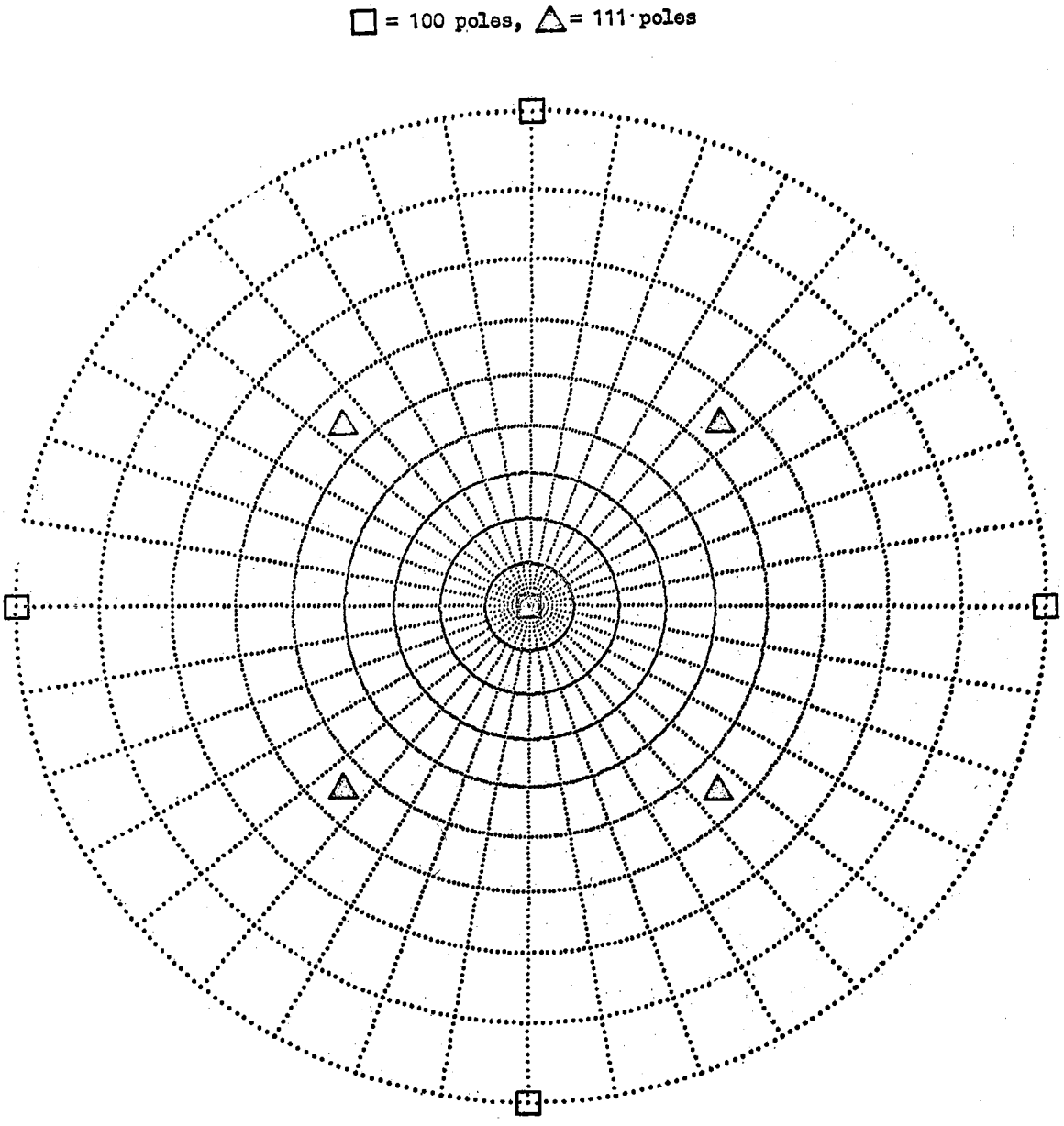

Figure 18. Ideal (111) Pole Figure for the (001) [100] Orientation

because of a rotation about [100] (hereafter referred to as RD). The maximum pole density of 4.6R occurs in the peak in the first quadrant.

Specimen 3A (36% cold work, outer, Figure 31, Table XXVIII) is symmetrical about the RD and exhibits the greatest orientation found in any of the 6061-T6 specimens. The maximum pole density of 5.2R lies again in the peak in the first quadrant but is only slightly greater than the intensities found in the other peaks.

Specimen 4A (50% cold work, outer, Figure 32, Table XXIX) shows a slightly less pronounced orientation than the previous specimens. The maximum pole density of 4.3R occurs in the fourth quadrant but there is only a small intensity difference between peaks as in the previous specimen.

The discussion now will proceed to the specimens obtained from the center section of the 6061-T6 material. Specimen 1B (zero cold work, inner, Figure 33, Table XXX) exhibits a barely discernible basic orientation rotated about RD. The maximum pole density of 3.2R and the scattered pattern probably represent the closest practical approach to random orientation for this material.

Specimen 2B (20% cold work, inner, Figure 34, Table XXXI) shows a well defined basic orientation. There is a slight intensity asymmetry due to a rotation about RD, with a maximum pole density of 4.6R occurring in the fourth quadrant.

Specimen 3B (36% cold work, inner, Figure 35, Table XXXII) again exhibits the basic orientation with a maximum pole density of 4.7R occurring in the peak in the third quadrant. There is only a slight density imbalance since the peaks in the other quadrants are within 0.5R of this value.

Specimen 4B (50% cold work, inner, Figure 36, Table XXXIII) is characterized by the basic orientation with a maximum pole density of 4.8R appearing in the first and second quadrant with the densities in the peaks in the other quadrants separated by only 0.1R.

Table IV summarizes the data obtained for the above specimens by presenting the preferred orientation in terms of pole density (random intensity, R) for the inner and outer specimens as a function of the amount of cold work received.

TABLE IV

PREFERRED ORIENTATION IN COLD-ROLLED 6061-T6 ALUMINUM

Percent Cold Work	Preferred Orientation (R)	
	Center Specimens	Surface Specimens
0	3.2	--
20	4.6	4.6
36	4.7	5.2
50	4.8	4.3

The data also are graphically illustrated in Figure 19. As indicated by the graph, the degree of orientation for the inner (center) specimens does not increase linearly with cold work as was the case for the 1100-0 center specimens.

In conclusion, the basic orientation for the 6061-T6 specimens is (001) [100] as opposed to (123) [$1\bar{2}1$] for the 1100-0 material. The extent of the

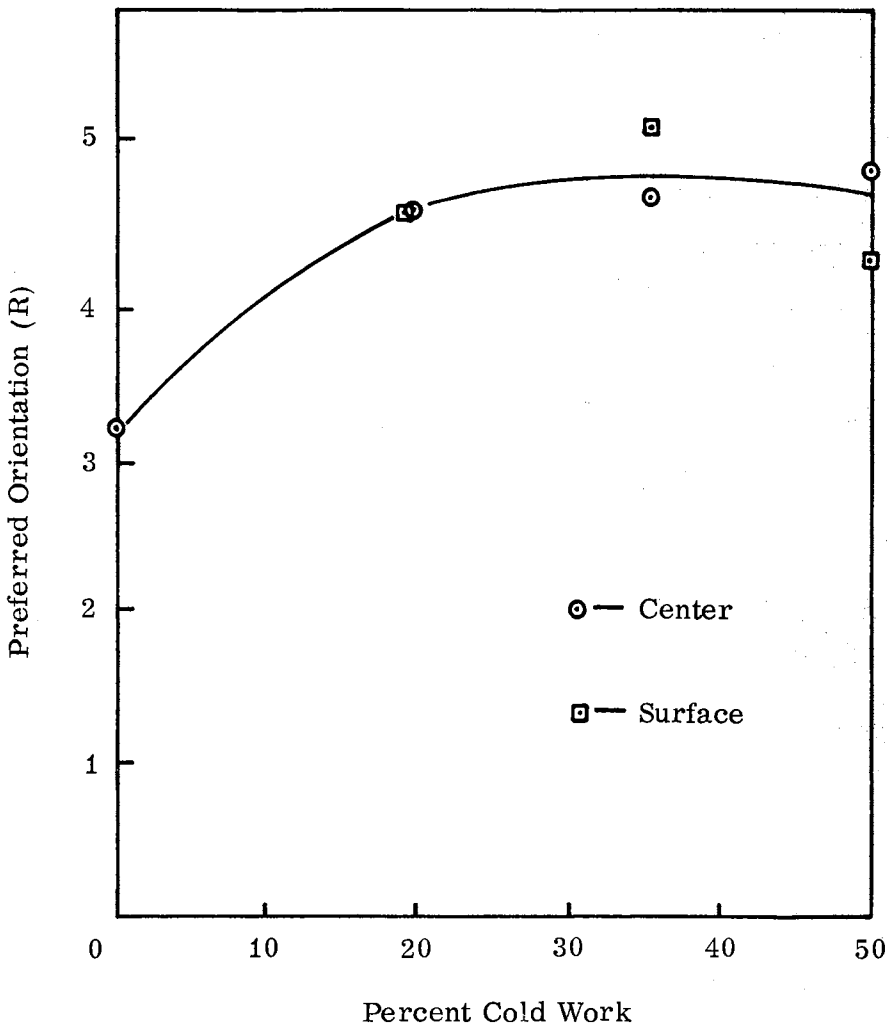

Figure 19. Preferred Orientation Versus Percent Cold Work for 6061-T6 Aluminum

orientation ranges from slight to moderate and the asymmetry of both the center and surface orientations decreases with increasing cold work.

Results of Birefringence Measurements

Birefringence measurements were made on the 1100-0 and 6061-T6 specimens using the technique and instrumentation described in Chapter III and

the experimental procedure outlined in this chapter. The fractional change in velocity was calculated using equation (3.32) after obtaining the necessary data for the specimen thickness (h) and the number of echoes to the first minimum in the echo pattern (p). The frequency (f) was 10 Mc for all tests.

Prior to making measurements on all the specimens, several were measured to determine if any variation in $\frac{\Delta V}{V}$ could be detected as a function of transducer position on the specimen surface. Of the twelve specimens randomly selected and tested, none showed any such variation. Thus, subsequent measurements were made at only one transducer location, that being at the center of the specimen face. The data obtained from these measurements are shown in Tables V and VI.

TABLE V

BIREFRINGENCE DATA FOR 1100-0 ALUMINUM

Cold Work (%)	Specimen	$\frac{\Delta V}{V}$ ($X10^3$)
	A11	4.362
	A12	4.381
0	A13	4.410
	A21	4.400
	A22	4.371
	A23	4.388
	A31	4.502
	A32	4.421
	A33	4.220

TABLE V (Continued)

Cold Work (%)	Specimen	$\frac{\Delta V}{V}$ ($X10^3$)
40	B11	5.526
	B12	5.438
	B13	5.492
	B21	5.613
	B22	6.101
	B23	5.825
	B31	5.510
	B32	5.480
	B33	5.562
60	C11	7.375
	C12	6.542
	C13	6.811
	C21	7.563
	C22	7.462
	C23	7.110
	C31	8.231
	C32	7.121
	C33	7.930
80	D11	3.171
	D12	3.030
	D13	3.138

TABLE V (Continued)

Cold Work (%)	Specimen	$\frac{\Delta V}{V}$ ($X10^3$)
	D21	3.279
	D22	3.420
	D23	3.402
	D31	3.138
	D32	3.092
	D33	3.256

TABLE VI

BIREFRINGENCE DATA FOR 6061-T6 ALUMINUM

Cold Work (%)	Specimen	$\frac{\Delta V}{V}$ ($X10^3$)
	111	1.914
	112	1.785
	113	1.776
0	121	1.776
	122	1.385
	123	1.524
	131	1.784
	132	1.238
	133	1.986
20	211	2.156
	212	1.827

TABLE VI (Continued)

Cold Work (%)	Specimen	$\frac{\Delta V}{V}$ ($X10^3$)
	213	1.762
	221	2.060
	222	1.832
	223	2.300
	231	2.831
	232	2.635
	233	2.741
36	311	2.603
	312	1.839
	313	2.049
	321	2.659
	322	2.670
	323	2.650
	331	2.782
	332	3.008
	333	2.633
50	411	3.870
	412	3.488
	413	3.678
	421	3.577

TABLE VI (Continued)

Cold Work (%)	Specimen	$\frac{\Delta V}{V}$ ($X10^3$)
	422	3.488
	423	3.610
	431	3.201
	432	2.736
	433	2.621

It was desired to determine if any significant variation existed along the rolling and transverse directions of the sheets. Therefore, the data obtained for the nine specimens removed from each of the eight sheets were statistically evaluated. An analysis of variance (AOV) as described by Ostle (22) was performed on the data for each sheet of each material. As was shown in Figure 10, each specimen occupied a position in a matrix in which the rows of the matrix were parallel to the rolling direction and the columns were parallel to the transverse direction. Thus, the procedure used was to partition the total sums of squares into mean, row, column, and experimental error sums of squares and use an F-test to determine the significance of the row and column variations as compared to that of the sheet. The AOV table and the calculations used to obtain the various sums of squares are given in Table VII.

The results of this statistical evaluation are given in Tables VIII through XV which present the numerical analyses of variance for the eight different sheets of aluminum which were tested. By comparing the calculated F- ratios in the AOV's with the tabulated F- Ratio of 4.32 corresponding to a significance level

TABLE VII

ANALYSIS OF VARIANCE TABLE AND CALCULATIONS

Source of Variation	Degrees of Freedom	Sums of Squares	Mean Square	F-Ratio
Total	9	Y_{ij}		
Mean	1	M_{yy}		
Row	2	R_{yy}	$R_{yy}/2 = R$	R/E
Column	2	C_{yy}	$C_{yy}/2 = C$	C/E
Error	4	E_{yy}	$E_{yy}/4 = E$	

Columns

Rows				
	y_{11}	y_{12}	y_{13}	R_1
	y_{21}	y_{22}	y_{23}	R_2
	y_{31}	y_{32}	y_{33}	R_3
	C_1	C_2	C_3	

Sums of Squares:

$$\text{Total} = y_{11}^2 + y_{12}^2 + \ldots + y_{33}^2 = y_{ij}$$

$$\text{Mean} = (y_{11} + y_{12} + \ldots + y_{33})^2/9 = M_{yy}$$

$$\text{Row} = (R_1^2 + R_2^2 + R_3^2)/3 - M_{yy} = R_{yy}$$

$$\text{Column} = (C_1^2 + C_2^2 + C_3^2)/3 - M_{yy} = C_{yy}$$

$$\text{Error} = y_{ij} - M_{yy} - R_{yy} - C_{yy} = E_{yy}$$

of 10% ($\alpha = 0.10$) and degrees of freedom of two and four, the hypotheses of (1) no significant variation of $\frac{\Delta V}{V}$ in the rolling direction and (2) no significant variation in $\frac{\Delta V}{V}$ in the transverse direction were tested. If the F-Ratio calculated from C/E in the AOV were greater than the tabulated value of 4.32, hypothesis (1) was rejected and it was concluded that there was a significant variation in $\frac{\Delta V}{V}$ in the rolling direction. If the calculated F-Ratio were less than 4.32, then hypothesis (1) was accepted. The same procedure was followed to test hypothesis (2) except that in this case the calculated F-Ratio obtained from R/E was used. Table XVI summarizes qualitatively the information obtained from the analyses of variance. Based on a 10% significance level ($\alpha = 0.10$), there is no indication of any significant variation in $\frac{\Delta V}{V}$ in the rolling direction for any sheet tested. For the same significance level, no significant variation in $\frac{\Delta V}{V}$ in the transverse direction is indicated for the sheets which had received zero cold work. However, all of the cold worked sheets show a significant variation in $\frac{\Delta V}{V}$ in the transverse direction (again for $\alpha = 0.10$). It is believed that this variation in $\frac{\Delta V}{V}$ for the cold worked material resulted from the material being subjected to a non-uniform distribution of stress caused by the springing of the rolls during the rolling process. Of course, the springing of the rolls would affect the properties of the material in the transverse direction but would have no effect along the rolling direction. Therefore, no significant variation in $\frac{\Delta V}{V}$ along the rolling direction would be expected, and none was measured. The mean value of $\frac{\Delta V}{V}$ for each sheet (plus or minus one standard deviation) was calculated and is shown in Table XVII.

TABLE VIII

AOV FOR 1100-0 ALUMINUM WITH ZERO COLD WORK

Source of Variation	Degrees of Freedom	Sums of Squares	Mean Square	F-Ratio (Calculated)
Total	9	173.0101		
Mean	1	172.9663		
Row	2	0.0001	0.00005	R/E = .0060*
Column	2	0.0103	0.00515	C/E = .6168*
Error	4	0.0334	0.00835	

* Not significant at 10% significance level

TABLE IX

AOV FOR 1100-0 ALUMINUM WITH 40% COLD WORK

Source of Variation	Degrees of Freedom	Sums of Squares	Mean Square	F-Ratio (Calculated)
Total	9	284.2555		
Mean	1	283.9663		
Row	2	0.2396	0.1198	R/E = 4.6077**
Column	2	0.0233	0.0117	C/E = 0.4500*
Error	4	0.1038	0.0260	

* Not significant at 10% significance level
** Significant at 10% significance level

TABLE X

AOV FOR 1100-0 ALUMINUM WITH 60% COLD WORK

Source of Variation	Degrees of Freedom	Sums of Squares	Mean Square	F-Ratio (Calculated)
Total	9	488.3535		
Mean	1	486.1290		
Row	2	1.0909	0.5455	R/E = 5.3480**
Column	2	0.7158	0.3579	C/E = 3.5088*
Error	4	0.4078	0.1020	

* Not significant at 10% significance level
** Significant at 10% significance level

TABLE XI

AOV FOR 1100-0 ALUMINUM WITH 80% COLD WORK

Source of Variation	Degrees of Freedom	Sums of Squares	Mean Square	F-Ratio (Calculated)
Total	9	93.1141		
Mean	1	92.9682		
Row	2	0.1089	0.0545	R/E = 8.7903**
Column	2	0.0122	0.0061	C/E = 0.9839*
Error	4	0.0248	0.0062	

* Not significant at 10% significance level
** Significant at 10% significance level

TABLE XII

AOV FOR 6061-T6 ALUMINUM WITH ZERO COLD WORK

Source of Variation	Degrees of Freedom	Sums of Squares	Mean Square	F-Ratio (Calculated)
Total	9	26.1280		
Mean	1	25.6299		
Rows	2	0.1012	0.0506	R/E = 1.1448*
Column	2	0.2202	0.1101	C/E = 2.4910*
Error	4	0.1767	0.0442	

* Not significant at 10% significance level

TABLE XIII

AOV FOR 6061-T6 ALUMINUM WITH 20% COLD WORK

Source of Variation	Degrees of Freedom	Sums of Squares	Mean Square	F-Ratio (Calculated)
Total	9	46.4676		
Mean	1	45.1038		
Row	2	1.1462	0.5731	R/E = 19.1993**
Column	2	0.0982	0.0491	C/E = 1.6445*
Error	4	0.1194	0.0299	

* Not significant at 10% significance level
** Significant at 10% significance level

TABLE XIV

AOV FOR 6061-T6 ALUMINUM WITH 36% COLD WORK

Source of Variation	Degrees of Freedom	Sums of Squares	Mean Square	F-Ratio (Calculated)
Total	9	59.3219		
Mean	1	58.2576		
Row	2	0.6828	0.3414	R/E = 4.6960**
Column	2	0.0910	0.0455	C/E = 0.6259*
Error	4	0.2905	0.0727	

* Not significant at 10% significance level
** Significant at 10% significance level

TABLE XV

AOV FOR 6061-T6 ALUMINUM WITH 50% COLD WORK

Source of Variation	Degrees of Freedom	Sums of Squares	Mean Square	F-Ratio (Calculated)
Total	9	103.3040		
Mean	1	101.8397		
Row	2	1.1956	0.5978	R/E = 22.4737**
Column	2	0.1623	0.0812	C/E = 3.0526*
Error	4	0.1064	0.0266	

* Not significant at 10% significance level
** Significant at 10% significance level

TABLE XVI

SIGNIFICANCE OF THE VARIATION IN $\frac{\Delta V}{V}$ WITH DIRECTION FOR COLD-ROLLED 1100-0 AND 6061-T6 ALUMINUM

Material	Percent Cold Work	Significant Variation in $\frac{\Delta V}{V}$ *	
		Rolling Direction	Transverse Direction
1100-0	0	No	No
	40	No	Yes
	60	No	Yes
	80	No	Yes
6061-T6	0	No	No
	20	No	Yes
	36	No	Yes
	50	No	Yes

* 10% significance level

The birefringence data obtained for the 1100-0 aluminum specimens are plotted in Figure 20 as a function of percent cold work. Note that $\frac{\Delta V}{V}$ increases with increasing cold work and then drops sharply to a value at 80% that is less than the birefringence in the unworked metal. The same general increase is noted in the 6061-T6 data shown in Figure 21 for up to 50% cold work. If specimens of 6061-T6 with greater than 50% cold work could be obtained, it would be interesting to see if they would exhibit the same sharp decrease in $\frac{\Delta V}{V}$ at the higher reductions in gage.

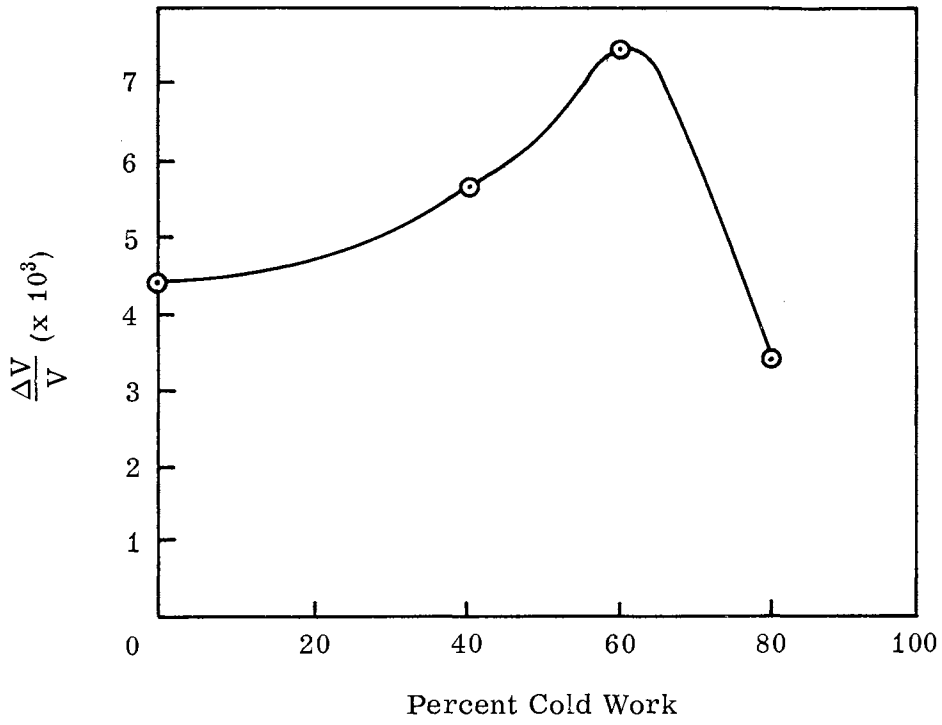

Figure 20. Birefringence Versus Percent Cold Work for 1100-0 Aluminum

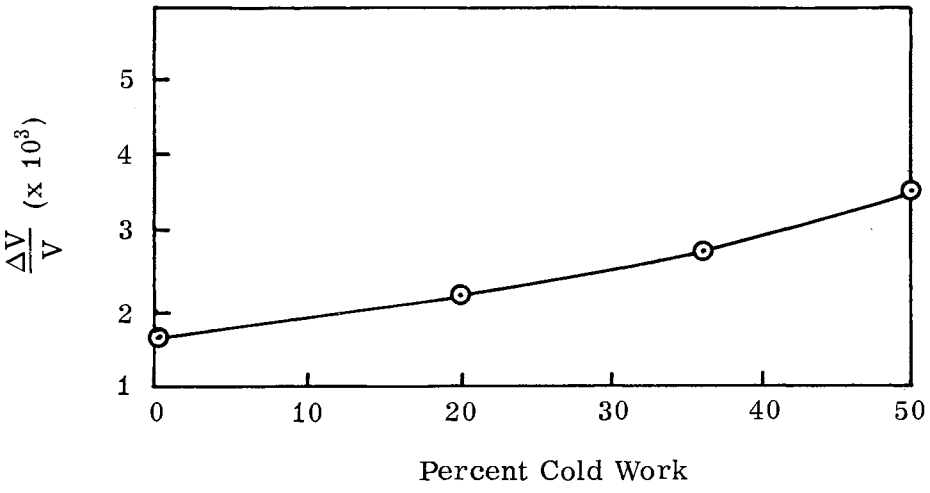

Figure 21. Birefringence Versus Percent Cold Work for 6061-T6 Aluminum

TABLE XVII

SUMMARY OF THE BIREFRINGENCE DATA FOR COLD-ROLLED 1100-0 AND 6061-T6 ALUMINUM

Percent Cold Work	$\frac{\Delta V}{V}$ $(x10^3)$*	
	1100-0	6061-T6
0	4.384 ± .074	1.688 ± .062
20		2.239 ± .413
36		2.544 ± .365
40	5.616 ± .214	
50		3.364 ± .428
60	7.349 ± .530	
80	3.214 ± .135	

* Each value represents the mean value plus or minus one standard deviation for nine specimens.

In order to compare the birefringence and preferred orientation data, Table XVIII was constructed by compiling the data given in Tables III, IV, and XVII. The quantity R_A in the table is the average value of the pole density in terms of Random Intensity. It is interesting to note that for the 1100-0 material, the minimum birefringence was measured in the specimens which had the greatest orientation, but the maximum birefringence did not occur in the specimens which had the least orientation. For the 6061-T6 material, two significantly different values of birefringence were measured in specimens which had approximately the same orientation. From the data in Table XVIII, it appears that the measured

birefringence in these materials was not produced principally by preferred orientation. This conclusion is supported by the theory presented in Chapter II if the basic orientations possessed by these materials are used to determine theoretically the effect of orientation on birefringence.

According to the theoretical considerations given in Chapter II, an estimate of the magnitude of the birefringence due to orientation can be made if the orientation of the crystallites is known with respect to the wave propagation direction. For the case of the 6061-T6 material, the wave propagation direction was [001] for which the direction cosines are $l_1 = l_2 = 0$ and $l_3 = 1$. If the D_{ij} coefficients are calculated using these values for the direction cosines and then are substituted into equation (2. 28), the resulting equation is:

$$\rho v^2 = c_{44} , \tag{4.1}$$

for which

$$v = \left(\frac{c_{44}}{\rho} \right)^{\frac{1}{2}}. \tag{4.2}$$

Since the solution of equation (2. 28) gives only one distinct velocity, no velocity difference is produced for a wave propagated in the [001] direction of a single crystal of aluminum. Hence, the value of $\frac{\Delta V}{V}$ (p) computed using equation (2.37) is zero. Thus, theoretically, preferred orientation is not a source of birefringence in cold-rolled 6061-T6 aluminum and the observed $\frac{\Delta V}{V}$ must be produced by some other source of anisotropy.

For the 1100-0 material, wave propagation was along the [123] direction. In this case, if the same type of calculations are made as were made for the

TABLE XVIII

COMPARISON OF BIREFRINGENCE AND PREFERRED ORIENTATION DATA

Material	Cold Work (%)	$\frac{\Delta V}{V}$ ($\times 10^3$)	Preferred Orientation*		
			R_S	R_C	R_A
1100-0	0	4.384 ± .074	2.4	--	--
	40	5.616 ± .214	6.6	4.0	5.3
	60	7.349 ± .530	6.3	6.2	6.25
	80	3.214 ± .135	6.5	8.6	7.55
6061-T6	0	1.688 ± .062	--	3.2	--
	20	2.239 ± .413	4.6	4.6	4.6
	36	2.544 ± .365	5.2	4.7	4.95
	50	3.364 ± .428	4.3	4.8	4.55

* R_S denotes the pole density for the crystallites near the surface whereas R_C signifies the pole density at the center of the material. R_A is the average of R_S and R_C.

6061-T6 material, two distinct quasi-distortional wave velocities are obtained. If these are substituted into equation (2.37), a $\frac{\Delta V}{V}$ is obtained which is a linear function of the fraction of the crystallites which are preferentially oriented. Thus, theoretically, the birefringence for this material will increase with increasing pole density. However, the magnitude of the birefringence resulting from this orientation is small compared to the experimentally determined $\frac{\Delta V}{V}$ shown in

Table XVIII. It appears then that some source of birefringence other than preferred orientation must be the major contributor to the $\frac{\Delta V}{V}$ observed in 1100-0 aluminum.

As discussed previously, residual stress is another source of birefringence. To investigate this source, tests were made to determine the effect of heat treatment on $\frac{\Delta V}{V}$. Twenty-four specimens were randomly assigned (using a table of random numbers) to two separate groups. The specimens in the first group were heat treated for 8 hours at 475° F and those in the second group for 2 hours at 650° F. After heat treatment, birefringence measurements were made to determine the change in $\frac{\Delta V}{V}$ produced in each specimen. No significant change was noted. An examination of the specimen photomicrographs taken prior and subsequent to heat treatment indicated that no observable changes in microstructure had occurred. Therefore, it seemed either that the residual stresses (which should have been relieved to some extent by the heat treatments) did not contribute appreciably to the birefringence or that possibly the heat treatments affected the residual stress distribution in such a way that the difference between the components of the residual stresses projected in the rolling and transverse directions remained the same. If the $\frac{\Delta V}{V}$ were due to this difference in stress, then no change in $\frac{\Delta V}{V}$ would be produced by the heat treatments.

The Effect of Applied Stress

It was mentioned in Chapter I that the stress-induced double refraction of distortional waves has been studied for several materials including aluminum. Thus, the objective of these tests was not to demonstrate this phenomenon, but

to establish the magnitude of the birefringence produced by stress on some of the specimens used in this study. In this way, it could be determined if the effect of stress was large enough to be the principal contributor to the observed birefringence.

The tests were made using the procedure and experimental apparatus described previously. The data which were obtained are illustrated in Figure 22 in which $\frac{\Delta V}{V}$ is plotted as a function of stress and cold work. Since it was desired to obtain data to as high a stress as possible, only specimens of the 6061-T6 material were tested because of the low strength of the 1100-0 material. As was predicted by equation (2.52), a linear relationship between $\frac{\Delta V}{V}$ and stress was obtained. It was stated previously in Chapter II that the third order constant n which appears in equation (2.52) could be calculated if the slope of the $\frac{\Delta V}{V}$ versus stress curve were determined experimentally. Theoretically, the slope should be equal to $\frac{-(4\mu + n)}{8\mu V^2 \rho}$. This may be simplified by recalling that $V^2 = \frac{\mu}{\rho}$ in which case the slope would be $\frac{-(4\mu + n)}{8\mu^2}$. The slope of the curve in Figure 22 for the unworked material is approximately 2.5×10^{-7} $\frac{\Delta V}{V}$ per psi. Therefore, the calculated value of n was -44.1×10^6 psi which agrees within two percent of that obtained by Rollins (7) from measurements made on 6061-T6 plate. It is interesting to note that cold work apparently had no appreciable effect on the slope, indicating that n is truly a constant for the material. If residual stresses are the major cause of birefringence, then in order to produce a $\frac{\Delta V}{V}$ of the magnitudes observed in this study, stresses on the order of 6,000 to 14,000 psi would prevail in the material. Based on the slope given above, Table XIX was constructed to illustrate the stresses which would exist if the birefringence were only

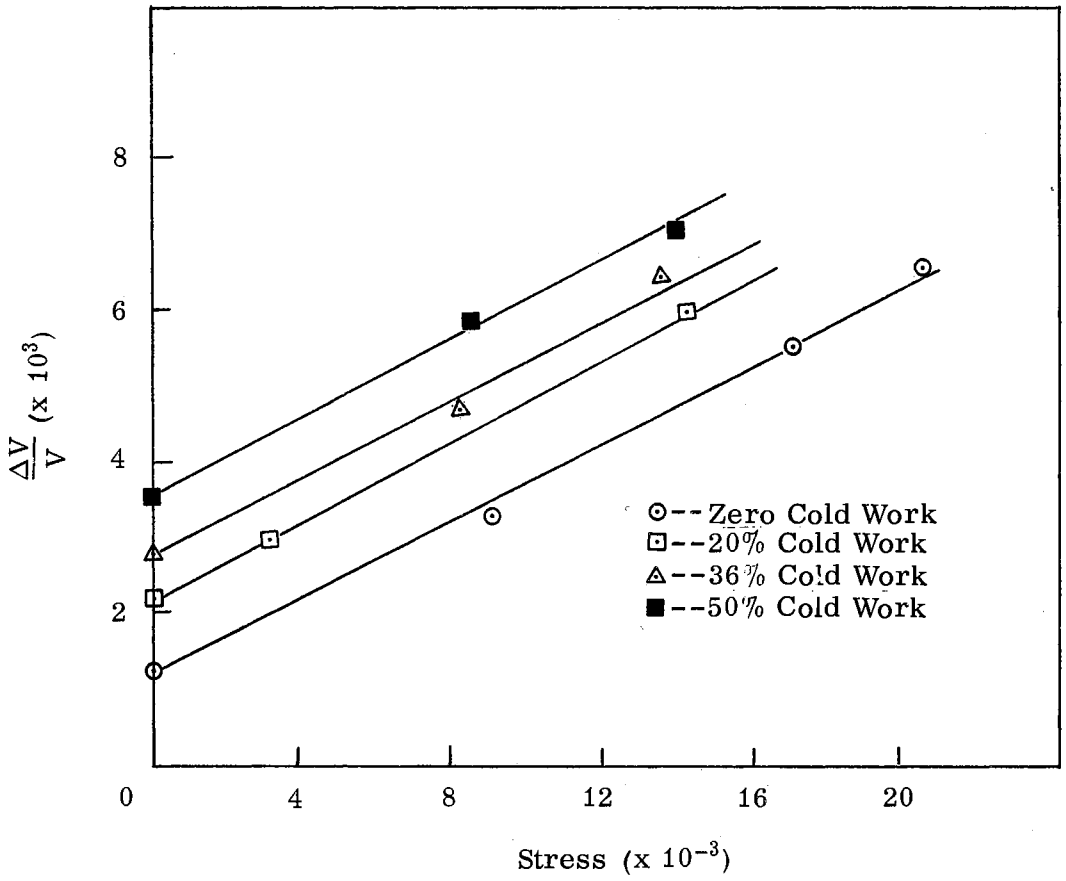

Figure 22. Stress-Induced Birefringence in Cold-Rolled 6061-T6 Aluminum

a function of stress. It should be remembered that the residual stress distribution in a rolled sheet is complex and that in spite of the great technological importance of rolling, there is very little published information on the residual stresses imposed by this process. Little information on the residual stresses in any direction except the rolling direction of the sheet is available, although it is very probable that a biaxial state of stress exists. Thus, the residual stress which affects wave propagation generally will be the difference between the residual stress components in the rolling and transverse directions.

TABLE XIX

CALCULATED STRESSES IN COLD-ROLLED
6061-T6 SHEET ALUMINUM

Cold Work (%)	$\frac{\Delta V}{V}$ ($x10^3$)	Stress (psi)*
0	1.688	6750
20	2.239	8960
36	2.544	10176
50	3.364	13456

* Stress here denotes the difference between the resultant residual stress components along the rolling and transverse directions.

This is based on the work of Kammer and Vigness (23) who made absolute velocity measurements with tensile loads applied parallel and normal to the direction of particle motion of a distortional wave. Their results showed that when the tensile stress was applied parallel to the particle motion, the velocity decreased whereas for the load applied normal to the particle motion, the velocity increased. Thus, the stresses listed in Table XIX of necessity have to be the difference in the residual stress components since the data were obtained by measuring the fractional difference in velocity between waves with particle motions parallel and perpendicular to the rolling and transverse directions.

From the measurements reported above, it was determined that the initial birefringence observed in the 6061-T6 specimens could be produced by stresses of reasonable magnitude. In addition, the measurements showed that the cold work did not affect the linear stress-birefringence relationship since the

birefringence produced by stress was not dependent on the value of the initial birefringence. The value of the third order constant n was calculated using the experimental data and was found to agree within two percent with the value obtained by Rollins for 6061-T6 plate.

CHAPTER V

CONCLUSIONS AND RECOMMENDATIONS

The purpose of this study was to investigate the effect of crystallite preferred orientation on the birefringence of distortional waves and to compare this effect, if any, with that caused by stress. Based on the results of this investigation, the following conclusions have been reached:

1. The cold rolling of 1100-0 aluminum produces a basic preferred orientation in which the (123) crystal plane is aligned parallel to the rolling plane and the $[1\bar{2}1]$ direction is oriented parallel to the rolling direction. In general, the degree of orientation of the crystallites near the surface and those at the center of the sheet differs. The surface orientation tends to be established early in the cold working process and changes only slightly with increasing cold work. The orientation at the center of the sheet, however, develops more slowly but increases linearly with increasing cold work.

2. Unlike 1100-0, the cold rolling of 6061-T6 up to a 50% reduction in gage produces a basic orientation which is described as (001) [100]. As in the case of 1100-0, the degree of orientation at the surface and the center generally is different. The surface orientation increases with increasing cold work until a 36% reduction in gage is achieved beyond which a decrease is noted. The center orientation exhibits an increase with increasing cold work but shows no linear relationship with reduction in gage.

3. Based on a statistical analysis of the birefringence measurements made on each sheet, there is no significant variation in birefringence in the rolling direction for either of the two test materials or in the transverse direction for the unworked material. However, cold rolling does produce a significant variation in $\frac{\Delta V}{V}$ in the transverse direction for both materials. This is ascribed to the springing of the rolls during the rolling operation.

4. The birefringence observed in both materials is not a linear function of cold work, but does increase with increasing cold work. However, cold working 1100-0 to 80% produces a sharp decrease in birefringence.

5. Heat treatments which produce no noticeable recrystallization or grain growth appear to have no measureable effect on birefringence.

6. A theoretical analysis based on the preferred orientation data indicates that orientation is not the principal source of the birefringence observed for the 6061-T6 and 1100-0 specimens which were tested. The experimental birefringence and preferred orientation data support this conclusion.

7. The birefringence increases linearly with externally applied stress for 6061-T6 aluminum in agreement with the theory presented. The value of the Murnaghan third order elastic constant n for 6061-T6 aluminum (based on the experimental data) is -44.1×10^6 psi and does not change when the material is cold-rolled.

In summary, there is no evidence that preferred orientation contributes significantly to the birefringence of shear waves in the two materials tested, whereas the stress-induced birefringence data show that stresses of reasonable magnitude can account for the observed birefringence.

Recommendations for Further Study

It is recommended that further study be conducted in the area of distortional wave birefringence in worked metals. It appears that the most fruitful results will come from making birefringence measurements on the material and then destructively measuring the residual stresses by using the methods developed by Sachs, Treuting and Read, or other suitable methods reported in the literature (20). Complete analysis of the residual stresses in the principal directions and their variation with depth in the material by these methods will be a laborious process. However, it is believed that the results would be well worth the effort since data would not only be obtained on residual stress distributions produced by the rolling process, but in all probablility, would validate the assumption that residual stresses affect birefringence in the same manner as do externally applied stresses.

SELECTED BIBLIOGRAPHY

(1) Benson, R. W., and Raelson, V. J. "Acoustoelasticity." Product Engineering. Vol. 30 (1959).

(2) Templin, R. L. "Effects of Cold Working on the Physical Properties of Metals." Proceedings, Amer. Inst. Mining Met. Engrs. (1929).

(3) Sullivan, P. F., and Papadakis, E. P. "Ultrasonic Double Refraction in Worked Metals." Journal Acoustical Society of America. Vol. 33, Number 11 (1961).

(4) Firestone, F. A., and Frederick, J. R. "Refinements in Supersonic Reflectoscopy. Polarized Sound." Journal, Acoustical Society of America. Vol. 18, Number 1 (1946).

(5) Hughes, D. S., and Kelly, J. L. "Second-Order Elastic Deformation of Solids." Physical Review. Vol. 92, Number 5 (1955).

(6) Bergman, R. H. and Shahbender, R. A. "Effect of Statically Applied Stresses on the Velocity of Propagation of Ultrasonic Waves." Journal, Applied Physics. Vol. 29, Number 12 (1958).

(7) Rollins, F. R. "Study of Methods for Non-Destructive Measurement of Residual Stress." WADC Technical Report 59-561 (1959).

(8) Crecraft, D. I. "Ultrasonic Wave Velocities in Stressed Nickel Steel." Nature. Vol. 195, Number 4847 (1962).

(9) Murnaghan, F. D. Finite Deformation of an Elastic Solid. John Wiley & Sons, Inc., New York (1951).

(10) Toupin, R. A., and Bernstein, B. "Sound Waves in Perfectly Elastic Materials. Acoustoelastic Effect." Journal, Acoustical Society of America. Vol. 33, Number 2 (1961).

(11) Smith, R. T. "Stress-Induced Anisotropy in Solids - The Acoustoelastic Effect." Ultrasonics (July - September, 1963).

(12) Lindsay, R. B. Mechanical Radiation. McGraw-Hill Book Company, Inc., New York (1960).

(13) Sokolnikoff, I. S. Mathematical Theory of Elasticity. McGraw-Hill Book Company, Inc., New York (1956).

(14) Hearmon, R. F. S. Applied Anisotropic Elasticity. Oxford University Press (1961).

(15) Taylor, A. X-Ray Metallography. John Wiley & Sons, Inc., New York (1961).

(16) Barrett, C. S. Structure of Metals. McGraw-Hill Book Company, Inc., New York (1952).

(17) Eichhorn, R. M. "Automatic Pole Figure Plotter." Review, Scientific Instruments. Vol. 36, Number 7 (1965).

(18) Roderick, R. L., and Truell, R. "The Measurement of Ultrasonic Attenuation in Solids by the Pulse Echo Technique and Some Results in Steel." Journal, Applied Physics. Vol. 23, Number 2 (1952).

(19) Crecraft, D. I. "Launching Ultrasonic Shear Waves Into Solids at Normal Incidence by Pressure Coupling." Journal, Sound Vibration. Vol. 1, Number 4 (1964).

(20) Dieter, G. E. Mechanical Metallurgy. McGraw-Hill Book Company, Inc., New York (1961).

(21) Hu, H., Sperry, P. R., and Beck, P. A. "Rolling Textures in Face-Centered Cubic Metals." Journal, Metals. Vol. 4, (1952).

(22) Ostle, B. Statistics in Research. Iowa State University Press, Ames (1963).

(23) Kammer, E. W., and Vigness, I. "The Use of Ultrasonic Waves for Stress Determinations." U. S. Naval Research Laboratory Report 64-13 (1964).

APPENDIX A

POLE FIGURE DATA

The pole figures and the supporting data tables discussed in Chapters III and IV appear on the following pages. The data were generated by using the automatic pole figure facility of the General Chemistry Department of the Lawrence Radiation Laboratory. Each pole figure and data sheet clearly denotes the specimen to which it pertains. The azimuthal angle is shown on the left hand side of each data Table whereas the radial angle is listed at the top. The rolling direction of the specimen coincides with the vertical axis in the pole figure.

POLE FIGURE DATA SHEET FOR SPECIMEN II-A-1

The normalized pole figure is based on Mo k-alpha radiation and the 111 reflection.

The 222 reflection was used to fill in the blind region from 80 through 90 degrees alpha.

The alpha-dependent two theta shift was taken into account.

Integrated intensities were used.

Normal smoothing was used.

Maximum and minimum corrected intensities are 212 and 14 counts/second, respectively.

Random intensity is 87 counts/second.

Maximum intensity is 2.42 times random.

Contour spacing is based on multiples of random intensity.

2 contours are to be plotted.

Their values are 1.000 2.000.

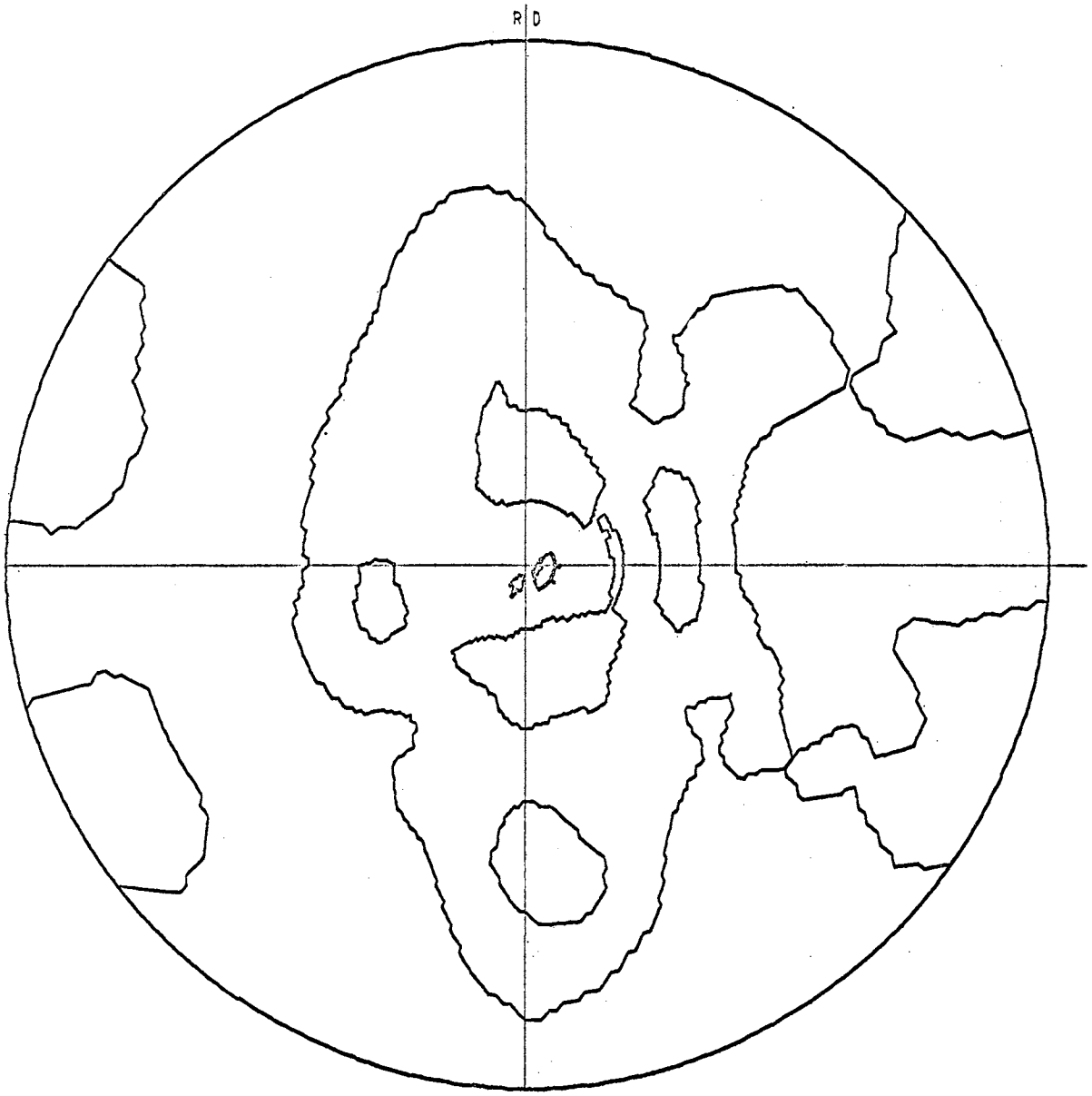

Figure 23. (111) Pole Figure for Specimen II-A-1

TABLE XX

POLE FIGURE DATA FOR SPECIMEN II-A-1

	0	5	10	15	20	25	30	35	40	45	50	55	60	65	70	75	80	85	90
2	0.8	0.7	0.8	0.9	1.0	1.1	1.2	1.4	1.4	1.3	1.1	1.0	0.9	0.6	0.6	0.9	1.3	1.8	1.9
4	0.8	0.7	0.8	0.9	1.0	1.2	1.3	1.4	1.4	1.3	1.1	1.0	0.9	0.7	0.6	0.9	1.3	1.8	1.9
6	0.7	0.7	0.8	0.9	1.0	1.2	1.3	1.4	1.4	1.2	1.0	1.0	0.9	0.7	0.6	0.9	1.3	1.8	1.9
8	0.7	0.6	0.7	0.9	1.0	1.3	1.4	1.5	1.4	1.2	1.0	1.0	0.9	0.8	0.6	0.9	1.3	1.8	1.9
10	0.6	0.6	0.7	0.9	1.0	1.3	1.4	1.5	1.4	1.2	1.0	1.0	1.0	0.8	0.6	0.9	1.3	1.8	1.9
12	0.5	0.5	0.6	0.8	1.0	1.3	1.5	1.6	1.5	1.3	1.0	1.0	1.0	0.8	0.6	0.9	1.3	1.8	1.9
14	0.4	0.5	0.6	0.8	1.0	1.3	1.5	1.6	1.5	1.3	1.1	1.0	1.0	0.8	0.6	0.8	1.4	1.8	1.9
16	0.4	0.4	0.5	0.7	1.0	1.3	1.6	1.6	1.6	1.3	1.1	1.0	1.0	0.8	0.6	0.8	1.4	1.9	1.9
18	0.3	0.4	0.4	0.6	0.9	1.2	1.5	1.7	1.6	1.4	1.1	1.0	1.0	0.9	0.7	0.9	1.5	1.9	1.9
20	0.2	0.3	0.4	0.6	0.8	1.2	1.5	1.6	1.6	1.4	1.2	1.1	1.0	0.9	0.7	0.9	1.5	1.9	1.9
22	0.2	0.3	0.3	0.5	0.7	1.1	1.4	1.6	1.6	1.5	1.2	1.1	1.0	0.9	0.7	0.9	1.5	1.9	1.9
24	0.2	0.2	0.3	0.4	0.6	1.0	1.3	1.5	1.6	1.5	1.2	1.2	1.0	0.9	0.7	0.9	1.5	1.9	1.9
26	0.2	0.2	0.2	0.4	0.5	0.9	1.2	1.4	1.6	1.5	1.2	1.2	1.1	1.0	0.8	1.0	1.6	1.9	1.9
28	0.2	0.2	0.2	0.3	0.5	0.8	1.1	1.4	1.6	1.5	1.3	1.3	1.1	1.1	0.8	1.0	1.6	1.9	1.9
30	0.2	0.1	0.2	0.3	0.4	0.7	1.0	1.3	1.5	1.5	1.3	1.3	1.2	1.1	0.9	1.1	1.6	1.9	1.9
32	0.2	0.1	0.2	0.3	0.4	0.6	0.9	1.2	1.4	1.4	1.3	1.3	1.2	1.2	0.9	1.1	1.6	1.9	1.9
34	0.2	0.2	0.2	0.3	0.4	0.6	0.8	1.1	1.4	1.4	1.3	1.3	1.2	1.2	1.0	1.1	1.5	1.9	1.9
36	0.2	0.2	0.2	0.3	0.4	0.6	0.8	1.1	1.3	1.3	1.3	1.3	1.3	1.2	1.0	1.2	1.5	1.9	1.9
38	0.3	0.3	0.3	0.4	0.4	0.6	0.8	1.0	1.2	1.3	1.3	1.4	1.3	1.2	1.1	1.2	1.5	1.9	1.9
40	0.4	0.3	0.3	0.4	0.5	0.6	0.8	1.0	1.2	1.2	1.3	1.4	1.3	1.2	1.1	1.2	1.4	1.9	1.9
42	0.4	0.4	0.4	0.5	0.5	0.6	0.8	1.0	1.1	1.2	1.3	1.4	1.4	1.3	1.2	1.3	1.4	1.9	1.9
44	0.5	0.5	0.5	0.5	0.6	0.7	0.8	1.0	1.1	1.2	1.3	1.4	1.4	1.3	1.2	1.3	1.4	1.9	1.9
46	0.6	0.6	0.5	0.6	0.6	0.7	0.8	0.9	1.1	1.2	1.2	1.4	1.4	1.3	1.3	1.4	1.4	1.9	1.9
48	0.7	0.7	0.6	0.7	0.7	0.7	0.8	0.9	1.1	1.2	1.2	1.4	1.4	1.4	1.3	1.4	1.4	1.9	1.9
50	0.8	0.8	0.7	0.7	0.7	0.8	0.8	0.9	1.1	1.2	1.2	1.4	1.5	1.4	1.3	1.5	1.4	1.9	1.9
52	0.9	0.9	0.7	0.7	0.8	0.8	0.8	0.8	1.1	1.2	1.3	1.4	1.5	1.5	1.4	1.6	1.5	1.9	1.9
54	1.0	1.0	0.8	0.8	0.8	0.8	0.8	0.8	1.0	1.2	1.3	1.4	1.5	1.5	1.4	1.6	1.5	1.9	1.9
56	1.1	1.0	0.8	0.8	0.8	0.8	0.8	0.8	1.0	1.2	1.3	1.4	1.6	1.5	1.4	1.7	1.5	1.9	1.9
58	1.1	1.1	0.9	0.8	0.8	0.7	0.8	0.8	1.0	1.2	1.3	1.5	1.6	1.5	1.5	1.7	1.5	1.9	1.9
60	1.1	1.2	0.9	0.9	0.8	0.7	0.7	0.8	1.0	1.1	1.4	1.5	1.6	1.5	1.5	1.7	1.5	1.9	1.9
62	1.2	1.3	0.9	0.9	0.8	0.7	0.7	0.8	1.0	1.1	1.4	1.6	1.6	1.5	1.5	1.8	1.5	1.9	1.9
64	1.2	1.3	1.0	0.9	0.8	0.7	0.7	0.8	1.0	1.1	1.5	1.7	1.7	1.5	1.6	1.8	1.5	1.8	1.9
66	1.3	1.4	1.0	0.9	0.7	0.7	0.7	0.7	1.0	1.1	1.5	1.7	1.7	1.5	1.6	1.8	1.5	1.8	1.9
68	1.4	1.5	1.0	0.9	0.7	0.7	0.7	0.7	0.9	1.1	1.5	1.8	1.7	1.5	1.6	1.8	1.5	1.8	1.9
70	1.4	1.5	1.1	0.9	0.7	0.7	0.6	0.7	0.9	1.1	1.5	1.9	1.8	1.5	1.6	1.8	1.5	1.8	1.9
72	1.4	1.6	1.1	0.9	0.7	0.6	0.6	0.7	0.9	1.1	1.5	1.9	1.8	1.5	1.6	1.8	1.5	1.8	1.9
74	1.5	1.6	1.1	0.9	0.7	0.6	0.6	0.6	0.9	1.1	1.5	1.9	1.9	1.5	1.6	1.8	1.5	1.8	1.9
76	1.4	1.5	1.1	0.9	0.7	0.6	0.6	0.6	0.9	1.1	1.5	2.0	1.9	1.5	1.5	1.8	1.5	1.8	1.9
78	1.4	1.5	1.1	0.9	0.7	0.6	0.6	0.6	0.9	1.1	1.5	2.0	1.9	1.5	1.5	1.8	1.5	1.8	1.9
80	1.3	1.4	1.1	0.8	0.7	0.6	0.6	0.6	0.9	1.1	1.5	2.0	1.9	1.4	1.5	1.8	1.4	1.9	1.9
82	1.2	1.2	1.0	0.8	0.7	0.6	0.6	0.6	0.8	1.1	1.5	2.0	1.9	1.4	1.5	1.8	1.4	1.9	1.9
84	1.0	1.1	1.0	0.8	0.7	0.6	0.6	0.6	0.8	1.1	1.5	2.0	2.0	1.4	1.5	1.8	1.4	1.9	1.9
86	0.9	0.9	0.9	0.8	0.7	0.7	0.6	0.6	0.8	1.1	1.5	2.0	2.0	1.3	1.4	1.8	1.4	1.9	1.9
88	0.7	0.8	0.8	0.8	0.7	0.7	0.6	0.6	0.8	1.0	1.5	2.0	2.0	1.3	1.4	1.8	1.4	1.9	1.9
90	0.6	0.6	0.7	0.8	0.8	0.7	0.6	0.7	0.8	1.1	1.5	2.0	2.0	1.3	1.4	1.7	1.4	1.9	1.9

TABLE XX (Continued)

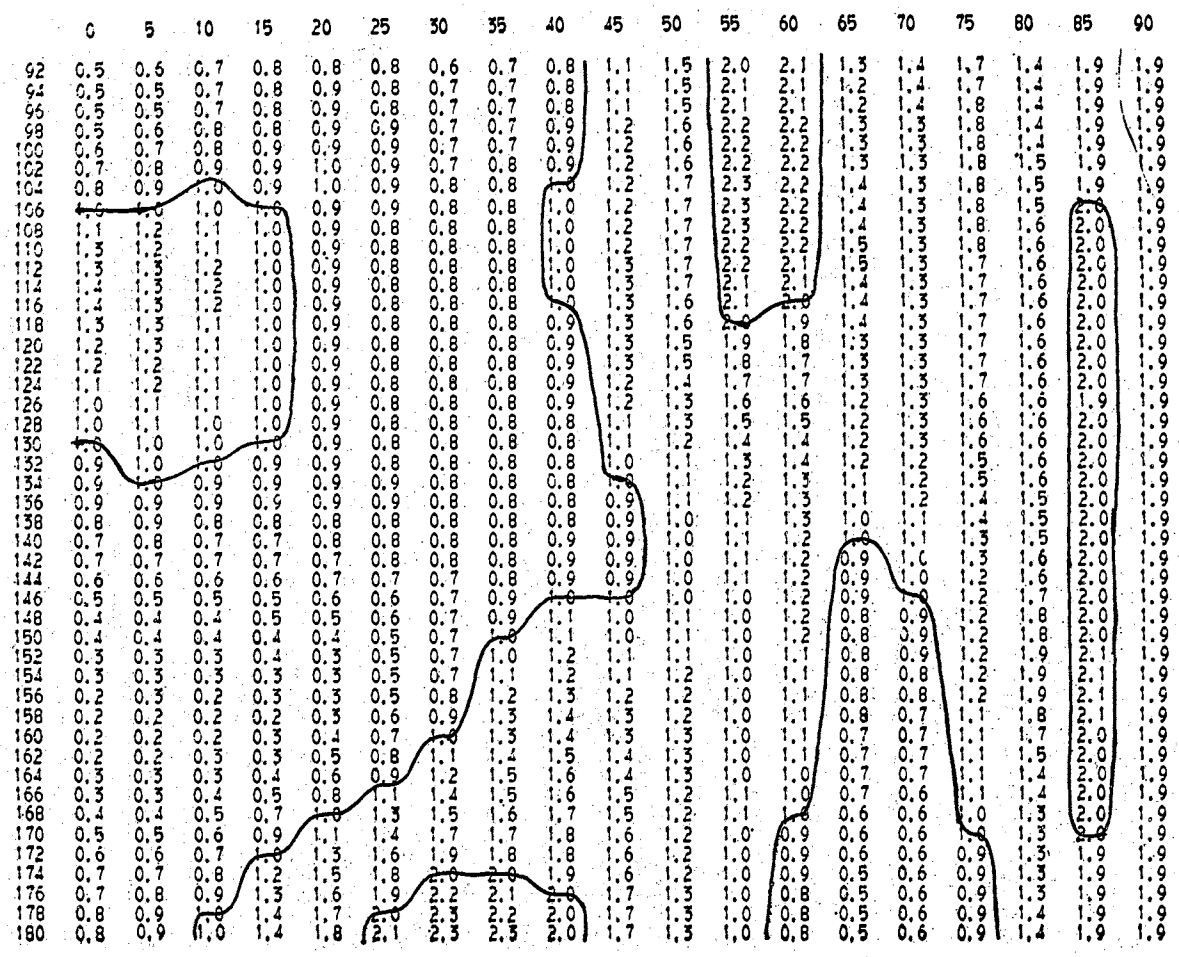

TABLE XX (Continued)

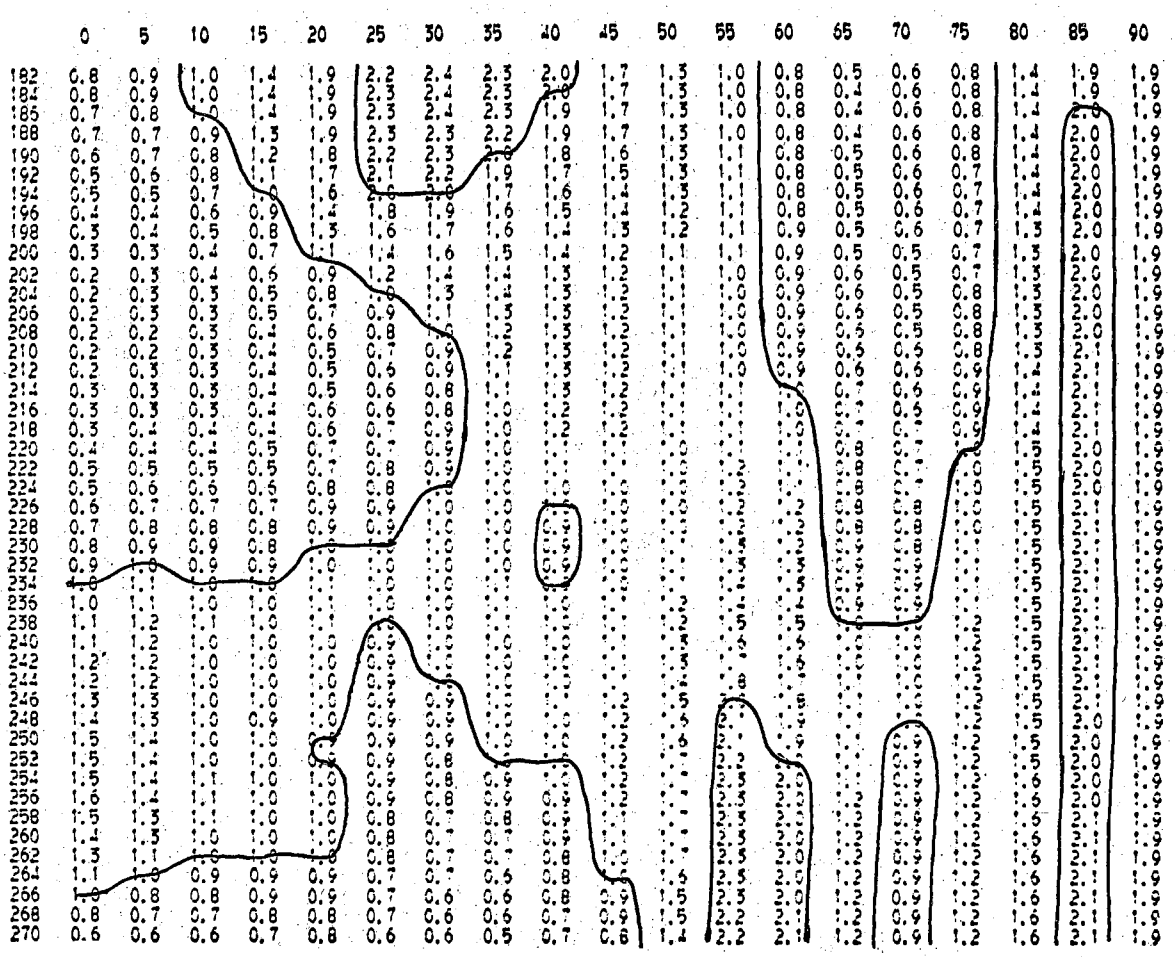

TABLE XX (Continued)

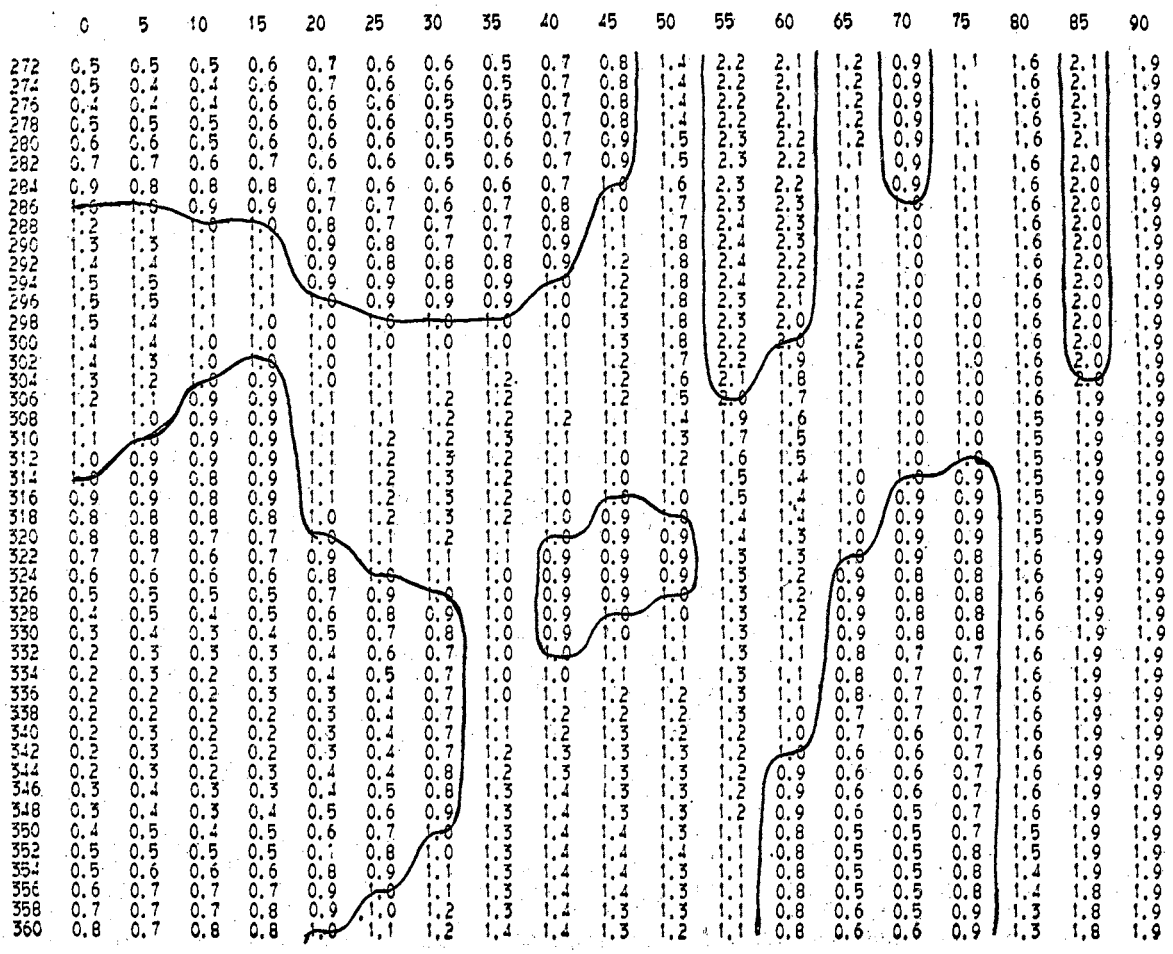

POLE FIGURE DATA SHEET FOR SPECIMEN II-B-1

The normalized pole figure is based on Mo k-alpha radiation and the 111 reflection.

The 222 reflection was used to fill in the blind region from 80 through 90 degrees alpha.

The alpha-dependent two theta shift was taken into account.

Integrated intensities were used.

Normal smoothing was used.

Maximum and minimum corrected intensities are 906 and 0 counts/second, respectively.

Random intensity is 136 counts/second.

Maximum intensity is 6.62 times random.

Contour spacing is based on multiples of random intensity.

6 contours are to be plotted.

Their values are 1.000 2.000 3.000 4.000 5.000 6.000.

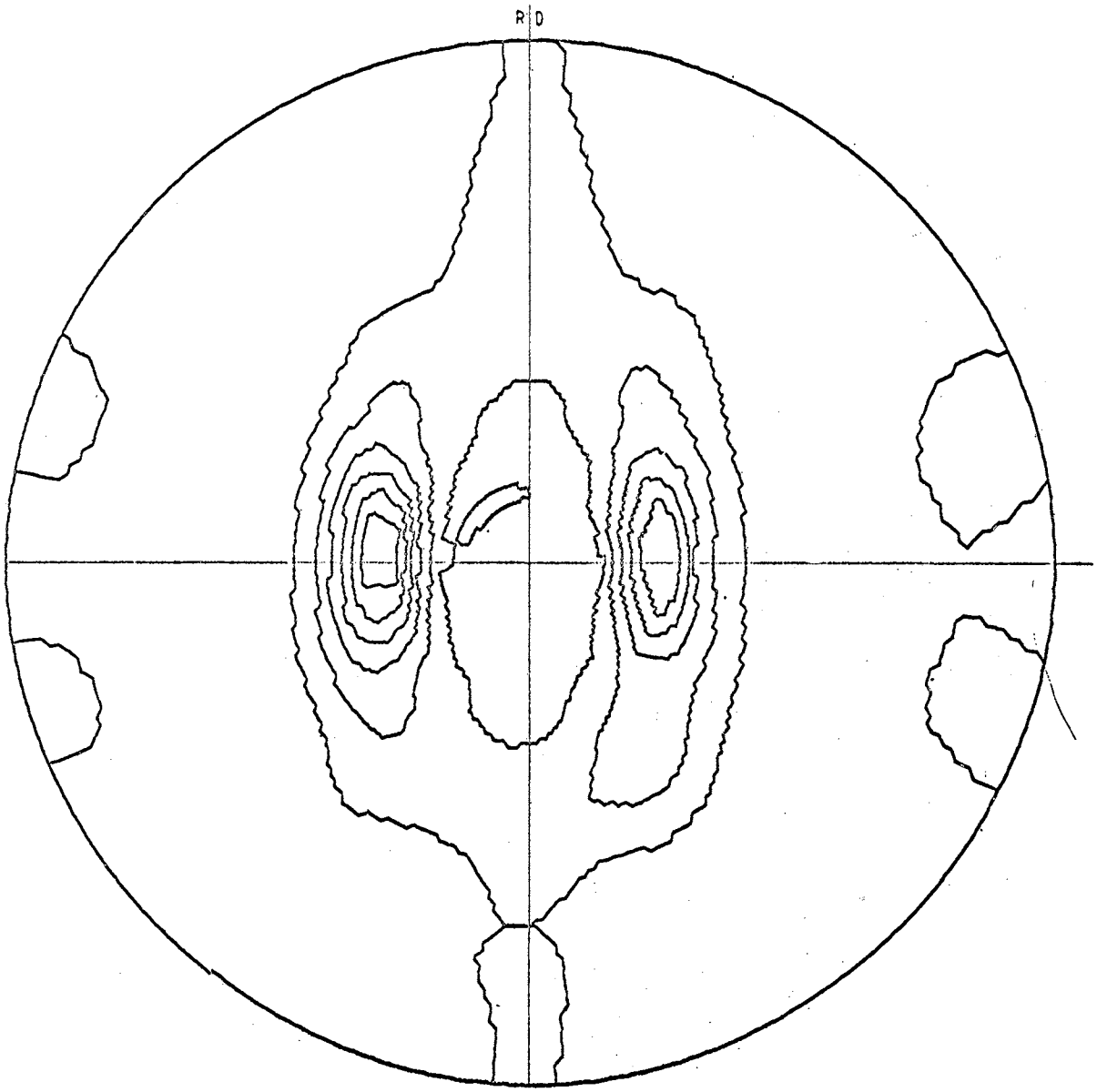

Figure 24. (111) Pole Figure for Specimen II-B-1

TABLE XXI

POLE FIGURE DATA FOR SPECIMEN II-B-1

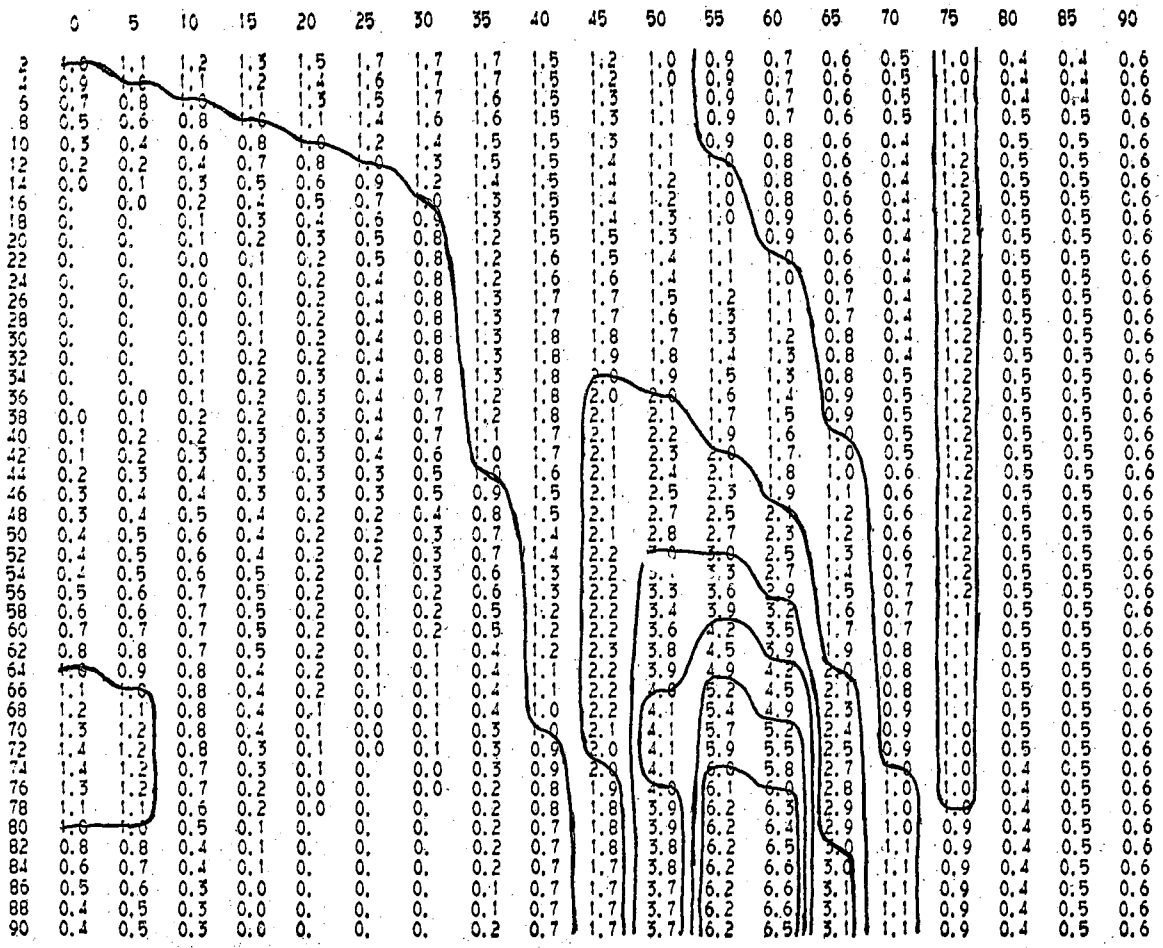

TABLE XXI (Continued)

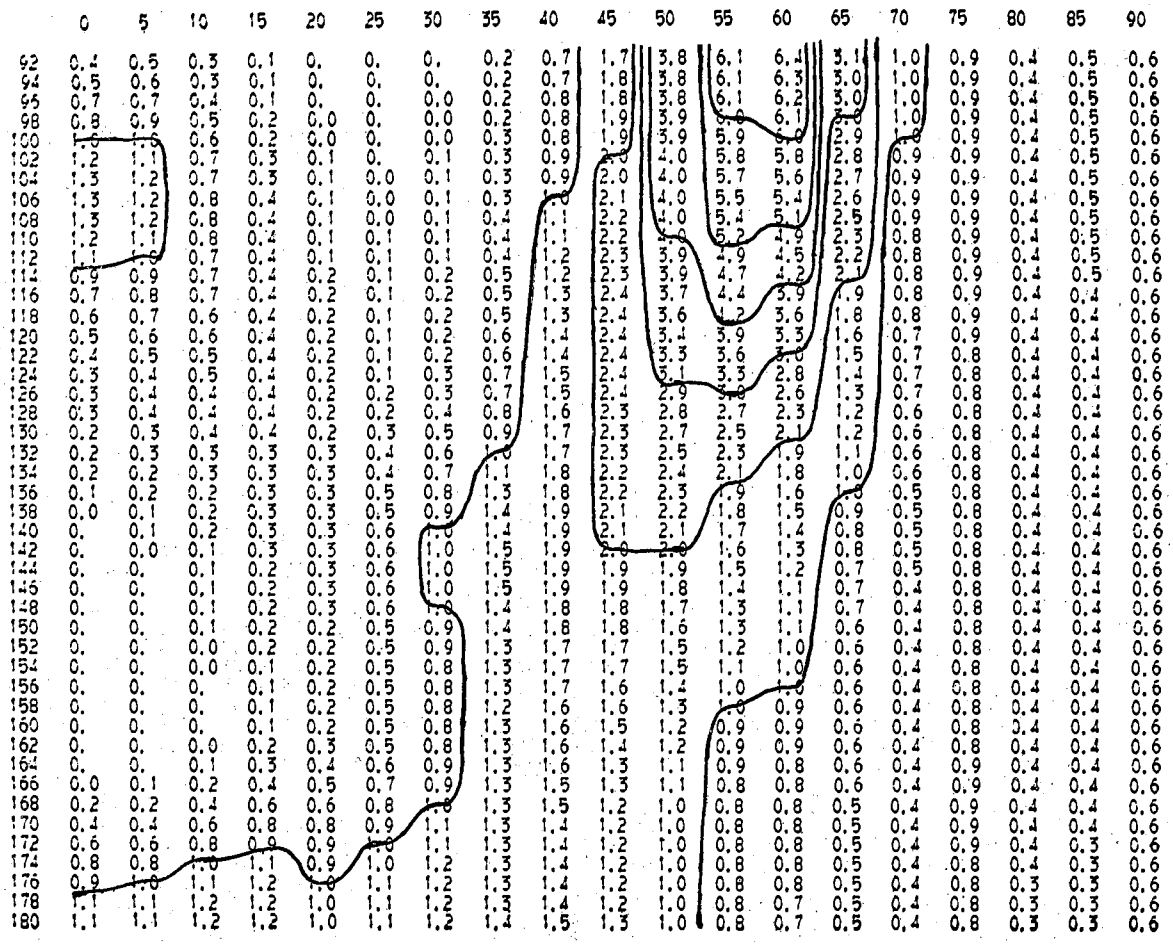

TABLE XXI (Continued)

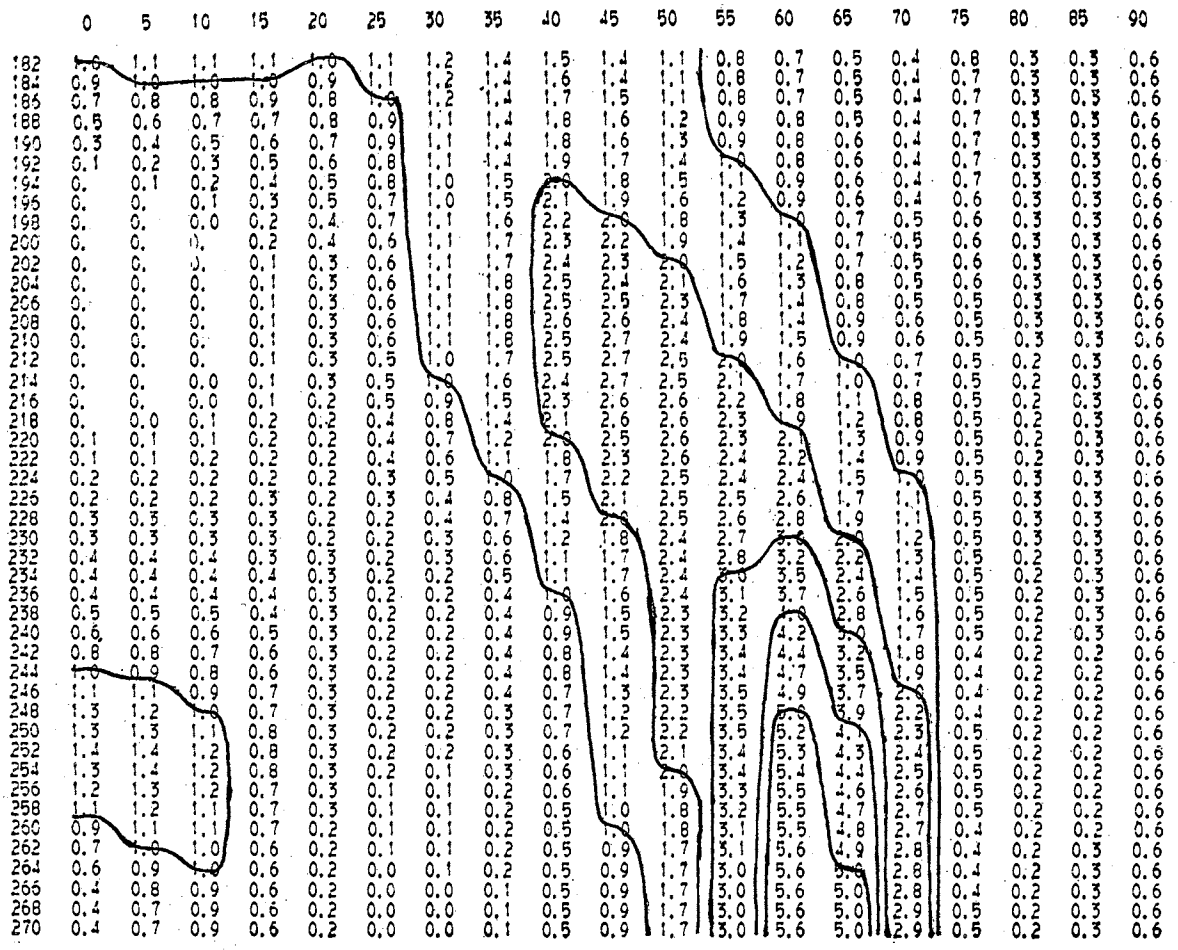

TABLE XXI (Continued)

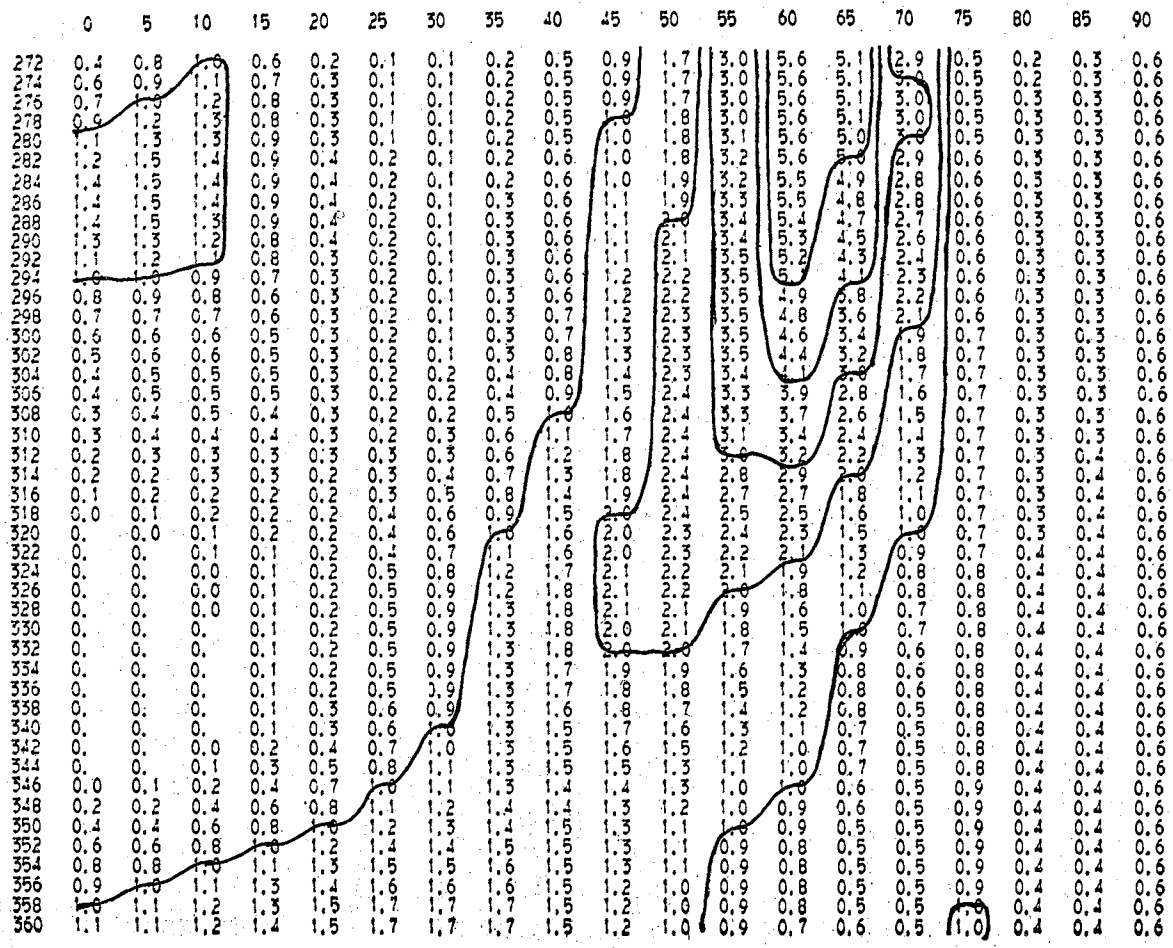

POLE FIGURE DATA SHEET FOR SPECIMEN II-C-1

The normalized pole figure is based on Mo k-alpha radiation and the 111 reflection.

The 222 reflection was used to fill in the blind region from 80 through 90 degrees alpha.

The alpha-dependent two theta shift was taken into account.

Integrated intensities were used.

Normal smoothing was used.

Maximum and minimum corrected intensities are 1323 and 72 counts/second, respectively.

Random intensity is 210 counts/second.

Maximum intensity is 6.29 times random.

Contour spacing is based on multiples of random intensity.

6 contours are to be plotted.

Their values are 1.000 2.000 3.000 4.000 5.000 6.000.

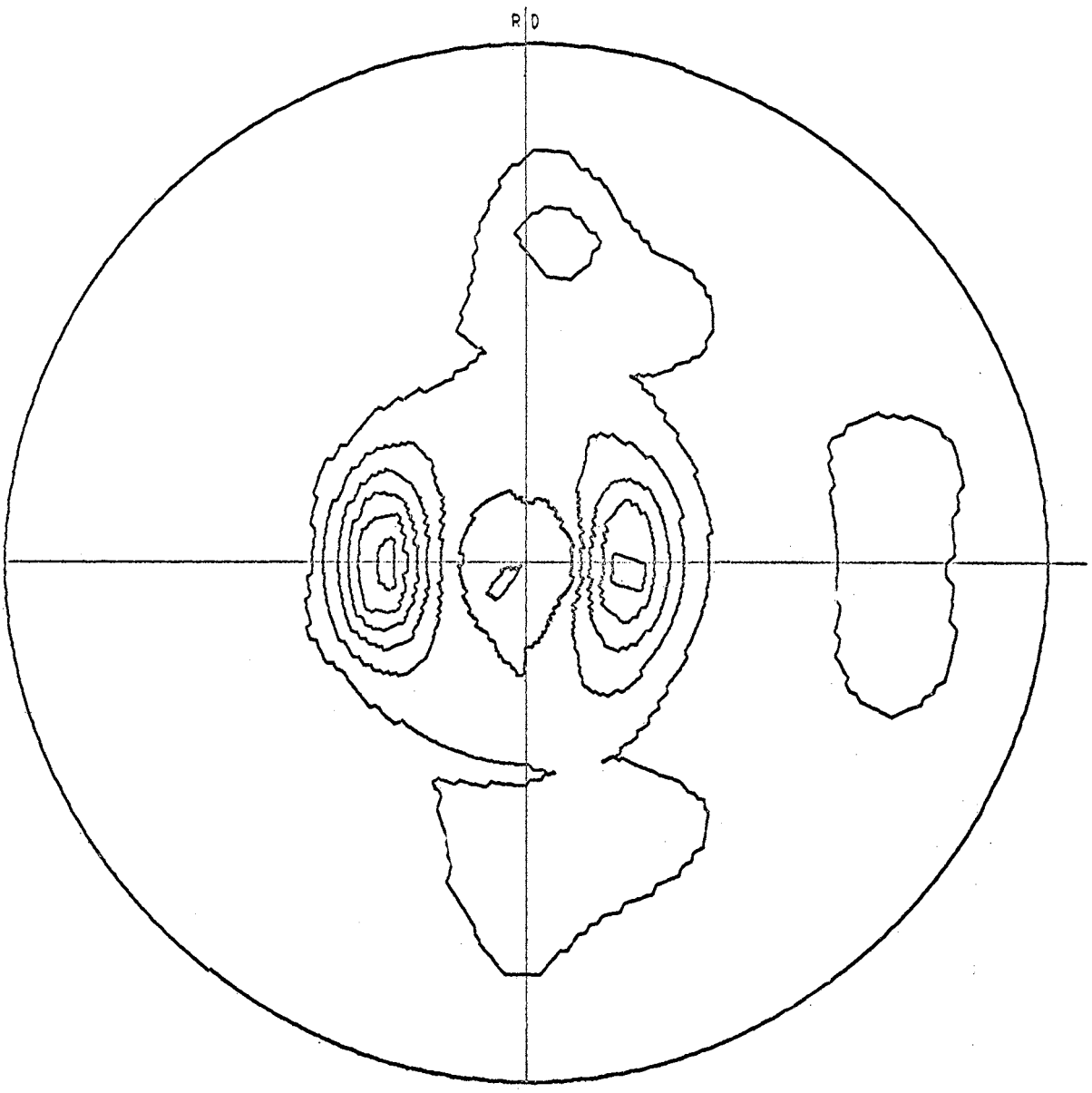

Figure 25. (111) Pole Figure for Specimen II-C-1

TABLE XXII

POLE FIGURE DATA FOR SPECIMEN II-C-1

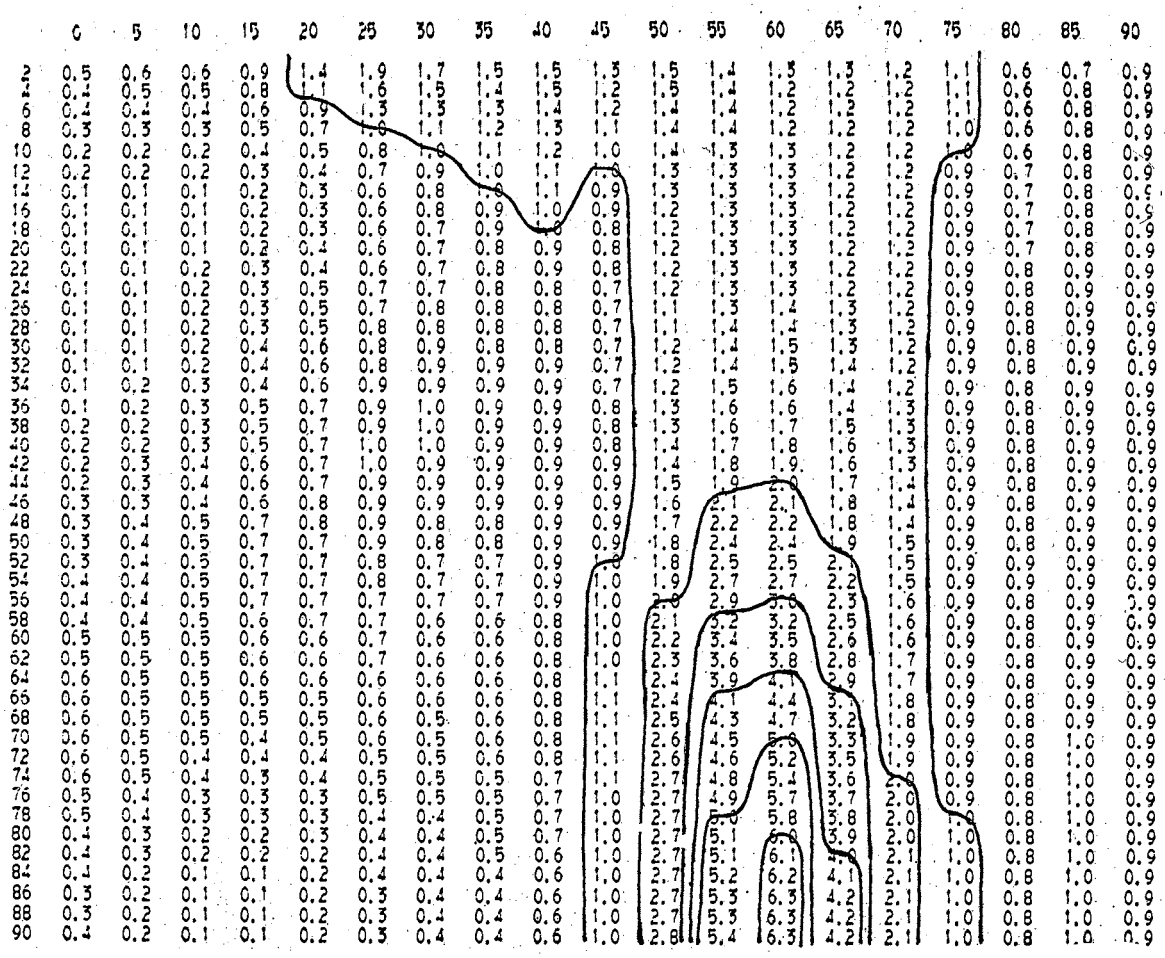

TABLE XXII (Continued)

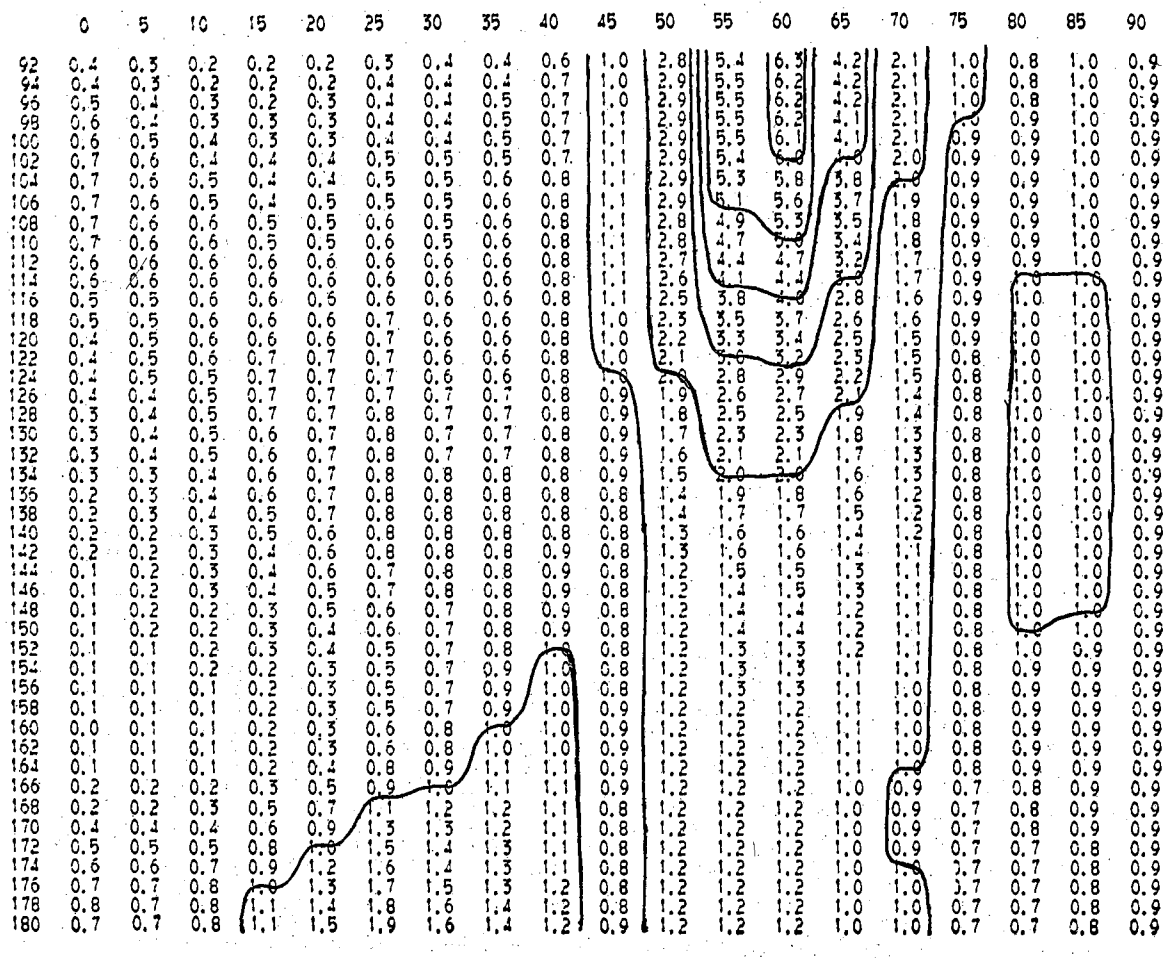

TABLE XXII (Continued)

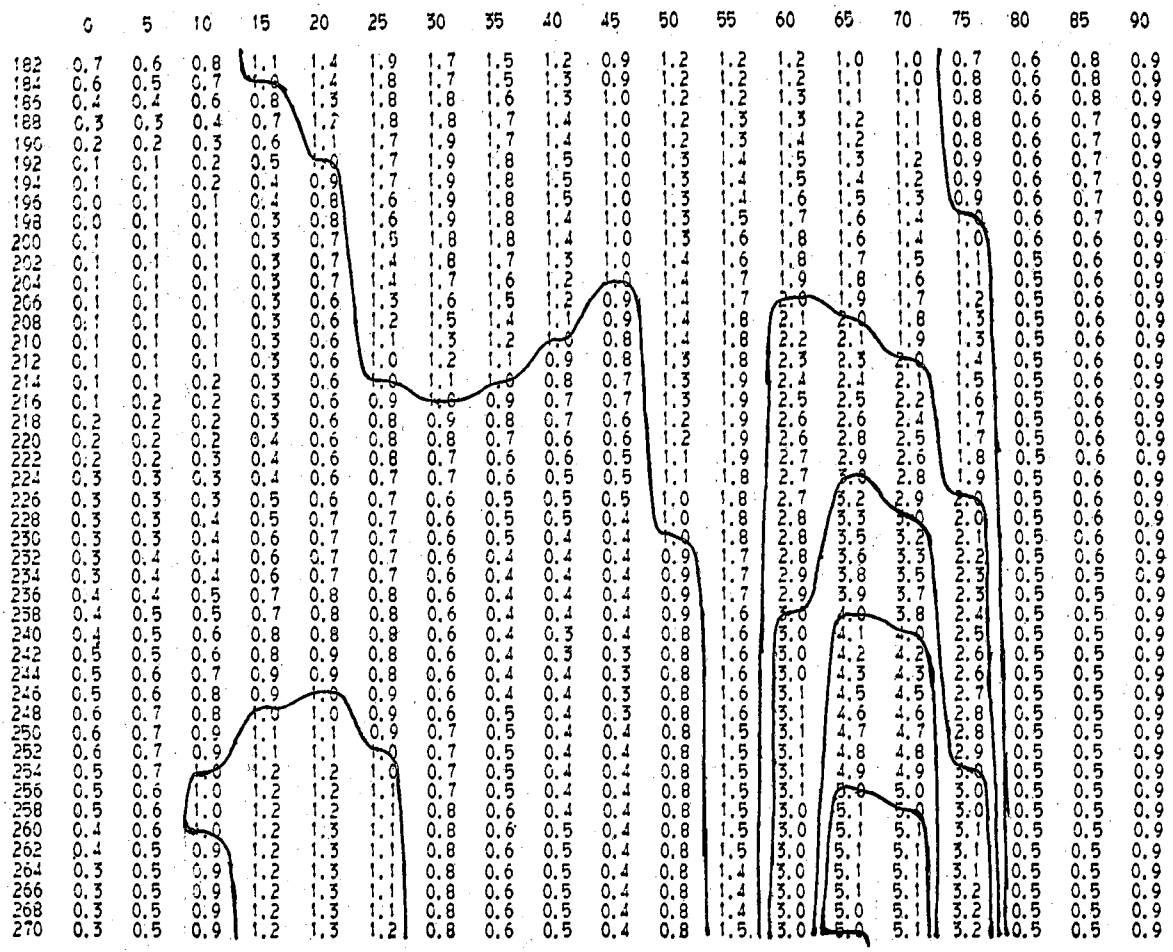

TABLE XXII (Continued)

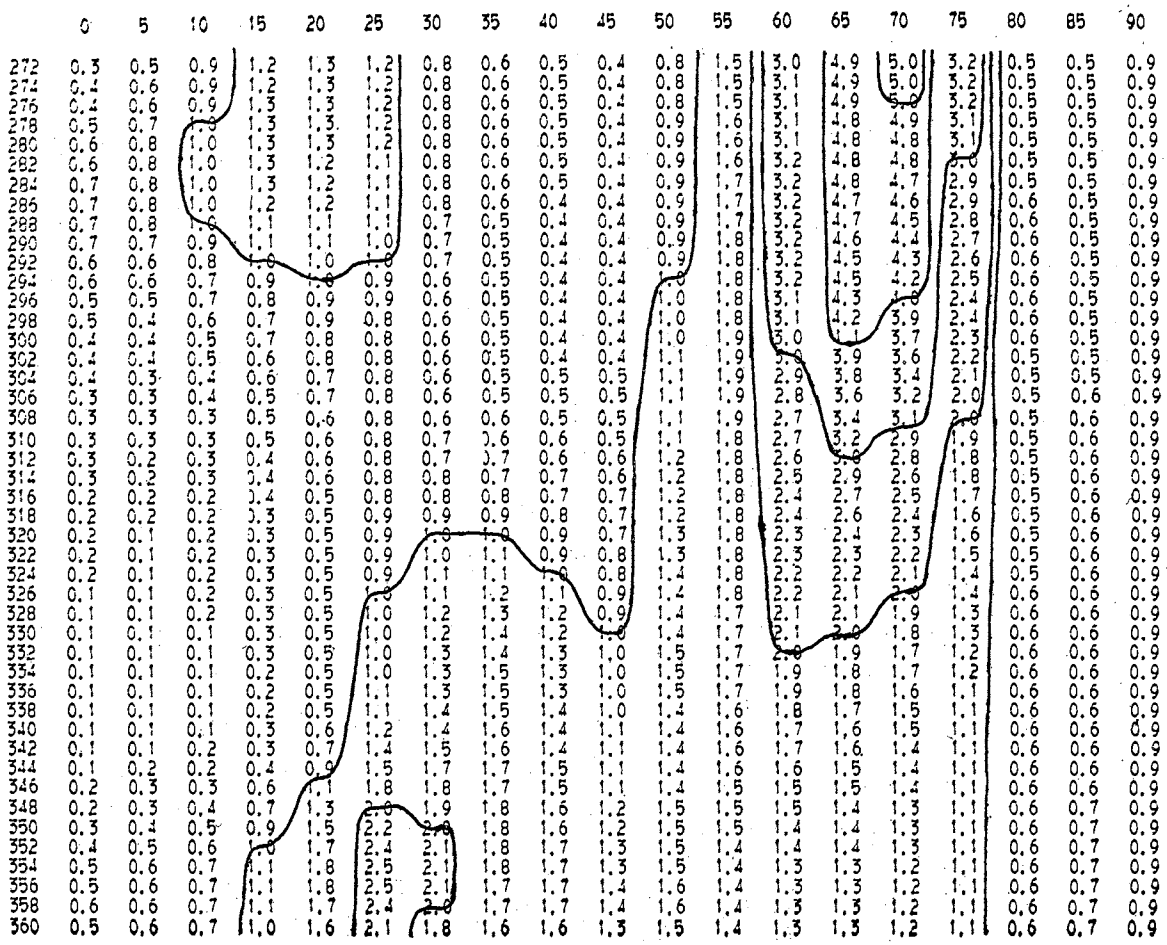

POLE FIGURE DATA SHEET FOR SPECIMEN II-D-1

The normalized pole figure is based on Mo k-alpha radiation and the 111 reflection.

The 222 reflection was used to fill in the blind region from 80 through 90 degrees alpha.

The alpha-dependent two theta shift was taken into account.

Integrated intensities were used.

Normal smoothing was used.

Maximum and minimum corrected intensities are 988 and 0 counts/second, respectively.

Random intensity is 151 counts/second.

Maximum intensity is 6.54 times random.

Contour spacing is based on multiples of random intensity.

6 contours are to be plotted.

Their values are 1.000 2.000 3.000 4.000 5.000 6.000.

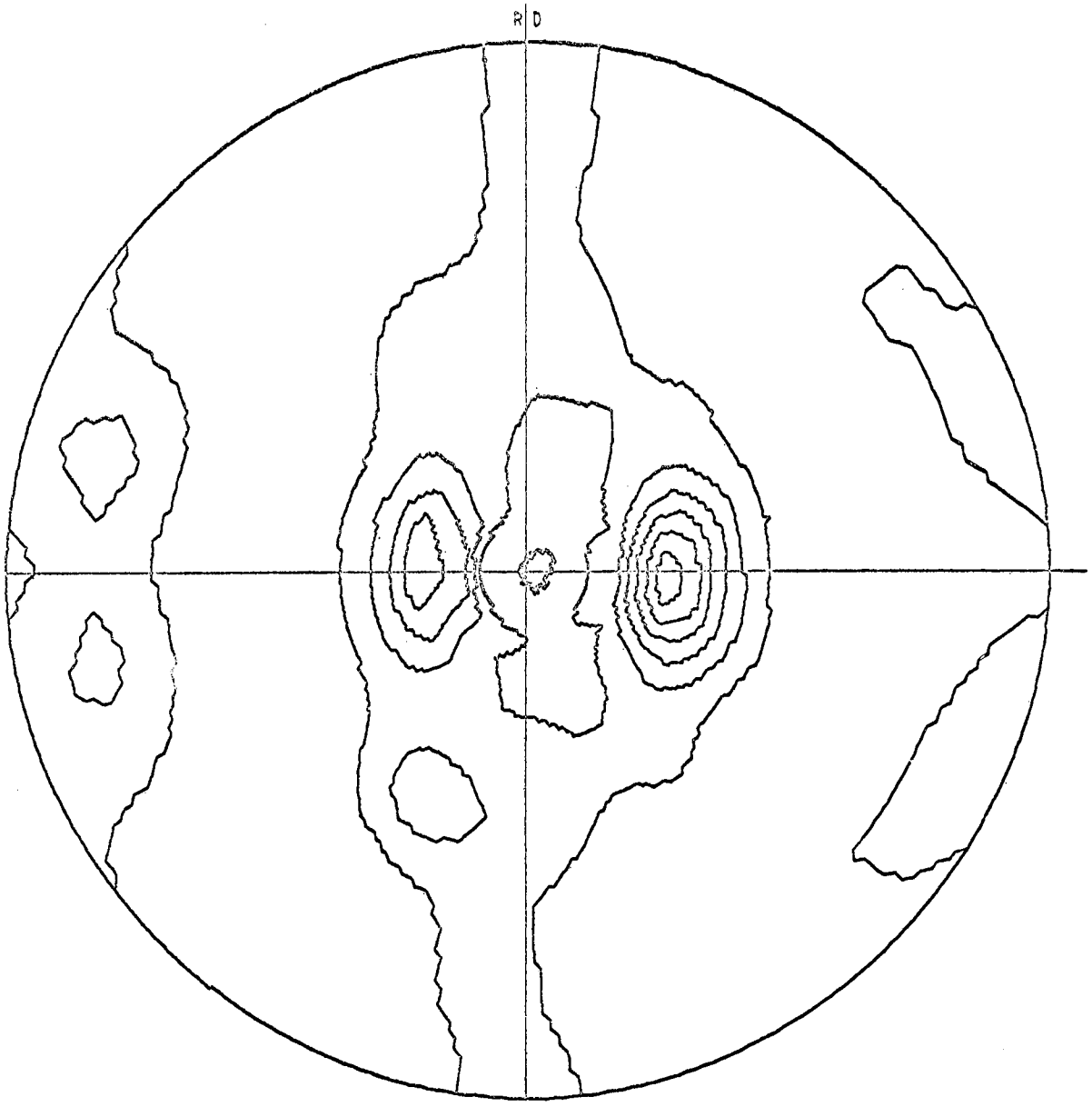

Figure 26. (111) Pole Figure for Specimen II-D-1

TABLE XXIII

POLE FIGURE DATA FOR SPECIMEN II-D-1

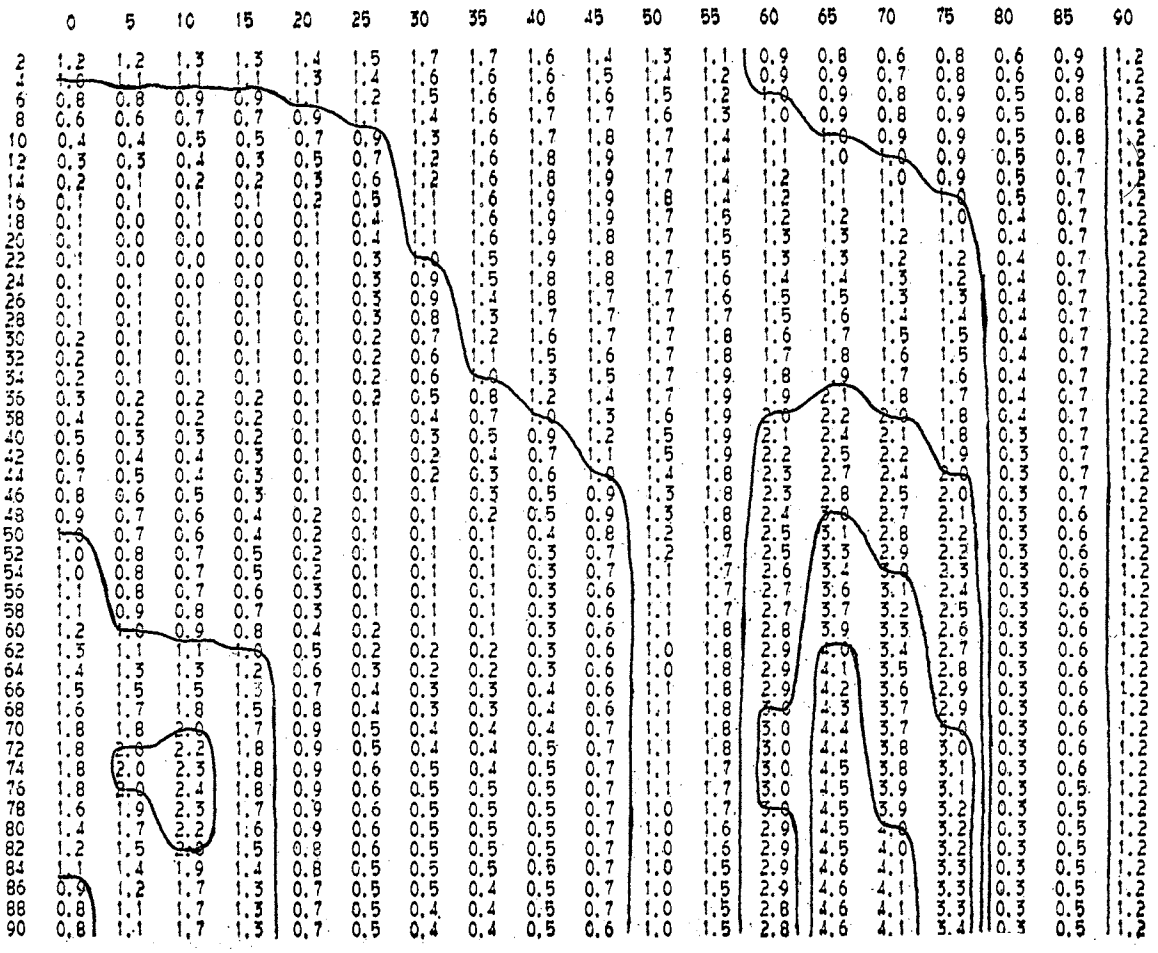

TABLE XXIII (Continued)

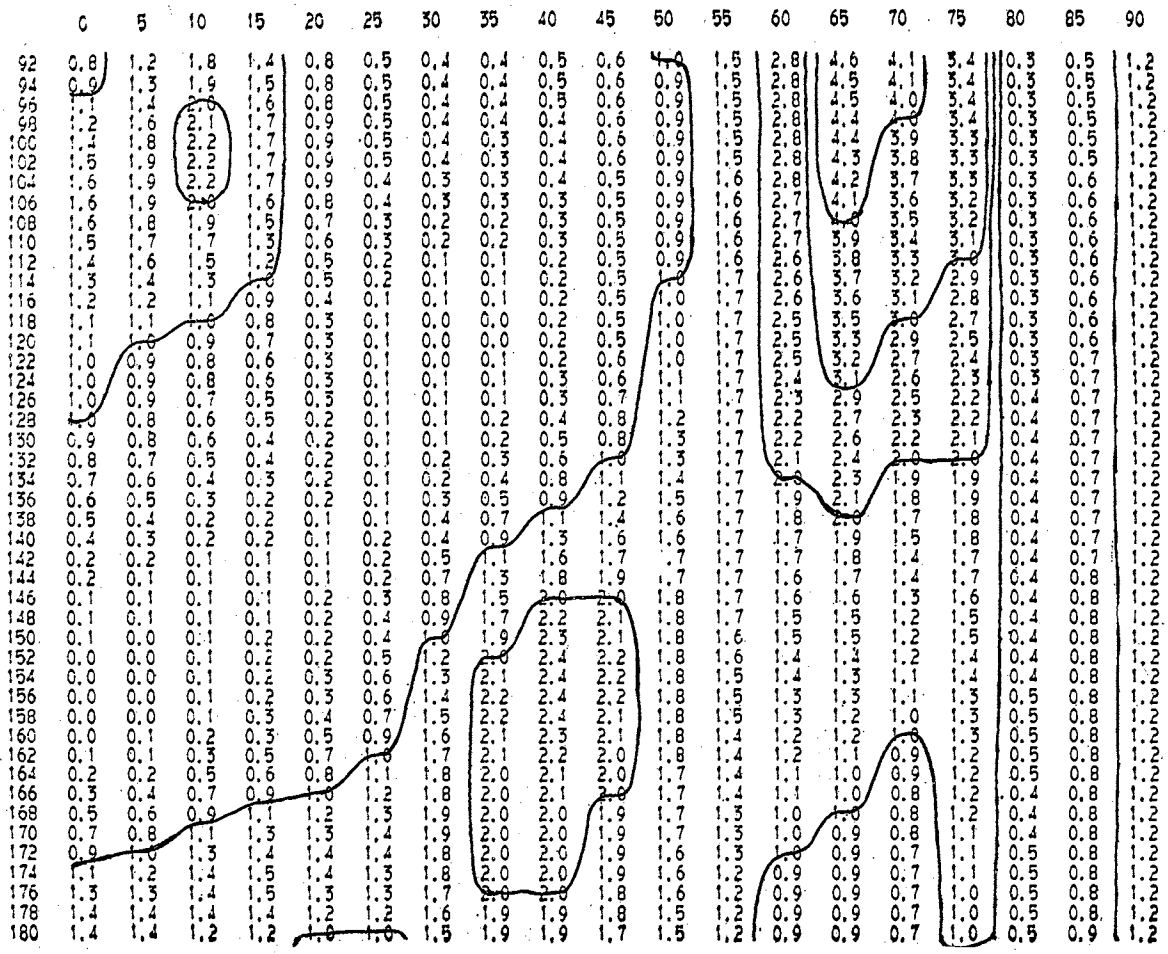

TABLE XXIII (Continued)

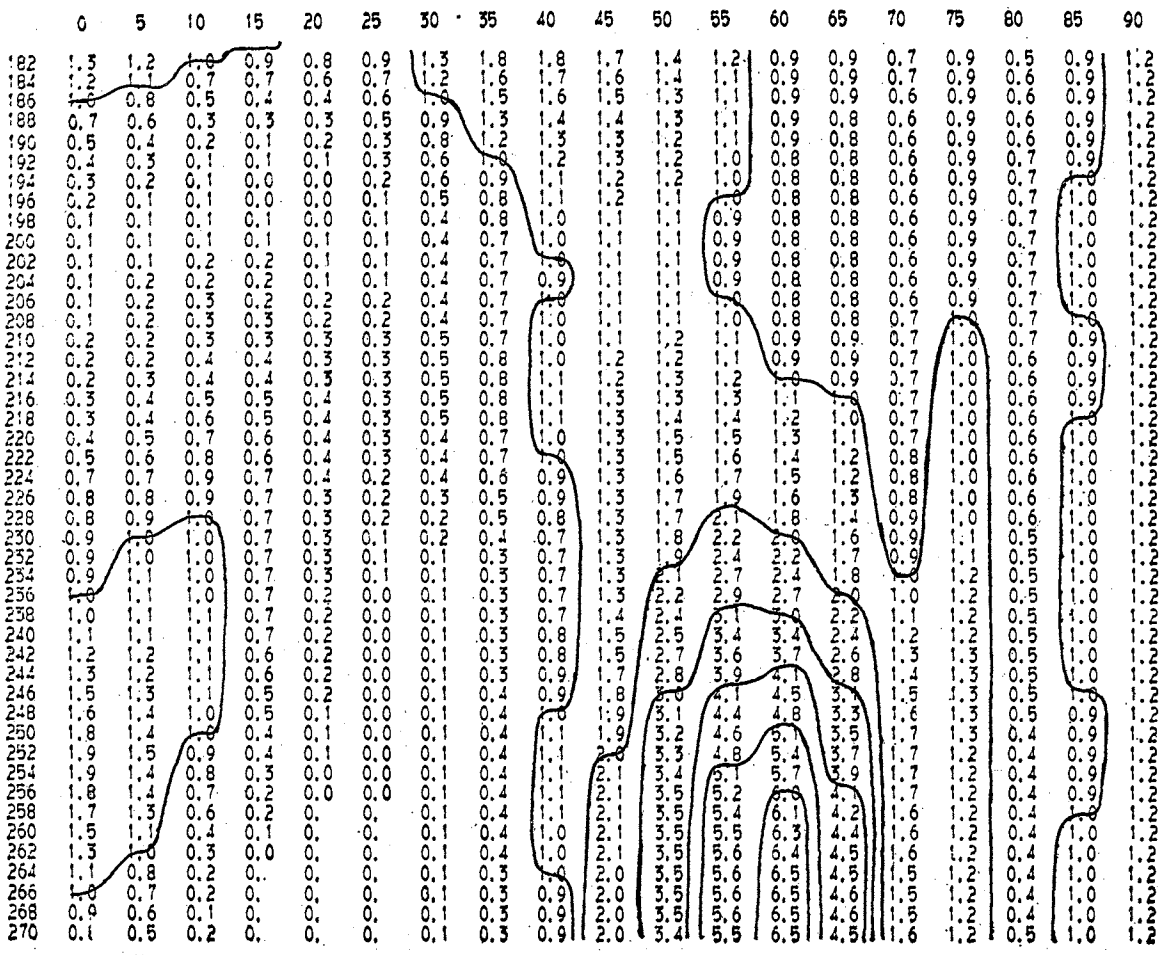

TABLE XXIII (Continued)

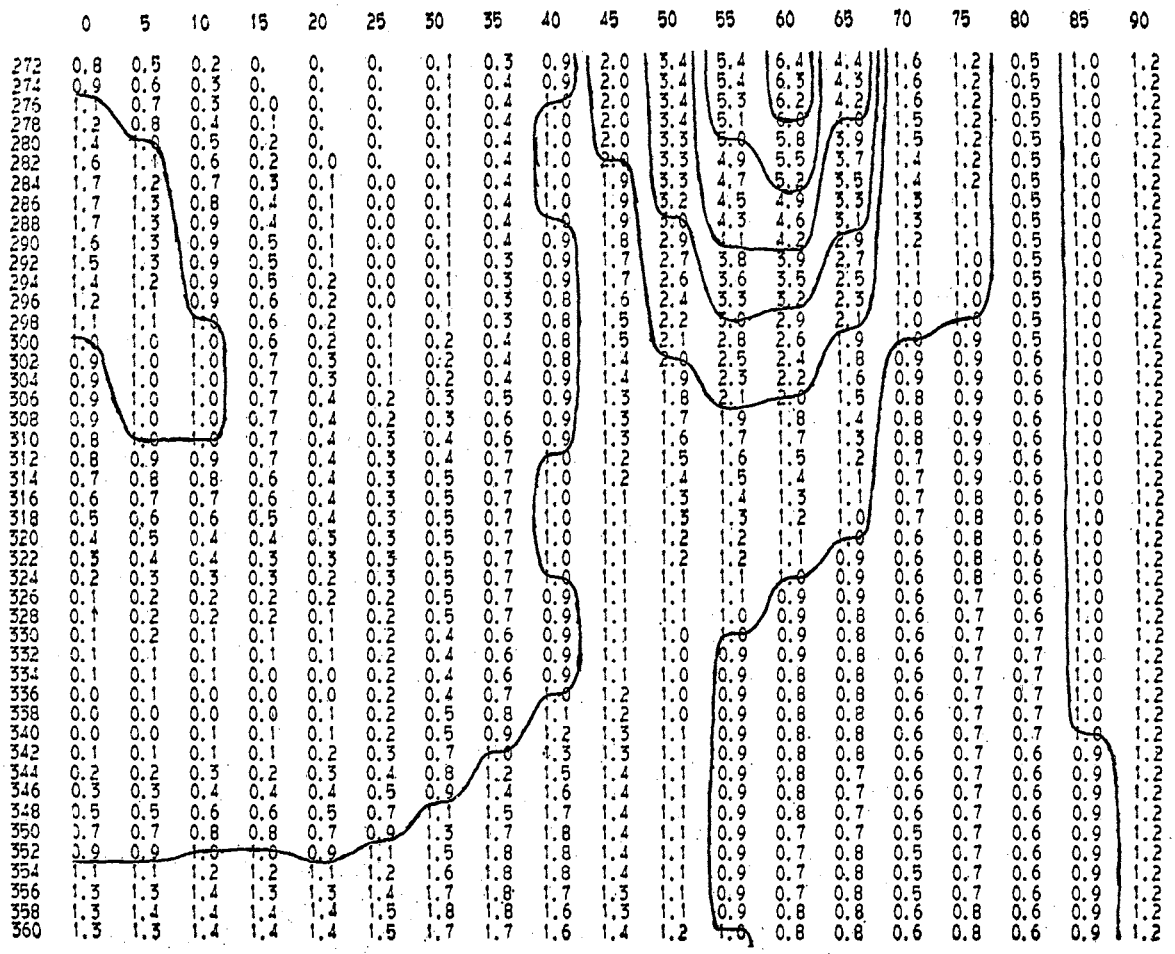

POLE FIGURE DATA SHEET FOR SPECIMEN II-B-2

The normalized pole figure is based on Mo k-alpha radiation and the 111 reflection.

The 222 reflection was used to fill in the blind region from 80 through 90 degrees alpha.

The alpha-dependent two theta shift was taken into account.

Integrated intensities were used.

Normal smoothing was used.

Maximum and minimum corrected intensities are 1041 and 0 counts/second, respectively.

Random intensity is 258 counts/second.

Maximum intensity is 4.02 times random.

Contour spacing is based on multiples of random intensity.

4 contours are to be plotted.

Their values are 1.000 2.000 3.000 4.000.

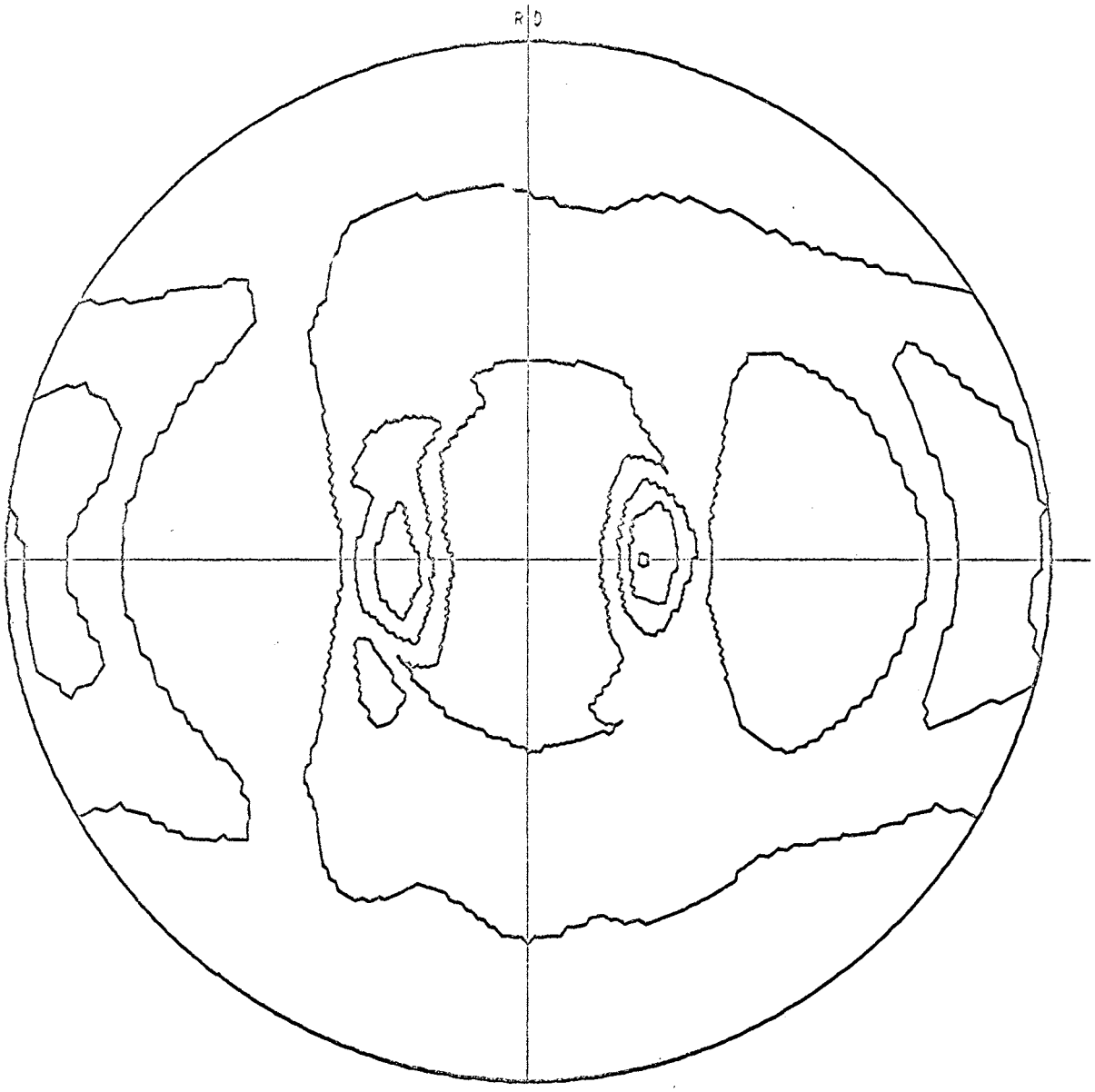

Figure 27. (111) Pole Figure for Specimen II-B-2

TABLE XXIV

POLE FIGURE DATA FOR SPECIMEN II-B-2

	0	5	10	15	20	25	30	35	40	45	50	55	60	65	70	75	80	85	90
2	0.5	0.6	0.7	0.8	1.0	1.4	1.5	1.5	1.4	1.2	0.8	0.5	0.3	0.3	0.2	0.3	0.2	0.3	0.4
4	0.5	0.5	0.7	0.8	1.0	1.4	1.6	1.5	1.4	1.1	0.9	0.5	0.3	0.3	0.2	0.3	0.3	0.3	0.4
6	0.5	0.5	0.7	0.9	1.0	1.4	1.6	1.5	1.4	1.1	0.9	0.6	0.3	0.3	0.2	0.3	0.3	0.3	0.4
8	0.5	0.5	0.7	0.9	1.1	1.4	1.6	1.5	1.4	1.1	0.9	0.7	0.3	0.3	0.2	0.3	0.3	0.3	0.4
10	0.4	0.5	0.8	0.9	1.0	1.4	1.6	1.5	1.4	1.1	0.9	0.8	0.3	0.2	0.2	0.3	0.3	0.3	0.4
12	0.4	0.5	0.8	0.9	1.0	1.4	1.5	1.4	1.4	1.2	0.9	0.8	0.3	0.2	0.2	0.2	0.3	0.3	0.4
14	0.4	0.5	0.8	0.9	1.1	1.4	1.5	1.4	1.4	1.2	0.9	0.9	0.3	0.2	0.2	0.2	0.3	0.3	0.4
16	0.3	0.5	0.8	0.9	1.1	1.3	1.4	1.4	1.4	1.2	0.9	1.0	0.3	0.2	0.2	0.2	0.3	0.3	0.4
18	0.3	0.5	0.8	0.9	1.1	1.3	1.4	1.4	1.4	1.2	1.0	1.1	0.3	0.2	0.2	0.2	0.3	0.3	0.4
20	0.3	0.5	0.7	0.9	1.1	1.3	1.4	1.4	1.3	1.2	1.0	1.2	0.4	0.2	0.2	0.2	0.3	0.3	0.4
22	0.3	0.5	0.7	0.9	1.1	1.3	1.4	1.4	1.3	1.3	1.1	1.3	0.4	0.3	0.2	0.2	0.3	0.3	0.4
24	0.3	0.5	0.7	0.9	1.1	1.3	1.4	1.4	1.3	1.3	1.2	1.4	0.4	0.3	0.2	0.2	0.3	0.3	0.4
26	0.2	0.5	0.7	0.9	1.1	1.3	1.4	1.4	1.3	1.3	1.3	1.5	0.4	0.3	0.2	0.2	0.3	0.3	0.4
28	0.2	0.5	0.7	0.9	1.1	1.2	1.4	1.4	1.3	1.4	1.3	1.6	0.5	0.3	0.2	0.2	0.3	0.4	0.4
30	0.2	0.5	0.7	0.9	1.0	1.2	1.4	1.4	1.4	1.4	1.4	1.8	0.6	0.4	0.2	0.2	0.3	0.4	0.4
32	0.2	0.4	0.7	0.9	1.0	1.1	1.4	1.4	1.4	1.4	1.5	1.9	0.6	0.4	0.2	0.2	0.3	0.4	0.4
34	0.2	0.4	0.7	0.9	1.0	1.1	1.4	1.4	1.4	1.5	1.6	2.0	0.7	0.4	0.2	0.2	0.3	0.4	0.4
36	0.2	0.4	0.7	0.9	0.9	1.0	1.3	1.4	1.5	1.5	1.7	2.2	0.8	0.5	0.2	0.2	0.3	0.4	0.4
38	0.2	0.4	0.7	0.9	0.9	1.0	1.3	1.4	1.5	1.5	1.8	2.3	0.9	0.5	0.2	0.2	0.3	0.4	0.4
40	0.2	0.4	0.8	0.9	0.9	0.9	1.2	1.4	1.5	1.6	1.9	2.4	1.0	0.6	0.3	0.2	0.3	0.4	0.4
42	0.3	0.4	0.8	0.9	0.9	0.9	1.2	1.3	1.5	1.6	1.9	2.5	1.1	0.7	0.3	0.2	0.3	0.4	0.4
44	0.3	0.4	0.8	1.0	0.9	0.9	1.1	1.3	1.5	1.7	2.0	2.5	1.3	0.7	0.3	0.2	0.3	0.4	0.4
46	0.3	0.5	0.8	1.0	0.9	0.9	1.0	1.2	1.5	1.7	2.1	2.6	1.4	0.8	0.3	0.2	0.3	0.4	0.4
48	0.4	0.5	0.9	1.1	1.0	0.8	0.9	1.1	1.5	1.7	2.1	2.6	1.6	0.9	0.4	0.3	0.3	0.3	0.4
50	0.4	0.6	0.9	1.1	1.0	0.8	0.8	1.0	1.4	1.7	2.2	2.5	1.7	1.0	0.4	0.3	0.3	0.3	0.4
52	0.5	0.7	1.0	1.2	1.0	0.7	0.7	0.9	1.3	1.7	2.2	2.5	1.9	1.1	0.5	0.3	0.3	0.3	0.4
54	0.6	0.8	1.1	1.2	1.0	0.7	0.6	0.8	1.2	1.6	2.3	2.4	2.1	1.3	0.5	0.3	0.3	0.3	0.4
56	0.7	0.9	1.2	1.3	1.0	0.6	0.5	0.6	1.0	1.5	2.3	2.3	2.2	1.4	0.5	0.3	0.3	0.3	0.4
58	0.8	1.1	1.3	1.3	0.9	0.5	0.4	0.5	0.9	1.4	2.3	2.3	2.4	1.6	0.6	0.3	0.3	0.3	0.4
60	1.0	1.2	1.4	1.3	0.9	0.4	0.3	0.3	0.7	1.3	2.3	2.2	2.5	1.7	0.6	0.4	0.3	0.3	0.4
62	1.2	1.4	1.5	1.3	0.8	0.4	0.2	0.2	0.6	1.2	2.2	2.1	2.7	1.8	0.7	0.4	0.3	0.3	0.4
64	1.4	1.6	1.7	1.3	0.7	0.3	0.1	0.1	0.4	1.1	2.1	2.1	2.8	2.0	0.8	0.4	0.3	0.3	0.4
66	1.5	1.8	1.8	1.2	0.7	0.2	0.1	0.1	0.3	0.9	2.0	2.0	2.9	2.1	0.8	0.4	0.3	0.3	0.4
68	1.7	1.9	1.9	1.2	0.6	0.2	0.0	0.0	0.2	0.8	1.9	2.0	3.1	2.2	0.9	0.5	0.2	0.3	0.4
70	1.9	2.1	1.9	1.1	0.5	0.1	0.0	0.	0.1	0.7	1.7	2.0	3.2	2.3	0.9	0.5	0.2	0.3	0.4
72	2.0	2.2	2.0	1.1	0.4	0.1	0.	0.	0.1	0.6	1.6	2.0	3.3	2.5	1.0	0.5	0.2	0.3	0.4
74	2.0	2.3	2.1	1.0	0.4	0.1	0.	0.	0.0	0.5	1.4	2.0	3.3	2.6	1.0	0.5	0.2	0.3	0.4
76	2.1	2.3	2.1	1.0	0.3	0.0	0.	0.	0.	0.4	1.3	2.1	3.4	2.6	1.1	0.6	0.2	0.3	0.4
78	2.0	2.3	2.0	0.9	0.3	0.0	0.	0.	0.	0.3	1.1	2.1	3.4	2.7	1.1	0.6	0.2	0.3	0.4
80	2.0	2.3	2.0	0.8	0.2	0.	0.	0.	0.	0.2	1.0	2.2	3.4	2.8	1.2	0.6	0.2	0.3	0.4
82	2.0	2.3	1.9	0.7	0.2	0.	0.	0.	0.	0.2	0.9	2.3	3.4	2.9	1.2	0.6	0.2	0.3	0.4
84	1.9	2.2	1.8	0.7	0.1	0.	0.	0.	0.	0.1	0.9	2.3	3.5	2.9	1.2	0.6	0.2	0.3	0.4
86	1.9	2.2	1.8	0.6	0.1	0.	0.	0.	0.	0.1	0.8	2.4	3.5	3.0	1.3	0.6	0.2	0.3	0.4
88	1.9	2.2	1.7	0.6	0.1	0.	0.	0.	0.	0.1	0.8	2.5	3.5	3.1	1.3	0.6	0.2	0.3	0.4
90	1.9	2.1	1.7	0.6	0.1	0.	0.	0.	0.	0.1	0.8	2.5	3.5	3.1	1.3	0.6	0.2	0.3	0.4

TABLE XXIV (Continued)

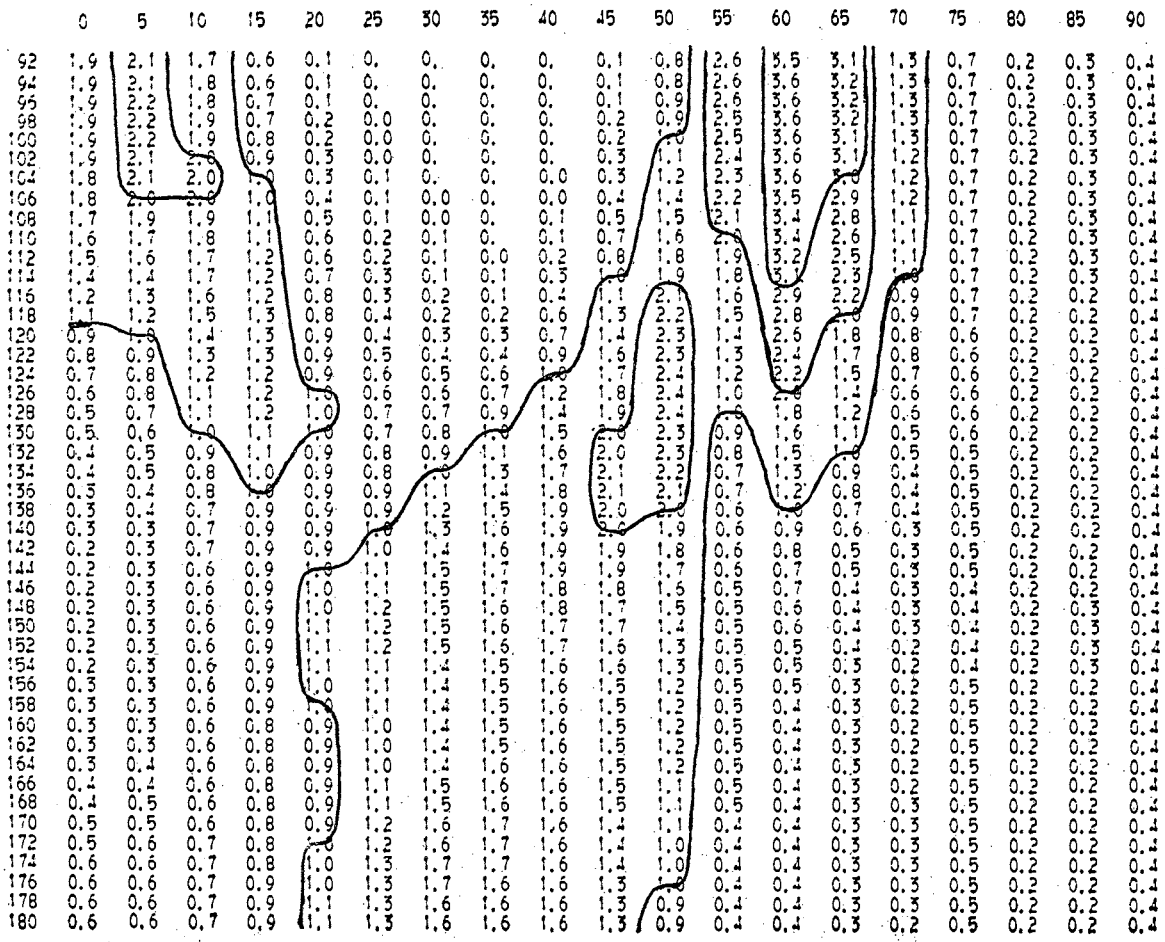

TABLE XXIV (Continued)

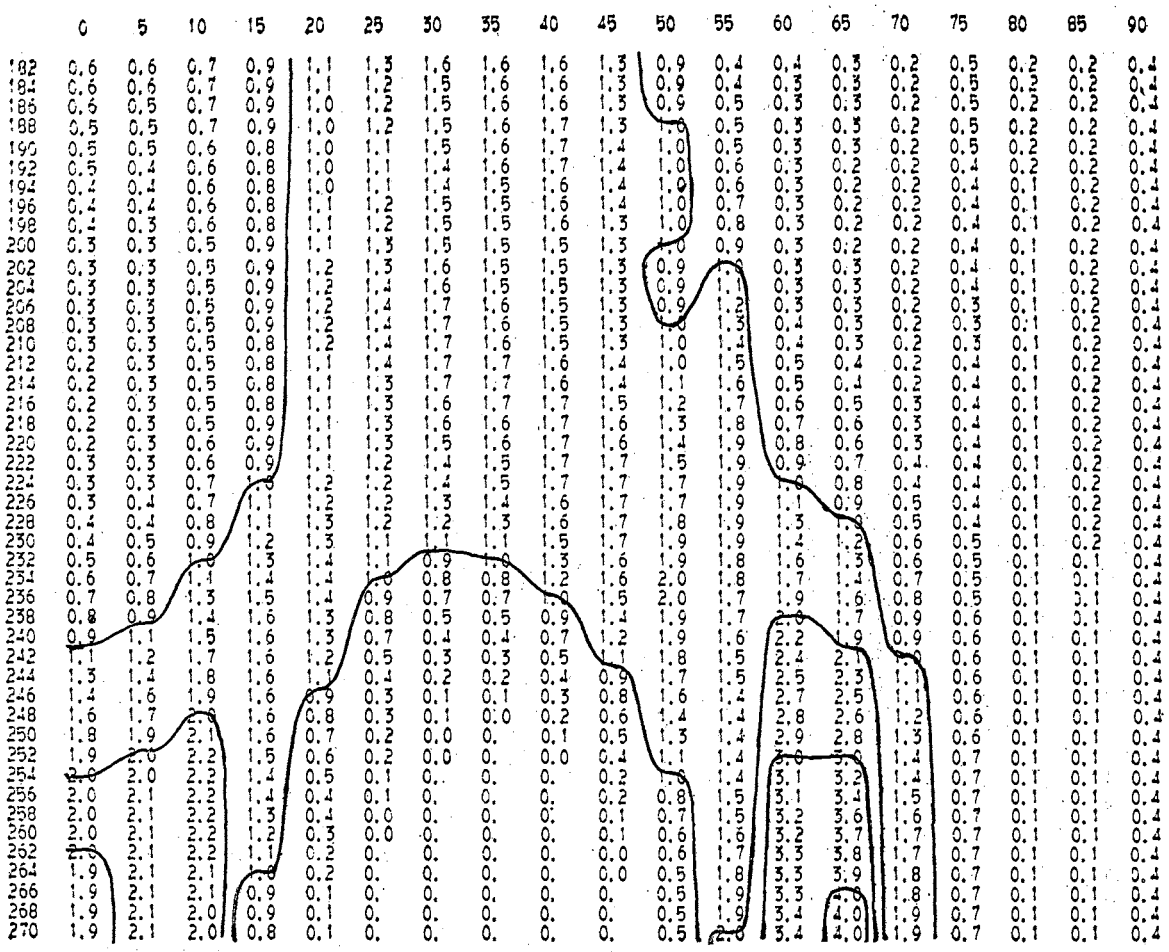

TABLE XXIV (Continued)

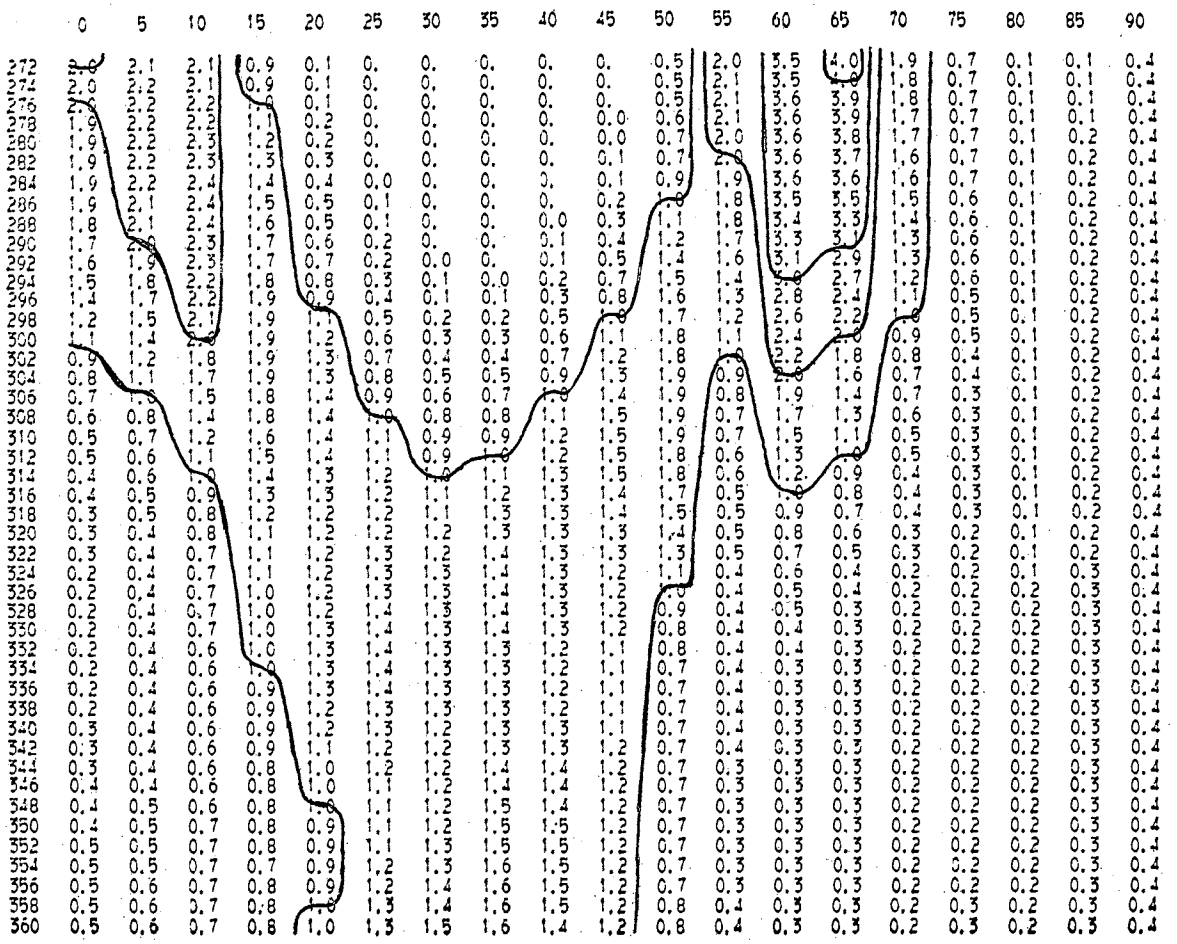

POLE FIGURE DATA SHEET FOR SPECIMEN II-C-2

The normalized pole figure is based on Mo k-alpha radiation and the 111 reflection.

The 222 reflection was used to fill in the blind region from 80 through 90 degrees alpha.

The alpha-dependent two theta shift was taken into account.

Integrated intensities were used.

Normal smoothing was used.

Maximum and minimum corrected intensities are 856 and 0 counts/second, respectively.

Random intensity is 137 counts/second.

Maximum intensity is 6.22 times random.

Contour spacing is based on multiples of random intensity.

6 contours are to be plotted.

Their values are 1.000 2.000 3.000 4.000 5.000 6.000.

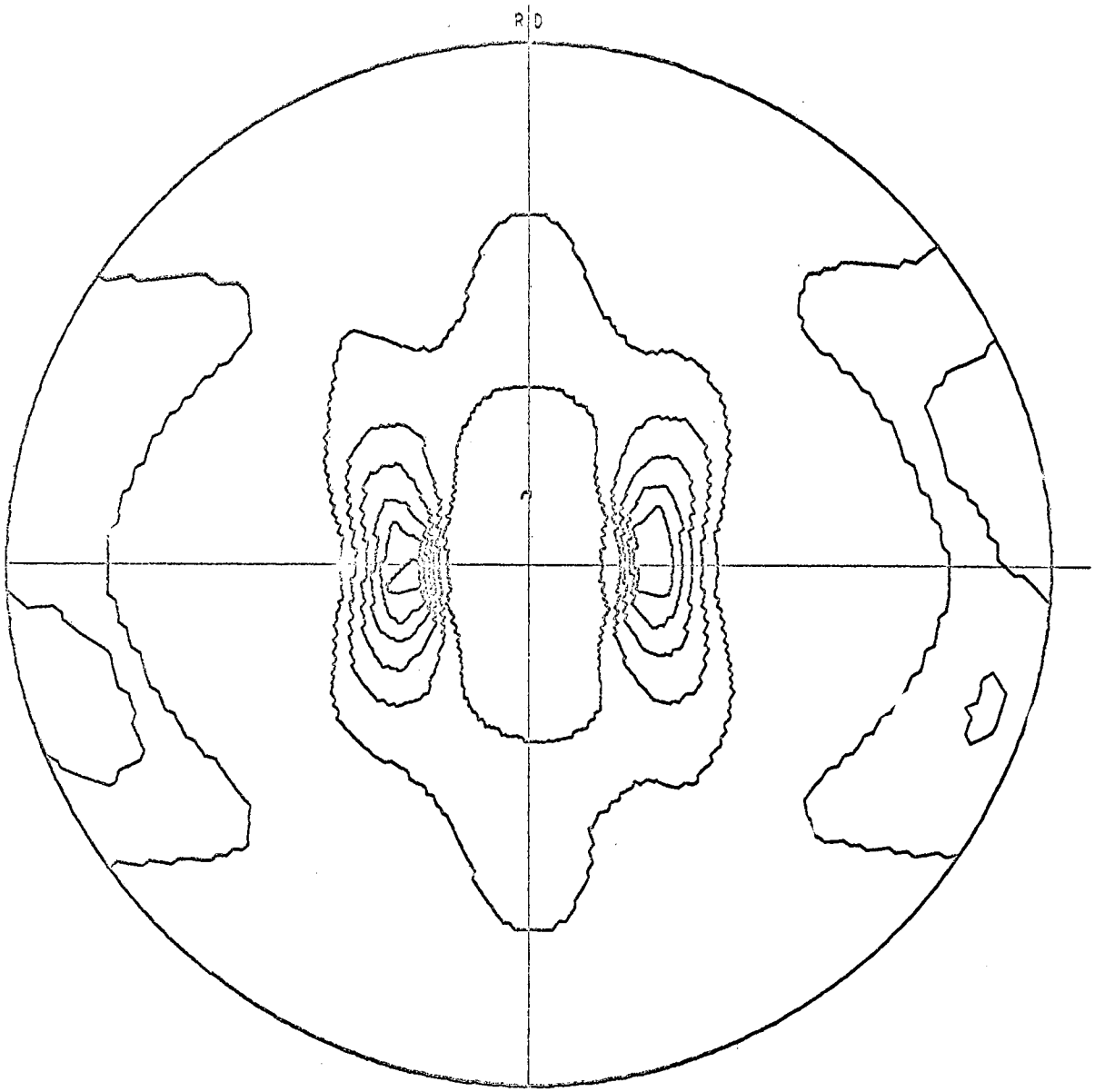

Figure 28. (111) Pole Figure for Specimen II-C-2

TABLE XXV

POLE FIGURE DATA FOR SPECIMEN II-C-2

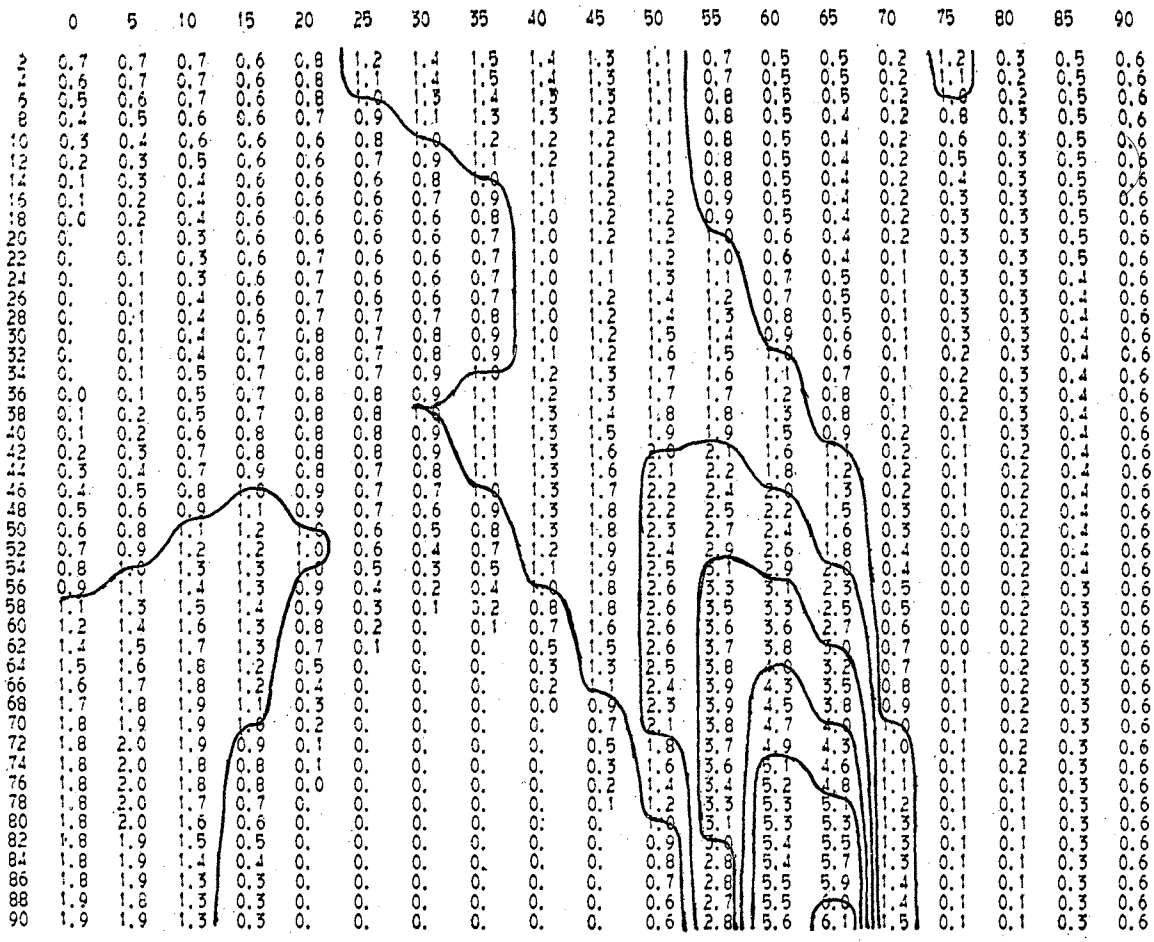

TABLE XXV (Continued)

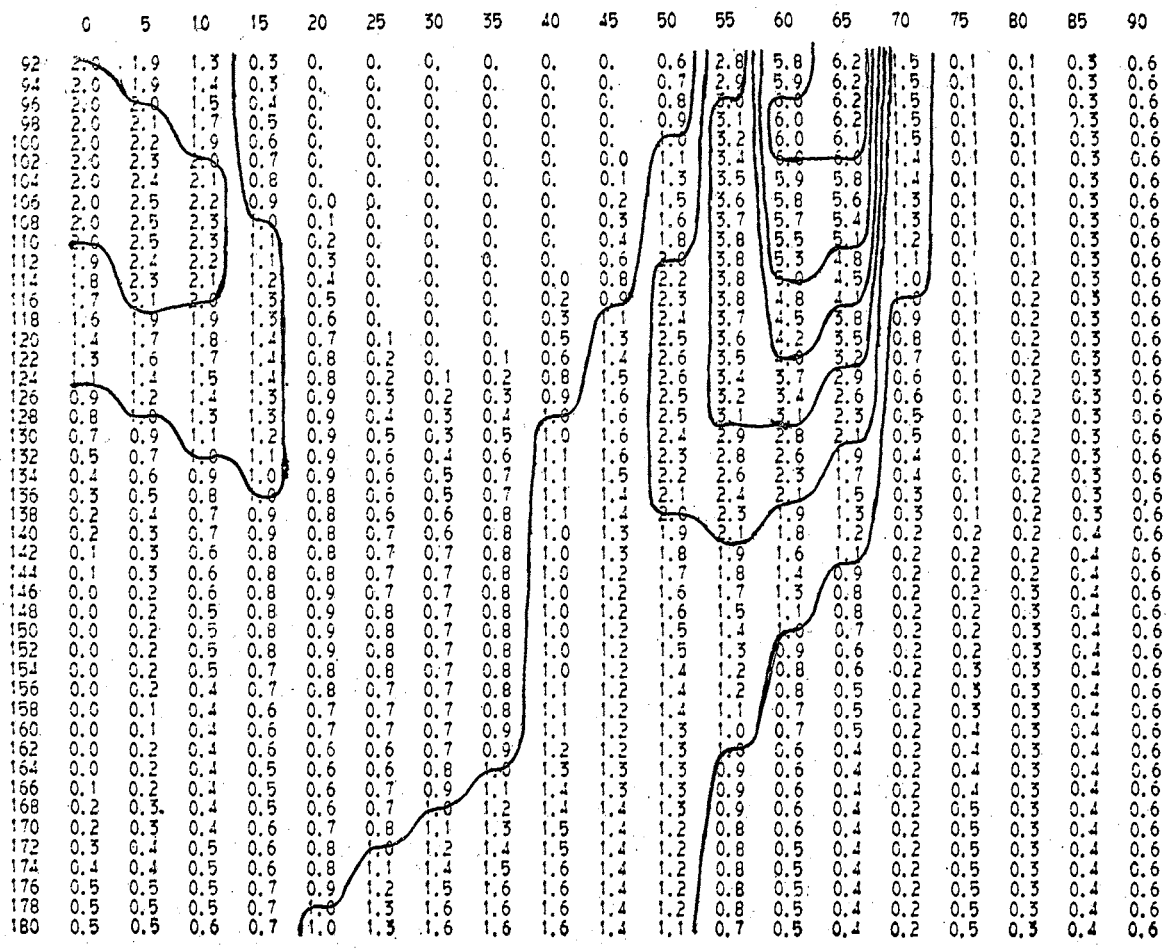

TABLE XXV (Continued)

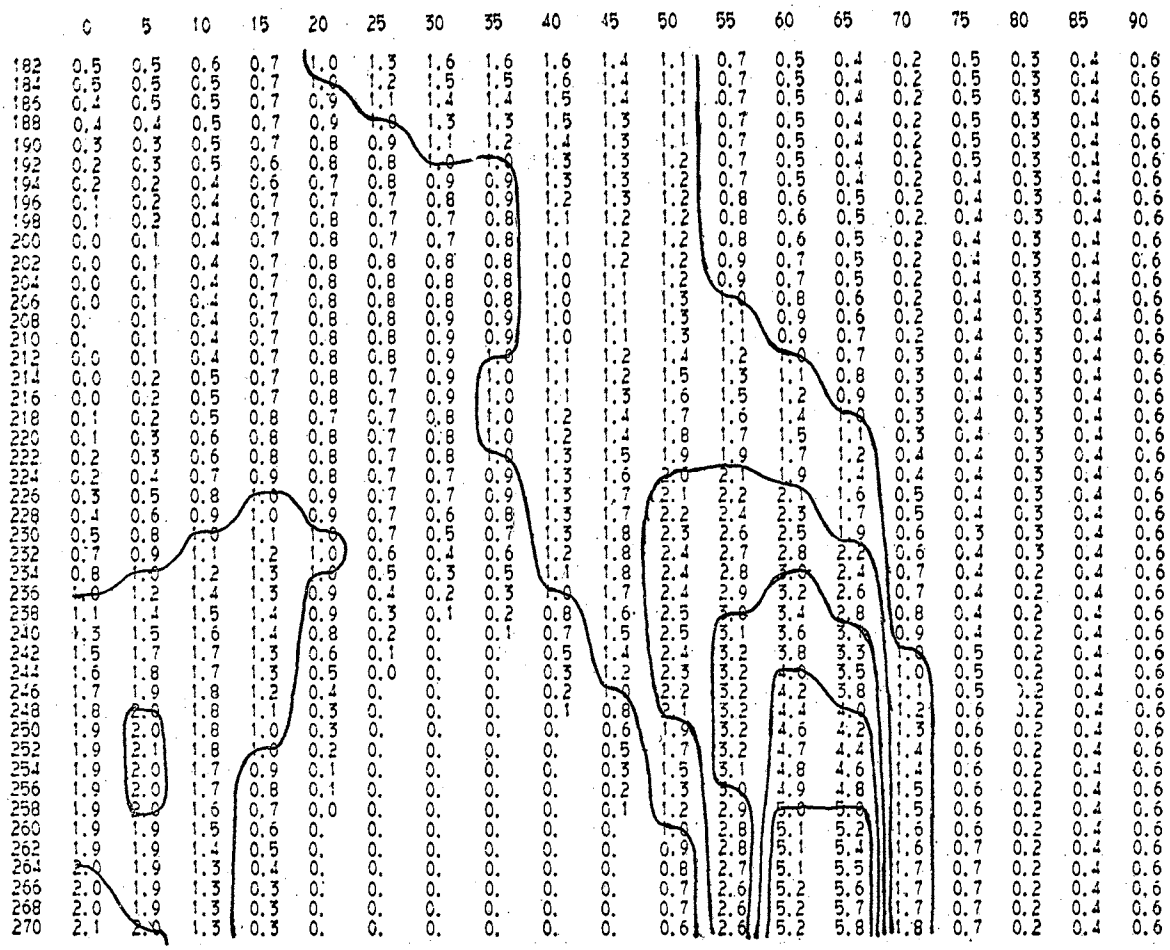

TABLE XXV (Continued)

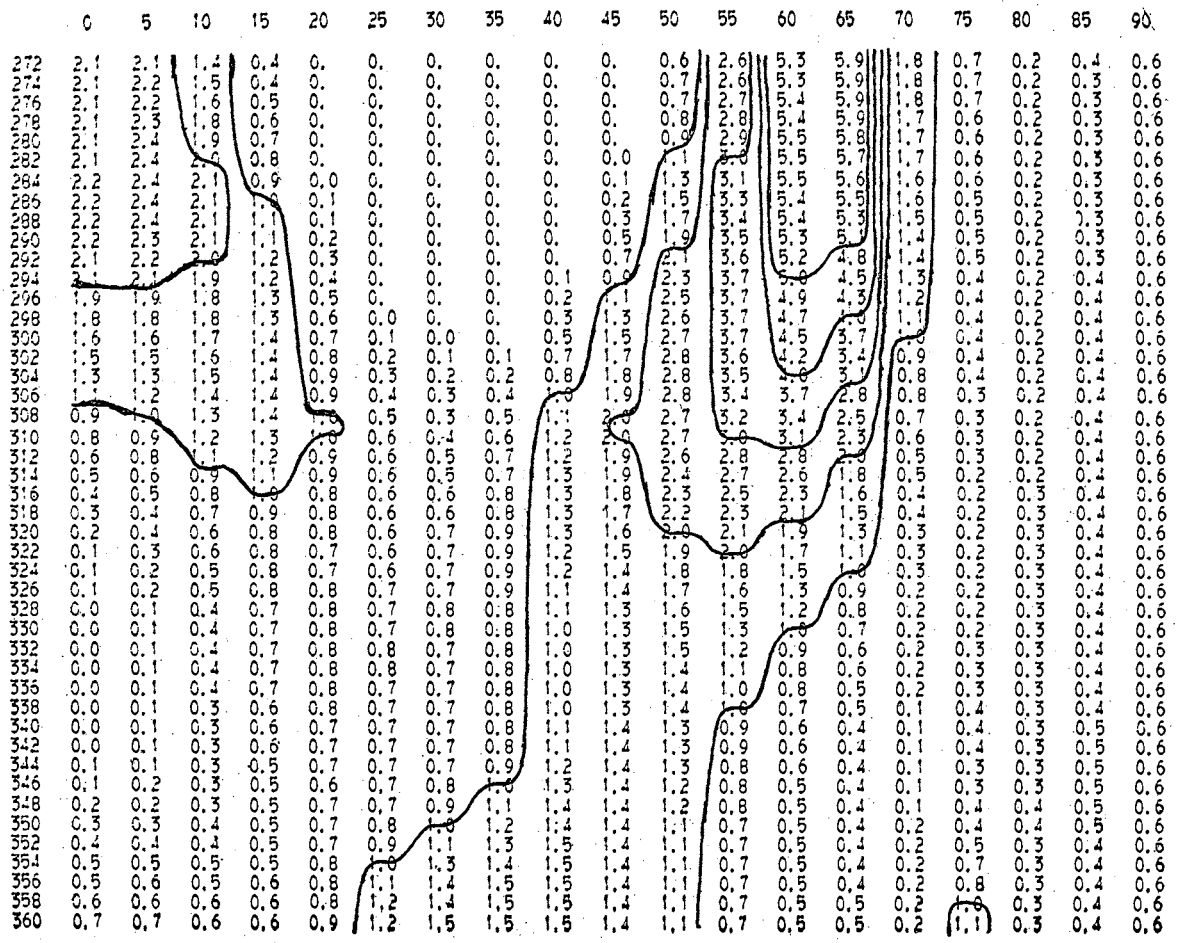

POLE FIGURE DATA SHEET FOR SPECIMEN II-D-2

The normalized pole figure is based on Mo k-alpha radiation and the 111 reflection.

The 222 reflection was used to fill in the blind region from 80 through 90 degrees alpha.

The alpha-dependent two theta shift was taken into account.

Integrated intensities were used.

Normal smoothing was used.

Maximum and minimum corrected intensities are 2065 and 0 counts/second, respectively.

Random intensity is 238 counts/second.

Maximum intensity is 8.65 times random.

Contour spacing is based on multiples of random intensity.

8 contours are to be plotted.

Their values are 1.000 2.000 3.000 4.000 5.000 6.000 7.000 8.000.

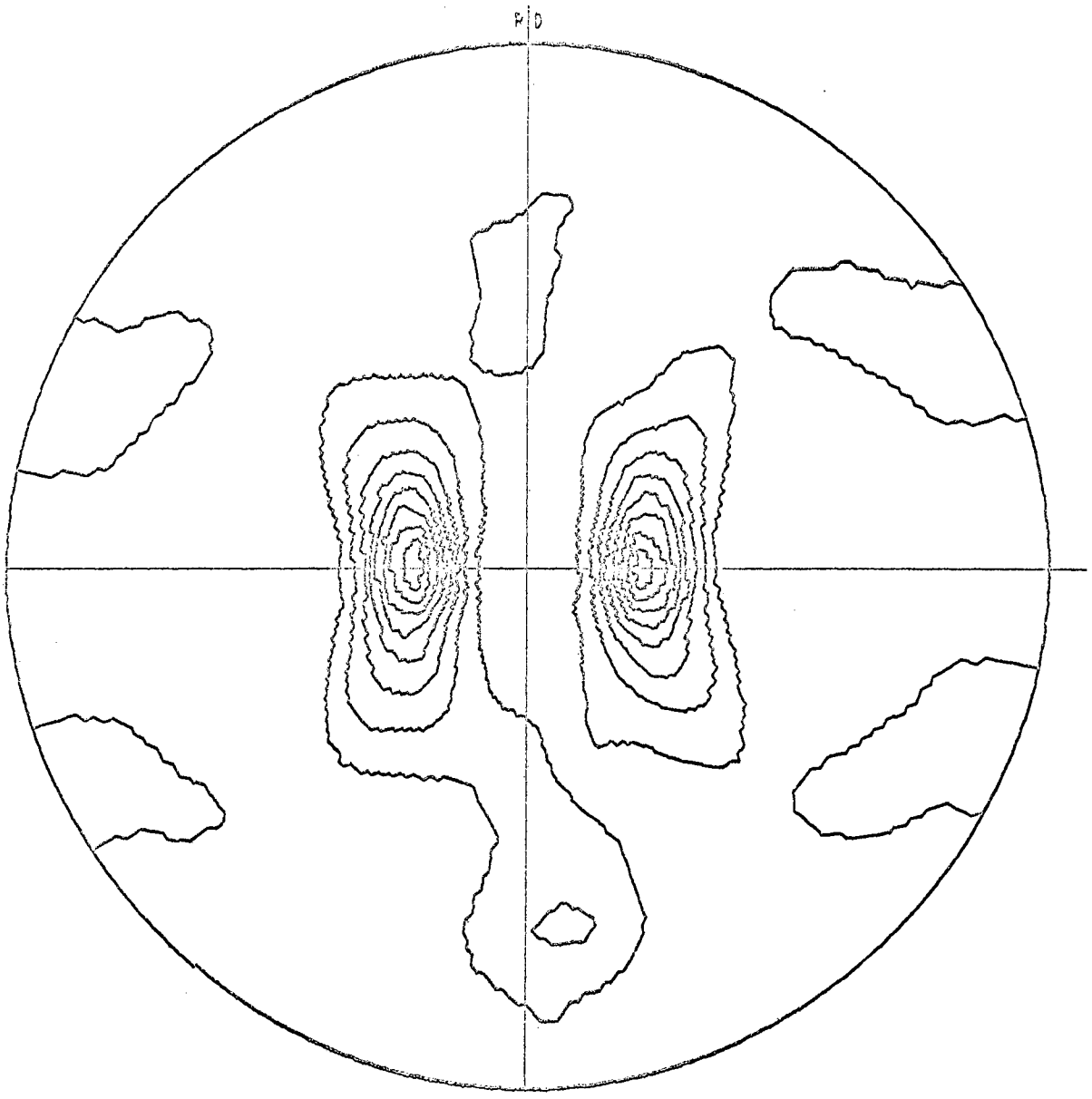

Figure 29. (111) Pole Figure for Specimen II-D-2

TABLE XXVI

POLE FIGURE DATA FOR SPECIMEN II-D-2

	0	5	10	15	20	25	30	35	40	45	50	55	60	65	70	75	80	85	90
2	0.5	0.5	0.7	0.8	0.9	1.0	1.1	1.1	1.1	1.1	0.9	0.8	0.7	0.5	0.5	0.4	0.5	0.6	0.9
4	0.4	0.4	0.6	0.7	0.9	1.0	1.1	1.1	1.1	1.1	0.9	0.8	0.7	0.6	0.5	0.4	0.5	0.6	0.9
6	0.3	0.3	0.5	0.7	0.9	1.0	1.1	1.1	1.1	1.1	0.9	0.8	0.7	0.6	0.5	0.4	0.5	0.6	0.9
8	0.2	0.2	0.3	0.6	0.8	1.0	1.0	1.0	1.1	1.1	0.9	0.8	0.8	0.6	0.5	0.5	0.5	0.6	0.9
10	0.0	0.0	0.2	0.6	0.8	1.0	1.0	1.0	1.1	1.1	0.9	0.8	0.8	0.7	0.5	0.5	0.5	0.6	0.9
12	0.	0.	0.2	0.5	0.8	0.9	0.9	0.9	1.0	1.1	0.9	0.9	0.8	0.7	0.5	0.5	0.5	0.6	0.9
14	0.	0.	0.1	0.5	0.8	0.9	0.8	0.9	1.0	1.0	0.9	0.9	0.8	0.7	0.5	0.5	0.6	0.6	0.9
16	0.	0.	0.1	0.5	0.7	0.8	0.7	0.8	0.9	1.0	1.0	0.9	0.9	0.8	0.6	0.5	0.6	0.6	0.9
18	0.	0.	0.1	0.5	0.7	0.7	0.7	0.7	0.8	1.0	1.0	1.0	0.9	0.8	0.6	0.5	0.5	0.6	0.9
20	0.	0.	0.1	0.5	0.6	0.6	0.6	0.6	0.8	0.9	1.0	1.0	1.0	0.9	0.7	0.5	0.5	0.6	0.9
22	0.	0.	0.1	0.4	0.6	0.5	0.5	0.6	0.7	0.9	1.1	1.1	1.1	0.9	0.7	0.6	0.5	0.7	0.9
24	0.	0.	0.1	0.4	0.5	0.5	0.4	0.5	0.6	0.9	1.1	1.2	1.2	1.0	0.8	0.6	0.5	0.7	0.9
26	0.	0.	0.1	0.4	0.5	0.4	0.4	0.5	0.6	0.9	1.2	1.3	1.3	1.1	0.8	0.6	0.5	0.7	0.9
28	0.	0.	0.1	0.4	0.5	0.4	0.3	0.4	0.6	1.0	1.3	1.5	1.4	1.2	0.9	0.7	0.5	0.7	0.9
30	0.	0.	0.1	0.4	0.4	0.3	0.3	0.4	0.6	1.0	1.4	1.6	1.6	1.3	1.0	0.7	0.5	0.7	0.9
32	0.	0.	0.1	0.4	0.4	0.3	0.3	0.4	0.7	1.1	1.5	1.8	1.8	1.5	1.0	0.8	0.5	0.7	0.9
34	0.	0.	0.1	0.4	0.4	0.3	0.3	0.5	0.8	1.2	1.7	2.0	2.0	1.6	1.1	0.8	0.5	0.7	0.9
36	0.	0.	0.1	0.4	0.4	0.3	0.3	0.5	0.8	1.3	1.8	2.1	2.2	1.7	1.2	0.9	0.5	0.7	0.9
38	0.	0.	0.1	0.4	0.4	0.3	0.3	0.6	1.0	1.4	1.9	2.3	2.4	1.9	1.3	0.9	0.5	0.7	0.9
40	0.	0.	0.2	0.4	0.4	0.3	0.4	0.7	1.1	1.5	2.0	2.5	2.6	2.1	1.4	1.0	0.5	0.7	0.9
42	0.	0.	0.2	0.5	0.4	0.4	0.4	0.7	1.2	1.6	2.2	2.7	2.9	2.3	1.5	1.0	0.5	0.7	0.9
44	0.	0.	0.3	0.6	0.5	0.4	0.4	0.8	1.2	1.7	2.2	2.9	3.2	2.6	1.6	1.0	0.5	0.7	0.9
46	0.	0.1	0.4	0.6	0.6	0.4	0.4	0.8	1.3	1.8	2.3	3.0	3.5	2.8	1.8	1.1	0.4	0.7	0.9
48	0.1	0.2	0.5	0.7	0.6	0.5	0.4	0.8	1.3	1.9	2.4	3.2	3.8	3.1	1.9	1.1	0.4	0.7	0.9
50	0.2	0.3	0.7	0.8	0.7	0.5	0.4	0.8	1.3	1.9	2.5	3.4	4.1	3.4	2.1	1.2	0.4	0.7	0.9
52	0.3	0.4	0.8	0.9	0.7	0.5	0.4	0.7	1.3	1.9	2.6	3.6	4.5	3.8	2.2	1.2	0.4	0.7	0.9
54	0.4	0.6	1.0	1.0	0.7	0.4	0.3	0.7	1.2	1.9	2.7	3.7	4.8	4.1	2.2	1.3	0.4	0.6	0.9
56	0.6	0.7	1.1	1.1	0.7	0.4	0.3	0.5	1.1	1.9	2.7	3.8	5.1	4.5	2.6	1.4	0.4	0.6	0.9
58	0.7	0.9	1.2	1.1	0.7	0.3	0.2	0.4	1.0	1.9	2.7	3.9	5.3	4.8	2.9	1.5	0.4	0.6	0.9
60	0.9	1.0	1.3	1.1	0.6	0.2	0.1	0.3	0.8	1.8	2.7	4.0	5.6	5.2	3.2	1.5	0.3	0.6	0.9
62	1.0	1.1	1.3	1.1	0.5	0.1	0.	0.2	0.7	1.6	2.7	4.0	5.8	5.6	3.4	1.6	0.3	0.6	0.9
64	1.2	1.2	1.4	1.0	0.4	0.1	0.	0.1	0.5	1.4	2.6	4.0	6.0	5.9	3.7	1.7	0.3	0.6	0.9
66	1.3	1.3	1.4	1.0	0.3	0.	0.	0.	0.4	1.2	2.4	4.0	6.1	6.3	3.9	1.7	0.3	0.6	0.9
68	1.4	1.4	1.4	0.9	0.3	0.	0.	0.	0.2	1.0	2.2	3.9	6.3	6.7	4.2	1.8	0.3	0.6	0.9
70	1.5	1.4	1.3	0.8	0.2	0.	0.	0.	0.1	0.8	2.0	3.8	6.4	7.0	4.4	1.8	0.3	0.6	0.9
72	1.5	1.4	1.3	0.7	0.1	0.	0.	0.	0.0	0.7	1.8	3.7	6.5	7.4	4.7	1.9	0.3	0.6	0.9
74	1.4	1.3	1.2	0.6	0.1	0.	0.	0.	0.	0.5	1.6	3.6	6.6	7.7	4.9	2.0	0.3	0.6	0.9
76	1.2	1.2	1.0	0.5	0.0	0.	0.	0.	0.	0.3	1.4	3.4	6.6	7.9	5.1	2.0	0.3	0.6	0.9
78	1.0	1.0	0.9	0.4	0.0	0.	0.	0.	0.	0.2	1.2	3.3	6.7	8.2	5.3	2.1	0.3	0.6	0.9
80	0.8	0.8	0.8	0.3	0.	0.	0.	0.	0.	0.1	1.1	3.2	6.7	8.3	5.4	2.2	0.3	0.6	0.9
82	0.6	0.7	0.6	0.2	0.	0.	0.	0.	0.	0.1	0.9	3.1	6.7	8.4	5.6	2.2	0.3	0.6	0.9
84	0.5	0.5	0.5	0.2	0.	0.	0.	0.	0.	0.0	0.8	3.0	6.7	8.5	5.7	2.3	0.3	0.6	0.9
86	0.3	0.4	0.4	0.1	0.	0.	0.	0.	0.	0.	0.7	2.9	6.7	8.6	5.7	2.3	0.3	0.6	0.9
88	0.2	0.3	0.3	0.1	0.	0.	0.	0.	0.	0.	0.7	2.8	6.7	8.6	5.8	2.3	0.2	0.6	0.9
90	0.2	0.2	0.3	0.0	0.	0.	0.	0.	0.	0.	0.6	2.8	6.6	8.6	5.8	2.3	0.2	0.6	0.9

TABLE XXVI (Continued)

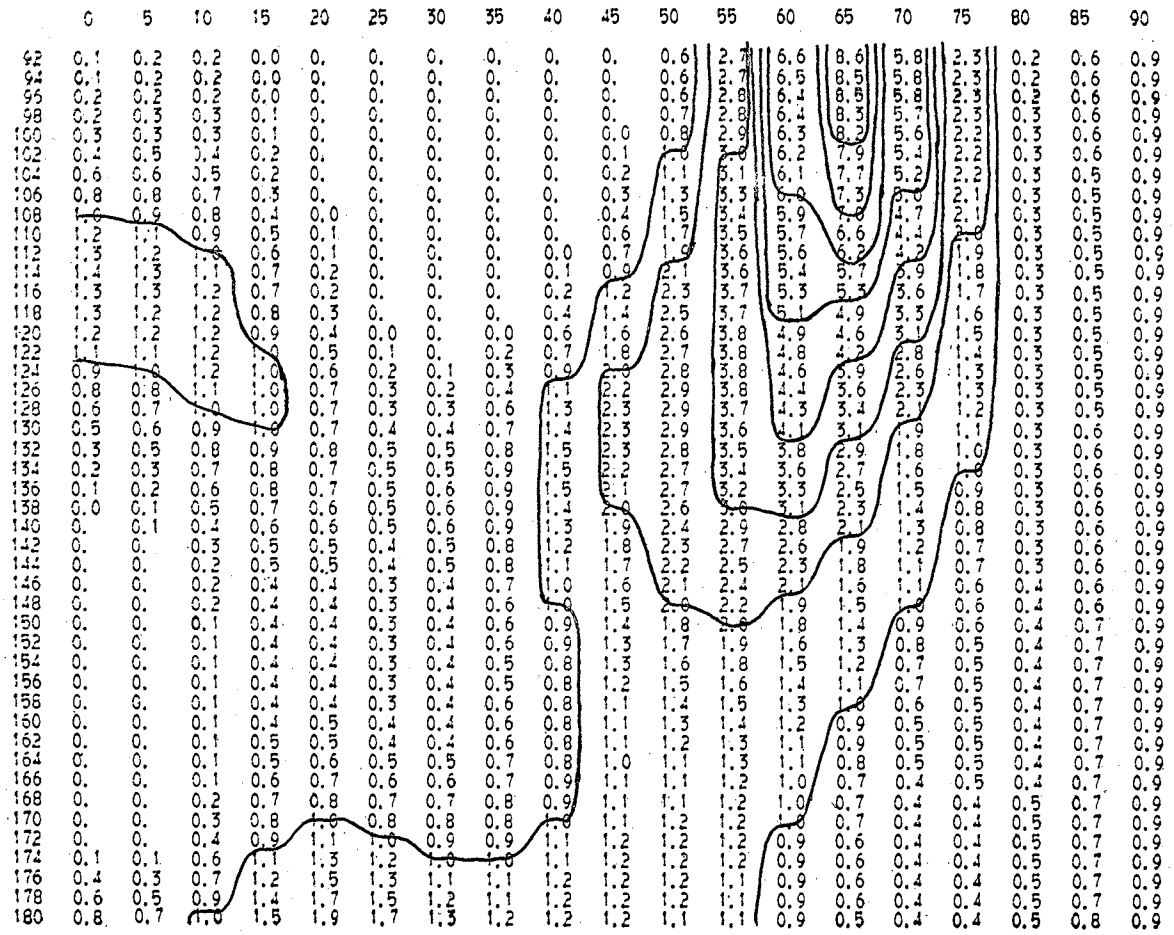

TABLE XXVI (Continued)

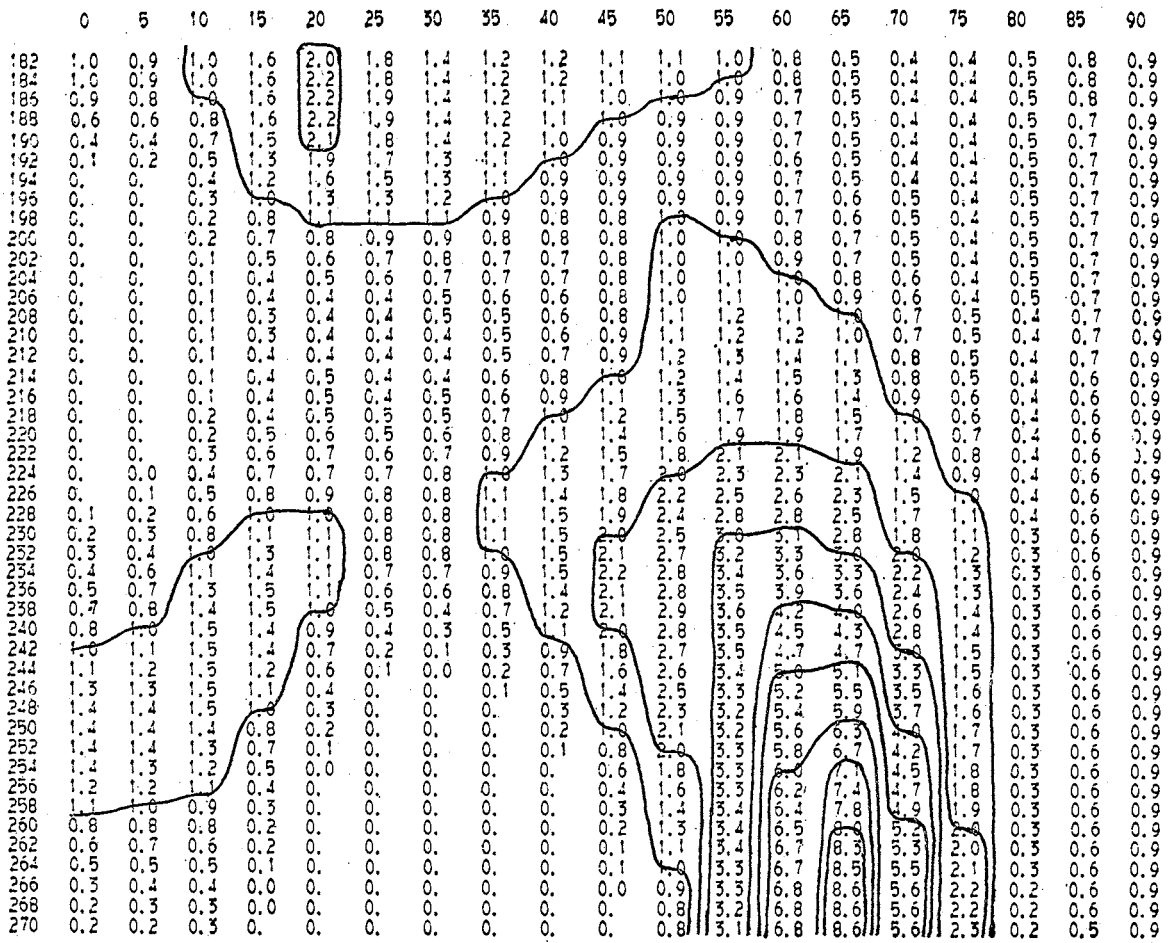

TABLE XXVI (Continued)

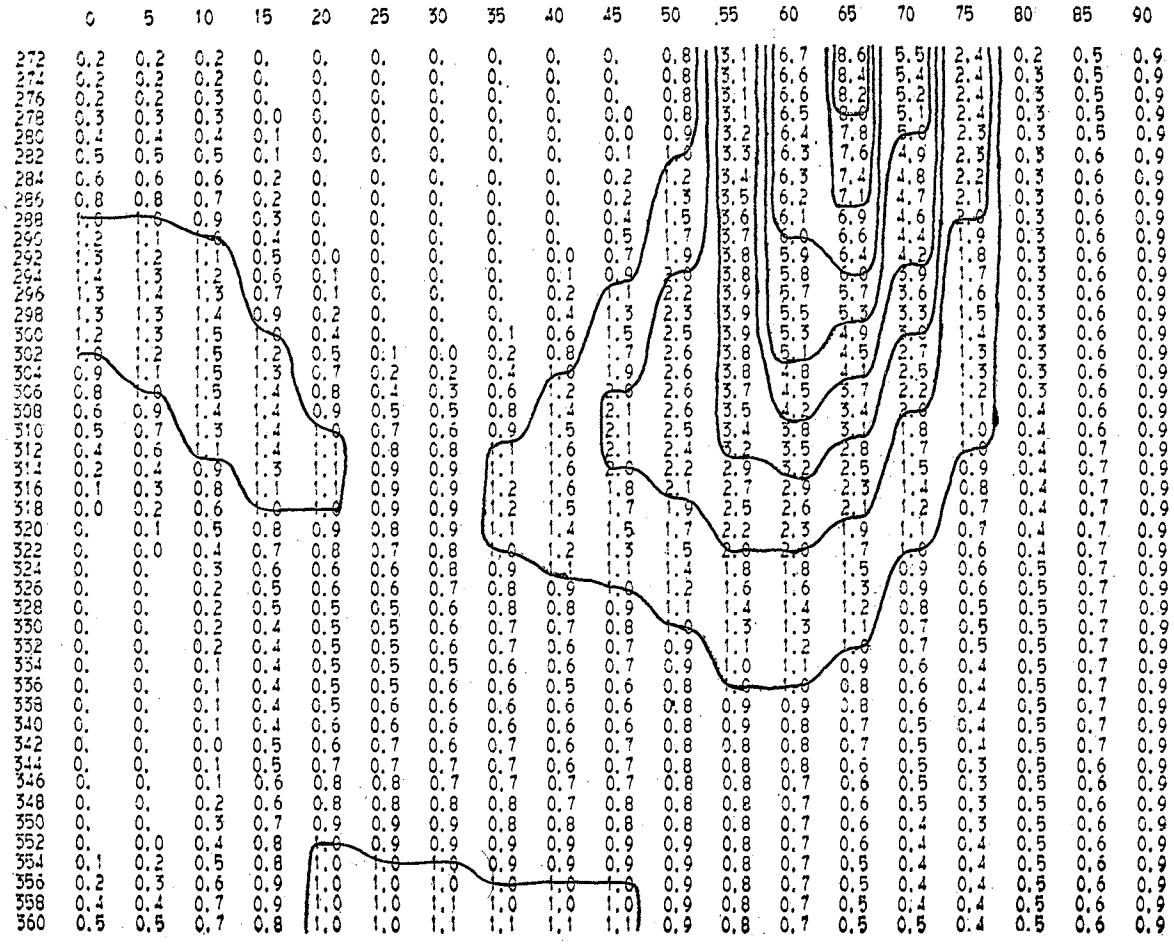

POLE FIGURE DATA SHEET FOR SPECIMEN 2A

The normalized pole figure is based on Mo k-alpha radiation and the 111 reflection.

The 222 reflection was used to fill in the blind region from 80 through 90 degrees alpha.

The alpha-dependent two theta shift was taken into account.

Integrated intensities were used.

Normal smoothing was used.

Maximum and minimum corrected intensities are 2207 and 0 counts/second, respectively.

Random intensity is 477 counts/second.

Contour spacing is based on multiples of random intensity.

4 contours are to be plotted.

Their values are 1.000 2.000 3.000 4.000.

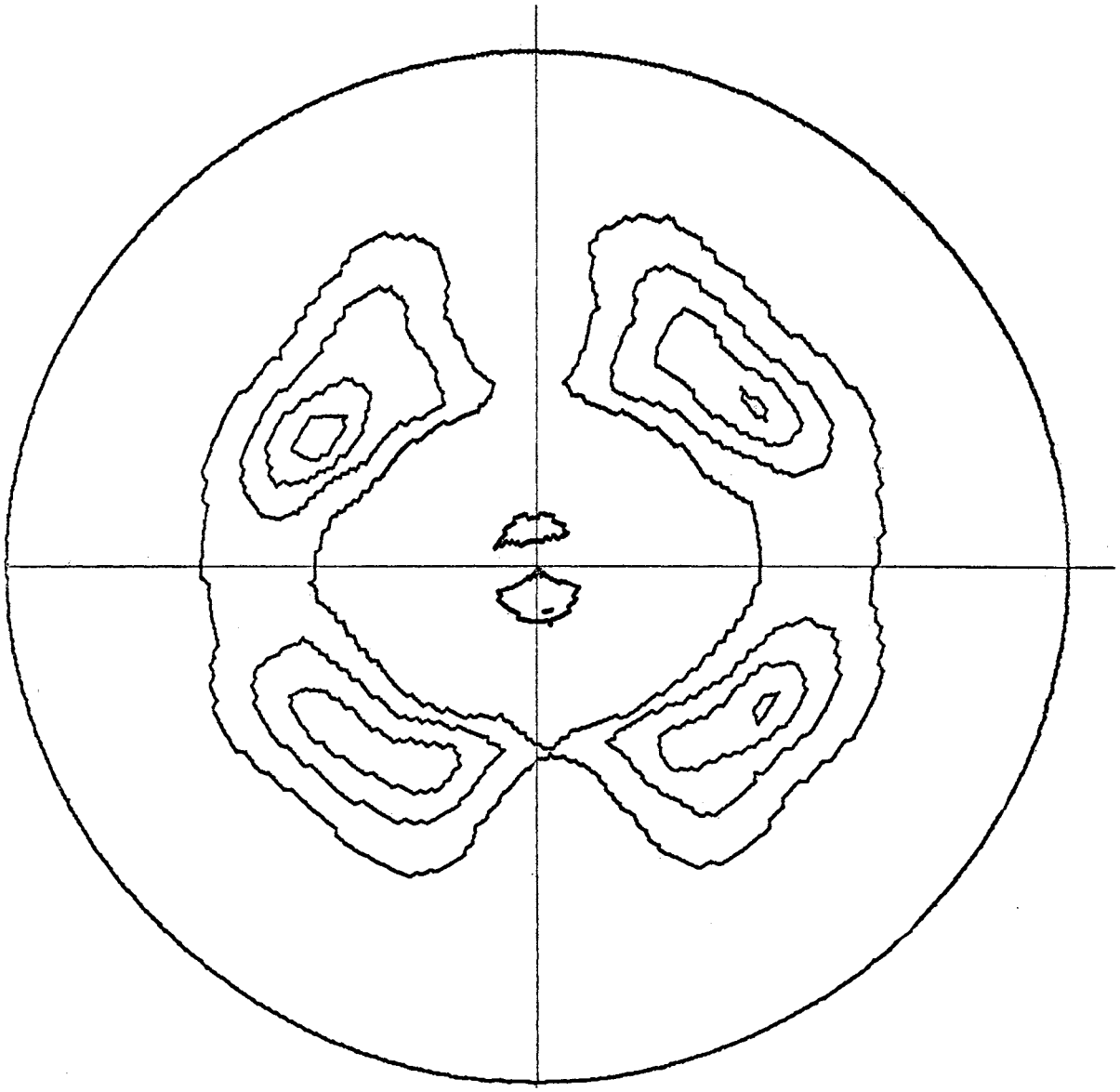

Figure 30. (111) Pole Figure for Specimen 2A

TABLE XXVII

POLE FIGURE DATA FOR SPECIMEN 2A

	0	5	10	15	20	25	30	35	40	45	50	55	60	65	70	75	80	85	9
2	0.5	0.7	0.6	0.6	0.7	0.6	0.5	0.4	0.4	0.4	0.6	0.7	1.0	0.7	0.5	0.5	1.2	1.0	0.
4	0.7	0.7	0.6	0.6	0.6	0.6	0.5	0.4	0.4	0.4	0.6	0.7	1.0	0.7	0.5	0.5	1.2	1.0	0.
6	0.6	0.7	0.6	0.6	0.6	0.6	0.5	0.4	0.4	0.4	0.7	0.7	1.0	0.7	0.5	0.5	1.2	1.0	0.
8	0.6	0.7	0.6	0.6	0.6	0.7	0.6	0.4	0.5	0.5	0.7	0.7	1.0	0.7	0.5	0.4	1.3	1.0	0.
10	0.6	0.6	0.7	0.6	0.6	0.7	0.6	0.5	0.5	0.6	0.8	0.7	1.0	0.7	0.5	0.4	1.4	0.9	0.
12	0.5	0.6	0.7	0.6	0.7	0.8	0.7	0.6	0.6	0.7	0.9	0.8	0.9	0.7	0.5	0.4	1.4	0.9	0.
14	0.5	0.6	0.7	0.7	0.7	0.9	0.8	0.6	0.7	0.8	1.1	0.8	0.9	0.7	0.5	0.4	1.5	0.9	0.
16	0.4	0.5	0.7	0.7	0.8	1.0	0.9	0.8	0.8	0.9	1.2	0.8	0.9	0.7	0.5	0.4	1.5	0.9	0.
18	0.4	0.5	0.7	0.7	0.9	1.1	1.1	0.9	1.0	1.1	1.4	0.9	0.9	0.7	0.5	0.4	1.5	0.9	0.
20	0.3	0.4	0.7	0.8	1.0	1.3	1.3	1.1	1.2	1.3	1.5	0.9	0.9	0.7	0.5	0.4	1.5	0.9	0.
22	0.2	0.3	0.6	0.8	1.0	1.5	1.6	1.3	1.4	1.5	1.7	0.9	0.8	0.7	0.5	0.4	1.5	1.0	0.
24	0.2	0.3	0.6	0.8	1.1	1.6	1.8	1.5	1.7	1.7	1.8	0.9	0.8	0.7	0.5	0.4	1.4	1.0	0.
26	0.1	0.2	0.5	0.8	1.1	1.8	2.1	1.8	1.9	1.9	1.9	0.9	0.7	0.6	0.5	0.4	1.4	1.0	0.
28	0.1	0.1	0.5	0.8	1.1	1.9	2.4	2.0	2.2	2.1	2.0	0.8	0.7	0.6	0.4	0.4	1.4	1.0	0.
30	0.0	0.1	0.4	0.7	1.1	2.0	2.6	2.3	2.4	2.3	2.0	0.8	0.6	0.6	0.4	0.3	1.3	1.0	0.
32	0.	0.0	0.4	0.7	1.0	2.0	2.7	2.5	2.6	2.4	2.1	0.7	0.6	0.6	0.4	0.3	1.3	1.0	0.
34	0.	0.0	0.3	0.6	1.0	1.9	2.8	2.7	2.7	2.5	2.1	0.7	0.5	0.6	0.4	0.3	1.3	1.0	0.
36	0.	0.	0.3	0.6	0.9	1.8	2.8	2.8	2.8	2.6	2.1	0.6	0.5	0.6	0.4	0.3	1.2	0.9	0.
38	0.	0.	0.2	0.5	0.8	1.7	2.8	2.8	2.8	2.6	2.0	0.5	0.5	0.6	0.4	0.3	1.2	0.9	0.
40	0.	0.	0.2	0.5	0.7	1.5	2.7	2.9	2.9	2.6	1.9	0.5	0.5	0.5	0.4	0.3	1.2	0.9	0.
42	0.	0.	0.2	0.4	0.7	1.4	2.5	2.9	3.0	2.6	1.9	0.5	0.5	0.5	0.4	0.3	1.2	0.9	0.
44	0.	0.	0.2	0.4	0.6	1.3	2.4	3.0	3.1	2.6	1.8	0.5	0.5	0.5	0.4	0.3	1.2	0.9	0.
46	0.	0.	0.2	0.4	0.6	1.2	2.4	3.1	3.3	2.6	1.7	0.4	0.5	0.5	0.4	0.3	1.1	0.8	0.
48	0.	0.	0.2	0.4	0.5	1.1	2.3	3.2	3.6	2.7	1.7	0.4	0.5	0.5	0.4	0.3	1.1	0.8	0.
50	0.	0.0	0.2	0.4	0.5	1.1	2.3	3.4	3.9	2.7	1.6	0.4	0.5	0.4	0.4	0.3	1.1	0.8	0.
52	0.0	0.0	0.3	0.4	0.6	1.1	2.4	3.6	4.2	2.8	1.6	0.4	0.5	0.4	0.4	0.3	1.1	0.8	0.
54	0.0	0.1	0.3	0.4	0.6	1.1	2.5	3.8	4.4	2.8	1.6	0.4	0.5	0.4	0.4	0.3	1.1	0.8	0.
56	0.1	0.1	0.4	0.4	0.6	1.2	2.7	4.0	4.6	2.8	1.5	0.4	0.5	0.4	0.3	0.3	1.1	0.8	0.
58	0.1	0.1	0.5	0.5	0.7	1.2	2.8	4.2	4.6	2.8	1.5	0.4	0.4	0.4	0.3	0.2	1.1	0.8	0.
60	0.1	0.2	0.5	0.5	0.7	1.3	2.9	4.2	4.5	2.6	1.4	0.3	0.4	0.4	0.3	0.2	1.0	0.7	0.
62	0.1	0.2	0.5	0.5	0.8	1.3	2.9	4.2	4.3	2.4	1.4	0.3	0.4	0.4	0.3	0.2	1.0	0.7	0.
64	0.1	0.2	0.5	0.6	0.8	1.3	2.9	4.1	4.0	2.2	1.3	0.3	0.4	0.4	0.3	0.2	1.0	0.7	0.
66	0.2	0.2	0.6	0.6	0.8	1.3	2.8	3.9	3.6	1.9	1.2	0.3	0.4	0.3	0.3	0.2	1.0	0.7	0.
68	0.2	0.2	0.6	0.6	0.8	1.3	2.7	3.6	3.2	1.7	1.1	0.3	0.4	0.3	0.3	0.2	1.0	0.7	0.
70	0.2	0.2	0.6	0.7	0.8	1.3	2.5	3.4	2.9	1.5	1.0	0.3	0.4	0.3	0.3	0.2	0.9	0.7	0.
72	0.2	0.2	0.6	0.7	0.7	1.2	2.3	3.1	2.6	1.3	0.9	0.2	0.3	0.4	0.3	0.2	0.9	0.7	0.
74	0.2	0.2	0.6	0.7	0.7	1.2	2.1	2.8	2.3	1.2	0.8	0.2	0.3	0.4	0.3	0.2	0.9	0.7	0.
76	0.2	0.2	0.6	0.7	0.7	1.1	1.9	2.5	2.1	1.1	0.7	0.2	0.3	0.4	0.3	0.2	0.9	0.7	0.
78	0.1	0.2	0.6	0.7	0.7	1.1	1.7	2.2	1.9	1.1	0.7	0.2	0.3	0.4	0.3	0.2	0.9	0.7	0.
80	0.1	0.2	0.6	0.6	0.7	1.1	1.6	2.0	1.8	1.1	0.7	0.2	0.3	0.4	0.3	0.2	0.8	0.6	0.
82	0.1	0.2	0.5	0.6	0.6	1.0	1.5	1.8	1.7	1.1	0.7	0.1	0.2	0.4	0.3	0.2	0.8	0.6	0.
84	0.1	0.2	0.5	0.6	0.6	1.0	1.4	1.6	1.6	1.0	0.7	0.1	0.2	0.4	0.3	0.2	0.8	0.6	0.
86	0.1	0.1	0.5	0.6	0.6	1.0	1.4	1.5	1.6	1.0	0.7	0.1	0.2	0.3	0.3	0.2	0.8	0.6	0.
88	0.1	.1	0.5	0.6	0.6	1.0	1.4	1.4	1.5	0.9	0.7	0.1	0.2	0.3	0.3	0.2	0.8	0.6	0.
90	0.1	.1	0.5	0.6	0.6	1.0	1.4	1.4	1.5	0.9	0.7	0.1	0.2	0.3	0.3	0.2	0.8	0.6	0.

TABLE XXVII (Continued)

	0	5	10	15	20	25	30	35	40	45	50	55	60	65	70	75	80	85	9
92	0.1	0.1	0.5	0.6	0.6	1.0	1.4	1.4	1.5	0.9	0.7	0.1	0.2	0.3	0.3	0.2	0.8	0.6	0.
94	0.1	0.1	0.5	0.6	0.6	1.0	1.4	1.4	1.4	0.9	0.7	0.1	0.2	0.3	0.3	0.2	0.8	0.6	0.
96	0.1	0.1	0.5	0.6	0.6	0.9	1.5	1.4	1.5	0.9	0.7	0.1	0.2	0.3	0.3	0.2	0.8	0.6	0.
98	0.1	0.1	0.5	0.6	0.6	0.9	1.5	1.5	1.5	1.0	0.7	0.1	0.2	0.3	0.3	0.2	0.8	0.7	0.
100	0.1	0.1	0.6	0.7	0.6	0.9	1.5	1.5	1.6	1.0	0.8	0.1	0.2	0.3	0.3	0.2	0.8	0.7	0.
102	0.1	0.1	0.6	0.7	0.6	0.9	1.5	1.6	1.7	1.1	0.8	0.1	0.2	0.3	0.3	0.2	0.8	0.7	0.
104	0.1	0.2	0.6	0.7	0.6	1.0	1.6	1.7	1.8	1.2	0.8	0.1	0.2	0.3	0.3	0.2	0.8	0.7	0.
106	0.1	0.2	0.6	0.7	0.7	1.0	1.7	1.8	1.9	1.3	0.8	0.1	0.2	0.3	0.3	0.2	0.8	0.7	0.
108	0.1	0.2	0.7	0.7	0.7	1.1	1.8	2.0	2.1	1.4	0.8	0.1	0.3	0.3	0.3	0.2	0.8	0.8	0.
110	0.1	0.2	0.7	0.7	0.7	1.2	2.0	2.2	2.3	1.6	0.9	0.1	0.3	0.3	0.3	0.2	0.8	0.8	0.
112	0.1	0.2	0.7	0.8	0.8	1.3	2.2	2.4	2.4	1.7	0.9	0.2	0.3	0.3	0.3	0.2	0.8	0.8	0.
114	0.1	0.2	0.7	0.8	0.8	1.3	2.3	2.6	2.6	1.8	1.0	0.2	0.3	0.3	0.3	0.2	0.9	0.8	0.
116	0.1	0.2	0.7	0.8	0.8	1.4	2.5	2.9	2.7	1.9	1.0	0.2	0.3	0.4	0.3	0.2	0.9	0.8	0.
118	0.1	0.2	0.7	0.8	0.8	1.4	2.6	3.1	2.8	2.0	1.1	0.2	0.4	0.4	0.3	0.2	1.0	0.8	0.
120	0.1	0.2	0.7	0.9	0.8	1.4	2.6	3.3	3.0	2.1	1.2	0.3	0.4	0.4	0.3	0.2	1.0	0.8	0.
122	0.1	0.2	0.7	0.8	0.8	1.3	2.6	3.4	3.1	2.2	1.2	0.3	0.4	0.4	0.3	0.2	1.0	0.8	0.
124	0.1	0.2	0.6	0.8	0.8	1.3	2.6	3.5	3.2	2.3	1.3	0.3	0.4	0.4	0.3	0.2	1.1	0.9	0.
126	0.1	0.2	0.5	0.8	0.8	1.2	2.5	3.5	3.3	2.3	1.3	0.3	0.4	0.4	0.3	0.2	1.1	0.9	0.
128	0.1	0.2	0.5	0.7	0.7	1.2	2.4	3.5	3.4	2.4	1.3	0.3	0.4	0.4	0.3	0.2	1.1	0.9	0.
130	0.0	0.1	0.4	0.7	0.7	1.1	2.3	3.4	3.5	2.5	1.3	0.3	0.4	0.4	0.3	0.2	1.2	1.0	0.
132	0.0	0.1	0.4	0.6	0.7	1.1	2.2	3.4	3.6	2.5	1.3	0.3	0.4	0.4	0.3	0.2	1.2	1.0	0.
134	0.	0.1	0.3	0.6	0.7	1.1	2.2	3.3	3.6	2.6	1.4	0.3	0.4	0.4	0.3	0.2	1.3	1.0	0.
136	0.	0.0	0.3	0.5	0.7	1.0	2.1	3.2	3.6	2.6	1.4	0.3	0.4	0.4	0.3	0.2	1.3	1.0	0.
138	0.	0.0	0.3	0.5	0.7	1.0	2.1	3.1	3.6	2.7	1.5	0.4	0.4	0.5	0.4	0.2	1.4	1.1	0.
140	0.	0.	0.3	0.5	0.6	1.1	2.0	3.0	3.6	2.8	1.7	0.4	0.4	0.5	0.4	0.2	1.4	1.1	0.
142	0.	0.	0.2	0.5	0.6	1.1	2.0	3.0	3.6	2.9	1.8	0.5	0.4	0.5	0.4	0.2	1.4	1.1	0.
144	0.	0.	0.2	0.5	0.7	1.1	2.0	2.9	3.6	3.0	2.0	0.5	0.4	0.5	0.4	0.2	1.4	1.1	0.
146	0.	0.	0.3	0.5	0.7	1.1	2.0	2.9	3.6	3.2	2.2	0.6	0.4	0.5	0.4	0.2	1.4	1.1	0.
148	0.	0.	0.3	0.6	0.7	1.1	1.9	2.8	3.6	3.3	2.3	0.7	0.5	0.5	0.4	0.2	1.4	1.1	0.
150	0.	0.	0.3	0.6	0.7	1.2	1.9	2.8	3.6	3.4	2.5	0.8	0.5	0.6	0.4	0.2	1.4	1.1	0.
152	0.	0.0	0.3	0.6	0.8	1.2	1.9	2.7	3.5	3.4	2.6	0.9	0.5	0.6	0.4	0.2	1.4	1.1	0.
154	0.	0.0	0.4	0.7	0.8	1.1	1.8	2.5	3.4	3.4	2.7	0.9	0.6	0.6	0.4	0.2	1.4	1.1	0.
156	0.	0.1	0.5	0.7	0.8	1.1	1.7	2.4	3.2	3.3	2.8	1.0	0.6	0.6	0.4	0.2	1.5	1.1	0.
158	0.0	0.1	0.5	0.7	0.8	1.1	1.6	2.1	2.9	3.1	2.8	1.1	0.7	0.6	0.4	0.2	1.5	1.1	0.
160	0.1	0.2	0.6	0.7	0.7	1.0	1.5	1.9	2.6	2.9	2.8	1.1	0.7	0.6	0.4	0.3	1.5	1.1	0.
162	0.1	0.2	0.6	0.7	0.7	0.9	1.4	1.7	2.3	2.6	2.7	1.1	0.7	0.6	0.4	0.3	1.6	1.2	0.
164	0.2	0.3	0.7	0.7	0.7	0.8	1.2	1.4	1.9	2.3	2.6	1.1	0.8	0.6	0.4	0.3	1.7	1.2	0.
166	0.2	0.3	0.8	0.7	0.6	0.8	1.0	1.2	1.6	2.0	2.4	1.1	0.8	0.6	0.4	0.3	1.7	1.2	0.
168	0.3	0.4	0.8	0.7	0.5	0.7	0.9	1.0	1.3	1.7	2.2	1.1	0.8	0.6	0.4	0.3	1.7	1.2	0.
170	0.4	0.5	0.8	0.7	0.5	0.6	0.7	0.8	1.1	1.5	2.0	1.1	0.8	0.6	0.4	0.3	1.8	1.2	0.
172	0.4	0.6	0.8	0.7	0.4	0.5	0.6	0.7	0.9	1.3	1.8	1.0	0.8	0.6	0.4	0.3	1.8	1.2	0.
174	0.5	0.6	0.8	0.7	0.4	0.5	0.5	0.6	0.8	1.1	1.6	1.0	0.8	0.6	0.4	0.3	1.8	1.3	0.
176	0.5	0.7	0.8	0.6	0.4	0.4	0.5	0.5	0.7	0.9	1.4	0.9	0.8	0.6	0.4	0.3	1.8	1.3	0.
178	0.6	0.7	0.8	0.6	0.4	0.4	0.4	0.4	0.6	0.8	1.2	0.9	0.8	0.6	0.4	0.3	1.8	1.3	0.
180	0.6	0.7	0.8	0.6	0.4	0.4	0.4	0.4	0.6	0.8	1.1	0.8	0.8	0.6	0.4	0.3	1.8	1.3	0.

TABLE XXVII (Continued)

	0	5	10	15	20	25	30	35	40	45	50	55	60	65	70	75	80	85	9
182	0.6	0.8	0.8	0.6	0.4	0.4	0.4	0.4	0.5	0.7	1.1	0.8	0.8	0.6	0.4	0.3	1.9	1.3	0.
184	0.6	0.8	0.8	0.6	0.4	0.4	0.4	0.4	0.5	0.7	1.1	0.9	0.8	0.6	0.4	0.3	1.9	1.3	0.
186	0.6	0.8	0.8	0.6	0.4	0.4	0.4	0.4	0.5	0.7	1.1	0.9	0.8	0.6	0.4	0.3	2.0	1.3	0.
188	0.6	0.7	0.8	0.6	0.4	0.4	0.4	0.4	0.5	0.7	1.1	0.9	0.8	0.6	0.4	0.3	2.0	1.3	0.
190	0.5	0.7	0.8	0.6	0.5	0.4	0.4	0.4	0.6	0.8	1.2	0.9	0.8	0.6	0.3	0.3	2.1	1.3	0.
192	0.5	0.6	0.8	0.6	0.5	0.5	0.5	0.5	0.7	0.9	1.3	1.0	0.8	0.6	0.3	0.3	2.1	1.3	0.
194	0.4	0.6	0.8	0.7	0.6	0.5	0.6	0.6	0.8	1.0	1.4	1.0	0.8	0.6	0.3	0.3	2.1	1.3	0.
196	0.4	0.5	0.8	0.7	0.6	0.6	0.7	0.7	0.9	1.1	1.6	1.0	0.8	0.6	0.3	0.3	2.1	1.3	0.
198	0.3	0.4	0.8	0.7	0.6	0.7	0.8	0.8	1.1	1.2	1.7	0.9	0.8	0.6	0.3	0.3	2.0	1.3	0.
200	0.3	0.4	0.7	0.7	0.7	0.7	0.9	1.0	1.3	1.4	1.9	0.9	0.7	0.6	0.3	0.2	2.0	1.3	0.
202	0.2	0.3	0.7	0.7	0.7	0.8	1.0	1.1	1.5	1.7	2.1	0.8	0.7	0.6	0.3	0.2	1.9	1.3	0.
204	0.2	0.2	0.6	0.7	0.7	0.9	1.2	1.3	1.8	1.9	2.3	0.8	0.7	0.6	0.3	0.2	1.9	1.3	0.
206	0.1	0.2	0.5	0.7	0.7	1.0	1.3	1.5	2.1	2.2	2.5	0.7	0.6	0.5	0.3	0.2	1.8	1.2	0.
208	0.1	0.1	0.5	0.7	0.8	1.2	1.5	1.8	2.4	2.5	2.6	0.6	0.6	0.5	0.3	0.2	1.8	1.2	0.
210	0.0	0.1	0.4	0.7	0.8	1.3	1.8	2.0	2.7	2.7	2.7	0.5	0.5	0.5	0.3	0.2	1.7	1.2	0.
212	0.	0.0	0.4	0.6	0.8	1.3	1.9	2.2	2.9	2.9	2.7	0.5	0.5	0.5	0.3	0.2	1.7	1.2	0.
214	0.	0.0	0.3	0.6	0.9	1.4	2.1	2.4	3.2	3.1	2.6	0.4	0.5	0.5	0.3	0.2	1.6	1.2	0.
216	0.	0.	0.3	0.6	0.9	1.4	2.2	2.6	3.4	3.2	2.5	0.4	0.5	0.5	0.3	0.2	1.5	1.2	0.
218	0.	0.	0.3	0.6	0.9	1.4	2.3	2.7	3.5	3.2	2.4	0.4	0.5	0.5	0.3	0.2	1.5	1.1	0.
220	0.	0.	0.3	0.6	0.8	1.3	2.3	2.8	3.6	3.2	2.3	0.4	0.5	0.5	0.3	0.2	1.4	1.1	0.
222	0.	0.	0.3	0.6	0.8	1.3	2.3	2.9	3.6	3.1	2.1	0.4	0.5	0.5	0.3	0.2	1.4	1.1	0.
224	0.	0.	0.4	0.6	0.8	1.2	2.2	3.0	3.6	3.0	1.9	0.4	0.5	0.4	0.3	0.2	1.3	1.1	0.
226	0.	0.0	0.4	0.6	0.8	1.2	2.2	3.1	3.7	2.9	1.8	0.3	0.4	0.4	0.3	0.2	1.3	1.1	0.
228	0.	0.0	0.4	0.6	0.7	1.1	2.2	3.3	3.7	2.8	1.6	0.3	0.4	0.4	0.3	0.2	1.2	1.0	0.
230	0.	0.1	0.5	0.6	0.7	1.2	2.3	3.5	3.7	2.7	1.5	0.3	0.4	0.4	0.3	0.2	1.2	1.0	0.
232	0.	0.1	0.5	0.6	0.7	1.2	2.4	3.8	3.8	2.5	1.4	0.3	0.4	0.5	0.3	0.2	1.2	1.0	0.
234	0.0	0.1	0.6	0.6	0.8	1.3	2.5	4.0	3.8	2.4	1.3	0.3	0.4	0.5	0.3	0.2	1.2	1.0	0.
236	0.0	0.2	0.6	0.7	0.8	1.4	2.7	4.2	3.8	2.2	1.2	0.2	0.4	0.5	0.3	0.2	1.1	1.0	0.
238	0.1	0.2	0.6	0.7	0.8	1.5	2.8	4.3	3.7	2.1	1.1	0.2	0.4	0.5	0.3	0.2	1.1	1.0	0.
240	0.1	0.2	0.6	0.7	0.8	1.6	2.9	4.3	3.6	2.0	1.1	0.2	0.4	0.5	0.3	0.2	1.1	1.0	0.
242	0.1	0.2	0.6	0.7	0.9	1.7	2.9	4.1	3.5	1.8	1.0	0.2	0.4	0.5	0.3	0.2	1.1	1.0	0.
244	0.2	0.2	0.6	0.8	0.9	1.7	2.9	3.9	3.3	1.7	1.0	0.1	0.3	0.4	0.3	0.2	1.0	1.0	0.
246	0.2	0.2	0.6	0.8	0.9	1.7	2.8	3.6	3.0	1.6	0.9	0.1	0.3	0.4	0.3	0.3	1.0	1.0	0.
248	0.2	0.2	0.7	0.8	0.9	1.7	2.8	3.2	2.8	1.5	0.9	0.1	0.3	0.4	0.4	0.3	0.9	0.9	0.
250	0.2	0.2	0.7	0.8	0.9	1.6	2.6	2.9	2.6	1.4	0.8	0.2	0.3	0.4	0.4	0.3	0.9	0.9	0.
252	0.2	0.2	0.7	0.8	0.9	1.6	2.5	2.7	2.3	1.3	0.8	0.2	0.3	0.4	0.4	0.3	0.9	0.9	0.
254	0.1	0.2	0.7	0.8	0.9	1.5	2.3	2.4	2.1	1.2	0.8	0.2	0.3	0.4	0.4	0.3	0.8	0.9	0.
256	0.1	0.2	0.7	0.8	0.8	1.4	2.2	2.3	2.0	1.1	0.7	0.2	0.3	0.4	0.4	0.3	0.8	0.9	0.
258	0.1	0.2	0.7	0.8	0.8	1.3	2.0	2.1	1.8	1.1	0.7	0.2	0.3	0.4	0.4	0.3	0.8	0.9	0.
260	0.1	0.2	0.7	0.8	0.8	1.2	1.9	2.0	1.7	1.1	0.7	0.2	0.3	0.4	0.4	0.3	0.8	0.9	0.
262	0.1	0.2	0.6	0.7	0.7	1.1	1.7	1.8	1.6	1.0	0.7	0.2	0.3	0.4	0.4	0.3	0.8	0.9	0.
264	0.1	0.2	0.6	0.7	0.7	1.1	1.6	1.7	1.5	1.0	0.7	0.1	0.3	0.4	0.4	0.3	0.8	0.9	0.
266	0.1	0.2	0.5	0.7	0.7	1.1	1.5	1.6	1.5	1.0	0.7	0.1	0.2	0.4	0.4	0.3	0.8	0.9	0.
268	0.1	0.1	0.5	0.6	0.6	1.1	1.4	1.5	1.	1.0	0.7	0.1	0.2	0.4	0.4	0.3	0.7	0.9	0.
270	0.0	0.1	0.5	0.6	0.6	1.1	1.3	1.5	1.4	1.0	0.7	0.1	0.2	0.4	0.4	0.3	0.7	0.9	0.

TABLE XXVII (Continued)

	0	5	10	15	20	25	30	35	40	45	50	55	60	65	70	75	80	85	9
272	0.0	0.1	0.4	0.6	0.6	1.1	1.3	1.4	1.4	1.0	0.6	0.1	0.2	0.4	0.4	0.3	0.7	0.9	0.
274	0.0	0.1	0.4	0.6	0.7	1.2	1.3	1.5	1.5	0.9	0.6	0.1	0.2	0.4	0.4	0.4	0.7	0.9	0.
276	0.0	0.1	0.4	0.6	0.7	1.2	1.3	1.5	1.5	0.9	0.6	0.1	0.2	0.4	0.4	0.4	0.8	0.9	0.
278	0.0	0.1	0.4	0.6	0.7	1.3	1.3	1.5	1.5	0.9	0.6	0.1	0.2	0.4	0.4	0.4	0.8	0.9	0.
280	0.1	0.1	0.4	0.7	0.7	1.3	1.4	1.6	1.5	0.9	0.7	0.2	0.2	0.4	0.4	0.4	0.8	0.9	0.
282	0.1	0.1	0.4	0.7	0.7	1.3	1.5	1.6	1.5	0.9	0.7	0.2	0.2	0.4	0.4	0.4	0.8	0.9	0.
284	0.1	0.1	0.4	0.7	0.8	1.3	1.6	1.7	1.5	0.9	0.7	0.2	0.2	0.4	0.4	0.4	0.7	0.8	0.
286	0.1	0.2	0.4	0.7	0.8	1.4	1.7	1.8	1.5	1.0	0.7	0.2	0.3	0.4	0.4	0.4	0.7	0.8	0.
288	0.1	0.2	0.4	0.8	0.9	1.4	1.9	1.9	1.5	1.0	0.7	0.3	0.3	0.4	0.4	0.4	0.7	0.8	0.
290	0.1	0.2	0.4	0.7	0.9	1.5	2.1	2.1	1.6	1.1	0.8	0.3	0.3	0.4	0.4	0.4	0.7	0.8	0.
292	0.1	0.2	0.4	0.7	1.0	1.6	2.3	2.3	1.7	1.1	0.8	0.3	0.3	0.4	0.4	0.4	0.7	0.8	0.
294	0.1	0.2	0.4	0.7	1.0	1.7	2.5	2.5	1.8	1.2	0.9	0.3	0.3	0.4	0.4	0.4	0.8	0.8	0.
296	0.1	0.2	0.5	0.7	1.0	1.8	2.8	2.8	2.0	1.3	1.0	0.3	0.3	0.4	0.4	0.4	0.8	0.8	0.
298	0.1	0.2	0.5	0.7	1.0	1.9	3.0	3.0	2.3	1.4	1.0	0.3	0.3	0.4	0.4	0.4	0.8	0.8	0.
300	0.1	0.2	0.5	0.7	1.0	1.9	3.2	3.2	2.5	1.6	1.0	0.3	0.3	0.4	0.4	0.4	0.8	0.8	0.
302	0.1	0.2	0.5	0.7	1.0	1.9	3.3	3.3	2.6	1.7	1.1	0.3	0.3	0.4	0.4	0.4	0.8	0.8	0.
304	0.1	0.2	0.5	0.7	0.9	1.8	3.3	3.3	2.6	1.7	1.1	0.3	0.4	0.4	0.4	0.4	0.8	0.9	0.
306	0.1	0.2	0.5	0.7	0.9	1.7	3.2	3.3	2.6	2.0	1.1	0.3	0.4	0.4	0.4	0.4	0.9	0.9	0.
308	0.1	0.1	0.5	0.7	0.8	1.6	3.1	3.2	2.5	2.1	1.1	0.3	0.4	0.4	0.4	0.4	0.9	0.8	0.
310	0.1	0.1	0.4	0.7	0.8	1.5	3.0	3.1	2.5	2.2	1.1	0.4	0.4	0.4	0.4	0.4	0.9	0.8	0.
312	0.1	0.1	0.4	0.6	0.8	1.4	2.9	3.0	2.5	2.3	1.2	0.4	0.4	0.4	0.4	0.4	0.9	0.8	0.
314	0.1	0.1	0.4	0.6	0.7	1.3	2.8	2.9	2.5	2.3	1.2	0.4	0.4	0.4	0.4	0.4	1.0	0.8	0.
316	0.0	0.0	0.3	0.6	0.7	1.3	2.8	2.9	2.5	2.4	1.2	0.4	0.4	0.5	0.4	0.4	1.0	0.8	0.
318	0.	0.0	0.3	0.5	0.7	1.4	2.8	2.9	2.5	2.4	1.3	0.4	0.4	0.5	0.4	0.4	1.0	0.9	0.
320	0.	0.	0.3	0.5	0.7	1.5	2.8	2.9	2.5	2.5	1.4	0.4	0.4	0.5	0.4	0.4	1.0	0.9	0.
322	0.	0.	0.2	0.5	0.7	1.6	2.9	3.0	2.5	2.5	1.5	0.4	0.4	0.5	0.4	0.5	1.1	0.9	0.
324	0.	0.	0.2	0.4	0.8	1.7	3.0	3.1	2.5	2.6	1.6	0.4	0.4	0.5	0.5	0.5	1.1	0.9	0.
326	0.	0.	0.2	0.4	0.8	1.8	3.1	3.2	2.5	2.6	1.7	0.4	0.4	0.5	0.5	0.5	1.1	0.9	0.
328	0.	0.	0.2	0.5	0.9	1.9	3.1	3.3	2.5	2.7	1.8	0.4	0.4	0.5	0.5	0.5	1.2	0.9	0.
330	0.	0.	0.2	0.5	1.0	2.0	3.1	3.2	2.5	2.7	1.9	0.4	0.5	0.5	0.5	0.5	1.2	0.9	0.
332	0.	0.	0.2	0.5	1.1	2.0	3.0	3.0	2.5	2.6	1.9	0.4	0.5	0.5	0.5	0.5	1.2	0.9	0.
334	0.	0.0	0.2	0.6	1.1	2.1	2.8	2.8	2.5	2.5	2.0	0.4	0.5	0.5	0.5	0.5	1.2	0.9	0.
336	0.0	0.1	0.3	0.7	1.2	2.0	2.7	2.6	2.5	2.4	2.0	0.4	0.6	0.6	0.5	0.5	1.2	0.9	0.
338	0.1	0.1	0.4	0.7	1.2	2.0	2.4	2.3	2.3	2.2	1.9	0.5	0.6	0.6	0.5	0.5	1.3	0.9	0.
340	0.1	0.1	0.5	0.8	1.2	1.9	2.2	2.0	2.3	2.0	1.8	0.5	0.6	0.6	0.5	0.5	1.3	0.9	0.
342	0.2	0.2	0.5	0.8	1.1	1.7	1.9	1.7	1.8	1.8	1.8	0.5	0.7	0.6	0.5	0.5	1.4	0.9	0.
344	0.2	0.2	0.6	0.8	1.1	1.6	1.7	1.4	1.5	1.5	1.6	0.6	0.7	0.6	0.5	0.5	1.4	0.9	0.
346	0.3	0.3	0.6	0.8	1.0	1.4	1.4	1.2	1.2	1.3	1.5	0.6	0.8	0.7	0.5	0.5	1.4	0.9	0.
348	0.3	0.4	0.7	0.7	0.9	1.2	1.2	1.0	1.0	1.4	1.5	0.7	0.8	0.7	0.5	0.5	1.5	0.9	0.
350	0.4	0.4	0.7	0.7	0.9	1.1	1.0	0.8	0.8	0.9	1.1	0.7	0.9	0.7	0.5	0.5	1.5	0.9	0.
352	0.4	0.5	0.7	0.7	0.8	1.0	0.8	0.7	0.7	0.8	1.0	0.7	0.9	0.7	0.5	0.5	1.5	0.9	0.
354	0.5	0.6	0.7	0.7	0.8	0.8	0.7	0.6	0.6	0.6	0.9	0.7	0.9	0.7	0.5	0.5	1.4	0.9	0.
356	0.5	0.6	0.6	0.6	0.7	0.8	0.6	0.5	0.5	0.5	0.8	0.7	1.0	0.7	0.5	0.5	1.4	1.0	0.
358	0.6	0.7	0.6	0.6	0.7	0.7	0.5	0.4	0.4	0.4	0.6	0.7	1.0	0.7	0.5	0.5	1.3	1.0	0.
360	0.6	0.7	0.6	0.6	0.7	0.7	0.5	0.4	0.4	0.4	0.6	0.7	1.0	0.7	0.5	0.5	1.3	1.0	0.

POLE FIGURE DATA SHEET FOR SPECIMEN 3A

The normalized pole figure is based on Mo k-alpha radiation and the 111 reflection.

The 222 reflection was used to fill in the blind region from 80 through 90 degrees alpha.

The alpha-dependent two theta shift was taken into account.

Integrated intensities were used.

Normal smoothing was used.

Maximum and minimum corrected intensities are 2501 and 0 counts/second, respectively.

Random intensity is 480 counts/second.

Contour spacing is based on multiples of random intensity.

4 contours are to be plotted.

Their values are 1.000 2.000 3.000 4.000.

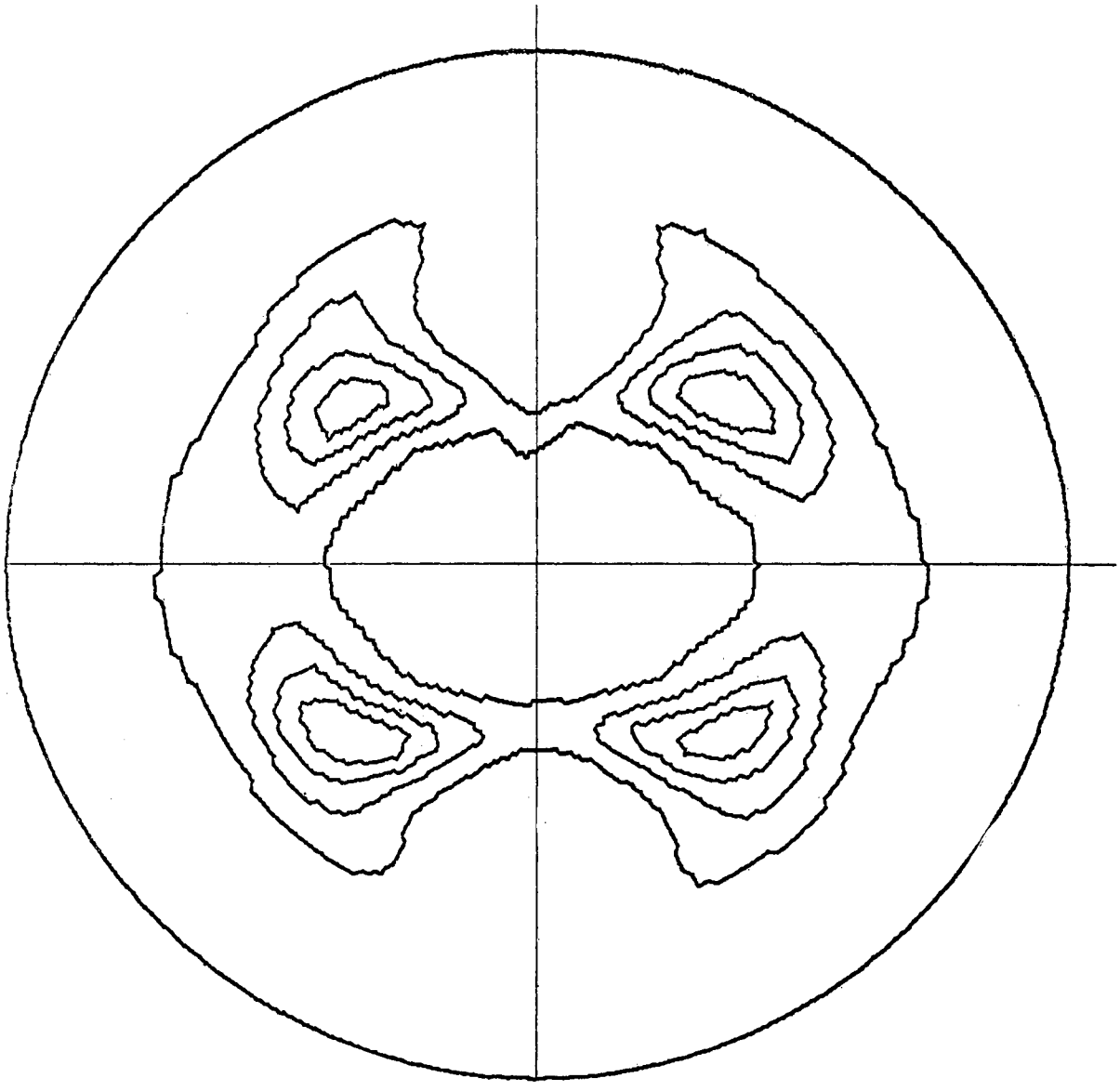

Figure 31. (111) Pole Figure for Specimen 3A

TABLE XXVIII

POLE FIGURE DATA FOR SPECIMEN 3A

	0	5	10	15	20	25	30	35	40	45	50	55	60	65	70	75	80	85	90
2	0.6	0.5	0.7	0.7	0.6	0.4	0.2	0.2	0.2	0.3	0.4	0.9	1.1	1.0	0.9	0.2	0.5	0.6	0.7
4	0.6	0.4	0.7	0.7	0.6	0.4	0.2	0.2	0.2	0.3	0.5	1.0	1.1	1.0	0.9	0.2	0.5	0.6	0.7
6	0.6	0.4	0.7	0.7	0.6	0.4	0.2	0.2	0.2	0.3	0.5	1.0	1.1	1.0	0.9	0.2	0.5	0.6	0.7
8	0.5	0.3	0.7	0.7	0.6	0.4	0.2	0.2	0.2	0.3	0.5	1.1	1.1	1.0	0.9	0.2	0.5	0.6	0.7
10	0.4	0.3	0.6	0.7	0.6	0.5	0.3	0.3	0.3	0.4	0.6	1.2	1.1	1.0	0.9	0.2	0.5	0.6	0.7
12	0.4	0.2	0.6	0.7	0.7	0.5	0.3	0.3	0.3	0.5	0.9	1.3	1.1	1.0	0.9	0.2	0.5	0.6	0.7
14	0.3	0.2	0.5	0.7	0.8	0.6	0.4	0.3	0.4	0.6	1.0	1.4	1.1	1.0	0.8	0.2	0.5	0.6	0.7
16	0.2	0.1	0.5	0.7	0.9	0.7	0.5	0.4	0.5	0.7	1.2	1.5	1.1	0.9	0.8	0.2	0.6	0.6	0.7
18	0.2	0.1	0.4	0.7	1.0	0.9	0.6	0.5	0.6	0.9	1.5	1.5	1.0	0.9	0.8	0.2	0.6	0.6	0.7
20	0.1	0.0	0.4	0.7	1.1	1.0	0.7	0.6	0.7	1.1	1.7	1.6	0.9	0.9	0.7	0.2	0.6	0.6	0.7
22	0.1	0.0	0.3	0.7	1.2	1.2	0.8	0.8	0.9	1.4	2.0	1.6	0.9	0.9	0.7	0.2	0.5	0.6	0.7
24	0.1	0.	0.3	0.7	1.3	1.4	1.0	0.9	1.1	1.7	2.2	1.7	0.9	0.8	0.6	0.1	0.5	0.6	0.7
26	0.0	0.	0.2	0.7	1.4	1.5	1.2	1.1	1.4	2.1	2.5	1.7	0.8	0.8	0.6	0.1	0.5	0.6	0.7
28	0.	0.	0.2	0.6	1.4	1.7	1.4	1.4	1.7	2.4	2.7	1.6	0.8	0.8	0.5	0.1	0.5	0.6	0.7
30	0.	0.	0.1	0.6	1.5	1.8	1.7	1.7	2.1	2.8	2.8	1.5	0.8	0.8	0.5	0.1	0.5	0.6	0.7
32	0.	0.	0.1	0.6	1.5	2.0	1.9	2.0	2.5	3.2	2.9	1.5	0.8	0.8	0.5	0.1	0.5	0.6	0.7
34	0.	0.	0.1	0.5	1.4	2.1	2.2	2.3	2.9	3.5	2.9	1.4	0.7	0.7	0.4	0.1	0.5	0.5	0.7
36	0.	0.	0.1	0.5	1.4	2.1	2.4	2.7	3.4	3.7	2.9	1.4	0.7	0.7	0.4	0.1	0.5	0.5	0.7
38	0.	0.	0.1	0.5	1.4	2.2	2.5	3.0	3.8	3.8	2.8	1.3	0.7	0.6	0.4	0.1	0.5	0.5	0.7
40	0.	0.	0.1	0.5	1.3	2.2	2.7	3.3	4.1	3.9	2.7	1.2	0.6	0.6	0.3	0.1	0.5	0.5	0.7
42	0.	0.	0.1	0.5	1.3	2.2	2.8	3.6	4.4	3.9	2.5	1.1	0.6	0.5	0.3	0.1	0.5	0.5	0.7
44	0.	0.	0.1	0.5	1.2	2.2	2.9	3.8	4.7	3.8	2.3	1.0	0.6	0.5	0.3	0.1	0.5	0.5	0.7
46	0.0	0.	0.2	0.5	1.1	2.1	3.0	4.0	4.8	3.7	2.1	1.0	0.6	0.5	0.3	0.1	0.5	0.5	0.7
48	0.0	0.	0.2	0.5	1.1	2.1	3.0	4.1	4.9	3.5	2.0	0.9	0.5	0.4	0.2	0.1	0.5	0.5	0.7
50	0.0	0.	0.2	0.5	1.0	2.0	3.0	4.2	4.9	3.2	1.9	0.9	0.5	0.4	0.2	0.1	0.5	0.5	0.7
52	0.0	0.	0.2	0.5	1.0	1.9	3.0	4.1	4.7	3.0	1.8	0.9	0.4	0.3	0.2	0.1	0.5	0.6	0.7
54	0.1	0.	0.2	0.5	0.9	1.8	2.9	4.1	4.5	3.0	1.7	0.9	0.4	0.3	0.2	0.1	0.5	0.6	0.7
56	0.1	0.	0.2	0.5	0.9	1.8	2.8	3.9	4.3	2.8	1.6	0.8	0.3	0.2	0.1	0.0	0.5	0.6	0.7
58	0.1	0.	0.2	0.5	0.9	1.7	2.8	3.7	4.0	2.6	1.6	0.8	0.3	0.2	0.1	0.0	0.5	0.6	0.7
60	0.1	0.	0.2	0.5	0.9	1.6	2.7	3.5	3.7	2.4	1.5	0.7	0.3	0.2	0.1	0.0	0.5	0.6	0.7
62	0.1	0.	0.2	0.5	0.9	1.5	2.5	3.3	3.4	2.3	1.4	0.7	0.2	0.1	0.1	0.0	0.5	0.6	0.7
64	0.0	0.	0.2	0.5	0.9	1.5	2.4	3.1	3.2	2.1	1.4	0.6	0.2	0.1	0.1	0.0	0.5	0.6	0.7
66	0.0	0.	0.2	0.6	0.9	1.4	2.3	2.8	2.9	2.0	1.3	0.5	0.2	0.1	0.0	0.0	0.5	0.6	0.7
68	0.0	0.	0.2	0.6	1.0	1.4	2.3	2.6	2.7	1.9	1.2	0.5	0.2	0.1	0.0	0.0	0.5	0.6	0.7
70	0.0	0.	0.2	0.6	1.0	1.4	2.3	2.4	2.5	1.7	1.1	0.5	0.1	0.0	0.0	0.0	0.5	0.6	0.7
72	0.0	0.	0.2	0.6	1.0	1.4	2.2	2.2	2.3	1.6	1.0	0.4	0.1	0.0	0.0	0.0	0.5	0.6	0.7
74	0.0	0.	0.2	0.6	1.1	1.4	1.7	2.1	2.2	1.5	0.9	0.4	0.1	0.0	0.0	0.0	0.5	0.5	0.7
76	0.0	0.	0.2	0.7	1.1	1.4	1.6	1.9	2.1	1.5	0.9	0.3	0.1	0.	0.	0.	0.5	0.5	0.7
78	0.0	0.	0.2	0.7	1.1	1.4	1.5	1.8	2.0	1.4	0.8	0.3	0.1	0.	0.	0.	0.4	0.5	0.7
80	0.0	0.	0.2	0.7	1.1	1.4	1.5	1.7	1.9	1.3	0.7	0.2	0.0	0.	0.	0.	0.4	0.5	0.7
82	0.0	0.	0.2	0.7	1.1	1.4	1.4	1.7	1.9	1.2	0.7	0.2	0.0	0.	0.	0.	0.4	0.5	0.7
84	0.0	0.	0.2	0.7	1.1	1.4	1.4	1.7	1.9	1.2	0.7	0.2	0.0	0.	0.	0.	0.4	0.5	0.7
86	0.0		0.2	0.7	1.1	1.4	1.4	1.7	1.9	1.2	0.7	0.2	0.0	0.	0.	0.	0.4	0.5	0.7
88	0.0		0.2	0.7	1.2	1.4	1.4	1.8	1.9	1.2	0.7	0.2	0.0	0.	0.	0.	0.4	0.5	0.7
90	0.0		0.2	0.7	1.2	1.3	1.4	1.8	1.9	1.2	0.7	0.2	0.0	0.	0.	0.	0.4	0.5	0.7

TABLE XXVIII (Continued)

	0	5	10	15	20	25	30	35	40	45	50	55	60	65	70	75	80	85	90
92	0.0	0.	0.2	0.7	1.2	1.3	1.4	1.8	1.9	1.2	0.7	0.2	0.0	0.	0.	0.	0.4	0.5	0.7
94	0.0	0.	0.2	0.7	1.2	1.3	1.4	1.9	1.9	1.2	0.7	0.2	0.0	0.	0.	0.	0.4	0.5	0.7
96	0.0	0.	0.2	0.7	1.2	1.3	1.5	1.9	1.9	1.3	0.7	0.3	0.0	0.	0.	0.	0.4	0.5	0.7
98	0.0	0.	0.3	0.7	1.2	1.3	1.5	1.9	1.9	1.3	0.8	0.3	0.0	0.	0.	0.	0.5	0.5	0.7
100	0.0	0.	0.3	0.7	1.2	1.3	1.6	1.9	1.9	1.3	0.8	0.3	0.0	0.	0.	0.	0.5	0.5	0.7
102	0.0	0.	0.3	0.7	1.1	1.3	1.6	2.0	2.0	1.4	0.8	0.3	0.0	0.	0.	0.	0.5	0.5	0.7
104	0.0	0.	0.3	0.6	1.1	1.4	1.7	2.0	2.0	1.5	0.9	0.4	0.0	0.	0.	0.	0.5	0.5	0.7
106	0.0	0.	0.3	0.6	1.1	1.4	1.8	2.1	2.2	1.5	1.0	0.4	0.0	0.	0.	0.	0.5	0.5	0.7
108	0.0	0.	0.3	0.6	1.0	1.4	1.9	2.3	2.3	1.6	1.0	0.4	0.0	0.	0.	0.	0.5	0.5	0.7
110	0.0	0.	0.3	0.6	1.0	1.5	2.0	2.5	2.5	1.7	1.1	0.5	0.0	0.	0.	0.	0.5	0.5	0.7
112	0.0	0.	0.2	0.6	1.0	1.5	2.2	2.7	2.7	1.8	1.2	0.5	0.1	0.	0.	0.	0.5	0.5	0.7
114	0.0	0.	0.2	0.6	0.9	1.6	2.4	3.0	2.9	1.9	1.3	0.5	0.1	0.	0.	0.	0.5	0.6	0.7
116	0.0	0.	0.2	0.5	0.9	1.7	2.6	3.3	3.1	1.9	1.4	0.6	0.1	0.0	0.	0.	0.5	0.6	0.7
118	0.0	0.	0.2	0.5	0.9	1.7	2.8	3.6	3.3	2.0	1.4	0.6	0.1	0.0	0.	0.	0.5	0.6	0.7
120	0.0	0.	0.2	0.5	0.9	1.8	3.0	3.9	3.5	2.1	1.4	0.6	0.2	0.0	0.	0.	0.5	0.6	0.7
122	0.1	0.	0.2	0.5	0.9	1.9	3.2	4.2	3.7	2.3	1.5	0.7	0.2	0.1	0.0	0.	0.6	0.6	0.7
124	0.1	0.	0.2	0.5	1.0	1.9	3.4	4.5	3.9	2.4	1.5	0.7	0.2	0.1	0.0	0.	0.6	0.6	0.7
126	0.1	0.	0.2	0.4	1.0	2.0	3.5	4.7	4.2	2.6	1.5	0.8	0.3	0.1	0.0	0.	0.6	0.6	0.7
128	0.1	0.	0.2	0.4	1.0	2.0	3.5	4.8	4.5	2.8	1.6	0.8	0.3	0.1	0.0	0.	0.6	0.6	0.7
130	0.0	0.	0.1	0.4	1.0	2.0	3.5	4.9	4.8	3.0	1.6	0.8	0.3	0.1	0.0	0.	0.6	0.6	0.7
132	0.0	0.	0.1	0.4	1.0	2.1	3.4	4.9	5.0	3.2	1.7	0.9	0.4	0.2	0.0	0.	0.6	0.6	0.7
134	0.	0.	0.1	0.4	1.1	2.0	3.3	4.7	5.1	3.5	1.9	0.9	0.4	0.2	0.0	0.	0.6	0.6	0.7
136	0.	0.	0.1	0.4	1.1	2.0	3.1	4.5	5.2	3.7	2.0	1.0	0.5	0.3	0.1	0.	0.6	0.6	0.7
138	0.	0.	0.0	0.4	1.1	2.0	2.9	4.2	5.1	3.9	2.2	1.0	0.5	0.3	0.1	0.	0.6	0.6	0.7
140	0.	0.	0.0	0.4	1.1	1.9	2.7	3.8	5.0	4.0	2.4	1.1	0.5	0.3	0.1	0.	0.6	0.6	0.7
142	0.	0.	0.0	0.5	1.1	1.9	2.5	3.4	4.7	4.1	2.5	1.2	0.6	0.4	0.1	0.	0.6	0.6	0.7
144	0.	0.	0.0	0.5	1.1	1.8	2.2	2.9	4.2	4.1	2.7	1.2	0.6	0.4	0.1	0.	0.6	0.6	0.7
146	0.	0.	0.0	0.5	1.1	1.7	2.0	2.5	3.8	3.9	2.8	1.3	0.6	0.5	0.1	0.	0.6	0.7	0.7
148	0.	0.	0.0	0.5	1.0	1.5	1.7	2.1	3.2	3.7	2.9	1.4	0.7	0.5	0.2	0.	0.6	0.7	0.7
150	0.	0.	0.1	0.5	1.0	1.4	1.5	1.7	2.7	3.4	2.9	1.5	0.7	0.5	0.2	0.	0.6	0.7	0.7
152	0.	0.	0.1	0.5	1.0	1.3	1.3	1.4	2.2	3.1	2.8	1.5	0.7	0.5	0.2	0.	0.6	0.7	0.7
154	0.1	0.	0.1	0.5	0.9	1.1	1.1	1.1	1.8	2.7	2.8	1.6	0.8	0.6	0.2	0.	0.7	0.7	0.7
156	0.1	0.	0.1	0.5	0.9	1.0	0.9	0.9	1.4	2.3	2.6	1.7	0.8	0.6	0.2	0.	0.7	0.7	0.7
158	0.1	0.	0.2	0.5	0.8	0.9	0.7	0.7	1.1	2.0	2.5	1.7	0.8	0.7	0.3	0.	0.7	0.7	0.7
160	0.2	0.	0.2	0.5	0.8	0.7	0.6	0.6	0.9	1.6	2.3	1.7	0.9	0.7	0.3	0.	0.7	0.7	0.7
162	0.3	0.0	0.2	0.5	0.7	0.6	0.5	0.5	0.7	1.4	2.2	1.8	0.9	0.7	0.3	0.	0.7	0.8	0.7
164	0.3	0.1	0.3	0.5	0.6	0.6	0.4	0.4	0.6	1.1	2.0	1.8	0.9	0.8	0.3	0.	0.7	0.8	0.7
166	0.4	0.1	0.3	0.5	0.6	0.5	0.4	0.3	0.5	0.9	1.8	1.8	0.9	0.8	0.3	0.	0.7	0.8	0.7
168	0.5	0.2	0.4	0.5	0.5	0.4	0.3	0.3	0.4	0.8	1.6	1.8	1.0	0.8	0.3	0.	0.7	0.8	0.7
170	0.6	0.2	0.4	0.5	0.5	0.4	0.3	0.3	0.4	0.7	1.4	1.8	1.0	0.8	0.4	0.	0.7	0.8	0.7
172	0.7	0.3	0.4	0.5	0.5	0.4	0.2	0.2	0.3	0.6	1.3	1.7	1.0	0.8	0.4	0.	0.7	0.8	0.7
174	0.7	0.3	0.4	0.5	0.4	0.3	0.2	0.2	0.3	0.5	1.2	1.7	1.0	0.8	0.4	0.	0.7	0.8	0.7
176	0.8	0.3	0.4	0.5	0.4	0.3	0.2	0.2	0.3	0.4	1.1	1.7	1.0	0.8	0.4	0.	0.7	0.8	0.7
178	0.8	.3	0.4	0.5	0.4	0.3	0.2	0.2	0.3	0.4	1.0	1.7	1.0	0.8	0.4	0.	0.8	0.8	0.7
180	0.8	.3	0.4	0.5	0.4	0.3	0.2	0.2	0.2	0.4	1.0	1.7	1.0	0.8	0.4	0.	0.8	0.8	0.7

TABLE XXVIII (Continued)

	0	5	10	15	20	25	30	35	40	45	50	55	60	65	70	75	80	85	90
182	0.8	0.3	0.4	0.5	0.4	0.3	0.2	0.2	0.2	0.4	1.0	1.7	1.8	0.8	0.4	0.	0.8	0.8	0.7
184	0.8	0.3	0.4	0.5	0.4	0.3	0.2	0.2	0.3	0.4	1.1	1.7	1.0	0.8	0.4	0.	0.8	0.8	0.7
186	0.7	0.3	0.4	0.5	0.4	0.3	0.2	0.2	0.3	0.5	1.1	1.7	1.0	0.8	0.4	0.	0.8	0.8	0.7
188	0.6	0.2	0.4	0.5	0.5	0.3	0.2	0.2	0.3	0.5	1.2	1.8	1.0	0.8	0.4	0.	0.8	0.8	0.7
190	0.5	0.2	0.4	0.5	0.5	0.4	0.3	0.2	0.3	0.5	1.3	1.8	1.0	0.8	0.3	0.	0.8	0.8	0.7
192	0.5	0.2	0.3	0.5	0.5	0.4	0.3	0.3	0.3	0.6	1.4	1.8	1.0	0.8	0.3	0.	0.8	0.8	0.7
194	0.4	0.1	0.3	0.5	0.6	0.4	0.3	0.3	0.4	0.7	1.6	1.8	1.0	0.8	0.3	0.	0.8	0.8	0.7
196	0.3	0.1	0.3	0.5	0.6	0.5	0.4	0.4	0.5	0.9	1.8	1.9	1.0	0.8	0.3	0.	0.8	0.8	0.7
198	0.2	0.0	0.3	0.6	0.7	0.6	0.5	0.4	0.6	1.1	2.0	1.9	0.9	0.8	0.3	0.	0.8	0.8	0.7
200	0.2	0.	0.2	0.6	0.8	0.7	0.6	0.6	0.8	1.4	2.2	1.9	0.9	0.7	0.3	0.	0.7	0.8	0.7
202	0.1	0.	0.2	0.6	0.8	0.8	0.7	0.7	1.0	1.7	2.5	1.9	0.9	0.7	0.3	0.	0.7	0.8	0.7
204	0.1	0.	0.2	0.6	0.9	1.0	0.8	0.9	1.3	2.1	2.7	1.9	0.9	0.7	0.2	0.	0.7	0.8	0.7
206	0.1	0.	0.1	0.6	1.0	1.1	1.0	1.1	1.6	2.4	2.8	1.8	0.8	0.6	0.2	0.	0.7	0.8	0.7
208	0.0	0.	0.1	0.6	1.1	1.3	1.2	1.4	2.0	2.8	3.0	1.8	0.8	0.6	0.2	0.	0.7	0.8	0.7
210	0.	0.	0.1	0.6	1.1	1.4	1.4	1.7	2.5	3.2	3.0	1.7	0.8	0.5	0.2	0.	0.7	0.8	0.7
212	0.	0.	0.1	0.6	1.2	1.6	1.7	2.1	3.0	3.5	3.0	1.6	0.7	0.5	0.2	0.	0.7	0.8	0.7
214	0.	0.	0.0	0.5	1.2	1.7	1.9	2.4	3.4	3.7	2.9	1.5	0.7	0.4	0.1	0.	0.7	0.8	0.7
216	0.	0.	0.0	0.5	1.3	1.9	2.2	2.8	3.8	3.8	2.8	1.4	0.7	0.4	0.1	0.	0.7	0.7	0.7
218	0.	0.	0.0	0.5	1.3	2.0	2.4	3.2	4.2	3.9	2.7	1.3	0.6	0.4	0.1	0.	0.7	0.7	0.7
220	0.	0.	0.0	0.5	1.3	2.1	2.6	3.6	4.5	3.8	2.5	1.2	0.6	0.3	0.1	0.	0.7	0.7	0.7
222	0.	0.	0.1	0.5	1.4	2.2	2.8	3.9	4.6	3.7	2.3	1.1	0.5	0.3	0.1	0.	0.7	0.7	0.7
224	0.	0.	0.1	0.5	1.4	2.3	3.0	4.2	4.7	3.5	2.1	1.1	0.5	0.2	0.1	0.	0.7	0.7	0.7
226	0.0	0.	0.1	0.5	1.4	2.3	3.2	4.4	4.7	3.2	2.0	1.0	0.5	0.2	0.0	0.	0.6	0.7	0.7
228	0.0	0.	0.1	0.6	1.3	2.3	3.3	4.6	4.5	3.0	1.9	1.0	0.4	0.2	0.0	0.	0.6	0.7	0.7
230	0.0	0.	0.1	0.6	1.3	2.3	3.3	4.7	4.4	2.8	1.8	0.9	0.4	0.1	0.0	0.	0.6	0.7	0.7
232	0.0	0.	0.2	0.6	1.2	2.2	3.4	4.7	4.2	2.6	1.7	0.9	0.3	0.1	0.0	0.	0.6	0.7	0.7
234	0.0	0.	0.2	0.6	1.2	2.1	3.3	4.6	3.9	2.4	1.7	0.8	0.3	0.1	0.0	0.	0.6	0.7	0.7
236	0.0	0.	0.2	0.5	1.1	2.0	3.2	4.4	3.6	2.2	1.6	0.8	0.2	0.1	0.	0.	0.6	0.7	0.7
238	0.0	0.	0.2	0.5	1.0	1.9	3.1	4.1	3.3	2.0	1.6	0.8	0.2	0.0	0.	0.	0.6	0.7	0.7
240	0.0	0.	0.2	0.5	1.0	1.8	2.9	3.9	3.1	2.0	1.5	0.7	0.2	0.0	0.	0.	0.6	0.7	0.7
242	0.0	0.	0.2	0.5	1.0	1.7	2.8	3.5	2.8	1.9	1.4	0.6	0.1	0.0	0.	0.	0.6	0.6	0.7
244	0.0	0.	0.2	0.5	1.0	1.6	2.6	3.2	2.6	1.8	1.3	0.6	0.1	0.	0.	0.	0.6	0.6	0.7
246	0.0	0.	0.2	0.6	1.0	1.5	2.4	2.9	2.4	1.7	1.2	0.5	0.1	0.	0.	0.	0.6	0.6	0.7
248	0.0	0.	0.2	0.6	1.0	1.5	2.2	2.7	2.2	1.6	1.1	0.4	0.0	0.	0.	0.	0.6	0.6	0.7
250	0.0	0.	0.2	0.6	1.0	1.5	2.0	2.4	2.1	1.5	1.0	0.4	0.0	0.	0.	0.	0.6	0.6	0.7
252	0.0	0.	0.2	0.6	1.0	1.5	1.9	2.3	2.0	1.4	0.9	0.4	0.0	0.	0.	0.	0.5	0.6	0.7
254	0.0	0.	0.2	0.6	1.1	1.5	1.8	2.1	1.8	1.3	0.8	0.3	0.	0.	0.	0.	0.5	0.6	0.7
256	0.0	0.	0.2	0.7	1.1	1.5	1.8	2.0	1.7	1.3	0.7	0.3	0.	0.	0.	0.	0.5	0.6	0.7
258	0.0	0.	0.3	0.7	1.2	1.6	1.8	1.9	1.7	1.2	0.6	0.3	0.	0.	0.	0.	0.5	0.6	0.7
260	0.0	0.	0.3	0.7	1.2	1.6	1.8	1.8	1.6	1.1	0.6	0.3	0.	0.	0.	0.	0.5	0.6	0.7
262	0.0	0.	0.3	0.8	1.3	1.7	1.8	1.8	1.5	1.1	0.6	0.2	0.	0.	0.	0.	0.5	0.6	0.7
264	0.0	0.	0.3	0.8	1.3	1.7	1.8	1.7	1.4	1.0	0.6	0.2	0.	0.	0.	0.	0.5	0.6	0.7
266	0.0	0.	0.3	0.8	1.4	1.7	1.9	1.7	1.4	1.0	0.6	0.2	0.	0.	0.	0.	0.5	0.6	0.7
268	0.0		0.3	0.8	1.4	1.7	1.9	1.7	1.4	1.0	0.6	0.2	0.	0.	0.	0.	0.5	0.6	0.7
270	0.0		0.3	0.8	1.4	1.7	1.8	1.7	1.3	1.0	0.6	0.2	0.	0.	0.	0.	0.5	0.6	0.7

TABLE XXVIII (Continued)

	0	5	10	15	20	25	30	35	40	45	50	55	60	65	70	75	80	85	90
272	0.0	0.	0.2	0.8	1.3	1.7	1.8	1.6	1.3	1.0	0.6	0.2	0.	0.	0.	0.0	0.5	0.6	0.7
274	0.0	0.	0.2	0.7	1.3	1.7	1.7	1.6	1.3	1.0	0.6	0.2	0.	0.	0.	0.0	0.5	0.6	0.7
276	0.0	0.	0.2	0.7	1.2	1.6	1.7	1.6	1.4	1.0	0.7	0.3	0.	0.	0.	0.0	0.5	0.6	0.7
278	0.	0.	0.2	0.7	1.2	1.6	1.7	1.7	1.4	1.0	0.7	0.3	0.	0.	0.	0.0	0.5	0.6	0.7
280	0.	0.	0.2	0.7	1.1	1.6	1.7	1.8	1.5	1.0	0.7	0.3	0.0	0.	0.	0.0	0.5	0.6	0.7
282	0.	0.	0.2	0.7	1.1	1.6	1.7	1.9	1.5	1.1	0.8	0.3	0.0	0.	0.0	0.0	0.5	0.6	0.7
284	0.	0.	0.2	0.7	1.1	1.6	1.8	2.0	1.6	1.1	0.8	0.4	0.0	0.	0.0	0.0	0.5	0.6	0.7
286	0.	0.	0.2	0.7	1.0	1.6	1.9	2.2	1.8	1.2	0.9	0.4	0.1	0.	0.0	0.0	0.5	0.6	0.7
288	0.	0.	0.2	0.7	1.0	1.6	2.0	2.5	1.9	1.3	1.0	0.5	0.1	0.0	0.0	0.0	0.5	0.6	0.7
290	0.	0.	0.2	0.6	1.0	1.6	2.2	2.7	2.1	1.4	1.1	0.5	0.1	0.0	0.0	0.0	0.5	0.6	0.7
292	0.	0.	0.2	0.6	1.0	1.7	2.4	3.0	2.3	1.5	1.2	0.6	0.1	0.1	0.0	0.0	0.5	0.6	0.7
294	0.	0.	0.2	0.6	1.0	1.7	2.6	3.2	2.6	1.6	1.2	0.6	0.2	0.1	0.0	0.0	0.5	0.6	0.7
296	0.	0.	0.3	0.6	1.0	1.8	2.8	3.5	2.8	1.8	1.3	0.7	0.2	0.1	0.0	0.0	0.5	0.6	0.7
298	0.	0.	0.3	0.6	1.0	1.9	3.0	3.8	3.1	2.0	1.4	0.7	0.2	0.1	0.0	0.	0.5	0.6	0.7
300	0.0	0.	0.3	0.5	1.0	1.9	3.1	4.0	3.4	2.2	1.5	0.7	0.3	0.2	0.1	0.	0.5	0.6	0.7
302	0.0	0.	0.3	0.5	1.0	2.0	3.3	4.2	3.8	2.4	1.6	0.8	0.3	0.2	0.1	0.0	0.5	0.6	0.7
304	0.0	0.	0.3	0.5	1.0	2.0	3.4	4.4	4.1	2.6	1.6	0.8	0.3	0.2	0.1	0.0	0.5	0.6	0.7
306	0.0	0.	0.3	0.5	1.0	2.0	3.5	4.6	4.4	2.9	1.7	0.8	0.4	0.3	0.1	0.0	0.5	0.6	0.7
308	0.0	0.	0.2	0.5	1.0	2.0	3.5	4.6	4.6	3.1	1.8	0.8	0.4	0.3	0.1	0.0	0.5	0.7	0.7
310	0.0	0.	0.2	0.5	1.0	2.0	3.5	4.6	4.8	3.4	1.9	0.8	0.4	0.3	0.2	0.0	0.5	0.7	0.7
312	0.0	0.	0.2	0.5	1.0	2.0	3.5	4.6	4.9	3.6	2.0	0.9	0.4	0.4	0.2	0.0	0.5	0.7	0.7
314	0.0	0.	0.1	0.5	1.0	2.0	3.4	4.4	5.0	3.8	2.1	0.9	0.5	0.4	0.2	0.0	0.5	0.7	0.7
316	0.	0.	0.1	0.4	1.0	2.0	3.2	4.2	4.9	3.9	2.2	1.0	0.5	0.4	0.2	0.0	0.6	0.7	0.7
318	0.	0.	0.1	0.4	1.1	1.9	3.0	3.9	4.7	4.0	2.3	1.1	0.5	0.5	0.3	0.1	0.6	0.7	0.7
320	0.	0.	0.1	0.4	1.1	1.9	2.8	3.6	4.5	4.0	2.5	1.2	0.5	0.5	0.3	0.1	0.6	0.7	0.7
322	0.	0.	0.0	0.5	1.1	1.9	2.6	3.2	4.1	3.9	2.6	1.2	0.6	0.5	0.3	0.1	0.6	0.7	0.7
324	0.	0.	0.0	0.5	1.1	1.8	2.3	2.8	3.7	3.7	2.6	1.3	0.6	0.6	0.4	0.1	0.6	0.6	0.7
326	0.	0.	0.1	0.5	1.2	1.8	2.1	2.5	3.3	3.5	2.7	1.4	0.6	0.6	0.4	0.1	0.6	0.6	0.7
328	0.	0.	0.1	0.5	1.2	1.7	1.8	2.1	2.8	3.2	2.6	1.4	0.7	0.6	0.4	0.1	0.6	0.6	0.7
330	0.	0.	0.1	0.6	1.2	1.6	1.6	1.8	2.3	2.8	2.6	1.5	0.7	0.7	0.5	0.1	0.6	0.6	0.7
332	0.	0.	0.1	0.6	1.2	1.5	1.4	1.5	1.9	2.4	2.4	1.5	0.7	0.7	0.5	0.1	0.6	0.6	0.7
334	0.0	0.	0.2	0.7	1.2	1.3	1.2	1.2	1.5	2.0	2.2	1.5	0.7	0.7	0.5	0.1	0.6	0.6	0.7
336	0.1	0.	0.2	0.7	1.2	1.2	1.0	1.0	1.1	1.6	2.0	1.5	0.8	0.8	0.6	0.1	0.6	0.6	0.7
338	0.1	0.0	0.3	0.7	1.1	1.1	0.8	0.8	0.9	1.3	1.7	1.4	0.8	0.8	0.6	0.1	0.6	0.6	0.7
340	0.2	0.0	0.4	0.7	1.0	0.9	0.7	0.6	0.7	1.0	1.5	1.4	0.8	0.8	0.6	0.2	0.6	0.6	0.7
342	0.2	0.1	0.4	0.8	1.0	0.8	0.6	0.5	0.5	0.8	1.3	1.3	0.9	0.8	0.7	0.2	0.6	0.6	0.7
344	0.3	0.1	0.5	0.8	0.9	0.7	0.5	0.4	0.4	0.6	1.1	1.3	0.9	0.9	0.7	0.2	0.6	0.6	0.7
346	0.3	0.2	0.6	0.8	0.8	0.6	0.4	0.3	0.4	0.5	0.9	1.2	0.9	0.9	0.7	0.2	0.6	0.6	0.7
348	0.4	0.3	0.6	0.8	0.8	0.5	0.4	0.3	0.3	0.4	0.8	1.2	1.0	0.9	0.7	0.2	0.6	0.6	0.7
350	0.5	0.3	0.7	0.8	0.7	0.5	0.3	0.3	0.3	0.4	0.7	1.2	1.0	0.9	0.8	0.2	0.6	0.6	0.7
352	0.5	0.4	0.7	0.8	0.7	0.4	0.3	0.2	0.3	0.3	0.6	1.1	1.1	0.9	0.8	0.2	0.6	0.6	0.7
354	0.6	0.4	0.7	0.7	0.6	0.4	0.3	0.2	0.3	0.3	0.5	1.1	1.1	0.9	0.8	0.2	0.6	0.6	0.7
356	0.6	0.5	0.7	0.7	0.6	0.4	0.2	0.2	0.2	0.3	0.5	1.0	1.1	1.0	0.8	0.2	0.6	0.6	0.7
358	0.7	.5	0.7	0.7	0.6	0.4	0.2	0.2	0.2	0.3	0.5	1.0	1.1	1.0	0.8	0.2	0.6	0.6	0.7
360	0.7	.5	0.7	0.7	0.6	0.4	0.2	0.2	0.2	0.3	0.4	0.9	1.1	1.0	0.9	0.2	0.5	0.6	0.7

POLE FIGURE DATA SHEET FOR SPECIMEN 4A

The normalized pole figure is based on Mo k-alpha radiation and the 111 reflection.

The 222 reflection was used to fill in the blind region from 80 through 90 degrees alpha.

The alpha-dependent two theta shift was taken into account.

Integrated intensities were used.

Normal smoothing was used.

Maximum and minimum corrected intensities are 2843 and 0 counts/second, respectively.

Random intensity is 667 counts/second.

Contour spacing is based on multiples of random intensity.

4 contours are to be plotted.

Their values are 1.000 2.000 3.000 4.000 .

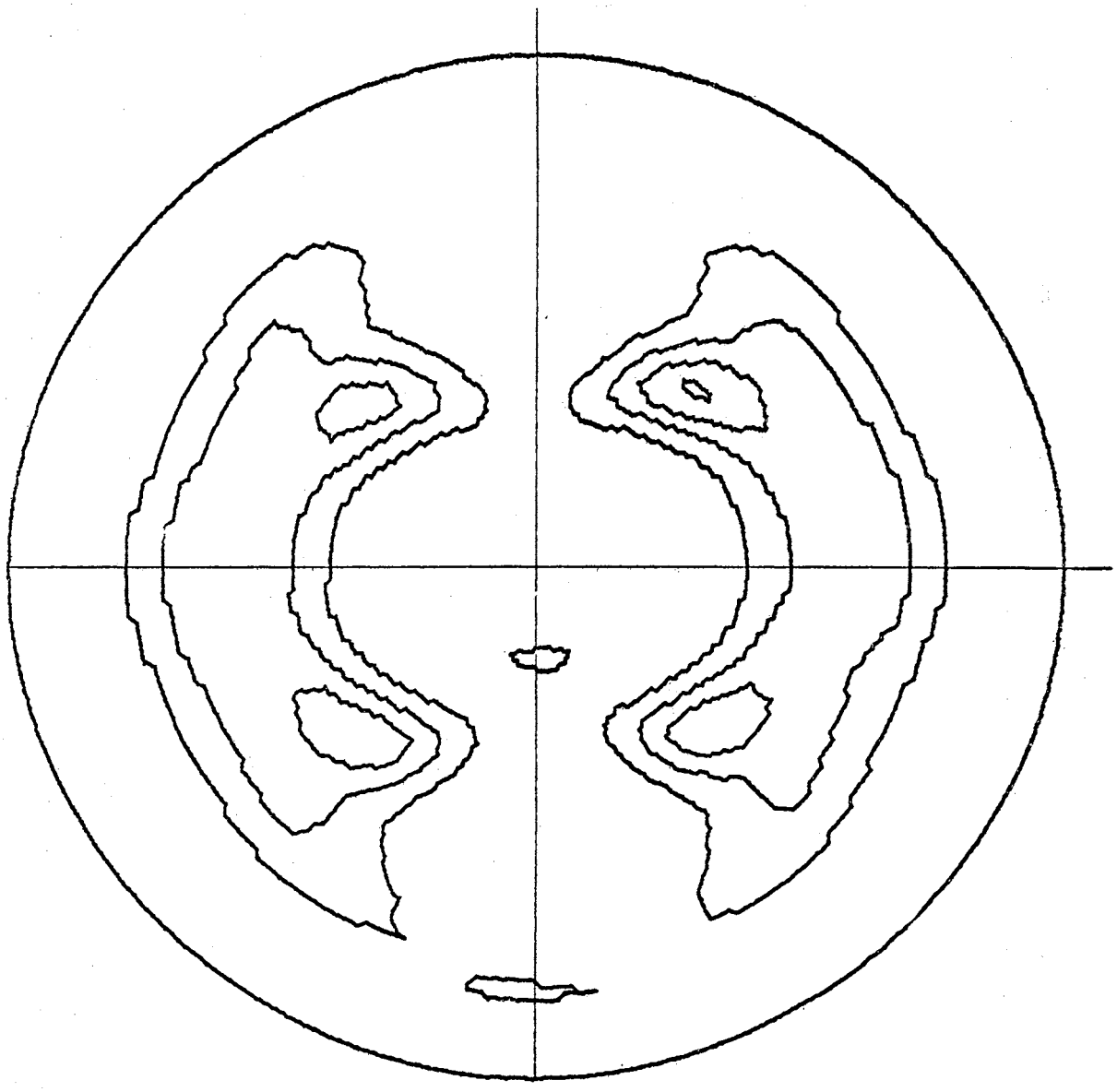

Figure 32. (111) Pole Figure for Specimen 4A

TABLE XXIX

POLE FIGURE DATA FOR SPECIMEN 4A

	0	5	10	15	20	25	30	35	40	45	50	55	60	65	70	75	80	85	90
2	0.6	0.6	0.6	0.5	0.3	0.2	0.2	0.2	0.3	0.3	0.6	0.8	0.9	0.9	0.6	0.2	0.1	0.1	0.2
4	0.6	0.6	0.6	0.5	0.3	0.2	0.2	0.2	0.3	0.3	0.6	0.8	0.9	0.9	0.6	0.2	0.1	0.1	0.2
6	0.6	0.6	0.6	0.5	0.3	0.3	0.2	0.2	0.3	0.4	0.6	0.8	0.9	0.9	0.6	0.2	0.1	0.1	0.2
8	0.6	0.6	0.6	0.5	0.4	0.3	0.2	0.2	0.3	0.4	0.7	0.8	0.9	0.9	0.6	0.2	0.1	0.1	0.2
10	0.6	0.6	0.6	0.5	0.4	0.3	0.2	0.3	0.3	0.4	0.7	0.9	0.9	0.9	0.6	0.2	0.2	0.2	0.2
12	0.6	0.6	0.6	0.5	0.4	0.3	0.3	0.3	0.3	0.5	0.8	0.9	0.9	0.9	0.6	0.2	0.2	0.2	0.2
14	0.5	0.5	0.6	0.6	0.5	0.3	0.3	0.3	0.4	0.6	0.9	0.9	0.9	0.9	0.6	0.2	0.2	0.2	0.2
16	0.5	0.5	0.6	0.6	0.5	0.4	0.3	0.3	0.4	0.7	1.0	1.0	0.9	0.8	0.5	0.2	0.2	0.2	0.2
18	0.5	0.5	0.5	0.6	0.6	0.4	0.3	0.3	0.5	0.8	1.2	1.0	0.8	0.8	0.5	0.2	0.2	0.2	0.2
20	0.5	0.5	0.5	0.7	0.6	0.5	0.3	0.4	0.6	1.0	1.3	1.0	0.8	0.7	0.5	0.2	0.2	0.2	0.2
22	0.4	0.4	0.5	0.7	0.7	0.5	0.4	0.5	0.7	1.2	1.5	1.1	0.8	0.7	0.5	0.2	0.2	0.2	0.2
24	0.4	0.4	0.5	0.7	0.8	0.6	0.4	0.6	0.9	1.5	1.6	1.1	0.8	0.6	0.4	0.2	0.2	0.2	0.2
26	0.3	0.3	0.5	0.8	0.9	0.7	0.5	0.7	1.1	1.7	1.8	1.1	0.7	0.6	0.4	0.2	0.2	0.1	0.2
28	0.3	0.3	0.5	0.8	1.0	0.8	0.6	0.8	1.4	2.0	1.9	1.1	0.7	0.5	0.4	0.2	0.2	0.1	0.2
30	0.3	0.3	0.5	0.9	1.1	0.9	0.7	1.0	1.7	2.3	2.0	1.1	0.6	0.5	0.3	0.2	0.2	0.1	0.2
32	0.2	0.3	0.5	1.0	1.2	1.1	0.9	1.3	2.0	2.5	2.0	1.0	0.6	0.4	0.3	0.2	0.2	0.1	0.2
34	0.2	0.2	0.5	1.0	1.4	1.2	1.1	1.5	2.4	2.7	2.1	1.0	0.5	0.4	0.3	0.2	0.2	0.1	0.2
36	0.1	0.2	0.5	1.1	1.5	1.4	1.3	1.8	2.7	2.9	2.1	0.9	0.5	0.3	0.2	0.2	0.2	0.1	0.2
38	0.1	0.2	0.5	1.1	1.6	1.6	1.4	2.1	3.0	3.0	2.0	0.9	0.4	0.3	0.2	0.2	0.2	0.1	0.2
40	0.1	0.2	0.5	1.2	1.8	1.7	1.5	2.4	3.3	3.0	2.0	0.8	0.4	0.2	0.2	0.2	0.2	0.1	0.2
42	0.1	0.1	0.5	1.2	1.9	1.9	1.8	2.7	3.5	3.1	1.9	0.8	0.4	0.2	0.2	0.2	0.2	0.1	0.2
44	0.1	0.1	0.4	1.2	1.9	2.0	2.0	2.9	3.6	3.0	1.8	0.7	0.3	0.2	0.1	0.2	0.2	0.1	0.2
46	0.0	0.1	0.4	1.2	2.0	2.1	2.1	3.0	3.6	2.9	1.7	0.6	0.3	0.1	0.1	0.2	0.2	0.1	0.2
48	0.0	0.1	0.4	1.2	2.0	2.2	2.2	3.1	3.6	2.8	1.6	0.6	0.2	0.1	0.1	0.2	0.2	0.1	0.2
50	0.0	0.1	0.3	1.2	2.0	2.3	2.3	3.1	3.5	2.7	1.5	0.5	0.2	0.1	0.1	0.2	0.2	0.1	0.2
52	0.	0.0	0.3	1.1	2.0	2.3	2.3	3.1	3.4	2.6	1.4	0.5	0.2	0.1	0.1	0.2	0.2	0.1	0.2
54	0.	0.0	0.3	1.1	2.0	2.3	2.4	3.0	3.2	2.4	1.3	0.4	0.1	0.0	0.1	0.2	0.2	0.1	0.2
56	0.	0.0	0.3	1.0	1.9	2.4	2.4	3.0	3.1	2.3	1.2	0.4	0.1	0.0	0.1	0.2	0.2	0.1	0.2
58	0.	0.	0.2	1.0	1.9	2.4	2.4	2.9	2.9	2.1	1.1	0.3	0.1	0.0	0.1	0.2	0.2	0.1	0.2
60	0.	0.	0.2	0.9	1.8	2.4	2.4	2.8	2.8	2.0	1.0	0.3	0.1	0.0	0.1	0.2	0.2	0.1	0.2
62	0.	0.	0.2	0.9	1.8	2.4	2.4	2.8	2.7	1.9	0.9	0.2	0.0	0.	0.1	0.2	0.2	0.1	0.2
64	0.	0.	0.2	0.9	1.8	2.4	2.5	2.8	2.6	1.7	0.9	0.2	0.0	0.	0.1	0.2	0.2	0.1	0.2
66	0.	0.	0.2	0.8	1.8	2.4	2.5	2.8	2.5	1.6	0.8	0.2	0.0	0.	0.1	0.2	0.2	0.1	0.2
68	0.	0.	0.2	0.8	1.8	2.4	2.5	2.7	2.5	1.5	0.7	0.2	0.0	0.	0.0	0.2	0.2	0.1	0.2
70	0.	0.	0.2	0.9	1.8	2.5	2.5	2.7	2.4	1.5	0.7	0.2	0.	0.	0.0	0.2	0.2	0.1	0.2
72	0.	0.	0.2	0.9	1.9	2.5	2.5	2.7	2.3	1.4	0.7	0.2	0.	0.	0.0	0.2	0.2	0.1	0.2
74	0.	0.	0.2	0.9	1.9	2.6	2.5	2.6	2.2	1.4	0.6	0.1	0.	0.	0.0	0.2	0.2	0.1	0.2
76	0.	0.0	0.3	1.0	2.0	2.6	2.5	2.6	2.2	1.3	0.6	0.1	0.	0.	0.0	0.2	0.2	0.1	0.2
78	0.	0.0	0.3	1.0	2.1	2.6	2.5	2.5	2.1	1.3	0.6	0.1	0.	0.	0.0	0.2	0.2	0.1	0.2
80	0.	0.0	0.3	1.1	2.1	2.6	2.5	2.5	2.1	1.3	0.6	0.1	0.	0.	0.0	0.2	0.2	0.1	0.2
82	0.0	0.1	0.4	1.2	2.2	2.6	2.5	2.4	2.1	1.3	0.6	0.1	0.	0.	0.0	0.2	0.2	0.1	0.2
84	0.0	0.1	0.4	1.2	2.2	2.6	2.4	2.4	2.1	1.3	0.6	0.1	0.	0.	0.0	0.2	0.2	0.1	0.2
86	0.0	0.1	0.4	1.3	2.3	2.6	2.4	2.4	2.1	1.3	0.6	0.1	0.	0.	0.0	0.2	0.2	0.1	0.2
88	0.1	0.1	0.4	1.3	2.3	2.6	2.4	2.4	2.1	1.3	0.6	0.1	0.	0.	0.1	0.2	0.2	0.1	0.2
90	0.1	0.1	0.4	1.3	2.3	2.6	2.4	2.4	2.0	1.3	0.6	0.1	0.	0.	0.1	0.2	0.2	0.1	0.2

TABLE XXIX (Continued)

TABLE XXIX (Continued)

	0	5	10	15	20	25	30	35	40	45	50	55	60	65	70	75	80	85	90
92	0.1	0.1	0.4	1.3	2.2	2.5	2.4	2.4	2.0	1.3	0.6	0.1	0.	0.	0.1	0.2	0.2	0.1	0.2
94	0.1	0.1	0.4	1.2	2.2	2.5	2.4	2.4	2.0	1.3	0.6	0.1	0.0	0.	0.0	0.2	0.2	0.1	0.2
96	0.1	0.1	0.4	1.2	2.2	2.5	2.4	2.4	2.0	1.3	0.6	0.1	0.0	0.	0.0	0.2	0.2	0.1	0.2
98	0.1	0.1	0.4	1.1	2.2	2.5	2.4	2.4	2.0	1.2	0.6	0.1	0.	0.	0.0	0.2	0.2	0.1	0.2
100	0.0	0.1	0.4	1.1	2.1	2.6	2.4	2.4	2.0	1.2	0.6	0.1	0.	0.	0.0	0.2	0.2	0.1	0.2
102	0.0	0.1	0.4	1.1	2.1	2.5	2.4	2.5	2.0	1.2	0.6	0.1	0.	0.	0.0	0.2	0.2	0.1	0.2
104	0.0	0.0	0.3	1.0	2.0	2.5	2.4	2.5	2.1	1.3	0.6	0.1	0.	0.	0.0	0.2	0.2	0.1	0.2
106	0.	0.0	0.3	1.0	2.0	2.5	2.4	2.6	2.1	1.3	0.6	0.1	0.	0.	0.0	0.2	0.2	0.1	0.2
108	0.	0.0	0.3	0.9	1.9	2.5	2.4	2.6	2.2	1.4	0.6	0.1	0.	0.	0.0	0.2	0.2	0.1	0.2
110	0.	0.	0.2	0.9	1.9	2.5	2.5	2.7	2.3	1.4	0.6	0.1	0.	0.	0.0	0.2	0.2	0.1	0.2
112	0.	0.	0.2	0.8	1.8	2.4	2.5	2.7	2.5	1.5	0.7	0.2	0.0	0.	0.1	0.2	0.1	0.1	0.2
114	0.	0.	0.2	0.8	1.8	2.4	2.5	2.8	2.6	1.6	0.7	0.2	0.0	0.	0.1	0.2	0.1	0.1	0.2
116	0.	0.	0.2	0.8	1.8	2.4	2.6	2.9	2.7	1.7	0.8	0.2	0.0	0.	0.1	0.2	0.1	0.1	0.2
118	0.	0.	0.2	0.8	1.8	2.4	2.6	3.0	2.9	1.8	0.9	0.2	0.0	0.	0.1	0.2	0.1	0.1	0.2
120	0.	0.	0.2	0.8	1.8	2.4	2.7	3.1	3.0	1.9	0.9	0.2	0.0	0.0	0.1	0.2	0.1	0.1	0.2
122	0.	0.	0.2	0.9	1.8	2.4	2.7	3.3	3.2	2.1	1.0	0.3	0.1	0.0	0.1	0.2	0.1	0.1	0.2
124	0.	0.	0.2	0.9	1.9	2.4	2.7	3.4	3.4	2.2	1.1	0.3	0.1	0.0	0.1	0.2	0.1	0.1	0.2
126	0.	0.	0.3	0.9	1.9	2.4	2.7	3.5	3.5	2.4	1.2	0.4	0.1	0.0	0.1	0.2	0.1	0.1	0.2
128	0.	0.0	0.3	1.0	2.0	2.4	2.7	3.5	3.7	2.6	1.3	0.4	0.1	0.1	0.1	0.2	0.1	0.1	0.2
130	0.	0.0	0.3	1.0	2.0	2.4	2.7	3.6	3.8	2.7	1.3	0.4	0.1	0.1	0.2	0.2	0.1	0.1	0.2
132	0.	0.0	0.3	1.1	2.0	2.4	2.6	3.5	3.9	2.9	1.4	0.5	0.2	0.1	0.2	0.3	0.1	0.1	0.2
134	0.0	0.0	0.3	1.1	2.0	2.4	2.6	3.5	4.0	3.0	1.5	0.5	0.2	0.1	0.2	0.3	0.1	0.1	0.2
136	0.0	0.1	0.4	1.2	2.0	2.3	2.4	3.4	4.0	3.2	1.6	0.6	0.3	0.2	0.3	0.3	0.1	0.1	0.2
138	0.0	0.1	0.4	1.2	2.0	2.2	2.3	3.2	3.9	3.2	1.7	0.7	0.3	0.2	0.3	0.3	0.1	0.1	0.2
140	0.0	0.1	0.4	1.2	2.0	2.1	2.1	2.9	3.8	3.2	1.8	0.7	0.3	0.2	0.3	0.3	0.1	0.1	0.2
142	0.1	0.1	0.4	1.2	1.9	1.9	1.9	2.7	3.5	3.2	1.9	0.8	0.4	0.3	0.4	0.3	0.1	0.1	0.2
144	0.1	0.2	0.5	1.2	1.8	1.8	1.7	2.3	3.3	3.1	1.9	0.8	0.4	0.3	0.4	0.3	0.1	0.1	0.2
146	0.1	0.2	0.5	1.2	1.7	1.6	1.5	2.0	2.9	2.9	1.9	0.8	0.5	0.4	0.5	0.4	0.1	0.1	0.2
148	0.1	0.2	0.5	1.2	1.6	1.4	1.2	1.7	2.5	2.7	1.9	0.9	0.5	0.4	0.5	0.4	0.1	0.1	0.2
150	0.1	0.3	0.6	1.2	1.5	1.2	1.0	1.4	2.1	2.5	1.9	0.9	0.5	0.4	0.6	0.4	0.1	0.1	0.2
152	0.1	0.3	0.6	1.1	1.3	1.1	0.9	1.1	1.8	2.2	1.8	0.9	0.5	0.5	0.6	0.4	0.1	0.1	0.2
154	0.2	0.4	0.6	1.1	1.2	0.9	0.7	0.9	1.4	1.9	1.7	0.9	0.6	0.5	0.7	0.4	0.1	0.1	0.2
156	0.2	0.4	0.7	1.1	1.1	0.8	0.6	0.7	1.1	1.6	1.5	0.9	0.6	0.6	0.7	0.5	0.1	0.1	0.2
158	0.2	0.4	0.7	1.0	1.0	0.7	0.5	0.6	0.9	1.3	1.4	0.8	0.6	0.6	0.8	0.5	0.1	0.1	0.2
160	0.3	0.5	0.7	1.0	0.9	0.6	0.4	0.5	0.7	1.0	1.2	0.8	0.6	0.6	0.9	0.5	0.1	0.1	0.2
162	0.3	0.6	0.8	1.0	0.9	0.5	0.4	0.4	0.5	0.8	1.0	0.8	0.6	0.7	0.9	0.5	0.1	0.1	0.2
164	0.4	0.6	0.8	1.0	0.8	0.5	0.3	0.4	0.4	0.7	0.9	0.7	0.6	0.7	1.0	0.6	0.1	0.1	0.2
166	0.4	0.6	0.9	1.0	0.7	0.4	0.3	0.3	0.4	0.5	0.7	0.7	0.6	0.7	1.1	0.6	0.1	0.1	0.2
168	0.4	0.7	0.9	1.0	0.7	0.4	0.3	0.3	0.3	0.4	0.6	0.6	0.6	0.7	1.1	0.6	0.1	0.1	0.2
170	0.5	0.7	1.0	1.0	0.6	0.3	0.2	0.3	0.3	0.3	0.5	0.6	0.6	0.8	1.2	0.6	0.1	0.1	0.2
172	0.5	0.8	1.0	1.0	0.6	0.3	0.2	0.3	0.3	0.3	0.4	0.5	0.6	0.8	1.2	0.6	0.1	0.1	0.2
174	0.5	0.8	1.1	1.0	0.5	0.3	0.2	0.3	0.3	0.3	0.4	0.5	0.6	0.8	1.2	0.6	0.1	0.1	0.2
176	0.6	0.8	1.1	0.9	0.5	0.2	0.2	0.3	0.3	0.3	0.3	0.4	0.6	0.8	1.2	0.6	0.1	0.1	0.2
178	0.6	0.8	1.1	0.9	0.5	0.2	0.2	0.3	0.2	0.2	0.3	0.4	0.6	0.8	1.3	0.6		0.1	0.2
180	0.6	0.8	1.1	0.9	0.5	0.2	0.2	0.3	0.2	0.2	0.3	0.4	0.6	0.8	1.3	0.6	0.4	0.1	0.2

TABLE XXIX (Continued)

	0	5	10	15	20	25	30	35	40	45	50	55	60	65	70	75	80	85	90
272	0.1	0.1	0.5	1.3	2.4	2.6	2.3	2.2	1.9	1.2	0.5	0.1	0.	0.	0.0	0.2	0.2	0.1	0.2
274	0.1	0.1	0.5	1.3	2.5	2.6	2.3	2.2	1.9	1.2	0.5	0.1	0.	0.	0.0	0.2	0.2	0.1	0.2
276	0.1	0.1	0.5	1.3	2.5	2.6	2.3	2.3	1.9	1.2	0.5	0.1	0.	0.	0.0	0.2	0.2	0.1	0.2
278	0.1	0.1	0.4	1.3	2.4	2.6	2.4	2.3	1.9	1.2	0.5	0.1	0.	0.	0.0	0.2	0.2	0.1	0.2
280	0.0	0.1	0.4	1.2	2.4	2.6	2.4	2.3	1.9	1.2	0.5	0.1	0.	0.	0.0	0.2	0.2	0.1	0.2
282	0.0	0.1	0.4	1.2	2.3	2.5	2.4	2.3	1.9	1.2	0.6	0.1	0.	0.	0.0	0.2	0.2	0.1	0.2
284	0.0	0.1	0.3	1.1	2.3	2.5	2.4	2.4	1.9	1.2	0.6	0.1	0.	0.	0.0	0.2	0.2	0.1	0.2
286	0.	0.0	0.3	1.1	2.2	2.5	2.4	2.4	1.9	1.3	0.6	0.1	0.	0.	0.0	0.2	0.2	0.1	0.2
288	0.	0.0	0.3	1.0	2.2	2.5	2.5	2.4	2.0	1.3	0.6	0.1	0.	0.	0.0	0.2	0.2	0.1	0.2
290	0.	0.	0.2	1.0	2.1	2.5	2.5	2.5	2.0	1.3	0.6	0.1	0.	0.	0.0	0.2	0.2	0.1	0.2
292	0.	0.	0.2	1.0	2.1	2.5	2.5	2.6	2.1	1.3	0.6	0.1	0.	0.	0.0	0.2	0.2	0.1	0.2
294	0.	0.	0.2	0.9	2.0	2.5	2.5	2.6	2.2	1.4	0.6	0.1	0.	0.	0.0	0.2	0.2	0.1	0.2
296	0.	0.	0.2	0.9	2.0	2.5	2.6	2.7	2.2	1.4	0.7	0.1	0.	0.	0.0	0.2	0.2	0.1	0.2
298	0.	0.	0.2	0.9	2.0	2.5	2.6	2.8	2.4	1.5	0.7	0.2	0.	0.	0.0	0.2	0.2	0.1	0.2
300	0.	0.	0.2	0.9	1.9	2.5	2.6	2.9	2.5	1.5	0.8	0.2	0.0	0.	0.0	0.2	0.2	0.1	0.2
302	0.	0.	0.2	0.9	1.9	2.5	2.7	3.0	2.7	1.7	0.8	0.2	0.0	0.	0.0	0.2	0.2	0.1	0.2
304	0.	0.	0.2	0.9	1.9	2.5	2.7	3.1	2.9	1.8	0.9	0.2	0.0	0.	0.0	0.2	0.2	0.1	0.2
306	0.	0.	0.2	0.9	1.9	2.5	2.7	3.2	3.1	2.0	1.0	0.3	0.1	0.	0.0	0.2	0.2	0.1	0.2
308	0.	0.	0.2	0.9	1.9	2.5	2.7	3.3	3.3	2.2	1.1	0.3	0.1	0.	0.1	0.2	0.2	0.1	0.2
310	0.	0.0	0.3	1.0	1.9	2.4	2.7	3.5	3.5	2.4	1.2	0.3	0.1	0.0	0.1	0.2	0.2	0.1	0.2
312	0.	0.0	0.3	1.0	1.9	2.4	2.7	3.5	3.8	2.6	1.3	0.4	0.1	0.0	0.1	0.1	0.2	0.1	0.2
314	0.	0.0	0.3	1.1	1.9	2.3	2.6	3.6	4.0	2.8	1.4	0.4	0.2	0.1	0.1	0.1	0.2	0.1	0.2
316	0.0	0.1	0.3	1.1	1.9	2.2	2.5	3.5	4.1	3.0	1.6	0.5	0.2	0.1	0.1	0.1	0.2	0.1	0.2
318	0.0	0.1	0.4	1.1	1.8	2.1	2.3	3.4	4.2	3.2	1.7	0.6	0.2	0.1	0.1	0.1	0.2	0.1	0.2
320	0.0	0.1	0.4	1.1	1.8	1.9	2.1	3.3	4.3	3.4	1.9	0.6	0.3	0.1	0.1	0.1	0.2	0.1	0.2
322	0.1	0.1	0.4	1.1	1.7	1.8	1.9	3.3	4.2	3.5	2.0	0.7	0.3	0.2	0.1	0.2	0.2	0.1	0.2
324	0.1	0.1	0.4	1.0	1.6	1.6	1.7	3.2	4.0	3.6	2.1	0.8	0.4	0.2	0.2	0.2	0.2	0.1	0.2
326	0.1	0.1	0.4	0.9	1.4	1.4	1.4	2.9	3.7	3.6	2.2	0.9	0.4	0.2	0.2	0.2	0.2	0.1	0.2
328	0.2	0.2	0.4	0.9	1.3	1.2	1.2	2.8	3.3	3.5	2.3	1.0	0.5	0.3	0.2	0.2	0.2	0.1	0.2
330	0.2	0.2	0.4	0.8	1.2	1.1	1.0	2.7	3.3	3.3	2.3	1.0	0.5	0.3	0.2	0.2	0.2	0.1	0.2
332	0.2	0.2	0.3	0.8	1.0	0.9	0.8	2.5	3.3	3.3	2.3	1.1	0.5	0.4	0.3	0.2	0.2	0.1	0.2
334	0.3	0.2	0.3	0.7	0.9	0.8	0.7	2.4	3.1	3.3	2.3	1.1	0.6	0.4	0.3	0.2	0.2	0.2	0.2
336	0.3	0.2	0.3	0.7	0.8	0.7	0.6	2.3	3.0	3.2	2.3	1.1	0.6	0.4	0.3	0.2	0.2	0.2	0.2
338	0.3	0.3	0.3	0.6	0.7	0.6	0.5	2.2	2.9	3.1	2.3	1.1	0.6	0.5	0.3	0.2	0.2	0.2	0.2
340	0.4	0.3	0.4	0.6	0.7	0.5	0.4	2.1	2.8	3.0	2.2	1.1	0.6	0.5	0.4	0.2	0.2	0.2	0.2
342	0.4	0.3	0.4	0.6	0.6	0.5	0.4	2.0	2.7	2.9	2.1	1.1	0.6	0.5	0.4	0.2	0.2	0.2	0.2
344	0.4	0.4	0.4	0.5	0.6	0.5	0.4	1.9	2.6	2.8	2.1	1.1	0.6	0.5	0.4	0.2	0.2	0.2	0.2
346	0.5	0.4	0.4	0.5	0.5	0.5	0.4	1.8	2.5	2.7	2.0	1.1	0.6	0.5	0.4	0.2	0.2	0.2	0.2
348	0.5	0.5	0.5	0.5	0.5	0.4	0.3	1.7	2.4	2.6	2.0	1.1	0.6	0.5	0.4	0.2	0.2	0.2	0.2
350	0.5	0.5	0.5	0.5	0.5	0.4	0.3	1.6	2.3	2.5	1.9	1.1	0.6	0.5	0.4	0.2	0.2	0.2	0.2
352	0.5	0.5	0.5	0.5	0.5	0.4	0.3	1.5	2.2	2.4	1.8	1.1	0.6	0.5	0.4	0.2	0.2	0.2	0.2
354	0.5	0.5	0.5	0.5	0.5	0.4	0.3	1.4	2.1	2.3	1.8	1.1	0.6	0.5	0.4	0.2	0.2	0.2	0.2
356	0.5	0.5	0.5	0.5	0.5	0.4	0.3	1.3	2.0	2.2	1.7	1.1	0.6	0.5	0.4	0.2	0.2	0.2	0.2
358	0.5	0.5	0.5	0.5	0.5	0.4	0.3	1.2	1.9	2.1	1.7	1.1	0.6	0.5	0.4	0.2	0.2	0.2	0.2
360	0.5	0.5	0.5	0.5	0.5	0.4	0.3	1.2	1.8	2.0	1.6	1.1	0.6	0.5	0.4	0.2	0.2	0.2	0.2
362	0.5	0.5	0.5	0.5	0.5	0.4	0.3	1.1	1.7	1.9	1.6	1.1	0.6	0.5	0.4	0.2	0.2	0.2	0.2
364	0.5	0.5	0.5	0.5	0.5	0.4	0.3	1.1	1.6	1.8	1.5	1.1	0.6	0.5	0.4	0.2	0.2	0.2	0.2
366	0.5	0.5	0.5	0.5	0.5	0.4	0.3	1.0	1.5	1.7	1.5	1.1	0.6	0.5	0.4	0.2	0.2	0.2	0.2
368	0.5	0.5	0.5	0.5	0.5	0.4	0.3	1.0	1.4	1.6	1.4	1.1	0.6	0.5	0.4	0.2	0.2	0.2	0.2
370	0.5	0.5	0.5	0.5	0.5	0.4	0.3	0.9	1.3	1.5	1.4	1.1	0.6	0.5	0.4	0.2	0.2	0.2	0.2
372	0.5	0.5	0.5	0.5	0.5	0.4	0.3	0.9	1.3	1.4	1.3	1.1	0.6	0.5	0.4	0.2	0.2	0.2	0.2
374	0.5	0.5	0.5	0.5	0.5	0.4	0.3	0.8	1.2	1.3	1.3	1.1	0.6	0.5	0.4	0.2	0.2	0.2	0.2
376	0.5	0.5	0.5	0.5	0.5	0.4	0.3	0.8	1.1	1.2	1.2	1.1	0.6	0.5	0.4	0.2	0.2	0.2	0.2
378	0.5	0.5	0.5	0.5	0.5	0.4	0.3	0.7	1.0	1.1	1.1	1.1	0.6	0.5	0.4	0.2	0.2	0.2	0.2
380	0.5	0.5	0.5	0.5	0.5	0.4	0.3	0.7	0.9	1.0	1.0	1.1	0.6	0.5	0.4	0.2	0.2	0.2	0.2
382	0.5	0.5	0.5	0.5	0.5	0.4	0.3	0.6	0.8	0.9	0.9	1.1	0.6	0.5	0.4	0.2	0.2	0.2	0.2
384	0.5	0.5	0.5	0.5	0.5	0.4	0.3	0.5	0.7	0.8	0.8	1.1	0.6	0.5	0.4	0.2	0.2	0.2	0.2
386	0.5	0.5	0.5	0.5	0.5	0.4	0.3	0.5	0.6	0.7	0.7	1.1	0.6	0.5	0.4	0.2	0.2	0.2	0.2
388	0.5	0.5	0.5	0.5	0.5	0.4	0.3	0.4	0.5	0.6	0.6	1.1	0.6	0.5	0.4	0.2	0.2	0.2	0.2
390	0.5	0.5	0.5	0.5	0.5	0.4	0.3	0.4	0.5	0.5	0.5	1.1	0.6	0.5	0.4	0.2	0.2	0.2	0.2
392	0.5	0.5	0.5	0.5	0.5	0.4	0.3	0.3	0.4	0.4	0.4	1.1	0.6	0.5	0.4	0.2	0.2	0.2	0.2
394	0.5	0.5	0.5	0.5	0.5	0.4	0.3	0.3	0.3	0.3	0.3	1.1	0.6	0.5	0.4	0.2	0.2	0.2	0.2
396	0.5	0.5	0.5	0.5	0.5	0.4	0.3	0.2	0.3	0.3	0.3	1.1	0.6	0.5	0.4	0.2	0.2	0.2	0.2
398	0.5	0.5	0.5	0.5	0.5	0.4	0.3	0.2	0.2	0.2	0.2	1.1	0.6	0.5	0.4	0.2	0.2	0.2	0.2
400	0.5	0.5	0.5	0.5	0.5	0.4	0.3	0.2	0.2	0.2	0.2	1.1	0.6	0.5	0.4	0.2	0.2	0.2	0.2
402	0.5	0.5	0.5	0.5	0.5	0.4	0.3	0.2	0.2	0.2	0.2	1.1	0.6	0.5	0.4	0.2	0.2	0.2	0.2
404	0.5	0.5	0.5	0.5	0.5	0.4	0.3	0.2	0.2	0.2	0.2	1.1	0.6	0.5	0.4	0.2	0.2	0.2	0.2
406	0.5	0.5	0.5	0.5	0.5	0.4	0.3	0.2	0.2	0.2	0.2	1.1	0.6	0.5	0.4	0.2	0.2	0.2	0.2
408	0.5	0.5	0.5	0.5	0.5	0.4	0.3	0.2	0.2	0.2	0.2	1.1	0.6	0.5	0.4	0.2	0.2	0.2	0.2
410	0.5	0.5	0.5	0.5	0.5	0.4	0.3	0.2	0.2	0.2	0.2	1.1	0.6	0.5	0.4	0.2	0.2	0.2	0.2
412	0.5	0.5	0.5	0.5	0.5	0.4	0.3	0.2	0.2	0.2	0.2	1.1	0.6	0.5	0.4	0.2	0.2	0.2	0.2
414	0.5	0.5	0.5	0.5	0.5	0.4	0.3	0.2	0.2	0.2	0.2	1.1	0.6	0.5	0.4	0.2	0.2	0.2	0.2
416	0.5	0.5	0.5	0.5	0.5	0.4	0.3	0.2	0.2	0.2	0.2	1.1	0.6	0.5	0.4	0.2	0.2	0.2	0.2
418	0.5	0.5	0.5	0.5	0.5	0.4	0.3	0.2	0.2	0.2	0.2	1.1	0.6	0.5	0.4	0.2	0.2	0.2	0.2
420	0.5	0.5	0.5	0.5	0.5	0.4	0.3	0.2	0.2	0.2	0.2	1.1	0.6	0.5	0.4	0.2	0.2	0.2	0.2
422	0.5	0.5	0.5	0.5	0.5	0.4	0.3	0.2	0.2	0.2	0.2	1.1	0.6	0.5	0.4	0.2	0.2	0.2	0.2
424	0.5	0.5	0.5	0.5	0.5	0.4	0.3	0.2	0.2	0.2	0.2	1.1	0.6	0.5	0.4	0.2	0.2	0.2	0.2
426	0.5	0.5	0.5	0.5	0.5	0.4	0.3	0.2	0.2	0.2	0.2	1.1	0.6	0.5	0.4	0.2	0.2	0.2	0.2
428	0.5	0.5	0.5	0.5	0.5	0.4	0.3	0.2	0.2	0.2	0.2	1.1	0.6	0.5	0.4	0.2	0.2	0.2	0.2
430	0.5	0.5	0.5	0.5	0.5	0.4	0.3	0.2	0.2	0.2	0.2	1.1	0.6	0.5	0.4	0.2	0.2	0.2	0.2
432	0.5	0.5	0.5	0.5	0.5	0.4	0.3	0.2	0.2	0.2	0.2	1.1	0.6	0.5	0.4	0.2	0.2	0.2	0.2
434	0.5	0.5	0.5	0.5	0.5	0.4	0.3	0.2	0.2	0.2	0.2	1.1	0.6	0.5	0.4	0.2	0.2	0.2	0.2
436	0.5	0.5	0.5	0.5	0.5	0.4	0.3	0.2	0.2	0.2	0.2	1.1	0.6	0.5	0.4	0.2	0.2	0.2	0.2
438	0.5	0.5	0.5	0.5	0.5	0.4	0.3	0.2	0.2	0.2	0.2	1.1	0.6	0.5	0.4	0.2	0.2	0.2	0.2
440	0.5	0.5	0.5	0.5	0.5	0.4	0.3	0.2	0.2	0.2	0.2	1.1	0.6	0.5	0.4	0.2	0.2	0.2	0.2

POLE FIGURE DATA SHEET FOR SPECIMEN 1B

The normalized pole figure is based on Mo k-alpha radiation and the 111 reflection.

The 222 reflection was used to fill in the blind region from 80 through 90 degrees alpha.

The alpha-dependent two theta shift was taken into account.

Integrated intensities were used.

Normal smoothing was used.

Maximum and minimum corrected intensities are 1098 and 0 counts/second, respectively.

Random intensity is 343 counts/second.

Contour spacing is based on multiples of random intensity.

4 contours are to be plotted.

Their values are 1.000 2.000 3.000 4.000.

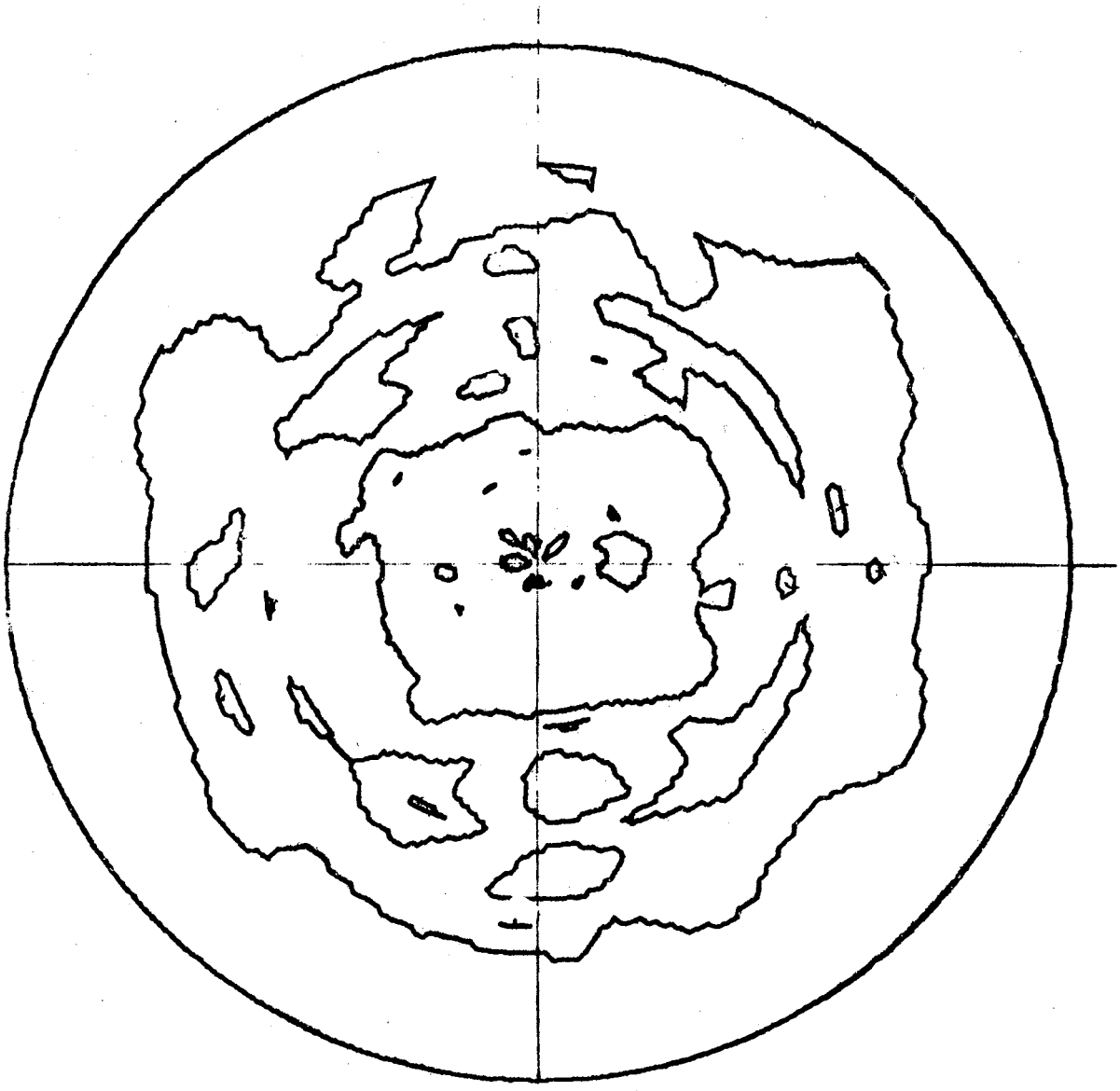

Figure 33. (111) Pole Figure for Specimen 1B

TABLE XXX

POLE FIGURE DATA FOR SPECIMEN 1B

	0	5	10	15	20	25	30	35	40	45	50	55	60	65	70	75	80	85
2	0.4	0.4	0.5	0.9	0.7	1.1	0.9	1.7	1.0	1.0	1.1	1.3	1.0	1.0	0.8	0.5	0.8	1.0
4	0.4	0.5	0.5	0.9	0.6	1.1	0.9	1.7	1.0	1.0	1.1	1.2	0.9	1.0	0.9	0.5	0.8	1.0
6	0.5	0.5	0.5	0.8	0.6	1.1	0.9	1.7	1.0	1.0	1.1	1.2	0.9	1.0	0.9	0.5	0.8	1.0
8	0.5	0.5	0.5	0.8	0.6	1.1	1.0	1.7	1.0	1.1	1.0	1.1	0.8	1.0	0.9	0.5	0.8	1.0
10	0.5	0.5	0.6	0.8	0.6	1.1	1.0	1.7	1.1	1.2	1.0	1.1	0.8	1.0	0.9	0.5	0.8	1.0
12	0.5	0.4	0.6	0.9	0.7	1.0	1.0	1.7	1.2	1.2	0.9	1.1	0.8	0.9	0.9	0.5	0.8	1.1
14	0.5	0.3	0.6	1.0	0.8	1.0	1.1	1.8	1.2	1.3	0.9	1.2	0.8	0.9	0.9	0.5	0.8	1.1
16	0.4	0.3	0.6	1.1	0.8	1.0	1.1	1.8	1.3	1.3	0.9	1.2	0.8	0.8	0.9	0.5	0.9	1.1
18	0.4	0.2	0.6	1.1	1.0	1.0	1.1	1.9	1.4	1.3	0.9	1.3	0.8	0.8	0.9	0.5	0.9	1.1
20	0.4	0.2	0.5	1.1	1.1	1.0	1.1	2.0	1.5	1.4	0.9	1.4	0.8	0.8	0.9	0.6	0.9	1.2
22	0.3	0.2	0.5	1.1	1.2	1.0	1.2	2.0	1.6	1.4	0.9	1.4	0.8	0.7	0.9	0.6	0.8	1.2
24	0.3	0.2	0.4	1.0	1.3	1.0	1.2	2.1	1.7	1.5	1.0	1.5	0.7	0.7	0.9	0.6	0.8	1.1
26	0.3	0.2	0.4	0.9	1.4	1.0	1.2	2.1	1.7	1.5	1.1	1.6	0.7	0.7	1.0	0.7	0.8	1.1
28	0.2	0.2	0.3	0.8	1.4	1.0	1.3	2.2	1.8	1.7	1.1	1.6	0.7	0.7	1.0	0.7	0.8	1.1
30	0.2	0.2	0.3	0.7	1.4	1.0	1.4	2.2	1.8	1.8	1.2	1.6	0.6	0.7	1.0	0.7	0.8	1.1
32	0.1	0.2	0.2	0.6	1.3	1.0	1.4	2.3	1.8	1.9	1.3	1.6	0.6	0.7	1.0	0.6	0.8	1.0
34	0.1	0.2	0.2	0.6	1.2	1.0	1.4	2.4	1.9	1.9	1.4	1.5	0.5	0.7	1.0	0.6	0.9	1.0
36	0.0	0.1	0.1	0.5	1.1	1.0	1.4	2.4	1.9	2.0	1.4	1.5	0.5	0.6	1.0	0.6	0.9	1.0
38	0.0	0.1	0.1	0.5	1.0	0.9	1.4	2.5	1.9	2.1	1.5	1.4	0.4	0.6	1.0	0.5	1.0	1.0
40	0.0	0.0	0.1	0.5	0.9	0.8	1.3	2.6	2.0	2.2	1.4	1.3	0.4	0.5	0.9	0.5	1.0	1.0
42	0.0	0.	0.1	0.5	0.9	0.8	1.2	2.6	2.1	2.3	1.4	1.2	0.3	0.5	0.8	0.5	1.1	1.0
44	0.0	0.	0.1	0.6	0.9	0.8	1.2	2.7	2.2	2.4	1.3	1.1	0.3	0.4	0.7	0.5	1.1	1.0
46	0.0	0.	0.2	0.7	0.9	0.9	1.2	2.7	2.2	2.4	1.2	1.0	0.2	0.4	0.6	0.5	1.1	1.0
48	0.0	0.	0.3	0.8	1.0	0.9	1.2	2.7	2.3	2.4	1.2	1.0	0.2	0.4	0.6	0.5	1.1	0.9
50	0.0	0.	0.4	1.0	1.0	1.0	1.3	2.8	2.3	2.4	1.1	1.0	0.2	0.4	0.5	0.5	1.1	0.9
52	0.1	0.	0.5	1.2	1.1	1.1	1.4	2.7	2.3	2.3	1.0	1.0	0.2	0.4	0.5	0.5	1.1	0.9
54	0.1	0.1	0.6	1.4	1.1	1.2	1.5	2.7	2.2	2.1	0.9	1.0	0.2	0.3	0.4	0.5	1.0	0.9
56	0.2	0.2	0.7	1.6	1.2	1.3	1.7	2.6	2.1	2.0	0.9	1.0	0.2	0.3	0.4	0.5	1.0	0.9
58	0.3	0.2	0.8	1.7	1.2	1.4	1.8	2.5	2.0	1.8	0.9	1.0	0.2	0.3	0.5	0.6	0.9	0.9
60	0.4	0.3	0.8	1.9	1.3	1.5	1.9	2.4	1.8	1.6	0.9	1.0	0.2	0.4	0.5	0.6	0.8	0.9
62	0.5	0.3	0.8	1.9	1.4	1.6	1.9	2.2	1.6	1.4	0.9	1.0	0.2	0.4	0.5	0.6	0.8	1.0
64	0.6	0.3	0.8	1.9	1.5	1.6	1.9	2.1	1.5	1.3	1.0	0.9	0.2	0.4	0.6	0.6	0.8	1.0
66	0.6	0.3	0.8	1.8	1.6	1.6	1.9	2.0	1.3	1.2	1.0	0.9	0.1	0.4	0.6	0.7	0.7	1.0
68	0.6	0.2	0.8	1.7	1.6	1.7	1.8	1.9	1.2	1.1	1.0	0.8	0.1	0.4	0.7	0.7	0.8	1.1
70	0.6	0.2	0.7	1.5	1.7	1.7	1.7	1.9	1.2	1.1	1.1	0.7	0.1	0.4	0.7	0.7	0.8	1.1
72	0.5	0.2	0.7	1.3	1.7	1.8	1.5	1.8	1.1	1.1	1.1	0.7	0.1	0.4	0.7	0.8	0.8	1.1
74	0.4	0.1	0.7	1.2	1.7	1.8	1.4	1.7	1.1	1.1	1.0	0.8	0.1	0.4	0.7	0.8	0.8	1.1
76	0.3	0.1	0.6	1.0	1.6	1.7	1.2	1.6	1.1	1.1	1.0	0.8	0.2	0.5	0.7	0.9	0.9	1.1
78	0.2	0.1	0.6	0.9	1.6	1.6	1.1	1.6	1.2	1.1	1.0	0.9	0.2	0.5	0.6	0.9	0.9	1.2
80	0.1	0.1	0.6	0.8	1.5	1.5	1.0	1.5	1.2	1.2	0.9	1.1	0.2	0.5	0.7	0.9	0.9	1.2
82	0.1	0.1	0.5	0.8	1.5	1.4	0.9	1.4	1.2	1.2	0.9	1.2	0.3	0.6	0.7	0.9	0.9	1.2
84	0.1	0.1	0.5	0.8	1.5	1.2	0.9	1.4	1 °	1.3	0.9	1.2	0.3	0.7	0.7	0.9	0.9	1.2
86	0.1	0.1	0.5	0.8	1.5	1.1	0.9	1.4	1	1.3	1.0	1.3	0.4	0.8	0.8	0.9	0.9	1.2
88	0.1	0.1	0.4	0.8	1.5	1.0	0.9	1.5	1.4	1.4	1.1	1.4	0.4	0.9	0.9	0.9	0.9	1.2

TABLE XXX (Continued)

	0	5	10	15	20	25	30	35	40	45	50	55	60	65	70	75	80	85	∞
92	0.1	0.1	0.3	0.8	1.4	0.9	1.0	1.8	1.6	1.4	1.2	1.4	0.5	0.9	1.1	0.9	0.9	1.2	0.
94	0.1	0.1	0.3	0.8	1.3	0.9	1.1	1.9	1.7	1.5	1.3	1.4	0.5	0.9	1.1	0.9	0.8	1.2	0.
96	0.1	0.1	0.2	0.8	1.2	1.0	1.1	2.0	1.7	1.5	1.3	1.4	0.5	0.9	1.1	0.9	0.8	1.2	0.
98	0.1	0.1	0.2	0.8	1.2	1.0	1.2	2.1	1.8	1.5	1.4	1.3	0.4	0.8	1.1	0.9	0.8	1.2	0.
100	0.1	0.0	0.3	0.8	1.2	1.1	1.2	2.1	1.8	1.5	1.4	1.3	0.4	0.8	1.0	0.9	0.8	1.1	0.
102	0.1	0.0	0.3	0.8	1.2	1.2	1.2	2.0	1.8	1.6	1.4	1.3	0.4	0.8	1.0	1.0	0.8	1.1	0.
104	0.1	0.0	0.3	0.8	1.2	1.2	1.3	1.9	1.7	1.6	1.3	1.3	0.4	0.8	0.9	1.0	0.8	1.0	0.
106	0.1	0.0	0.4	0.8	1.2	1.1	1.3	1.9	1.7	1.7	1.3	1.2	0.4	0.8	0.8	1.0	0.8	1.0	0.
108	0.1	0.0	0.4	0.8	1.2	1.1	1.3	1.8	1.6	1.7	1.3	1.2	0.4	0.9	0.8	1.0	0.9	1.0	0.
110	0.1	0.0	0.4	0.8	1.2	1.0	1.4	1.8	1.5	1.7	1.2	1.1	0.5	0.9	0.8	1.0	0.9	0.9	0.
112	0.1	0.1	0.5	0.8	1.3	0.9	1.4	1.9	1.4	1.6	1.2	1.1	0.5	1.0	0.8	0.9	0.9	0.9	0.
114	0.2	0.1	0.6	0.8	1.3	0.9	1.4	2.0	1.3	1.6	1.1	1.0	0.4	1.0	0.9	0.9	0.8	0.9	0.
116	0.2	0.2	0.6	0.8	1.4	0.9	1.5	2.1	1.3	1.5	1.1	1.0	0.4	1.0	1.0	0.9	0.8	0.8	0.
118	0.3	0.2	0.7	0.8	1.5	0.9	1.5	2.2	1.3	1.5	1.1	1.0	0.4	0.9	1.0	0.9	0.8	0.8	0.
120	0.3	0.2	0.7	0.9	1.6	1.0	1.6	2.3	1.4	1.5	1.1	1.0	0.3	0.8	1.0	0.9	0.8	0.8	0.
122	0.4	0.3	0.7	0.9	1.7	1.1	1.6	2.3	1.4	1.5	1.1	1.0	0.3	0.8	1.0	0.9	0.8	0.8	0.
124	0.5	0.3	0.7	1.0	1.7	1.2	1.6	2.3	1.5	1.5	1.2	1.1	0.2	0.7	1.0	0.9	0.7	0.9	0.
126	0.5	0.3	0.7	1.1	1.7	1.3	1.6	2.2	1.5	1.5	1.2	1.1	0.2	0.6	0.9	0.9	0.7	0.9	0.
128	0.5	0.3	0.7	1.1	1.7	1.3	1.6	2.2	1.6	1.5	1.1	1.1	0.2	0.6	0.9	0.9	0.7	0.9	0.
130	0.6	0.3	0.6	1.2	1.5	1.4	1.6	2.1	1.6	1.5	1.1	1.1	0.2	0.5	0.8	1.0	0.7	0.9	0.
132	0.5	0.3	0.6	1.2	1.4	1.4	1.6	2.0	1.6	1.5	1.1	1.1	0.2	0.5	0.7	1.0	0.8	0.9	0.
134	0.5	0.3	0.5	1.2	1.3	1.3	1.6	2.0	1.6	1.4	1.1	1.0	0.3	0.5	0.7	1.0	0.8	0.9	0.
136	0.4	0.2	0.4	1.1	1.2	1.3	1.6	2.0	1.7	1.3	1.0	1.0	0.3	0.5	0.7	1.0	0.8	1.0	0.
138	0.3	0.2	0.4	1.0	1.1	1.3	1.7	2.1	1.8	1.2	1.0	0.9	0.3	0.5	0.7	1.0	0.8	1.0	0.
140	0.2	0.1	0.3	0.9	1.0	1.3	1.8	2.2	1.9	1.2	1.0	0.8	0.3	0.4	0.8	1.0	0.8	1.0	0.
142	0.1	0.0	0.3	0.8	1.0	1.3	1.9	2.3	2.1	1.2	1.0	0.8	0.2	0.4	0.8	0.9	0.8	1.0	0.
144	0.1	0.	0.2	0.7	1.1	1.3	2.0	2.4	2.3	1.2	1.0	0.7	0.2	0.4	0.9	0.9	0.8	1.0	0.
146	0.	0.	0.2	0.7	1.1	1.4	2.1	2.6	2.5	1.3	1.0	0.7	0.2	0.4	0.9	0.9	0.8	1.0	0.
148	0.	0.	0.2	0.6	1.2	1.5	2.2	2.8	2.7	1.5	1.0	0.8	0.2	0.4	0.9	0.9	0.8	1.0	0.
150	0.	0.	0.1	0.7	1.2	1.6	2.3	2.9	2.8	1.6	1.1	0.8	0.2	0.4	0.9	0.9	0.9	1.0	0.
152	0.	0.	0.1	0.7	1.2	1.7	2.2	3.1	2.8	1.8	1.2	0.9	0.2	0.5	0.9	0.8	0.9	1.1	0.
154	0.	0.	0.1	0.8	1.2	1.8	2.2	3.2	2.7	1.9	1.4	1.0	0.2	0.5	0.8	0.8	0.9	1.1	0.
156	0.	0.	0.1	0.9	1.2	1.8	2.1	3.2	2.5	2.0	1.5	1.1	0.3	0.5	0.8	0.8	0.9	1.1	0.
158	0.	0.	0.2	0.9	1.2	1.8	2.0	3.2	2.3	2.1	1.7	1.2	0.3	0.5	0.7	0.8	0.9	1.1	0.
160	0.0	0.	0.2	0.9	1.2	1.7	1.9	3.1	2.1	2.1	1.8	1.3	0.3	0.5	0.7	0.7	0.8	1.1	0.
162	0.0	0.	0.3	0.9	1.3	1.6	1.7	2.9	1.8	2.0	1.9	1.4	0.3	0.5	0.6	0.7	0.8	1.1	0.
164	0.1	0.0	0.3	0.9	1.3	1.5	1.6	2.7	1.7	1.9	2.0	1.5	0.3	0.5	0.6	0.7	0.8	1.0	0.
166	0.1	0.0	0.4	0.9	1.5	1.3	1.5	2.4	1.5	1.8	2.0	1.5	0.3	0.6	0.6	0.6	0.7	1.0	0.
168	0.1	0.1	0.4	0.8	1.6	1.2	1.4	2.2	1.4	1.7	1.9	1.6	0.3	0.6	0.7	0.6	0.7	1.0	0.
170	0.2	0.1	0.4	0.8	1.7	1.1	1.3	1.9	1.4	1.5	1.8	1.6	0.3	0.6	0.7	0.6	0.7	1.0	0.
172	0.3	0.2	0.4	0.8	1.9	1.0	1.2	1.7	1.3	1.3	1.6	1.7	0.4	0.5	0.8	0.6	0.6	1.0	0.
174	0.3	.2	0.3	0.8	2.0	0.9	1.1	1.6	1.	1.2	1.4	1.7	0.4	0.5	0.9	0.6	.6	1.0	0.
176	0.4	.2	0.3	0.9	2.1	0.9	1.0	1.5	1.1	1.1	1.3	1.8	0.4	0.5	0.9	0.5	0.6	1.0	0.
178	0.5	0.2	0.3	0.9	2.1	0.9	0.	1.4	1.0	0.9	1.2	1.9	0.4	0.5	0.9	0.6	0.6	1.	0.

TABLE XXX (Continued)

	0	5	10	15	20	25	30	35	40	45	50	55	60	65	70	75	80	85	9
182	0.6	0.2	0.2	1.0	1.8	0.9	0.8	1.3	0.8	0.8	1.0	2.0	0.4	0.6	0.9	0.6	0.6	1.1	0.
184	0.6	0.2	0.2	1.0	1.5	1.0	0.7	1.3	0.7	0.7	1.0	2.1	0.4	0.6	0.8	0.6	0.7	1.1	0.
186	0.6	0.2	0.2	1.0	1.3	1.0	0.7	1.3	0.7	0.7	1.1	2.2	0.4	0.6	0.8	0.6	0.7	1.1	0.
188	0.6	0.2	0.2	1.0	1.1	1.0	0.7	1.4	0.7	0.6	1.1	2.2	0.4	0.7	0.8	0.5	0.7	1.1	0.
190	0.5	0.3	0.3	0.9	1.1	1.0	0.8	1.5	0.7	0.6	1.2	2.2	0.4	0.7	0.7	0.5	0.7	1.1	0.
192	0.5	0.3	0.3	0.8	1.0	1.0	0.8	1.6	0.7	0.7	1.2	2.2	0.4	0.7	0.7	0.5	0.8	1.0	0.
194	0.4	0.3	0.4	0.8	1.1	1.1	0.9	1.8	0.7	0.7	1.2	2.2	0.4	0.7	0.7	0.5	0.8	1.0	0.
196	0.4	0.3	0.4	0.8	1.1	1.1	1.0	1.9	0.8	0.8	1.3	2.1	0.4	0.6	0.7	0.4	0.8	1.0	0.
198	0.3	0.3	0.5	0.9	1.2	1.1	1.1	2.1	0.8	0.9	1.3	2.0	0.4	0.6	0.7	0.5	0.8	1.0	0.
200	0.3	0.3	0.5	0.9	1.3	1.1	1.2	2.2	0.9	1.1	1.4	1.9	0.4	0.6	0.7	0.5	0.8	1.0	0.
202	0.3	0.3	0.5	1.0	1.3	1.1	1.2	2.3	1.0	1.2	1.5	1.8	0.4	0.6	0.7	0.6	0.8	1.0	0.
204	0.2	0.2	0.4	1.1	1.3	1.2	1.3	2.4	1.2	1.4	1.5	1.7	0.4	0.5	0.6	0.6	0.8	1.0	0.
206	0.2	0.1	0.4	1.2	1.3	1.2	1.4	2.5	1.3	1.5	1.6	1.5	0.3	0.5	0.6	0.7	0.8	1.0	0.
208	0.1	0.1	0.4	1.2	1.3	1.3	1.5	2.5	1.4	1.6	1.7	1.4	0.3	0.5	0.6	0.8	0.8	1.0	0.
210	0.1	0.0	0.3	1.2	1.3	1.4	1.6	2.5	1.6	1.8	1.7	1.2	0.3	0.6	0.6	0.8	0.8	1.0	0.
212	0.1	0.	0.3	1.1	1.3	1.5	1.8	2.5	1.7	1.9	1.7	1.1	0.2	0.5	0.6	0.8	0.8	1.0	0.
214	0.0	0.	0.2	1.0	1.3	1.6	1.9	2.5	1.8	1.9	1.6	1.0	0.2	0.5	0.7	0.8	0.7	1.0	0.
216	0.0	0.	0.2	0.8	1.3	1.7	2.0	2.5	2.0	2.0	1.6	0.8	0.2	0.5	0.8	0.8	0.7	1.0	0.
218	0.	0.	0.2	0.7	1.3	1.8	2.0	2.5	2.0	2.0	1.5	0.7	0.2	0.5	0.8	0.8	0.7	0.9	0.
220	0.	0.	0.1	0.6	1.3	1.8	2.0	2.5	2.1	2.1	1.3	0.6	0.2	0.4	0.9	0.8	0.6	0.9	0.
222	0.	0.	0.1	0.5	1.2	1.8	2.0	2.6	2.1	2.0	1.2	0.6	0.2	0.4	0.9	0.7	0.6	0.9	0.
224	0.	0.	0.1	0.4	1.1	1.8	1.9	2.7	2.1	2.0	1.1	0.5	0.2	0.4	0.9	0.7	0.7	0.9	0.
226	0.	0.	0.1	0.4	1.1	1.8	1.9	2.8	2.1	1.9	0.9	0.5	0.2	0.4	0.9	0.7	0.7	0.9	0.
228	0.	0.	0.1	0.4	1.1	1.7	1.8	2.8	2.1	1.9	0.8	0.5	0.1	0.4	0.9	0.7	0.8	0.9	0.
230	0.0	0.	0.2	0.5	1.1	1.7	1.7	2.8	2.0	1.8	0.7	0.5	0.1	0.5	0.8	0.7	0.8	0.9	0.
232	0.1	0.0	0.3	0.6	1.2	1.7	1.7	2.8	1.9	1.7	0.6	0.6	0.1	0.5	0.8	0.7	0.9	0.9	0.
234	0.2	0.1	0.4	0.8	1.3	1.7	1.6	2.8	1.9	1.6	0.6	0.6	0.1	0.6	0.7	0.7	0.9	1.0	0.
236	0.3	0.1	0.5	0.9	1.4	1.7	1.6	2.7	1.8	1.5	0.6	0.7	0.1	0.6	0.7	0.6	1.0	1.0	0.
238	0.3	0.2	0.6	1.1	1.5	1.7	1.6	2.6	1.7	1.5	0.7	0.7	0.2	0.6	0.8	0.6	1.0	1.0	0.
240	0.4	0.2	0.7	1.2	1.5	1.7	1.6	2.6	1.7	1.4	0.7	0.7	0.2	0.6	0.8	0.6	1.0	0.9	0.
242	0.4	0.3	0.7	1.2	1.5	1.7	1.6	2.6	1.6	1.4	0.9	0.8	0.2	0.6	0.9	0.6	1.0	0.9	0.
244	0.4	0.3	0.7	1.3	1.5	1.7	1.7	2.6	1.6	1.3	1.0	0.8	0.2	0.6	0.9	0.6	1.0	0.9	0.
246	0.4	0.4	0.7	1.3	1.4	1.7	1.7	2.5	1.6	1.3	1.1	0.9	0.2	0.6	1.0	0.6	1.0	0.9	0.
248	0.4	0.4	0.6	1.2	1.3	1.7	1.7	2.5	1.5	1.3	1.1	0.9	0.2	0.6	1.0	0.7	1.0	0.9	0.
250	0.3	0.3	0.5	1.2	1.3	1.6	1.7	2.4	1.6	1.4	1.1	1.0	0.2	0.7	1.0	0.7	1.0	0.9	0.
252	0.3	0.3	0.5	1.1	1.2	1.6	1.7	2.3	1.6	1.4	1.1	1.0	0.2	0.7	1.0	0.8	1.0	0.9	0.
254	0.2	0.2	0.5	1.0	1.2	1.5	1.6	2.2	1.7	1.5	1.1	1.0	0.2	0.7	1.0	0.8	1.0	0.9	0.
256	0.2	0.2	0.4	0.9	1.2	1.4	1.6	2.1	1.8	1.5	1.0	1.0	0.3	0.7	1.1	0.9	1.0	0.9	0.
258	0.2	0.1	0.4	0.8	1.2	1.3	1.5	2.0	1.8	1.6	1.0	1.0	0.4	0.7	1.2	1.0	1.0	0.9	0.
260	0.2	0.1	0.4	0.8	1.2	1.2	1.5	2.0	1.9	1.7	0.9	1.0	0.5	0.7	1.3	1.0	0.9	0.9	0.
262	0.1	0.0	0.4	0.8	1.2	1.1	1.4	1.9	2.0	1.7	1.0	1.0	0.7	0.7	1.4	1.1	0.9	0.9	0.
264	0.2	0.	0.3	0.8	1.2	1.1	1.3	1.9	2.1	1.7	1.0	1.1	0.8	0.7	1.5	1.1	0.8	0.9	0.
266	0.2	0.	0.3	0.8	1.2	1.0	1.2	1.9	2.1	1.8	1.0	1.1	0.8	0.7	1.6	1.2	0.8	0.9	0.
268	0.2		0.3	0.9	1.2	1.0	1.2	1.9	2..	1.8	1.1	1.1	0.9	0.7	1.7	1.2	.7	0.9	0.
270	0.2	.0	0.2	0.9	1.2	1.0	1.1	1.9	2.0	1.8	1.1	1.2	0.8	0.8	1.7	1.1	0.7	0.9	0.

TABLE XXX (Continued)

	0	5	10	15	20	25	30	35	40	45	50	55	60	65	70	75	80	85	∞
272	0.2	0.1	0.2	0.9	1.2	1.0	1.1	1.8	1.9	1.9	1.2	1.2	0.8	0.8	1.7	1.1	0.7	0.9	0.
274	0.2	0.1	0.2	0.9	1.2	1.0	1.1	1.8	1.7	1.8	1.2	1.1	0.7	0.9	1.6	1.1	0.6	0.9	0.
276	0.2	0.1	0.3	0.9	1.2	1.1	1.0	1.7	1.6	1.8	1.2	1.1	0.6	0.9	1.5	1.0	0.6	0.9	0.
278	0.2	0.2	0.3	0.8	1.2	1.2	1.0	1.7	1.4	1.6	1.1	1.0	0.5	0.9	1.4	1.0	0.7	0.9	0.
280	0.1	0.2	0.4	0.8	1.2	1.2	1.0	1.7	1.3	1.5	1.1	0.9	0.5	0.9	1.3	1.0	0.7	0.9	0.
282	0.1	0.2	0.4	0.7	1.1	1.3	1.0	1.8	1.2	1.4	1.1	0.9	0.4	0.9	1.2	1.0	0.8	0.9	0.
284	0.1	0.2	0.5	0.7	1.1	1.4	1.0	2.0	1.1	1.3	1.0	0.8	0.4	0.9	1.2	1.0	0.8	0.9	0.
286	0.0	0.2	0.5	0.7	1.1	1.5	1.0	2.1	1.1	1.2	1.0	0.8	0.3	0.8	1.1	1.1	0.9	0.9	0.
288	0.0	0.1	0.5	0.8	1.2	1.6	1.1	2.2	1.1	1.2	1.0	0.7	0.3	0.8	1.1	1.1	0.9	0.9	0.
290	0.0	0.1	0.5	0.9	1.2	1.6	1.1	2.3	1.2	1.2	1.0	0.7	0.3	0.8	1.0	1.1	0.9	0.8	0.
292	0.0	0.1	0.5	1.0	1.4	1.6	1.2	2.5	1.2	1.2	0.9	0.7	0.3	0.8	1.0	1.1	0.9	0.8	0.
294	0.1	0.0	0.5	1.1	1.5	1.6	1.2	2.6	1.2	1.3	0.9	0.7	0.2	0.8	1.0	1.0	0.8	0.8	0.
296	0.2	0.0	0.5	1.3	1.7	1.5	1.3	2.7	1.2	1.3	0.9	0.8	0.2	0.8	1.0	1.0	0.8	0.8	0.
298	0.2	0.1	0.6	1.4	1.8	1.4	1.3	2.7	1.2	1.4	0.8	0.8	0.1	0.8	1.0	0.9	0.7	0.8	0.
300	0.3	0.1	0.6	1.4	1.9	1.3	1.4	2.7	1.2	1.4	0.8	0.8	0.1	0.7	1.0	0.8	0.7	0.9	0.
302	0.4	0.1	0.7	1.5	1.9	1.2	1.4	2.7	1.2	1.4	0.8	0.8	0.0	0.7	1.0	0.8	0.7	0.9	0.
304	0.5	0.2	0.8	1.5	1.9	1.2	1.5	2.8	1.2	1.4	0.7	0.8	0.0	0.6	1.1	0.7	0.7	1.0	0.
306	0.5	0.3	0.9	1.6	1.8	1.2	1.5	2.8	1.2	1.4	0.7	0.7	0.0	0.6	1.1	0.7	0.7	1.1	0.
308	0.5	0.3	1.0	1.6	1.7	1.3	1.6	2.8	1.2	1.4	0.7	0.7	0.0	0.5	1.1	0.6	0.8	1.2	0.
310	0.5	0.4	1.1	1.5	1.6	1.4	1.7	2.8	1.3	1.5	0.7	0.6	0.1	0.4	1.0	0.6	0.8	1.3	0.
312	0.5	0.4	1.1	1.4	1.6	1.5	1.7	2.7	1.4	1.6	0.7	0.5	0.1	0.4	1.0	0.6	0.9	1.3	0.
314	0.5	0.4	1.0	1.4	1.5	1.6	1.8	2.7	1.5	1.8	0.7	0.5	0.2	0.4	0.9	0.6	0.9	1.3	0.
316	0.4	0.4	0.9	1.2	1.4	1.7	1.7	2.6	1.6	1.9	0.8	0.5	0.2	0.4	0.7	0.6	1.0	1.3	0.
318	0.3	0.3	0.8	1.1	1.4	1.6	1.7	2.6	1.7	2.0	0.9	0.5	0.2	0.4	0.6	0.6	1.0	1.3	0.
320	0.2	0.2	0.6	1.0	1.4	1.6	1.6	2.5	1.8	2.2	1.0	0.6	0.2	0.4	0.6	0.6	1.0	1.2	0.
322	0.1	0.1	0.5	0.8	1.4	1.4	1.4	2.4	1.9	2.2	1.1	0.7	0.2	0.4	0.5	0.6	0.9	1.2	0.
324	0.1	0.1	0.3	0.7	1.3	1.3	1.3	2.4	2.0	2.3	1.2	0.8	0.2	0.4	0.5	0.6	0.9	1.1	0.
326	0.	0.	0.2	0.6	1.3	1.1	1.2	2.4	2.0	2.3	1.3	1.0	0.3	0.5	0.5	0.6	0.9	1.1	0.
328	0.	0.	0.2	0.5	1.2	1.0	1.1	2.4	2.0	2.2	1.4	1.1	0.3	0.5	0.6	0.6	0.8	1.1	0.
330	0.	0.	0.2	0.5	1.2	0.9	1.0	2.4	2.0	2.2	1.5	1.3	0.3	0.5	0.6	0.5	0.8	1.0	0.
332	0.	0.	0.2	0.5	1.1	0.9	1.0	2.5	1.9	2.1	1.6	1.4	0.4	0.5	0.7	0.5	0.8	1.0	0.
334	0.	0.	0.2	0.5	1.0	0.9	1.0	2.6	1.8	2.0	1.6	1.5	0.5	0.5	0.7	0.5	0.8	1.0	0.
336	0.	0.	0.2	0.5	1.0	0.9	1.0	2.6	1.8	2.0	1.7	1.6	0.5	0.5	0.8	0.4	0.8	0.9	0.
338	0.	0.	0.2	0.5	1.0	0.9	1.1	2.7	1.8	2.0	1.7	1.7	0.6	0.5	0.8	0.4	0.8	0.9	0.
340	0.	0.0	0.2	0.6	0.9	0.9	1.2	2.7	1.8	2.0	1.7	1.7	0.7	0.6	0.9	0.3	0.8	0.9	0.
342	0.0	0.1	0.3	0.7	0.9	1.0	1.3	2.6	1.8	2.0	1.6	1.7	0.7	0.6	0.9	0.3	0.8	0.9	0.
344	0.1	0.1	0.3	0.7	1.0	1.0	1.4	2.4	1.8	2.0	1.5	1.7	0.8	0.6	0.9	0.3	0.9	0.9	0.
346	0.1	0.1	0.3	0.9	1.0	1.0	1.5	2.2	1.8	2.0	1.4	1.7	0.9	0.6	0.8	0.3	0.9	0.9	0.
348	0.2	0.1	0.3	0.9	1.0	1.0	1.6	2.0	1.8	1.9	1.3	1.7	0.9	0.6	0.8	0.3	0.9	0.9	0.
350	0.2	0.2	0.3	1.0	1.0	1.1	1.6	1.8	1.7	1.8	1.2	1.7	1.0	0.7	0.8	0.3	0.9	0.9	0.
352	0.3	0.2	0.4	1.0	1.0	1.1	1.5	1.7	1.6	1.7	1.2	1.6	1.0	0.7	0.7	0.4	0.9	1.0	0.
354	0.3	0.2	0.4	1.1	0.9	1.1	1.4	1.7	1.4	1.5	1.1	1.6	1.1	0.8	0.7	0.4	0.9	1.0	0.
356	0.4	0.3	0.4	1.1	0.9	1.1	1.3	1.6	1.3	1.3	1.1	1.5	1.1	0.8	0.8	0.4	0.9	1.0	0.
358	0.4	0.3	0.4	1.1	0.8	1.1	1.1	1.6	1.	1.1	1.1	1.4	1.0	0.9	0.8	0.5	0.8	1.0	0.
360	0.4	0.4	0.5	1.0	0.7	1.1	1.0	1.6	1.6	1.0	1.1	1.3	1.0	0.9	0.8	0.5	0.8	1.0	0.

POLE FIGURE DATA SHEET FOR SPECIMEN 2B

The normalized pole figure is based on Mo k-alpha radiation and the 111 reflection.

The 222 reflection was used to fill in the blind region from 80 through 90 degrees alpha.

The alpha-dependent two theta shift was taken into account.

Integrated intensities were used.

Normal smoothing was used.

Maximum and minimum corrected intensities are 2084 and 0 counts/second, respectively.

Random intensity is 453 counts/second.

Contour spacing is based on multiples of random intensity.

4 contours are to be plotted.

Their values are 1.000 2.000 3.000 4.000.

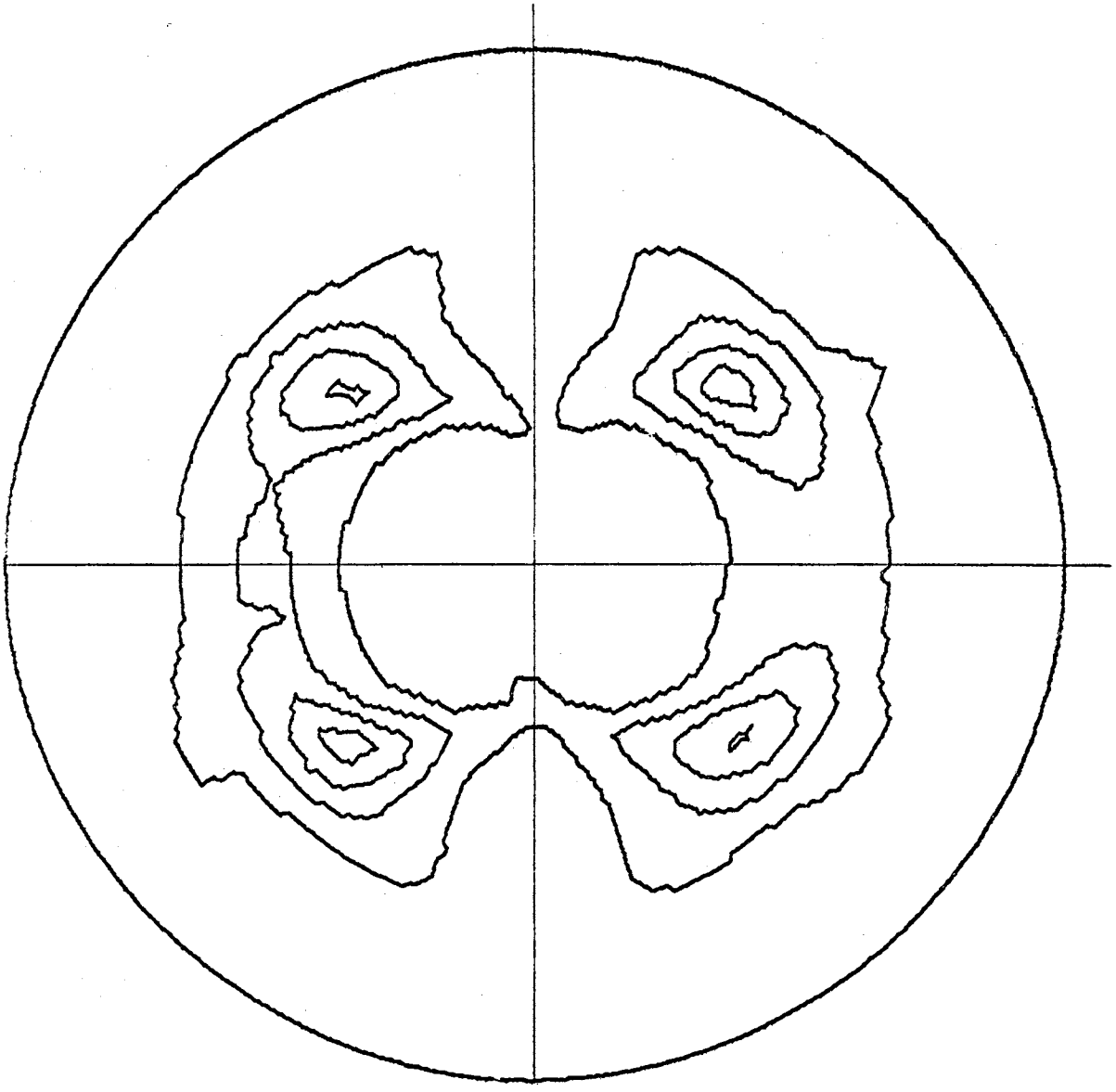

Figure 34. (111) Pole Figure for Specimen 2B

TABLE XXXI

POLE FIGURE DATA FOR SPECIMEN 2B

	0	5	10	15	20	25	30	35	40	45	50	55	60	65	70	75	80	85	9
2	0.6	0.6	0.7	0.7	0.5	0.6	0.5	0.5	0.5	0.6	0.7	0.9	1.0	0.9	0.8	0.7	0.3	0.4	0.
4	0.6	0.6	0.6	0.8	0.5	0.6	0.5	0.5	0.6	0.7	0.7	1.0	1.0	0.9	0.8	0.7	0.3	0.4	0.
6	0.5	0.5	0.6	0.8	0.6	0.6	0.5	0.5	0.6	0.7	0.8	1.0	1.0	0.9	0.8	0.7	0.3	0.4	0.
8	0.5	0.5	0.6	0.8	0.6	0.7	0.6	0.6	0.6	0.8	0.9	1.1	1.1	0.9	0.8	0.7	0.3	0.5	0.
10	0.4	0.4	0.6	0.8	0.6	0.7	0.7	0.6	0.7	0.8	1.0	1.1	1.1	0.9	0.8	0.6	0.3	0.5	0.
12	0.4	0.3	0.6	0.9	0.7	0.8	0.7	0.7	0.8	0.9	1.1	1.2	1.0	0.9	0.8	0.6	0.3	0.5	0.
14	0.3	0.3	0.6	0.9	0.7	0.9	0.8	0.7	0.8	1.0	1.2	1.2	1.0	0.9	0.7	0.6	0.4	0.5	0.
16	0.3	0.2	0.5	0.9	0.7	1.0	0.9	0.8	0.9	1.1	1.3	1.2	1.0	0.9	0.7	0.6	0.4	0.5	0.
18	0.2	0.2	0.5	0.8	0.8	1.0	1.0	0.9	1.0	1.2	1.5	1.2	0.9	0.8	0.7	0.5	0.4	0.5	0.
20	0.2	0.1	0.4	0.8	0.8	1.1	1.2	1.0	1.1	1.3	1.6	1.2	0.9	0.8	0.7	0.5	0.4	0.5	0.
22	0.1	0.1	0.4	0.8	0.8	1.2	1.3	1.2	1.2	1.4	1.8	1.2	0.8	0.8	0.7	0.5	0.4	0.5	0.
24	0.1	0.1	0.3	0.7	0.8	1.2	1.4	1.3	1.4	1.6	1.9	1.2	0.8	0.8	0.6	0.5	0.4	0.5	0.
26	0.0	0.0	0.3	0.6	0.8	1.2	1.4	1.5	1.6	1.7	2.0	1.1	0.8	0.7	0.6	0.5	0.4	0.5	0.
28	0.	0.0	0.2	0.6	0.7	1.3	1.5	1.7	1.8	1.9	2.1	1.1	0.7	0.7	0.6	0.5	0.4	0.5	0.
30	0.	0.	0.2	0.6	0.7	1.3	1.6	1.9	2.1	2.1	2.2	1.1	0.7	0.7	0.6	0.5	0.4	0.5	0.
32	0.	0.	0.2	0.5	0.7	1.3	1.8	2.2	2.4	2.4	2.2	1.0	0.6	0.7	0.6	0.5	0.4	0.5	0.
34	0.	0.	0.2	0.5	0.8	1.3	1.9	2.4	2.8	2.6	2.2	0.9	0.6	0.6	0.6	0.5	0.4	0.5	0.
36	0.	0.	0.2	0.5	0.8	1.4	2.1	2.7	3.2	2.8	2.1	0.8	0.5	0.6	0.6	0.5	0.4	0.5	0.
38	0.	0.0	0.2	0.5	0.8	1.5	2.4	3.0	3.5	2.9	2.0	0.7	0.5	0.6	0.5	0.5	0.4	0.5	0.
40	0.	0.0	0.2	0.6	0.9	1.7	2.6	3.4	3.8	3.0	1.9	0.7	0.4	0.6	0.5	0.5	0.4	0.5	0.
42	0.0	0.1	0.2	0.6	0.9	1.8	2.9	3.6	4.0	3.0	1.7	0.6	0.4	0.5	0.5	0.4	0.4	0.5	0.
44	0.0	0.1	0.3	0.6	0.9	2.0	3.1	3.9	4.1	2.9	1.6	0.5	0.4	0.5	0.5	0.4	0.4	0.5	0.
46	0.1	0.1	0.3	0.7	1.0	2.1	3.3	4.0	4.1	2.8	1.5	0.5	0.4	0.5	0.5	0.4	0.4	0.5	0.
48	0.1	0.1	0.3	0.7	1.0	2.2	3.4	4.1	3.9	2.7	1.4	0.5	0.4	0.5	0.4	0.4	0.4	0.5	0.
50	0.1	0.2	0.4	0.7	1.0	2.3	3.5	4.0	3.7	2.4	1.3	0.5	0.4	0.5	0.4	0.4	0.4	0.5	0.
52	0.1	0.2	0.4	0.8	1.0	2.2	3.4	3.9	3.4	2.2	1.2	0.5	0.4	0.4	0.4	0.4	0.4	0.5	0.
54	0.2	0.2	0.5	0.8	1.0	2.2	3.3	3.7	3.1	2.0	1.1	0.5	0.4	0.4	0.4	0.4	0.4	0.5	0.
56	0.2	0.2	0.5	0.9	1.0	2.1	3.2	3.5	2.8	1.8	1.1	0.5	0.4	0.4	0.3	0.4	0.3	0.5	0.
58	0.2	0.2	0.5	0.9	1.0	2.0	3.0	3.2	2.5	1.7	1.1	0.5	0.4	0.4	0.3	0.4	0.3	0.5	0.
60	0.2	0.2	0.5	1.0	1.0	1.9	2.8	3.0	2.2	1.6	1.1	0.5	0.3	0.4	0.3	0.4	0.3	0.5	0.
62	0.2	0.2	0.5	1.0	1.0	1.8	2.6	2.7	2.1	1.5	1.1	0.5	0.3	0.3	0.3	0.4	0.3	0.5	0.
64	0.1	0.1	0.5	0.9	1.0	1.7	2.4	2.5	1.9	1.4	1.1	0.5	0.3	0.3	0.3	0.4	0.3	0.5	0.
66	0.1	0.1	0.5	0.9	1.0	1.7	2.2	2.3	1.8	1.4	1.1	0.5	0.3	0.3	0.3	0.4	0.3	0.5	0.
68	0.1	0.1	0.5	0.8	1.0	1.6	2.0	2.2	1.8	1.4	1.1	0.5	0.3	0.3	0.3	0.4	0.3	0.5	0.
70	0.1	0.1	0.4	0.8	1.0	1.6	1.9	2.1	1.7	1.4	1.1	0.4	0.2	0.3	0.3	0.4	0.3	0.5	0.
72	0.0	0.1	0.4	0.7	1.0	1.6	1.8	2.1	1.7	1.4	1.0	0.4	0.2	0.2	0.3	0.4	0.3	0.5	0.
74	0.0	0.0	0.3	0.7	1.0	1.6	1.8	2.1	1.7	1.4	1.0	0.4	0.2	0.2	0.3	0.4	0.3	0.5	0.
76	0.	0.0	0.3	0.7	0.9	1.6	1.7	2.1	1.7	1.4	1.0	0.4	0.2	0.2	0.3	0.4	0.3	0.5	0.
78	0.	0.0	0.3	0.6	0.9	1.6	1.8	2.2	1.7	1.4	1.0	0.4	0.2	0.2	0.3	0.4	0.3	0.5	0.
80	0.	0.0	0.2	0.7	0.9	1.6	1.8	2.3	1.8	1.5	1.0	0.4	0.2	0.2	0.2	0.4	0.3	0.5	0.
82	0.	0.0	0.2	0.7	0.8	1.6	1.8	2.4	1.9	1.5	1.0	0.3	0.2	0.2	0.2	0.4	0.3	0.5	0.
84	0.	0.0	0.2	0.7	0.8	1.5	1.9	2.5	1.9	1.5	0.9	0.3	0.2	0.2	0.2	0.5	0.3	0.5	0.
86	0.0	0.1	0.2	0.7	0.8	1.5	1.9	2.5	2.0	1.6	0.9	0.3	0.2	0.2	0.2	0.5	0.3	0.5	0.
88	0.0	0.1	0.3	0.8	0.8	1.4	2.0	2.5	2.0	1.6	0.9	0.3	0.2	0.2	0.2	0.5		0.5	0.
90	0.0	.1	0.3	0.8	0.7	1.4	2.0	2.4	2.1	1.6	0.9	0.3	0.2	0.2	0.2	0.5	0.3	0.4	0.

TABLE XXXI (Continued)

	0	5	10	15	20	25	30	35	40	45	50	55	60	65	70	75	80	85	90
92	0.0	0.0	0.3	0.8	0.7	1.4	2.0	2.3	2.1	1.5	1.0	0.3	0.2	0.2	0.2	0.5	0.3	0.4	0.
94	0.0	0.0	0.3	0.8	0.7	1.4	2.0	2.2	2.1	1.5	1.0	0.3	0.2	0.2	0.2	0.5	0.3	0.4	0.
96	0.0	0.0	0.3	0.8	0.8	1.5	2.0	2.1	2.0	1.5	1.0	0.3	0.2	0.2	0.2	0.5	0.3	0.4	0.
98	0.	0.0	0.3	0.8	0.8	1.6	2.0	2.0	2.0	1.4	1.0	0.3	0.2	0.2	0.2	0.5	0.3	0.4	0.
100	0.	0.	0.3	0.8	0.9	1.6	2.0	2.0	2.0	1.4	1.0	0.3	0.2	0.2	0.2	0.5	0.3	0.4	0.
102	0.	0.	0.3	0.8	0.9	1.7	2.0	2.0	2.0	1.4	1.0	0.4	0.2	0.2	0.2	0.5	0.3	0.4	0.
104	0.	0.0	0.3	0.8	1.0	1.8	2.0	2.0	2.0	1.4	1.1	0.4	0.2	0.2	0.2	0.4	0.3	0.4	0.
106	0.0	0.0	0.3	0.8	1.1	1.9	2.0	2.1	2.0	1.4	1.1	0.4	0.3	0.2	0.3	0.4	0.3	0.4	0.
108	0.0	0.0	0.4	0.8	1.1	1.9	2.0	2.2	2.0	1.4	1.1	0.4	0.3	0.2	0.3	0.4	0.3	0.4	0.
110	0.1	0.1	0.4	0.8	1.2	1.9	2.1	2.3	2.0	1.4	1.1	0.4	0.3	0.3	0.3	0.4	0.3	0.4	0.
112	0.1	0.1	0.4	0.9	1.2	1.9	2.1	2.5	2.0	1.4	1.1	0.4	0.3	0.3	0.3	0.4	0.3	0.4	0.
114	0.1	0.1	0.4	0.9	1.3	1.9	2.2	2.6	2.1	1.5	1.1	0.4	0.3	0.3	0.3	0.4	0.3	0.4	0.
116	0.1	0.1	0.5	1.0	1.2	1.9	2.3	2.7	2.1	1.5	1.1	0.5	0.4	0.3	0.3	0.4	0.3	0.4	0.
118	0.1	0.1	0.5	1.0	1.2	1.8	2.5	2.9	2.2	1.5	1.1	0.5	0.4	0.3	0.3	0.4	0.3	0.4	0.
120	0.1	0.1	0.5	1.0	1.2	1.8	2.6	3.1	2.3	1.5	1.1	0.5	0.4	0.3	0.3	0.4	0.3	0.4	0.
122	0.1	0.1	0.5	1.0	1.1	1.8	2.8	3.4	2.5	1.5	1.1	0.5	0.4	0.4	0.3	0.4	0.3	0.4	0.
124	0.1	0.1	0.5	1.0	1.0	1.8	2.9	3.6	2.7	1.6	1.1	0.5	0.4	0.4	0.4	0.4	0.3	0.4	0.
126	0.1	0.1	0.5	1.0	1.0	1.8	3.1	3.9	3.0	1.7	1.1	0.5	0.4	0.4	0.4	0.4	0.3	0.4	0.
128	0.1	0.1	0.4	0.9	0.9	1.8	3.2	4.1	3.3	1.8	1.1	0.5	0.4	0.4	0.4	0.4	0.3	0.4	0.
130	0.1	0.1	0.4	0.8	0.9	1.8	3.3	4.3	3.6	2.0	1.1	0.5	0.4	0.5	0.5	0.4	0.3	0.4	0.
132	0.1	0.1	0.3	0.8	0.8	1.8	3.3	4.4	3.8	2.2	1.2	0.5	0.4	0.5	0.5	0.4	0.3	0.4	0.
134	0.0	0.0	0.3	0.7	0.8	1.8	3.3	4.4	4.0	2.4	1.3	0.5	0.4	0.5	0.5	0.4	0.3	0.4	0.
136	0.0	0.0	0.3	0.6	0.8	1.8	3.2	4.3	4.1	2.6	1.4	0.5	0.5	0.5	0.5	0.4	0.3	0.4	0.
138	0.	0.0	0.2	0.6	0.8	1.8	3.0	4.0	4.2	2.8	1.6	0.6	0.5	0.6	0.5	0.5	0.3	0.4	0.
140	0.	0.	0.2	0.6	0.8	1.7	2.9	3.7	4.1	3.0	1.7	0.6	0.5	0.6	0.5	0.5	0.3	0.4	0.
142	0.	0.	0.2	0.5	0.8	1.7	2.6	3.4	3.9	3.1	1.9	0.7	0.5	0.6	0.5	0.5	0.3	0.4	0.
144	0.	0.	0.2	0.5	0.8	1.7	2.4	3.0	3.6	3.1	2.0	0.7	0.6	0.6	0.5	0.6	0.3	0.4	0.
146	0.	0.	0.2	0.5	0.8	1.6	2.2	2.7	3.2	3.0	2.1	0.8	0.6	0.7	0.5	0.6	0.3	0.4	0.
148	0.	0.	0.2	0.6	0.8	1.6	2.0	2.3	2.9	2.8	2.2	0.9	0.6	0.7	0.6	0.6	0.3	0.4	0.
150	0.	0.	0.2	0.6	0.8	1.5	1.9	2.1	2.5	2.6	2.2	0.9	0.6	0.7	0.6	0.6	0.3	0.4	0.
152	0.0	0.0	0.3	0.6	0.8	1.5	1.7	1.8	2.2	2.3	2.1	1.0	0.7	0.7	0.6	0.6	0.3	0.4	0.
154	0.1	0.1	0.3	0.7	0.9	1.4	1.6	1.6	1.9	2.1	2.0	1.1	0.7	0.8	0.6	0.6	0.4	0.4	0.
156	0.1	0.1	0.3	0.7	0.9	1.3	1.5	1.5	1.6	1.8	1.9	1.1	0.8	0.8	0.7	0.6	0.4	0.4	0.
158	0.1	0.1	0.4	0.8	0.9	1.2	1.4	1.3	1.4	1.6	1.8	1.1	0.8	0.8	0.7	0.7	0.4	0.4	0.
160	0.2	0.2	0.4	0.8	0.9	1.1	1.2	1.2	1.2	1.4	1.6	1.2	0.9	0.9	0.8	0.7	0.4	0.4	0.
162	0.2	0.2	0.5	0.8	0.9	1.0	1.1	1.0	1.0	1.2	1.5	1.2	0.9	0.9	0.8	0.7	0.4	0.4	0.
164	0.3	0.3	0.5	0.8	0.8	0.9	0.9	0.9	0.9	1.0	1.4	1.2	0.9	0.9	0.9	0.7	0.4	0.4	0.
166	0.3	0.3	0.5	0.8	0.8	0.8	0.8	0.7	0.7	0.9	1.2	1.2	1.0	1.0	0.9	0.7	0.4	0.5	0.
168	0.4	0.4	0.6	0.8	0.7	0.7	0.7	0.6	0.6	0.8	1.1	1.2	1.0	1.0	0.9	0.7	0.4	0.5	0.
170	0.4	0.4	0.6	0.8	0.7	0.7	0.6	0.5	0.5	0.7	1.0	1.1	1.0	1.0	0.9	0.7	0.4	0.5	0.
172	0.5	0.4	0.6	0.7	0.6	0.6	0.5	0.5	0.5	0.6	1.0	1.1	1.0	1.0	0.9	0.7	0.4	0.5	0.
174	0.6	0.5	0.6	0.7	0.6	0.6	0.5	0.4	0.4	0.5	0.9	1.1	1.1	1.0	0.9	0.7	0.4	0.5	0.
176	0.6	0.5	0.6	0.7	0.5	0.6	0.5	0.4	0.4	0.5	0.8	1.0	1.1	1.0	0.9	0.7	0.4	0.5	0.
178	0.6	0.5	0.6	0.7	0.5	0.6	0.5	0.4	0.4	0.5	0.8	1.0	1.1	1.0	0.9	0.7	0.4	0.5	0.
180	0.6	0.5	0.6	0.7	0.5	0.6	0.5	0.4	0.4	0.5	0.8	1.0	1.1	1.0	0.8	0.7	0.4	0.5	0.

TABLE XXXI (Continued)

	0	5	10	15	20	25	30	35	40	45	50	55	60	65	70	75	80	85	%
182	0.6	0.6	0.6	0.7	0.8	0.6	0.5	0.4	0.4	0.5	0.8	1.0	1.1	1.0	0.8	0.8	0.4	0.5	0.5
184	0.6	0.6	0.6	0.7	0.6	0.7	0.5	0.5	0.5	0.6	0.8	1.0	1.1	1.0	0.8	0.8	0.4	0.5	0.5
186	0.5	0.5	0.6	0.7	0.6	0.7	0.6	0.5	0.5	0.6	0.9	1.1	1.0	1.0	0.8	0.8	0.4	0.5	0.5
188	0.5	0.5	0.6	0.7	0.6	0.7	0.6	0.6	0.6	0.7	0.9	1.1	1.0	1.0	0.9	0.8	0.4	0.4	0.5
190	0.4	0.4	0.6	0.7	0.7	0.8	0.7	0.6	0.7	0.8	1.0	1.1	1.0	0.9	0.9	0.8	0.4	0.4	0.5
192	0.4	0.4	0.6	0.7	0.7	0.8	0.7	0.7	0.8	0.9	1.1	1.2	1.0	0.9	0.9	0.8	0.4	0.4	0.5
194	0.3	0.3	0.5	0.7	0.8	0.9	0.8	0.8	0.9	1.0	1.3	1.2	1.0	0.9	0.9	0.8	0.4	0.4	0.5
196	0.3	0.3	0.5	0.7	0.8	1.0	0.9	0.9	1.0	1.2	1.4	1.2	0.9	0.9	0.9	0.8	0.4	0.4	0.5
198	0.2	0.2	0.5	0.7	0.8	1.1	1.1	1.1	1.2	1.3	1.6	1.2	0.9	0.9	0.8	0.7	0.4	0.4	0.5
200	0.2	0.2	0.4	0.7	0.9	1.2	1.2	1.2	1.3	1.5	1.8	1.2	0.9	0.9	0.8	0.7	0.4	0.4	0.5
202	0.1	0.1	0.4	0.7	0.9	1.3	1.3	1.3	1.4	1.7	1.9	1.1	0.8	0.8	0.8	0.7	0.4	0.4	0.5
204	0.1	0.1	0.3	0.7	1.0	1.4	1.5	1.5	1.6	1.9	2.0	1.1	0.8	0.8	0.7	0.7	0.4	0.4	0.5
206	0.0	0.0	0.3	0.7	1.0	1.5	1.6	1.6	1.8	2.1	2.1	1.0	0.7	0.8	0.7	0.6	0.4	0.4	0.5
208	0.0	0.0	0.2	0.6	0.9	1.5	1.7	1.8	2.0	2.3	2.1	1.0	0.7	0.7	0.7	0.6	0.4	0.4	0.5
210	0.	0.	0.2	0.6	0.9	1.6	1.8	2.0	2.3	2.5	2.1	0.9	0.6	0.7	0.6	0.6	0.4	0.4	0.5
212	0.	0.	0.2	0.6	0.9	1.6	1.9	2.2	2.6	2.6	2.1	0.8	0.6	0.6	0.6	0.6	0.4	0.4	0.5
214	0.	0.	0.1	0.5	0.8	1.7	2.1	2.5	2.8	2.7	2.0	0.8	0.5	0.6	0.6	0.6	0.4	0.4	0.5
216	0.	0.	0.1	0.5	0.8	1.7	2.2	2.8	3.1	2.8	1.9	0.7	0.5	0.5	0.6	0.6	0.4	0.4	0.5
218	0.	0.	0.2	0.5	0.8	1.7	2.3	3.1	3.4	2.8	1.7	0.6	0.5	0.5	0.6	0.6	0.4	0.4	0.5
220	0.	0.	0.2	0.5	0.8	1.8	2.5	3.4	3.6	2.7	1.6	0.6	0.4	0.5	0.5	0.6	0.3	0.4	0.5
222	0.	0.0	0.2	0.5	0.8	1.8	2.7	3.6	3.7	2.6	1.5	0.5	0.4	0.5	0.5	0.6	0.3	0.4	0.5
224	0.0	0.1	0.3	0.6	0.9	1.9	2.9	3.9	3.8	2.5	1.4	0.5	0.4	0.4	0.5	0.6	0.3	0.4	0.5
226	0.0	0.1	0.4	0.6	0.9	1.9	3.1	4.0	3.8	2.3	1.2	0.5	0.4	0.4	0.5	0.6	0.3	0.4	0.5
228	0.1	0.2	0.4	0.7	1.0	2.0	3.2	4.1	3.7	2.2	1.2	0.5	0.4	0.4	0.5	0.6	0.3	0.4	0.5
230	0.1	0.2	0.5	0.7	1.1	2.1	3.3	4.2	3.5	2.0	1.1	0.5	0.4	0.4	0.5	0.5	0.3	0.4	0.5
232	0.2	0.2	0.5	0.8	1.1	2.1	3.4	4.1	3.3	1.9	1.0	0.5	0.3	0.4	0.4	0.5	0.3	0.4	0.5
234	0.2	0.2	0.5	0.8	1.2	2.1	3.4	4.0	3.1	1.7	1.0	0.5	0.3	0.4	0.4	0.5	0.3	0.4	0.5
236	0.2	0.2	0.6	0.9	1.2	2.1	3.4	3.8	2.8	1.6	1.0	0.5	0.3	0.4	0.4	0.5	0.3	0.4	0.5
238	0.2	0.2	0.6	0.9	1.2	2.1	3.3	3.6	2.6	1.5	1.0	0.5	0.3	0.4	0.4	0.5	0.3	0.4	0.5
240	0.2	0.2	0.6	0.9	1.2	2.1	3.1	3.3	2.4	1.4	1.0	0.5	0.3	0.4	0.4	0.5	0.3	0.4	0.5
242	0.2	0.2	0.5	1.0	1.2	2.1	3.0	3.0	2.2	1.3	1.0	0.5	0.3	0.4	0.3	0.5	0.3	0.4	0.5
244	0.2	0.2	0.5	1.0	1.1	2.0	2.8	2.8	2.1	1.3	1.0	0.5	0.3	0.4	0.3	0.5	0.3	0.4	0.5
246	0.1	0.1	0.5	0.9	1.1	2.0	2.6	2.6	2.0	1.2	1.0	0.5	0.3	0.4	0.3	0.5	0.3	0.4	0.5
248	0.1	0.1	0.4	0.9	1.1	1.9	2.4	2.3	1.9	1.2	1.1	0.5	0.3	0.3	0.3	0.5	0.3	0.4	0.5
250	0.1	0.1	0.4	0.9	1.0	1.9	2.2	2.2	1.9	1.2	1.1	0.5	0.3	0.3	0.3	0.5	0.3	0.4	0.5
252	0.0	0.0	0.3	0.8	1.0	1.8	2.1	2.1	1.8	1.2	1.1	0.5	0.2	0.3	0.3	0.5	0.3	0.4	0.5
254	0.0	0.0	0.3	0.8	1.0	1.7	2.0	2.0	1.8	1.2	1.1	0.5	0.2	0.3	0.3	0.5	0.3	0.4	0.5
256	0.	0.0	0.3	0.7	0.9	1.7	2.0	1.9	1.8	1.2	1.1	0.5	0.2	0.3	0.3	0.5	0.3	0.4	0.5
258	0.	0.0	0.2	0.7	0.9	1.6	1.9	1.9	1.7	1.2	1.1	0.5	0.2	0.3	0.3	0.5	0.3	0.4	0.5
260	0.	0.0	0.2	0.7	0.8	1.5	1.9	1.9	1.7	1.3	1.1	0.5	0.2	0.3	0.3	0.5	0.3	0.4	0.5
262	0.	0.0	0.2	0.6	0.8	1.4	1.8	1.9	1.7	1.3	1.1	0.5	0.2	0.3	0.3	0.5	0.3	0.4	0.5
264	0.	0.0	0.2	0.6	0.8	1.4	1.8	1.9	1.7	1.3	1.1	0.5	0.2	0.3	0.3	0.5	0.3	0.4	0.5
266	0.	0.0	0.2	0.6	0.8	1.3	1.8	1.8	1.8	1.3	1.1	0.5	0.2	0.3	0.3	0.5	0.3	0.4	0.5
268	0.0	0.0	0.3	0.6	0.8	1.3	1.7	1.8	1.8	1.4	1.0	0.4	0.2	0.3	0.3	0.5		0.4	0.5
270	0.0	0.0	0.3	0.6	0.8	1.3	1.7	1.8	1.8	1.4	1.0	0.4	0.2	0.3	0.3	0.5		0.4	0.5

TABLE XXXI (Continued)

	0	5	10	15	20	25	30	35	40	45	50	55	60	65	70	75	80	85	90
272	0.0	0.0	0.3	0.6	0.8	1.4	1.7	1.7	1.8	1.4	1.0	0.4	0.3	0.3	0.3	0.5	0.3	0.4	0.5
274	0.0	0.0	0.3	0.7	0.8	1.4	1.7	1.7	1.8	1.4	1.0	0.4	0.3	0.3	0.3	0.5	0.3	0.4	0.5
276	0.	0.0	0.3	0.7	0.9	1.5	1.7	1.7	1.8	1.4	1.0	0.4	0.3	0.3	0.3	0.5	0.3	0.4	0.5
278	0.	0.0	0.3	0.7	0.9	1.5	1.7	1.7	1.7	1.4	1.0	0.3	0.3	0.3	0.3	0.5	0.3	0.4	0.5
280	0.	0.0	0.3	0.7	0.9	1.5	1.8	1.7	1.7	1.4	1.0	0.3	0.3	0.3	0.3	0.5	0.3	0.4	0.5
282	0.	0.0	0.3	0.7	0.9	1.6	1.8	1.8	1.6	1.4	1.0	0.3	0.3	0.3	0.3	0.5	0.3	0.4	0.5
284	0.	0.0	0.3	0.8	1.0	1.6	1.8	1.9	1.6	1.4	1.0	0.3	0.3	0.3	0.3	0.5	0.3	0.4	0.5
286	0.0	0.0	0.3	0.8	1.0	1.6	1.9	2.0	1.6	1.4	1.0	0.4	0.3	0.3	0.2	0.5	0.3	0.4	0.5
288	0.0	0.1	0.3	0.8	1.0	1.6	2.0	2.1	1.7	1.3	1.0	0.4	0.3	0.3	0.2	0.5	0.3	0.4	0.5
290	0.0	0.1	0.4	0.9	1.0	1.7	2.1	2.2	1.8	1.4	1.0	0.4	0.3	0.3	0.2	0.5	0.3	0.4	0.5
292	0.1	0.1	0.5	0.9	1.0	1.7	2.2	2.3	1.9	1.4	1.0	0.4	0.3	0.3	0.2	0.5	0.3	0.4	0.5
294	0.1	0.1	0.5	0.9	1.0	1.8	2.3	2.5	2.0	1.4	1.0	0.4	0.3	0.4	0.2	0.5	0.3	0.4	0.5
296	0.1	0.1	0.6	1.0	1.0	1.8	2.4	2.6	2.2	1.5	1.0	0.5	0.3	0.4	0.3	0.5	0.3	0.4	0.5
298	0.1	0.2	0.6	1.0	1.0	1.9	2.6	2.8	2.4	1.5	1.0	0.5	0.3	0.4	0.3	0.4	0.3	0.5	0.5
300	0.1	0.2	0.6	1.0	1.0	2.0	2.8	3.1	2.6	1.6	1.0	0.5	0.3	0.4	0.3	0.4	0.3	0.5	0.5
302	0.1	0.2	0.7	1.0	1.0	2.0	2.9	3.4	2.8	1.7	1.0	0.5	0.3	0.4	0.3	0.4	0.3	0.5	0.5
304	0.1	0.2	0.6	1.0	1.0	2.1	3.1	3.7	3.0	1.8	1.0	0.4	0.3	0.4	0.4	0.4	0.3	0.5	0.5
306	0.1	0.2	0.6	0.9	1.0	2.1	3.2	4.0	3.3	1.9	1.0	0.4	0.3	0.4	0.4	0.4	0.4	0.5	0.5
308	0.1	0.2	0.5	0.9	1.0	2.1	3.3	4.3	3.5	2.1	1.1	0.4	0.4	0.5	0.4	0.4	0.4	0.5	0.5
310	0.1	0.1	0.5	0.8	1.0	2.1	3.4	4.5	3.7	2.2	1.1	0.4	0.4	0.5	0.4	0.4	0.4	0.5	0.5
312	0.1	0.1	0.4	0.8	0.9	2.0	3.4	4.6	3.9	2.3	1.2	0.5	0.4	0.5	0.4	0.5	0.4	0.5	0.5
314	0.1	0.1	0.4	0.7	0.8	2.0	3.3	4.6	4.0	2.5	1.3	0.5	0.4	0.5	0.5	0.5	0.4	0.4	0.5
316	0.0	0.0	0.3	0.6	0.8	1.9	3.1	4.4	4.0	2.6	1.5	0.5	0.4	0.5	0.5	0.5	0.4	0.4	0.5
318	0.0	0.	0.2	0.6	0.7	1.8	3.0	4.1	4.0	2.7	1.6	0.6	0.5	0.6	0.5	0.5	0.4	0.4	0.5
320	0.	0.	0.2	0.5	0.7	1.7	2.7	3.8	3.8	2.7	1.7	0.6	0.5	0.6	0.5	0.5	0.4	0.4	0.5
322	0.	0.	0.2	0.5	0.7	1.6	2.5	3.3	3.5	2.7	1.8	0.7	0.5	0.6	0.5	0.5	0.4	0.4	0.5
324	0.	0.	0.2	0.5	0.7	1.5	2.3	2.9	3.2	2.6	1.8	0.7	0.5	0.6	0.5	0.5	0.4	0.4	0.5
326	0.	0.	0.2	0.5	0.7	1.5	2.1	2.5	2.8	2.5	1.9	0.8	0.6	0.6	0.5	0.5	0.4	0.4	0.5
328	0.	0.	0.2	0.5	0.7	1.4	1.9	2.2	2.5	2.4	1.9	0.9	0.6	0.6	0.5	0.5	0.4	0.4	0.5
330	0.	0.	0.2	0.5	0.8	1.4	1.8	1.9	2.1	2.2	1.9	1.0	0.6	0.7	0.5	0.5	0.4	0.5	0.5
332	0.0	0.0	0.2	0.6	0.8	1.4	1.7	1.7	1.8	2.1	1.8	1.0	0.7	0.7	0.6	0.5	0.4	0.5	0.5
334	0.1	0.1	0.3	0.6	0.8	1.4	1.5	1.5	1.6	1.9	1.8	1.1	0.8	0.7	0.6	0.5	0.4	0.5	0.5
336	0.1	0.1	0.4	0.7	0.8	1.3	1.4	1.3	1.4	1.7	1.7	1.2	0.8	0.8	0.6	0.5	0.4	0.5	0.5
338	0.1	0.1	0.4	0.7	0.8	1.2	1.3	1.2	1.3	1.6	1.7	1.2	0.9	0.8	0.6	0.6	0.4	0.5	0.5
340	0.2	0.2	0.5	0.8	0.8	1.1	1.1	1.1	1.2	1.5	1.6	1.3	0.9	0.8	0.6	0.6	0.4	0.5	0.5
342	0.2	0.2	0.5	0.8	0.8	1.0	1.0	1.0	1.1	1.3	1.5	1.3	1.0	0.8	0.7	0.6	0.4	0.5	0.5
344	0.3	0.3	0.6	0.8	0.8	0.9	0.9	0.9	1.0	1.2	1.4	1.3	1.0	0.8	0.7	0.5	0.4	0.5	0.5
346	0.3	0.3	0.7	0.8	0.7	0.8	0.8	0.8	0.9	1.1	1.3	1.3	1.0	0.9	0.7	0.5	0.4	0.5	0.5
348	0.3	0.4	0.7	0.8	0.7	0.8	0.7	0.7	0.8	1.0	1.2	1.2	1.0	0.9	0.7	0.5	0.4	0.5	0.5
350	0.4	0.5	0.7	0.8	0.7	0.7	0.6	0.6	0.7	0.9	1.1	1.1	1.0	0.9	0.7	0.5	0.4	0.5	0.5
352	0.5	0.5	0.7	0.8	0.7	0.7	0.6	0.6	0.6	0.8	0.9	1.0	1.0	0.9	0.8	0.6	0.4	0.5	0.5
354	0.5	0.6	0.7	0.8	0.6	0.6	0.5	0.5	0.6	0.7	0.8	1.0	0.9	0.9	0.8	0.6	0.4	0.5	0.5
356	0.6	0.6	0.7	0.8	0.6	0.6	0.5	0.5	0.6	0.7	0.8	0.9	0.9	0.9	0.8	0.6	0.4	0.5	0.5
358	0.6	0.6	0.7	0.8	0.6	0.6	0.5	0.5	0.5	0.6	0.7	0.9	1.0	0.9	0.8	0.6	0.4	0.5	0.5
360	0.6	0.6	0.7	0.8	0.6	0.6	0.5	0.4	0.5	0.6	0.7	0.9	1.0	0.9	0.8	0.6	0.4	0.5	0.5

POLE FIGURE DATA SHEET FOR SPECIMEN 3B

The normalized pole figure is based on Mo k-alpha radiation and the 111 reflection.

The 222 reflection was used to fill in the blind region from 80 through 90 degrees alpha.

The alpha-dependent two theta shift was taken into account.

Integrated intensities were used.

Normal smoothing was used.

Maximum and minimum corrected intensities are 2179 and 0 counts/second, respectively.

Random intensity is 464 counts/second.

Contour spacing is based on multiples of random intensity.

4 contours are to be plotted.

Their values are 1.000 2.000 3.000 4.000.

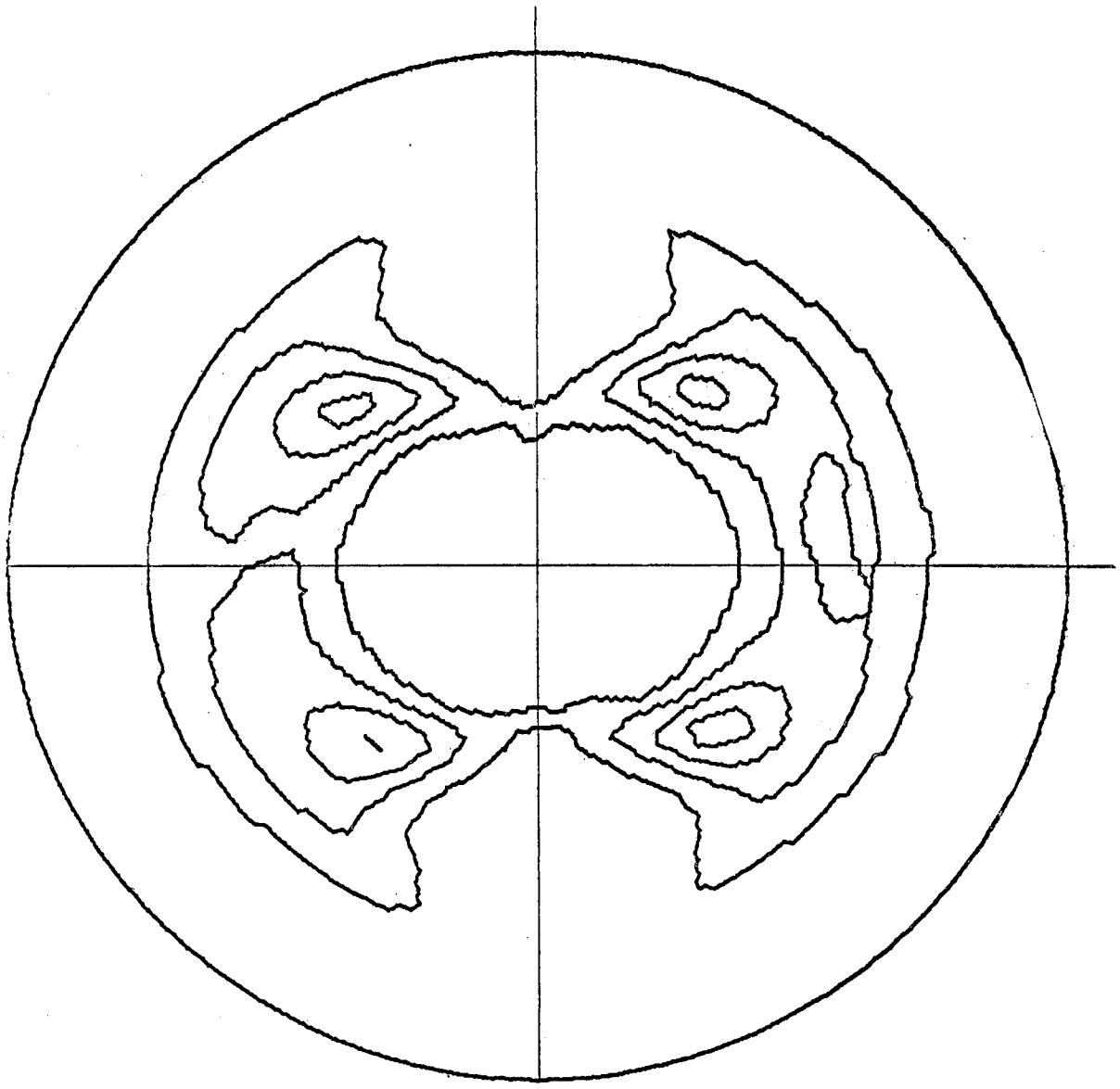

Figure 35. (111) Pole Figure for Specimen 3B

TABLE XXXII

POLE FIGURE DATA FOR SPECIMEN 3B

	0	5	10	15	20	25	30	35	40	45	50	55	60	65	70	75	80	85	90
2	0.7	0.7	0.8	0.7	0.5	0.2	0.2	0.2	0.2	0.3	0.6	1.1	1.0	1.0	0.8	0.3	0.2	0.2	0.3
4	0.7	0.7	0.8	0.7	0.5	0.2	0.2	0.2	0.2	0.4	0.5	1.1	1.0	1.0	0.8	0.3	0.2	0.2	0.3
6	0.7	0.7	0.7	0.7	0.5	0.3	0.2	0.2	0.2	0.4	0.7	1.1	1.0	1.0	0.8	0.3	0.2	0.3	0.3
8	0.6	0.6	0.7	0.7	0.5	0.3	0.2	0.2	0.2	0.4	0.7	1.1	1.0	1.0	0.8	0.3	0.2	0.3	0.3
10	0.6	0.6	0.7	0.7	0.5	0.3	0.2	0.2	0.2	0.4	0.8	1.1	1.0	1.0	0.8	0.3	0.2	0.3	0.3
12	0.5	0.5	0.6	0.7	0.5	0.3	0.2	0.2	0.3	0.5	0.9	1.2	1.0	0.9	0.8	0.3	0.2	0.3	0.3
14	0.4	0.4	0.6	0.7	0.6	0.4	0.2	0.2	0.3	0.5	1.0	1.2	0.9	0.9	0.8	0.3	0.2	0.3	0.3
16	0.4	0.4	0.5	0.7	0.6	0.4	0.3	0.2	0.3	0.6	1.2	1.2	0.9	0.9	0.7	0.3	0.2	0.3	0.3
18	0.3	0.3	0.5	0.7	0.7	0.5	0.3	0.3	0.4	0.8	1.3	1.3	0.9	0.9	0.7	0.3	0.2	0.3	0.3
20	0.2	0.3	0.4	0.7	0.8	0.6	0.4	0.3	0.5	0.9	1.5	1.3	0.8	0.9	0.6	0.3	0.2	0.3	0.3
22	0.2	0.2	0.4	0.7	0.9	0.7	0.5	0.4	0.6	1.1	1.7	1.3	0.8	0.8	0.6	0.3	0.2	0.3	0.3
24	0.2	0.2	0.4	0.7	1.0	0.8	0.5	0.5	0.7	1.4	1.9	1.3	0.8	0.8	0.5	0.3	0.2	0.3	0.3
26	0.1	0.1	0.3	0.8	1.1	0.9	0.7	0.6	0.9	1.7	2.1	1.3	0.8	0.8	0.5	0.2	0.2	0.3	0.3
28	0.1	0.1	0.3	0.8	1.2	1.1	0.8	0.8	1.2	2.1	2.3	1.3	0.7	0.7	0.5	0.2	0.2	0.3	0.3
30	0.1	0.1	0.3	0.7	1.3	1.2	0.9	0.9	1.5	2.5	2.4	1.2	0.7	0.7	0.4	0.2	0.2	0.3	0.3
32	0.0	0.0	0.2	0.7	1.3	1.3	1.1	1.1	1.9	2.8	2.5	1.2	0.6	0.7	0.4	0.2	0.2	0.3	0.3
34	0.0	0.0	0.2	0.7	1.4	1.4	1.2	1.4	2.3	3.3	2.6	1.1	0.6	0.6	0.3	0.2	0.2	0.3	0.3
36	0.	0.	0.2	0.7	1.4	1.5	1.4	1.7	2.7	3.4	2.5	1.0	0.6	0.6	0.3	0.2	0.2	0.3	0.3
38	0.	0.	0.1	0.6	1.4	1.6	1.6	2.1	3.2	3.6	2.5	1.0	0.5	0.5	0.3	0.2	0.2	0.3	0.3
40	0.	0.	0.1	0.6	1.4	1.7	1.8	2.5	3.6	3.7	2.3	0.9	0.5	0.5	0.2	0.2	0.2	0.3	0.3
42	0.	0.	0.1	0.6	1.4	1.8	2.0	2.8	3.9	3.8	2.2	0.8	0.4	0.4	0.2	0.2	0.2	0.3	0.3
44	0.	0.	0.2	0.6	1.4	1.9	2.3	3.2	4.2	3.7	2.0	0.7	0.4	0.4	0.2	0.2	0.2	0.3	0.3
46	0.	0.0	0.2	0.6	1.4	2.0	2.5	3.5	4.4	3.6	1.9	0.7	0.4	0.3	0.2	0.2	0.2	0.3	0.3
48	0.	0.0	0.2	0.7	1.4	2.1	2.7	3.8	4.5	3.5	1.7	0.6	0.4	0.3	0.1	0.2	0.3	0.3	0.3
50	0.	0.0	0.2	0.7	1.4	2.2	2.9	3.9	4.4	3.3	1.6	0.6	0.3	0.3	0.1	0.1	0.3	0.3	0.3
52	0.0	0.1	0.3	0.7	1.4	2.3	3.0	4.0	4.3	3.1	1.5	0.6	0.3	0.2	0.1	0.1	0.3	0.3	0.3
54	0.0	0.1	0.3	0.8	1.5	2.4	3.1	4.0	4.1	2.9	1.4	0.5	0.3	0.2	0.1	0.1	0.3	0.3	0.3
56	0.0	0.1	0.3	0.8	1.5	2.4	3.1	3.9	3.9	2.7	1.4	0.5	0.2	0.1	0.0	0.1	0.3	0.3	0.3
58	0.0	0.1	0.3	0.8	1.5	2.5	3.1	3.8	3.6	2.5	1.4	0.5	0.2	0.1	0.0	0.1	0.3	0.3	0.3
60	0.0	0.1	0.3	0.8	1.5	2.5	3.0	3.6	3.3	2.4	1.3	0.4	0.1	0.1	0.0	0.1	0.3	0.3	0.3
62	0.0	0.0	0.3	0.8	1.6	2.5	2.9	3.4	3.1	2.2	1.3	0.4	0.1	0.0	0.0	0.1	0.3	0.3	0.3
64	0.0	0.0	0.3	0.8	1.6	2.4	2.8	3.1	2.9	2.1	1.3	0.4	0.1	0.0	0.	0.1	0.3	0.3	0.3
66	0.0	0.0	0.3	0.8	1.6	2.4	2.7	2.9	2.7	2.0	1.3	0.3	0.0	0.	0.	0.1	0.3	0.3	0.3
68	0.	0.0	0.2	0.8	1.6	2.4	2.6	2.7	2.5	1.9	1.2	0.3	0.0	0.	0.	0.1	0.3	0.3	0.3
70	0.	0.	0.2	0.8	1.7	2.3	2.4	2.5	2.4	1.9	1.2	0.3	0.	0.	0.	0.1	0.3	0.3	0.3
72	0.	0.	0.2	0.8	1.7	2.3	2.3	2.3	2.3	1.8	1.1	0.2	0.	0.	0.	0.1	0.3	0.3	0.3
74	0.	0.	0.2	0.8	1.7	2.3	2.3	2.2	2.1	1.8	1.1	0.2	0.	0.	0.	0.2	0.3	0.3	0.3
76	0.	0.	0.2	0.8	1.7	2.2	2.2	2.1	2.1	1.7	1.0	0.2	0.	0.	0.	0.2	0.3	0.3	0.3
78	0.	0.	0.2	0.8	1.6	2.2	2.2	2.0	2.0	1.7	1.0	0.2	0.	0.	0.	0.2	0.3	0.3	0.3
80	0.	0.	0.2	0.8	1.6	2.1	2.1	1.9	1.8	1.7	0.9	0.1	0.	0.	0.	0.2	0.3	0.3	0.3
82	0.	0.	0.2	0.8	1.6	2.1	2.1	1.9	1.9	1.6	0.9	0.1	0.	0.	0.	0.2	0.3	0.3	0.3
84	0.	0.	0.2	0.8	1.5	2.0	2.0	1.9	2.0	1.6	0.8	0.1	0.	0.	0.	0.2	0.3	0.3	0.3
86	0.	0.	0.2	0.8	1.5	2.0	2.0	1.9	2.0	1.7	0.8	0.1	0.	0.	0.	0.2	0.3	0.3	0.3
88	0.		0.2	0.8	1.5	1.9	2.0	2.0	2.1	1.7	0.8	0.1	0.	0.	0.	0.2	0.	0.3	0.3
90	0.		0.2	0.8	1.5	1.9	2.0	2.0	2.1	1.7	0.8	0.1	0.	0.	0.	0.2	0.3	0.3	0.3

TABLE XXXII (Continued)

	0	5	10	15	20	25	30	35	40	45	50	55	60	65	70	75	80	85	90
92	0.	0.	0.2	0.8	1.5	1.9	2.0	2.1	2.2	1.7	0.8	0.1	0.	0.	0.	0.2	0.3	0.3	0.3
94	0.	0.	0.2	0.8	1.6	1.9	2.0	2.1	2.2	1.7	0.8	0.1	0.	0.	0.	0.2	0.3	0.3	0.3
96	0.	0.	0.2	0.8	1.6	2.0	2.0	2.2	2.2	1.7	0.8	0.1	0.	0.	0.	0.2	0.3	0.3	0.3
98	0.	0.	0.2	0.8	1.7	2.0	2.1	2.2	2.2	1.7	0.8	0.1	0.	0.	0.	0.2	0.3	0.3	0.3
100	0.	0.	0.2	0.8	1.7	2.0	2.1	2.2	2.2	1.7	0.8	0.1	0.	0.	0.	0.2	0.3	0.3	0.3
102	0.	0.	0.2	0.8	1.7	2.0	2.1	2.2	2.1	1.7	0.9	0.1	0.	0.	0.	0.2	0.3	0.3	0.3
104	0.	0.	0.2	0.8	1.7	2.0	2.1	2.2	2.1	1.7	0.9	0.1	0.	0.	0.	0.2	0.3	0.3	0.3
106	0.	0.	0.2	0.8	1.7	2.1	2.2	2.3	2.1	1.7	0.9	0.1	0.	0.	0.	0.2	0.3	0.3	0.3
108	0.	0.	0.2	0.8	1.7	2.1	2.2	2.3	2.2	1.8	0.9	0.2	0.	0.	0.	0.2	0.3	0.3	0.3
110	0.	0.	0.2	0.8	1.7	2.2	2.2	2.4	2.2	1.8	1.0	0.2	0.	0.	0.	0.2	0.3	0.3	0.3
112	0.	0.	0.2	0.8	1.8	2.2	2.3	2.4	2.2	1.8	1.0	0.2	0.	0.	0.	0.2	0.3	0.3	0.3
114	0.	0.	0.2	0.8	1.8	2.3	2.3	2.5	2.3	1.8	1.1	0.2	0.	0.	0.	0.2	0.3	0.3	0.3
116	0.	0.	0.2	0.8	1.8	2.3	2.4	2.6	2.4	1.9	1.2	0.3	0.	0.	0.0	0.2	0.3	0.3	0.3
118	0.	0.0	0.3	0.8	1.7	2.4	2.5	2.7	2.5	1.9	1.2	0.3	0.0	0.	0.0	0.2	0.3	0.3	0.3
120	0.0	0.0	0.3	0.8	1.7	2.4	2.6	2.9	2.6	2.0	1.3	0.3	0.0	0.0	0.0	0.2	0.3	0.3	0.3
122	0.0	0.0	0.3	0.8	1.7	2.4	2.6	3.0	2.7	2.1	1.3	0.4	0.1	0.0	0.0	0.2	0.3	0.3	0.3
124	0.0	0.0	0.3	0.8	1.7	2.4	2.7	3.1	2.9	2.2	1.4	0.4	0.1	0.1	0.0	0.2	0.3	0.3	0.3
126	0.0	0.0	0.3	0.8	1.6	2.4	2.8	3.3	3.1	2.4	1.4	0.4	0.1	0.1	0.1	0.2	0.3	0.3	0.3
128	0.0	0.0	0.3	0.8	1.6	2.4	2.9	3.4	3.3	2.5	1.5	0.5	0.2	0.1	0.1	0.2	0.3	0.3	0.3
130	0.0	0.1	0.3	0.7	1.5	2.4	2.9	3.6	3.5	2.8	1.5	0.5	0.2	0.2	0.1	0.2	0.3	0.3	0.3
132	0.0	0.1	0.3	0.7	1.5	2.4	3.0	3.7	3.8	3.0	1.6	0.6	0.3	0.2	0.1	0.2	0.3	0.3	0.3
134	0.0	0.0	0.3	0.7	1.5	2.4	3.0	3.7	4.0	3.2	1.7	0.6	0.3	0.2	0.1	0.2	0.3	0.3	0.3
136	0.0	0.0	0.2	0.6	1.5	2.4	3.0	3.7	4.1	3.4	1.8	0.7	0.3	0.3	0.2	0.2	0.3	0.3	0.3
138	0.0	0.0	0.2	0.6	1.5	2.3	2.8	3.5	4.1	3.5	1.9	0.7	0.4	0.3	0.2	0.2	0.3	0.3	0.3
140	0.0	0.0	0.2	0.6	1.5	2.3	2.7	3.3	4.0	3.7	2.1	0.8	0.4	0.4	0.2	0.2	0.3	0.3	0.3
142	0.0	0.0	0.1	0.6	1.4	2.2	2.5	3.0	3.9	3.7	2.2	0.8	0.5	0.4	0.3	0.2	0.3	0.3	0.3
144	0.0	0.0	0.1	0.6	1.4	2.1	2.2	2.7	3.6	3.7	2.3	0.9	0.5	0.5	0.3	0.3	0.3	0.3	0.3
146	0.0	0.0	0.1	0.6	1.4	2.0	2.0	2.3	3.2	3.5	2.3	0.9	0.5	0.5	0.3	0.3	0.3	0.3	0.3
148	0.	0.0	0.1	0.6	1.4	1.8	1.7	2.0	2.8	3.3	2.4	1.0	0.6	0.6	0.4	0.3	0.3	0.3	0.3
150	0.	0.0	0.2	0.6	1.4	1.7	1.4	1.7	2.4	3.1	2.4	1.0	0.6	0.6	0.4	0.3	0.2	0.3	0.3
152	0.0	0.0	0.2	0.7	1.4	1.5	1.2	1.4	2.0	2.8	2.3	1.0	0.7	0.7	0.5	0.3	0.2	0.3	0.3
154	0.0	0.0	0.2	0.7	1.3	1.4	1.1	1.1	1.7	2.4	2.3	1.0	0.7	0.7	0.5	0.3	0.2	0.3	0.3
156	0.0	0.1	0.2	0.7	1.3	1.2	0.9	0.9	1.3	2.1	2.1	1.1	0.7	0.8	0.5	0.3	0.2	0.3	0.3
158	0.1	0.1	0.3	0.7	1.2	1.1	0.8	0.8	1.1	1.8	2.0	1.1	0.8	0.8	0.6	0.3	0.2	0.3	0.3
160	0.1	0.1	0.3	0.7	1.1	0.9	0.7	0.6	0.9	1.5	1.8	1.1	0.8	0.9	0.6	0.4	0.2	0.3	0.3
162	0.2	0.1	0.3	0.7	1.0	0.8	0.6	0.5	0.7	1.2	1.6	1.1	0.8	0.9	0.7	0.4	0.2	0.3	0.3
164	0.2	0.2	0.4	0.7	0.9	0.7	0.5	0.5	0.6	1.0	1.5	1.1	0.9	0.9	0.7	0.4	0.2	0.3	0.3
166	0.3	0.2	0.4	0.7	0.8	0.6	0.4	0.4	0.5	0.8	1.3	1.1	0.9	0.9	0.7	0.4	0.2	0.3	0.3
168	0.3	0.3	0.5	0.6	0.7	0.5	0.4	0.3	0.4	0.7	1.1	1.1	0.9	1.0	0.8	0.4	0.2	0.3	0.3
170	0.4	0.3	0.5	0.6	0.6	0.4	0.3	0.3	0.3	0.6	1.0	1.1	0.9	1.0	0.8	0.4	0.2	0.3	0.3
172	0.4	0.4	0.5	0.6	0.5	0.3	0.2	0.2	0.3	0.5	0.9	1.1	1.0	1.0	0.8	0.4	0.2	0.3	0.3
174	0.5	0.5	0.6	0.6	0.5	0.3	0.2	0.2	0.3	0.4	0.8	1.1	1.0	1.0	0.8	0.4	0.2	0.3	0.3
176	0.6	0.5	0.6	0.6	0.5	0.3	0.2	0.2	0.2	0.4	0.7	1.1	1.0	1.0	0.8	0.4	0.2	0.3	0.3
178	0.6	.6	0.7	0.6	0.4	0.2	0.2	0.2	0.2	0.3	0.7	1.1	1.0	1.0	0.8	0.4	0.2	0.3	0.3
180	0.7	.6	0.7	0.6	0.4	0.2	0.2	0.2	0.2	0.3	0.6	1.1	1.0	1.0	0.8	0.4	0.2	0.3	0.3

TABLE XXXII (Continued)

	0	5	10	15	20	25	30	35	40	45	50	55	60	65	70	75	80	85	90
182	0.7	0.7	0.7	0.6	0.4	0.2	0.2	0.2	0.2	0.3	0.6	1.0	1.0	1.0	0.8	0.4	0.2	0.2	0.3
184	0.7	0.6	0.7	0.6	0.4	0.2	0.2	0.2	0.2	0.3	0.6	1.0	1.0	1.0	0.8	0.4	0.2	0.2	0.3
186	0.7	0.6	0.7	0.6	0.4	0.2	0.2	0.2	0.2	0.3	0.7	1.0	1.0	1.0	0.8	0.4	0.2	0.2	0.3
188	0.6	0.6	0.6	0.6	0.4	0.2	0.2	0.2	0.2	0.3	0.7	1.1	1.0	1.0	0.8	0.4	0.2	0.2	0.3
190	0.5	0.5	0.6	0.6	0.5	0.3	0.2	0.2	0.2	0.4	0.8	1.1	1.0	1.0	0.8	0.4	0.2	0.2	0.3
192	0.5	0.5	0.6	0.6	0.5	0.3	0.2	0.2	0.3	0.5	1.0	1.1	1.0	1.0	0.8	0.3	0.2	0.2	0.3
194	0.4	0.4	0.5	0.6	0.6	0.4	0.3	0.2	0.3	0.6	1.2	1.2	1.0	0.9	0.7	0.3	0.2	0.2	0.3
196	0.4	0.4	0.5	0.7	0.6	0.4	0.3	0.3	0.4	0.7	1.4	1.3	1.0	0.9	0.7	0.3	0.2	0.2	0.3
198	0.3	0.3	0.5	0.7	0.7	0.5	0.3	0.3	0.4	0.9	1.6	1.3	1.0	0.9	0.7	0.3	0.2	0.2	0.3
200	0.3	0.3	0.4	0.7	0.8	0.6	0.4	0.4	0.5	1.1	1.8	1.3	1.0	0.9	0.7	0.3	0.2	0.2	0.3
202	0.2	0.2	0.4	0.7	0.9	0.7	0.5	0.4	0.6	1.3	2.0	1.4	0.9	0.9	0.7	0.3	0.2	0.2	0.3
204	0.2	0.2	0.4	0.7	0.9	0.8	0.5	0.5	0.8	1.6	2.2	1.4	0.9	0.9	0.6	0.3	0.2	0.3	0.3
206	0.1	0.1	0.3	0.7	1.0	0.9	0.6	0.6	1.0	1.9	2.4	1.3	0.8	0.9	0.6	0.3	0.2	0.3	0.3
208	0.1	0.1	0.3	0.7	1.1	1.0	0.8	0.8	1.3	2.2	2.5	1.3	0.8	0.8	0.6	0.3	0.3	0.3	0.3
210	0.1	0.1	0.2	0.7	1.2	1.1	0.9	1.0	1.6	2.6	2.6	1.2	0.7	0.8	0.5	0.3	0.3	0.3	0.3
212	0.0	0.0	0.2	0.7	1.2	1.3	1.1	1.2	2.0	2.9	2.6	1.2	0.7	0.7	0.5	0.3	0.3	0.3	0.3
214	0.0	0.	0.2	0.6	1.2	1.4	1.2	1.5	2.4	3.2	2.6	1.1	0.6	0.7	0.4	0.2	0.3	0.3	0.3
216	0.	0.	0.1	0.6	1.3	1.5	1.5	1.9	2.9	3.5	2.6	1.0	0.6	0.6	0.4	0.2	0.2	0.3	0.3
218	0.	0.	0.1	0.6	1.3	1.7	1.7	2.3	3.4	3.8	2.5	0.9	0.5	0.5	0.3	0.2	0.2	0.3	0.3
220	0.	0.	0.1	0.5	1.3	1.8	2.0	2.7	3.8	3.9	2.3	0.8	0.5	0.5	0.3	0.2	0.2	0.3	0.3
222	0.	0.	0.1	0.5	1.3	1.9	2.2	3.0	4.2	4.0	2.2	0.8	0.4	0.4	0.3	0.2	0.2	0.3	0.3
224	0.	0.	0.1	0.5	1.3	2.0	2.5	3.4	4.5	3.9	2.1	0.7	0.4	0.4	0.2	0.2	0.2	0.3	0.3
226	0.	0.	0.2	0.6	1.3	2.1	2.7	3.7	4.7	3.8	1.9	0.7	0.4	0.3	0.2	0.2	0.2	0.3	0.3
228	0.	0.0	0.2	0.6	1.4	2.1	2.9	3.9	4.7	3.6	1.8	0.6	0.3	0.3	0.2	0.2	0.2	0.3	0.3
230	0.0	0.0	0.2	0.6	1.4	2.2	3.0	4.0	4.6	3.4	1.7	0.6	0.3	0.2	0.1	0.2	0.3	0.3	0.3
232	0.0	0.0	0.2	0.7	1.4	2.2	3.0	4.0	4.4	3.1	1.6	0.6	0.3	0.2	0.1	0.2	0.3	0.3	0.3
234	0.0	0.0	0.3	0.7	1.5	2.3	3.0	4.0	4.1	2.9	1.5	0.5	0.3	0.2	0.1	0.2	0.3	0.3	0.3
236	0.0	0.0	0.3	0.8	1.5	2.3	2.9	3.8	3.8	2.7	1.5	0.5	0.3	0.1	0.1	0.2	0.3	0.3	0.3
238	0.0	0.0	0.3	0.8	1.5	2.3	2.9	3.6	3.5	2.5	1.4	0.5	0.2	0.1	0.1	0.2	0.3	0.3	0.3
240	0.0	0.0	0.3	0.8	1.6	2.3	2.8	3.4	3.2	2.3	1.4	0.5	0.2	0.1	0.0	0.2	0.3	0.3	0.3
242	0.0	0.0	0.3	0.9	1.6	2.3	2.7	3.1	2.9	2.2	1.3	0.4	0.2	0.1	0.0	0.2	0.3	0.3	0.3
244	0.0	0.	0.3	0.9	1.7	2.3	2.6	2.9	2.7	2.1	1.3	0.4	0.1	0.0	0.0	0.2	0.3	0.3	0.3
246	0.0	0.	0.3	0.9	1.7	2.3	2.5	2.7	2.5	2.0	1.3	0.4	0.1	0.0	0.0	0.2	0.3	0.3	0.3
248	0.	0.	0.2	0.9	1.7	2.3	2.4	2.5	2.4	2.0	1.2	0.3	0.1	0.0	0.0	0.2	0.3	0.3	0.3
250	0.	0.	0.2	0.8	1.7	2.2	2.3	2.3	2.3	1.9	1.2	0.3	0.0	0.	0.0	0.2	0.3	0.3	0.3
252	0.	0.	0.2	0.8	1.7	2.2	2.2	2.2	2.2	1.9	1.1	0.3	0.0	0.	0.0	0.2	0.3	0.3	0.3
254	0.	0.	0.2	0.8	1.7	2.2	2.2	2.2	2.1	1.8	1.1	0.2	0.0	0.	0.0	0.2	0.3	0.3	0.3
256	0.	0.	0.2	0.7	1.7	2.1	2.1	2.1	2.1	1.8	1.0	0.2	0.	0.	0.	0.2	0.3	0.3	0.3
258	0.	0.	0.2	0.7	1.7	2.1	2.0	2.1	2.1	1.7	1.0	0.2	0.	0.	0.	0.2	0.2	0.2	0.3
260	0.	0.	0.2	0.7	1.7	2.0	2.0	2.1	2.0	1.7	0.9	0.2	0.	0.	0.	0.2	0.2	0.2	0.3
262	0.	0.	0.2	0.7	1.7	2.0	2.0	2.1	2.0	1.6	0.9	0.1	0.	0.	0.	0.2	0.2	0.2	0.3
264	0.	0.	0.2	0.7	1.7	2.0	1.9	2.1	2.0	1.6	0.8	0.1	0.	0.	0.	0.2	0.2	0.2	0.3
266	0.	0.	0.2	0.7	1.7	2.0	1.9	2.1	2.0	1.5	0.8	0.1	0.	0.	0.	0.2	0.2	0.2	0.3
268	0.		0.3	0.8	1.7	2.0	1.9	2.0	2.0	1.5	0.8	0.1	0.	0.	0.	0.2	0.2	0.2	0.3
270	0.		0.3	0.8	1.7	2.1	1.9	2.0	2.1	1.5	0.8	0.1	0.	0.	0.	0.2	0.2	0.2	0.3

TABLE XXXII (Continued)

	0	5	10	15	20	25	30	35	40	45	50	55	60	65	70	75	80	85	90
272	0.	0.	0.3	0.8	1.7	2.1	1.9	2.0	2.1	1.5	0.8	0.1	0.	0.	0.	0.2	0.2	0.2	0.3
274	0.	0.	0.3	0.8	1.7	2.2	1.9	2.0	2.1	1.5	0.8	0.1	0.	0.	0.	0.2	0.2	0.3	0.3
276	0.	0.	0.2	0.8	1.7	2.2	1.9	2.0	2.2	1.5	0.8	0.1	0.	0.	0.	0.2	0.3	0.3	0.3
278	0.	0.	0.2	0.8	1.7	2.2	1.9	2.0	2.2	1.5	0.8	0.1	0.	0.	0.	0.2	0.3	0.3	0.3
280	0.	0.	0.2	0.8	1.7	2.2	1.9	2.0	2.2	1.6	0.8	0.1	0.	0.	0.	0.2	0.3	0.3	0.3
282	0.	0.	0.2	0.8	1.7	2.2	1.9	2.0	2.2	1.6	0.9	0.1	0.	0.	0.	0.2	0.3	0.3	0.3
284	0.	0.	0.1	0.8	1.7	2.1	1.9	2.0	2.2	1.7	0.9	0.2	0.	0.	0.	0.2	0.3	0.3	0.3
286	0.	0.	0.1	0.7	1.6	2.1	1.9	2.0	2.2	1.7	0.9	0.2	0.	0.	0.	0.2	0.3	0.3	0.3
288	0.	0.	0.2	0.7	1.6	2.1	1.9	2.1	2.2	1.7	0.9	0.2	0.	0.	0.	0.2	0.3	0.3	0.3
290	0.	0.	0.2	0.8	1.6	2.1	1.9	2.1	2.2	1.7	0.9	0.2	0.	0.	0.	0.2	0.3	0.3	0.3
292	0.	0.	0.2	0.8	1.6	2.1	2.0	2.2	2.2	1.7	1.0	0.2	0.	0.	0.	0.2	0.3	0.3	0.3
294	0.	0.	0.2	0.8	1.6	2.1	2.1	2.3	2.2	1.7	1.0	0.3	0.0	0.	0.0	0.2	0.3	0.3	0.3
296	0.	0.0	0.3	0.8	1.6	2.2	2.2	2.4	2.3	1.8	1.1	0.3	0.0	0.	0.0	0.2	0.3	0.3	0.3
298	0.	0.0	0.3	0.9	1.6	2.2	2.3	2.6	2.4	1.8	1.1	0.3	0.1	0.0	0.0	0.2	0.3	0.3	0.3
300	0.	0.0	0.3	0.9	1.6	2.2	2.5	2.7	2.5	1.9	1.2	0.4	0.1	0.0	0.0	0.2	0.3	0.3	0.3
302	0.	0.0	0.3	0.9	1.6	2.3	2.6	2.9	2.7	2.0	1.2	0.4	0.1	0.0	0.0	0.2	0.3	0.3	0.3
304	0.	0.0	0.3	0.9	1.6	2.3	2.8	3.1	2.9	2.2	1.3	0.4	0.2	0.1	0.1	0.2	0.2	0.3	0.3
306	0.0	0.1	0.3	0.8	1.6	2.4	2.9	3.4	3.2	2.4	1.4	0.5	0.2	0.1	0.1	0.2	0.2	0.3	0.3
308	0.0	0.1	0.3	0.8	1.5	2.4	3.0	3.6	3.5	2.7	1.4	0.5	0.2	0.1	0.1	0.2	0.2	0.3	0.3
310	0.0	0.1	0.3	0.8	1.5	2.4	3.1	3.7	3.8	2.9	1.5	0.6	0.2	0.2	0.1	0.2	0.2	0.3	0.3
312	0.0	0.1	0.3	0.8	1.4	2.4	3.1	3.9	4.1	3.1	1.6	0.6	0.3	0.2	0.1	0.2	0.2	0.3	0.3
314	0.0	0.1	0.3	0.7	1.4	2.4	3.0	3.9	4.4	3.4	1.7	0.7	0.3	0.2	0.1	0.2	0.2	0.3	0.3
316	0.0	0.1	0.2	0.7	1.4	2.3	2.9	3.9	4.5	3.6	1.8	0.7	0.3	0.3	0.2	0.2	0.2	0.3	0.3
318	0.0	0.0	0.2	0.7	1.4	2.2	2.7	3.7	4.6	3.7	1.9	0.7	0.4	0.3	0.2	0.2	0.2	0.3	0.3
320	0.0	0.0	0.2	0.6	1.4	2.1	2.5	3.5	4.5	3.9	2.1	0.8	0.4	0.4	0.2	0.2	0.2	0.3	0.3
322	0.	0.0	0.2	0.6	1.3	2.0	2.3	3.1	4.3	3.9	2.2	0.8	0.4	0.4	0.2	0.2	0.2	0.3	0.3
324	0.	0.	0.1	0.6	1.3	1.9	2.0	2.8	4.0	3.9	2.4	0.9	0.5	0.5	0.3	0.2	0.2	0.3	0.3
326	0.	0.	0.1	0.6	1.3	1.8	1.8	2.4	3.5	3.8	2.5	0.9	0.5	0.5	0.3	0.2	0.2	0.3	0.3
328	0.	0.	0.1	0.6	1.2	1.6	1.6	2.0	3.1	3.6	2.6	1.0	0.6	0.6	0.3	0.2	0.2	0.3	0.3
330	0.	0.	0.1	0.6	1.2	1.5	1.3	1.6	2.6	3.4	2.6	1.1	0.6	0.6	0.4	0.2	0.2	0.3	0.3
332	0.	0.	0.2	0.6	1.2	1.3	1.1	1.3	2.1	3.0	2.6	1.1	0.6	0.7	0.4	0.2	0.2	0.3	0.3
334	0.0	0.0	0.2	0.6	1.1	1.2	1.0	1.0	1.7	2.7	2.5	1.2	0.7	0.7	0.5	0.3	0.2	0.3	0.3
336	0.0	0.1	0.2	0.7	1.1	1.1	0.8	0.8	1.3	2.3	2.4	1.2	0.7	0.7	0.5	0.3	0.2	0.3	0.3
338	0.1	0.1	0.3	0.7	1.0	1.0	0.7	0.7	1.0	1.9	2.2	1.3	0.8	0.8	0.5	0.3	0.2	0.3	0.3
340	0.1	0.1	0.3	0.7	1.0	0.9	0.6	0.5	0.8	1.6	2.1	1.3	0.8	0.8	0.6	0.3	0.2	0.3	0.3
342	0.2	0.2	0.4	0.8	0.9	0.8	0.5	0.5	0.6	1.3	1.9	1.4	0.8	0.8	0.6	0.3	0.2	0.3	0.3
344	0.2	0.2	0.4	0.8	0.9	0.7	0.4	0.4	0.5	1.0	1.7	1.4	0.9	0.8	0.6	0.3	0.2	0.3	0.3
346	0.3	0.3	0.5	0.8	0.8	0.6	0.4	0.3	0.4	0.8	1.5	1.3	0.9	0.9	0.7	0.3	0.2	0.3	0.3
348	0.3	0.4	0.5	0.8	0.7	0.5	0.3	0.3	0.4	0.7	1.3	1.3	0.9	0.9	0.7	0.3	0.2	0.2	0.3
350	0.4	0.4	0.6	0.7	0.6	0.4	0.3	0.3	0.3	0.6	1.1	1.3	1.0	0.9	0.7	0.3	0.2	0.2	0.3
352	0.4	0.5	0.6	0.7	0.6	0.4	0.2	0.2	0.3	0.5	1.0	1.2	1.0	0.9	0.7	0.3	0.2	0.2	0.3
354	0.5	0.5	0.7	0.7	0.5	0.3	0.2	0.2	0.3	0.4	0.9	1.2	1.0	0.9	0.8	0.3	0.2	0.2	0.3
356	0.6	0.6	0.7	0.7	0.5	0.3	0.2	0.2	0.2	0.4	0.8	1.2	1.0	0.9	0.8	0.3	0.2	0.2	0.3
358	0.6	0.6	0.7	0.7	0.5	0.3	0.2	0.2	0.2	0.4	0.7	1.1	1.0	0.9	0.8	0.3	0	0.2	0.3
360	0.7	0.7	0.8	0.7	0.5	0.2	0.2	0.2	0.2	0.3	0.7	1.1	1.0	0.9	0.8	0.3	0.2	0.2	0.3

POLE FIGURE DATA SHEET FOR SPECIMEN 4B

The normalized pole figure is based on Mo k-alpha radiation and the 111 reflection.

The 222 reflection was used to fill in the blind region from 80 through 90 degrees alpha.

The alpha-dependent two theta shift was taken into account.

Integrated intensities were used.

Normal smoothing was used.

Maximum and minimum corrected intensities are 2466 and 0 counts/second, respectively.

Random intensity is 514 counts/second.

Contour spacing is based on multiples of random intensity.

4 contours are to be plotted.

Their values are 1.000 2.000 3.000 4.000.

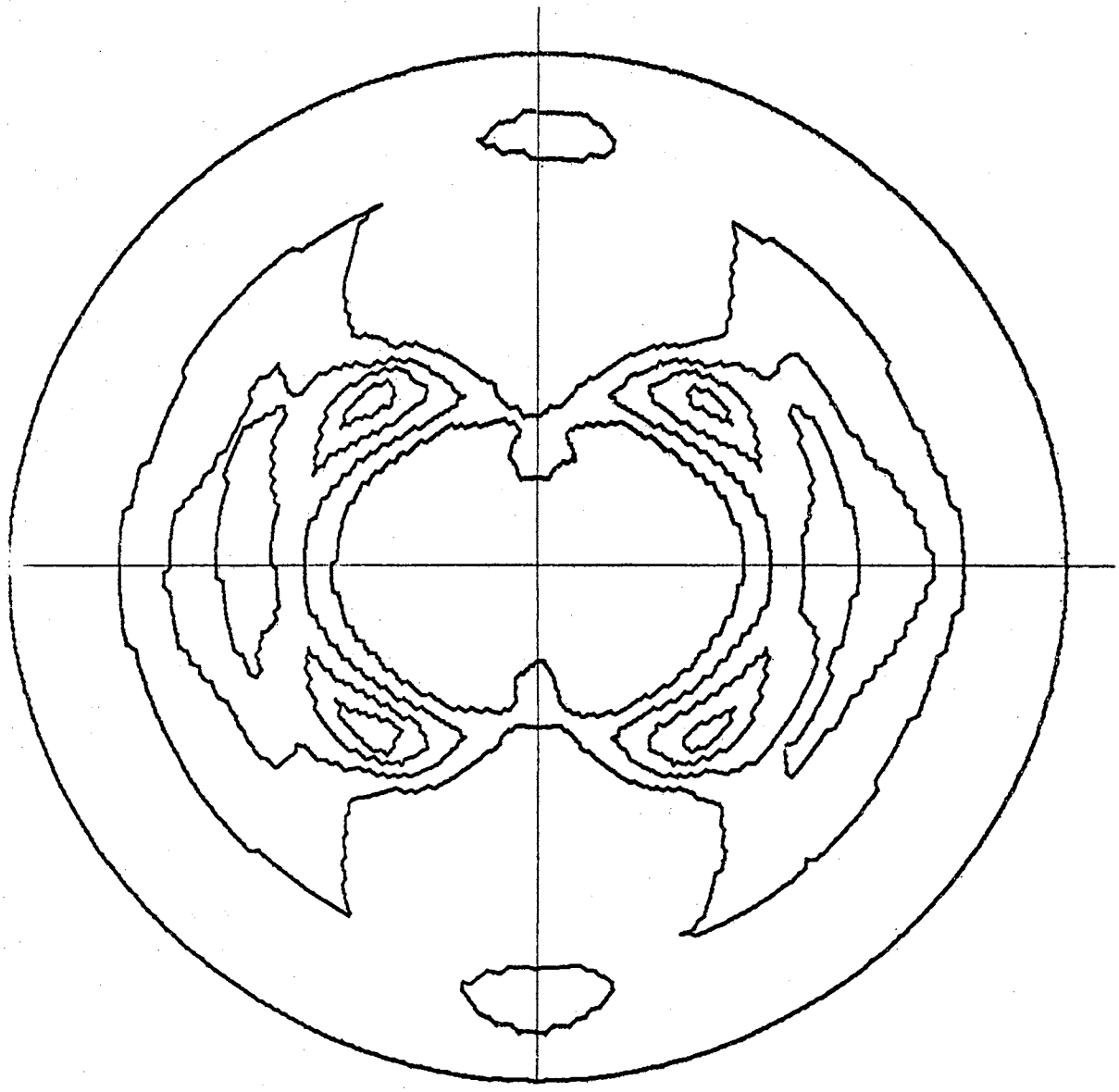

Figure 36. (111) Pole Figure for Specimen 4B

TABLE XXXIII

POLE FIGURE DATA FOR SPECIMEN 4B

	0	5	10	15	20	25	30	35	40	45	50	55	60	65	70	75	80	85	90
2	0.6	0.9	1.1	0.9	0.3	0.1	0.	0.0	0.2	0.2	0.5	1.0	1.1	1.1	1.1	0.4	0.2	0.3	0.4
4	0.6	0.9	1.1	0.9	0.3	0.1	0.	0.0	0.2	0.2	0.5	1.0	1.0	1.1	1.1	0.4	0.2	0.3	0.4
6	0.6	0.9	1.1	0.9	0.3	0.1	0.	0.0	0.2	0.2	0.6	1.0	1.0	1.1	1.1	0.4	0.2	0.3	0.4
8	0.5	0.8	1.0	0.9	0.3	0.1	0.	0.0	0.2	0.3	0.7	1.0	1.0	1.1	1.0	0.4	0.2	0.3	0.4
10	0.5	0.8	1.0	0.9	0.3	0.1	0.0	0.0	0.2	0.3	0.8	1.0	1.0	1.1	1.0	0.4	0.2	0.3	0.4
12	0.5	0.7	0.9	0.9	0.4	0.1	0.0	0.0	0.2	0.4	0.9	1.1	0.9	1.0	1.0	0.4	0.2	0.3	0.4
14	0.4	0.7	0.8	0.9	0.4	0.2	0.0	0.1	0.3	0.5	1.1	1.1	0.9	1.0	0.9	0.4	0.2	0.3	0.4
16	0.4	0.6	0.8	0.9	0.5	0.2	0.1	0.1	0.3	0.7	1.3	1.1	0.9	1.0	0.9	0.4	0.2	0.3	0.4
18	0.4	0.6	0.8	0.9	0.5	0.3	0.1	0.1	0.4	0.9	1.5	1.1	0.9	0.9	0.8	0.4	0.2	0.3	0.4
20	0.3	0.5	0.7	0.9	0.6	0.3	0.1	0.1	0.6	1.1	1.7	1.1	0.8	0.9	0.8	0.3	0.2	0.3	0.4
22	0.3	0.4	0.7	1.0	0.7	0.4	0.1	0.2	0.8	1.4	1.9	1.1	0.8	0.8	0.7	0.3	0.2	0.3	0.4
24	0.3	0.4	0.6	1.0	0.7	0.4	0.2	0.3	1.0	1.8	2.1	1.1	0.7	0.8	0.6	0.3	0.2	0.3	0.4
26	0.2	0.3	0.6	1.1	0.8	0.5	0.3	0.4	1.3	2.1	2.3	1.1	0.7	0.7	0.6	0.2	0.2	0.3	0.4
28	0.2	0.3	0.5	1.1	0.9	0.6	0.3	0.5	1.7	2.5	2.4	1.1	0.6	0.6	0.5	0.2	0.2	0.3	0.4
30	0.1	0.2	0.5	1.1	1.0	0.7	0.4	0.7	2.2	2.9	2.5	1.0	0.6	0.5	0.5	0.2	0.2	0.3	0.4
32	0.1	0.2	0.5	1.1	1.1	0.8	0.6	1.0	2.7	3.2	2.5	1.0	0.5	0.5	0.4	0.2	0.2	0.3	0.4
34	0.1	0.2	0.4	1.1	1.2	0.9	0.7	1.2	3.2	3.5	2.5	0.9	0.5	0.4	0.3	0.2	0.2	0.3	0.4
36	0.1	0.2	0.4	1.1	1.2	1.1	0.9	1.5	3.7	3.7	2.5	0.8	0.4	0.3	0.3	0.1	0.2	0.3	0.4
38	0.1	0.2	0.4	1.2	1.3	1.2	1.1	1.8	4.1	3.8	2.5	0.8	0.3	0.3	0.2	0.1	0.2	0.4	0.4
40	0.1	0.2	0.4	1.2	1.4	1.4	1.2	2.1	4.5	3.9	2.4	0.7	0.3	0.2	0.2	0.1	0.2	0.4	0.4
42	0.1	0.2	0.4	1.2	1.5	1.5	1.4	2.4	4.7	3.8	2.3	0.7	0.2	0.2	0.1	0.1	0.2	0.4	0.4
44	0.1	0.2	0.5	1.2	1.5	1.7	1.6	2.5	4.8	3.8	2.1	0.6	0.2	0.1	0.1	0.1	0.2	0.4	0.4
46	0.1	0.2	0.5	1.3	1.6	1.8	1.7	2.7	4.8	3.6	2.0	0.5	0.2	0.1	0.1	0.1	0.2	0.4	0.4
48	0.1	0.2	0.5	1.3	1.7	1.9	1.8	2.7	4.6	3.5	1.9	0.5	0.1	0.1	0.0	0.1	0.2	0.4	0.4
50	0.1	0.2	0.5	1.3	1.7	2.0	1.9	2.8	4.5	3.3	1.7	0.4	0.1	0.0	0.0	0.1	0.3	0.4	0.4
52	0.0	0.2	0.5	1.3	1.7	2.0	2.0	2.8	4.2	3.1	1.6	0.3	0.0	0.	0.	0.0	0.3	0.4	0.4
54	0.0	0.2	0.5	1.2	1.7	2.1	2.0	2.7	4.0	2.9	1.5	0.3	0.0	0.	0.	0.0	0.3	0.4	0.4
56	0.0	0.2	0.5	1.2	1.7	2.1	2.0	2.7	3.8	2.7	1.4	0.2	0.	0.	0.	0.0	0.3	0.4	0.4
58	0.	0.1	0.5	1.2	1.7	2.1	2.0	2.6	3.6	2.6	1.2	0.2	0.	0.	0.	0.0	0.3	0.4	0.4
60	0.	0.1	0.5	1.1	1.7	2.1	2.0	2.5	3.5	2.5	1.1	0.2	0.	0.	0.	0.0	0.3	0.4	0.4
62	0.	0.1	0.4	1.1	1.7	2.1	1.9	2.4	3.3	2.3	1.1	0.1	0.	0.	0.	0.0	0.3	0.4	0.4
64	0.	0.1	0.4	1.1	1.7	2.0	1.9	2.3	3.2	2.2	1.0	0.1	0.	0.	0.	0.0	0.3	0.4	0.4
66	0.	0.1	0.4	1.1	1.7	2.0	1.9	2.3	3.1	2.1	0.9	0.1	0.	0.	0.	0.0	0.3	0.4	0.4
68	0.	0.0	0.3	1.1	1.7	2.1	1.9	2.2	3.0	2.0	0.8	0.1	0.	0.	0.	0.0	0.3	0.4	0.4
70	0.	0.0	0.3	1.1	1.8	2.1	1.8	2.1	2.9	1.9	0.8	0.0	0.	0.	0.	0.0	0.3	0.4	0.4
72	0.	0.0	0.3	1.1	1.8	2.1	1.8	2.1	2.7	1.8	0.7	0.0	0.	0.	0.	0.0	0.3	0.4	0.4
74	0.	0.0	0.3	1.2	1.9	2.1	1.8	2.0	2.6	1.7	0.7	0.0	0.	0.	0.	0.0	0.3	0.4	0.4
76	0.	0.0	0.3	1.2	1.9	2.1	1.8	2.0	2.6	1.7	0.7	0.0	0.	0.	0.	0.0	0.3	0.4	0.4
78	0.	0.0	0.4	1.3	1.9	2.2	1.8	2.0	2.5	1.6	0.7	0.0	0.	0.	0.	0.0	0.3	0.4	0.4
80	0.	0.0	0.4	1.3	2.0	2.2	1.8	2.0	2.5	1.6	0.7	0.0	0.	0.	0.	0.0	0.3	0.4	0.4
82	0.	0.1	0.4	1.4	2.0	2.2	1.8	1.9	2.5	1.6	0.7	0.0	0.	0.	0.	0.0	0.3	0.4	0.4
84	0.	0.1	0.5	1.5	2.1	2.2	1.8	1.9	2.5	1.6	0.6	0.	0.	0.	0.	0.0	0.3	0.4	0.4
86	0.	0.1	0.5	1.5	2.1	2.2	1.8	1.9	2.5	1.6	0.6	0.	0.	0.	0.	0.0	0.3	0.4	0.4
88	0.	.1	0.6	1.6	2.1	2.2	1.8	1.9	2.5	1.5	0.6	0.	0.	0.	0.	0.0	0.3	0.4	0.4
90	0.	0.1	0.6	1.6	2.1	2.2	1.8	1.9	2.5	1.5	0.6	0.	0.	0.	0.	0.0	0.3	0.4	0.4

TABLE XXXIII (Continued)

	0	5	10	15	20	25	30	35	40	45	50	55	60	65	70	75	80	85	90
92	0.	0.1	0.6	1.6	2.1	2.3	1.8	1.9	2.4	1.5	0.6	0.	0.	0.	0.	0.0	0.3	0.4	0.4
94	0.	0.1	0.5	1.5	2.1	2.3	1.8	1.8	2.4	1.5	0.6	0.	0.	0.	0.	0.0	0.3	0.4	0.4
96	0.	0.0	0.5	1.5	2.1	2.3	1.8	1.8	2.3	1.5	0.6	0.	0.	0.	0.	0.0	0.3	0.4	0.4
98	0.	0.0	0.5	1.5	2.1	2.4	1.8	1.9	2.3	1.5	0.6	0.	0.	0.	0.	0.0	0.3	0.4	0.4
100	0.	0.0	0.4	1.4	2.1	2.4	1.8	1.9	2.4	1.6	0.6	0.	0.	0.	0.	0.1	0.3	0.4	0.4
102	0.	0.	0.4	1.4	2.0	2.4	1.9	2.0	2.5	1.6	0.7	0.	0.	0.	0.	0.1	0.3	0.4	0.4
104	0.	0.	0.4	1.3	2.0	2.4	1.9	2.1	2.6	1.7	0.7	0.	0.	0.	0.	0.0	0.3	0.4	0.4
106	0.	0.	0.3	1.3	1.9	2.3	1.9	2.2	2.8	1.8	0.7	0.0	0.	0.	0.	0.0	0.3	0.4	0.4
108	0.	0.	0.3	1.2	1.9	2.3	1.9	2.3	2.9	1.8	0.8	0.0	0.	0.	0.	0.0	0.3	0.4	0.4
110	0.	0.0	0.3	1.2	1.8	2.3	2.0	2.4	3.1	1.9	0.9	0.0	0.	0.	0.	0.0	0.3	0.4	0.4
112	0.	0.0	0.3	1.2	1.7	2.2	2.0	2.5	3.2	2.0	0.9	0.1	0.	0.	0.	0.0	0.3	0.4	0.4
114	0.	0.0	0.4	1.2	1.7	2.2	2.0	2.5	3.3	2.1	1.0	0.1	0.	0.	0.	0.0	0.3	0.4	0.4
116	0.	0.1	0.4	1.2	1.7	2.2	2.1	2.6	3.4	2.2	1.1	0.1	0.	0.	0.	0.0	0.3	0.4	0.4
118	0.	0.1	0.4	1.2	1.6	2.2	2.1	2.6	3.6	2.4	1.2	0.2	0.	0.	0.	0.0	0.3	0.4	0.4
120	0.	0.1	0.4	1.2	1.6	2.2	2.1	2.7	3.7	2.5	1.3	0.2	0.	0.	0.	0.0	0.3	0.4	0.4
122	0.0	0.1	0.5	1.2	1.6	2.1	2.1	2.7	3.9	2.7	1.3	0.2	0.	0.	0.	0.0	0.3	0.4	0.4
124	0.0	0.1	0.5	1.2	1.6	2.1	2.1	2.8	4.1	2.9	1.4	0.3	0.0	0.	0.	0.1	0.2	0.3	0.4
126	0.1	0.2	0.5	1.2	1.6	2.1	2.0	2.8	4.3	3.1	1.5	0.3	0.0	0.	0.	0.1	0.2	0.3	0.4
128	0.1	0.2	0.5	1.2	1.6	2.0	2.0	2.8	4.5	3.3	1.6	0.4	0.1	0.	0.	0.1	0.2	0.3	0.4
130	0.1	0.2	0.5	1.2	1.6	2.0	1.9	2.8	4.6	3.5	1.7	0.4	0.1	0.0	0.	0.1	0.2	0.3	0.4
132	0.1	0.2	0.5	1.2	1.6	1.9	1.8	2.8	4.7	3.7	1.8	0.4	0.1	0.1	0.	0.1	0.2	0.3	0.4
134	0.1	0.2	0.4	1.2	1.6	1.8	1.7	2.7	4.8	3.9	2.0	0.5	0.2	0.1	0.0	0.1	0.2	0.3	0.4
136	0.1	0.2	0.4	1.1	1.5	1.7	1.5	2.5	4.7	4.0	2.1	0.6	0.2	0.1	0.0	0.1	0.2	0.3	0.4
138	0.1	0.2	0.4	1.1	1.5	1.5	1.4	2.3	4.6	4.1	2.2	0.6	0.3	0.2	0.1	0.1	0.2	0.3	0.4
140	0.1	0.2	0.4	1.1	1.4	1.4	1.2	2.0	4.3	4.1	2.3	0.7	0.3	0.2	0.1	0.1	0.2	0.3	0.4
142	0.1	0.2	0.4	1.1	1.3	1.2	1.0	1.7	4.0	4.0	2.4	0.7	0.4	0.3	0.1	0.1	0.2	0.3	0.4
144	0.1	0.2	0.4	1.1	1.2	1.1	0.8	1.5	3.6	3.8	2.5	0.8	0.4	0.4	0.2	0.1	0.2	0.3	0.4
146	0.1	0.2	0.4	1.1	1.1	1.0	0.7	1.2	3.1	3.6	2.5	0.9	0.5	0.4	0.2	0.2	0.2	0.3	0.4
148	0.1	0.2	0.5	1.1	1.0	0.8	0.5	0.9	2.7	3.3	2.5	0.9	0.5	0.5	0.3	0.2	0.2	0.3	0.4
150	0.1	0.2	0.5	1.0	0.9	0.7	0.4	0.7	2.2	2.9	2.5	1.0	0.6	0.6	0.3	0.2	0.2	0.3	0.4
152	0.2	0.3	0.6	1.0	0.8	0.6	0.3	0.5	1.7	2.5	2.4	1.0	0.6	0.6	0.4	0.2	0.2	0.3	0.4
154	0.2	0.4	0.6	1.0	0.8	0.5	0.2	0.4	1.4	2.2	2.3	1.1	0.7	0.7	0.4	0.2	0.2	0.3	0.4
156	0.3	0.4	0.6	1.0	0.7	0.4	0.2	0.3	1.0	1.8	2.2	1.1	0.7	0.7	0.5	0.3	0.2	0.3	0.4
158	0.3	0.5	0.7	0.9	0.6	0.3	0.1	0.2	0.8	1.5	2.0	1.1	0.8	0.8	0.5	0.3	0.2	0.3	0.4
160	0.4	0.5	0.7	0.9	0.5	0.3	0.1	0.2	0.6	1.2	1.8	1.1	0.8	0.8	0.6	0.3	0.2	0.3	0.4
162	0.4	0.6	0.8	0.9	0.5	0.2	0.1	0.1	0.4	0.9	1.6	1.1	0.9	0.9	0.6	0.3	0.2	0.3	0.4
164	0.5	0.7	0.8	0.8	0.4	0.2	0.0	0.1	0.3	0.7	1.3	1.1	0.9	0.9	0.7	0.3	0.2	0.3	0.4
166	0.5	0.7	0.9	0.8	0.4	0.2	0.0	0.1	0.3	0.5	1.2	1.1	0.9	1.0	0.7	0.4	0.2	0.3	0.4
168	0.5	0.8	1.0	0.8	0.3	0.1	0.0	0.0	0.2	0.4	1.0	1.1	1.0	1.0	0.8	0.4	0.2	0.3	0.4
170	0.6	0.8	1.0	0.9	0.3	0.1	0.	0.0	0.2	0.3	0.8	1.1	1.0	1.0	0.8	0.4	0.2	0.3	0.4
172	0.6	0.9	1.1	0.9	0.3	0.1	0.	0.0	0.2	0.3	0.7	1.1	1.0	1.1	0.9	0.4	0.2	0.3	0.4
174	0.6	0.9	1.2	0.9	0.3	0.1	0.	0.0	0.1	0.2	0.6	1.0	1.0	1.1	0.9	0.4	0.2	0.3	0.4
176	0.7	1.0	1.2	1.0	0.3	0.1	0.	0.0	0.1	0.2	0.6	1.0	1.1	1.1	1.0	0.4	0.2	0.3	0.4
178	0.7	0	1.3	1.0	0.3	0.1	0.	0.0	0.1	0.2	0.5	1.0	1.1	1.1	1.0	0.4	0.2	0.3	0.4
180	0.7	0	1.3	1.0	0.3	0.1	0.	0.0	0.1	0.2	0.5	1.0	1.1	1.1	1.0	0.4	0.2	0.3	0.4

TABLE XXXIII (Continued)

	0	5	10	15	20	25	30	35	40	45	50	55	60	65	70	75	80	85	90
182	0.7	1.0	1.3	1.0	0.3	0.1	0.	0.0	0.1	0.2	0.5	1.0	1.1	1.1	1.0	0.4	0.2	0.3	0.4
184	0.6	1.0	1.2	1.0	0.3	0.1	0.	0.0	0.1	0.2	0.5	1.0	1.1	1.0	1.0	0.4	0.2	0.3	0.4
186	0.6	0.9	1.2	1.0	0.3	0.1	0.	0.0	0.2	0.2	0.5	1.0	1.1	1.0	1.0	0.4	0.2	0.3	0.4
188	0.6	0.9	1.1	0.9	0.3	0.1	0.	0.0	0.2	0.3	0.7	1.1	1.0	1.0	1.0	0.4	0.2	0.3	0.4
190	0.5	0.8	1.0	0.9	0.3	0.1	0.	0.0	0.2	0.3	0.8	1.1	1.0	1.0	0.9	0.4	0.2	0.3	0.4
192	0.5	0.8	1.0	0.9	0.4	0.1	0.0	0.0	0.2	0.4	1.0	1.1	1.0	0.9	0.9	0.3	0.2	0.3	0.4
194	0.5	0.7	0.9	0.9	0.4	0.2	0.0	0.1	0.3	0.5	1.1	1.1	0.9	0.9	0.9	0.3	0.2	0.3	0.4
196	0.4	0.7	0.9	0.9	0.4	0.2	0.0	0.1	0.3	0.7	1.3	1.1	0.9	0.9	0.8	0.3	0.2	0.3	0.4
198	0.4	0.6	0.8	0.9	0.5	0.2	0.1	0.1	0.4	0.9	1.5	1.1	0.8	0.8	0.8	0.3	0.2	0.3	0.4
200	0.3	0.6	0.8	1.0	0.6	0.3	0.1	0.1	0.6	1.2	1.7	1.1	0.8	0.8	0.7	0.3	0.2	0.3	0.4
202	0.3	0.5	0.7	1.0	0.7	0.4	0.1	0.2	0.7	1.5	1.9	1.0	0.7	0.7	0.7	0.3	0.2	0.3	0.4
204	0.2	0.4	0.7	1.1	0.7	0.4	0.2	0.3	1.0	1.8	2.1	1.0	0.7	0.7	0.6	0.3	0.2	0.3	0.4
206	0.2	0.4	0.7	1.1	0.9	0.5	0.3	0.4	1.3	2.2	2.3	1.0	0.6	0.6	0.6	0.2	0.2	0.3	0.4
208	0.1	0.3	0.6	1.2	1.0	0.6	0.3	0.5	1.7	2.6	2.5	1.0	0.6	0.6	0.5	0.2	0.2	0.3	0.4
210	0.1	0.3	0.6	1.2	1.1	0.8	0.4	0.7	2.1	2.9	2.5	0.9	0.5	0.5	0.5	0.2	0.2	0.3	0.4
212	0.1	0.2	0.5	1.2	1.2	0.9	0.6	0.9	2.6	3.3	2.6	0.9	0.5	0.5	0.4	0.2	0.2	0.3	0.4
214	0.1	0.2	0.5	1.2	1.3	1.0	0.7	1.2	3.1	3.5	2.6	0.9	0.4	0.4	0.4	0.2	0.2	0.3	0.4
216	0.1	0.2	0.5	1.2	1.3	1.2	0.9	1.5	3.5	3.7	2.5	0.8	0.4	0.3	0.3	0.2	0.2	0.3	0.4
218	0.1	0.2	0.4	1.2	1.4	1.4	1.1	1.8	4.0	3.9	2.4	0.7	0.3	0.3	0.3	0.2	0.2	0.3	0.4
220	0.1	0.2	0.4	1.1	1.5	1.5	1.3	2.1	4.3	3.9	2.3	0.7	0.3	0.2	0.2	0.1	0.2	0.4	0.4
222	0.1	0.2	0.4	1.1	1.6	1.7	1.5	2.4	4.5	3.9	2.1	0.6	0.2	0.2	0.2	0.1	0.2	0.4	0.4
224	0.1	0.2	0.4	1.1	1.6	1.8	1.7	2.6	4.7	3.8	2.0	0.5	0.2	0.1	0.1	0.1	0.2	0.4	0.4
226	0.1	0.2	0.4	1.2	1.6	1.9	1.8	2.7	4.7	3.6	1.9	0.5	0.2	0.1	0.1	0.1	0.2	0.4	0.4
228	0.1	0.2	0.5	1.2	1.7	2.0	1.9	2.8	4.6	3.5	1.7	0.4	0.1	0.0	0.0	0.1	0.2	0.4	0.4
230	0.1	0.2	0.5	1.2	1.7	2.0	2.0	2.8	4.4	3.3	1.7	0.4	0.1	0.0	0.0	0.1	0.2	0.4	0.4
232	0.1	0.2	0.5	1.2	1.7	2.0	2.0	2.8	4.3	3.1	1.6	0.3	0.0	0.	0.	0.1	0.2	0.4	0.4
234	0.1	0.2	0.5	1.2	1.7	2.0	2.0	2.7	4.1	3.0	1.5	0.3	0.0	0.	0.	0.1	0.2	0.4	0.4
236	0.0	0.1	0.4	1.1	1.7	2.0	2.0	2.7	3.9	2.9	1.4	0.2	0.	0.	0.	0.1	0.2	0.4	0.4
238	0.0	0.1	0.4	1.1	1.6	2.1	2.0	2.6	3.8	2.8	1.4	0.2	0.	0.	0.	0.1	0.2	0.4	0.4
240	0.0	0.1	0.4	1.1	1.6	2.1	2.0	2.5	3.6	2.7	1.3	0.2	0.	0.	0.	0.1	0.2	0.4	0.4
242	0.	0.1	0.4	1.1	1.7	2.1	1.9	2.5	3.5	2.6	1.2	0.1	0.	0.	0.	0.1	0.2	0.4	0.4
244	0.	0.1	0.4	1.1	1.7	2.1	1.9	2.4	3.4	2.4	1.2	0.1	0.	0.	0.	0.1	0.2	0.4	0.4
246	0.	0.0	0.4	1.1	1.7	2.2	1.9	2.4	3.3	2.3	1.1	0.1	0.	0.	0.	0.1	0.2	0.4	0.4
248	0.	0.0	0.4	1.2	1.8	2.2	1.9	2.3	3.2	2.2	1.0	0.1	0.	0.	0.	0.1	0.2	0.3	0.4
250	0.	0.0	0.3	1.2	1.8	2.2	1.9	2.3	3.1	2.1	0.9	0.1	0.	0.	0.	0.1	0.2	0.3	0.4
252	0.	0.0	0.3	1.2	1.9	2.3	1.9	2.2	2.9	2.0	0.9	0.0	0.	0.	0.	0.1	0.2	0.3	0.4
254	0.	0.0	0.3	1.3	2.0	2.3	1.9	2.2	2.8	1.9	0.8	0.0	0.	0.	0.	0.1	0.2	0.3	0.4
256	0.	0.0	0.3	1.4	2.0	2.3	1.9	2.1	2.7	1.8	0.8	0.0	0.	0.	0.	0.1	0.2	0.3	0.4
258	0.	0.0	0.4	1.5	2.1	2.3	1.9	2.0	2.6	1.7	0.7	0.0	0.	0.	0.	0.1	0.2	0.3	0.4
260	0.	0.0	0.4	1.6	2.2	2.3	1.9	2.0	2.5	1.6	0.7	0.	0.	0.	0.	0.1	0.2	0.3	0.4
262	0.	0.1	0.5	1.7	2.2	2.3	1.8	2.0	2.5	1.6	0.6	0.	0.	0.	0.	0.1	0.3	0.3	0.4
264	0.	0.1	0.5	1.8	2.3	2.4	1.8	1.9	2.5	1.6	0.6	0.	0.	0.	0.	0.1	0.3	0.3	0.4
266	0.	0.1	0.6	1.8	2.3	2.3	1.7	1.9	2.5	1.6	0.6	0.	0.	0.	0.	0.1	0.3	0.3	0.4
268	0.	0.1	0.6	1.9	2.4	2.3	1.7	1.9	2.5	1.6	0.6	0.	0.	0.	0.	0.1	0.3	0.3	0.4
270	0.	0.1	0.7	1.9	2.4	2.3	1.7	1.9	2.6	1.6	0.6	0.	0.	0.	0.	0.1	0.3	0.3	0.4

TABLE XXXIII (Continued)

	0	5	10	15	20	25	30	35	40	45	50	55	60	65	70	75	80	85	90
272	0.	0.1	0.7	1.9	2.4	2.3	1.7	1.9	2.6	1.6	0.6	0.	0.	0.	0.	0.1	0.3	0.3	0.4
274	0.	0.1	0.7	1.9	2.4	2.3	1.6	1.9	2.6	1.6	0.6	0.	0.	0.	0.	0.1	0.3	0.3	0.4
276	0.	0.1	0.6	1.8	2.4	2.3	1.7	2.0	2.6	1.5	0.6	0.	0.	0.	0.	0.1	0.3	0.4	0.4
278	0.	0.1	0.6	1.7	2.3	2.3	1.7	2.0	2.6	1.5	0.6	0.	0.	0.	0.	0.1	0.3	0.4	0.4
280	0.	0.0	0.5	1.6	2.3	2.3	1.7	2.0	2.6	1.5	0.6	0.	0.	0.	0.	0.1	0.3	0.4	0.4
282	0.	0.0	0.5	1.4	2.2	2.3	1.8	2.1	2.6	1.5	0.6	0.	0.	0.	0.	0.1	0.3	0.4	0.4
284	0.	0.0	0.4	1.4	2.1	2.3	1.8	2.1	2.7	1.6	0.6	0.0	0.	0.	0.	0.1	0.3	0.4	0.4
286	0.	0.0	0.4	1.3	2.0	2.3	1.9	2.2	2.7	1.6	0.7	0.0	0.	0.	0.	0.1	0.3	0.4	0.4
288	0.	0.0	0.4	1.2	1.9	2.3	1.9	2.2	2.8	1.7	0.7	0.0	0.	0.	0.	0.1	0.3	0.4	0.4
290	0.	0.0	0.4	1.2	1.8	2.3	1.9	2.2	2.8	1.8	0.7	0.0	0.	0.	0.	0.1	0.3	0.4	0.4
292	0.	0.0	0.4	1.1	1.7	2.2	1.9	2.2	2.8	1.9	0.8	0.0	0.	0.	0.	0.1	0.3	0.4	0.4
294	0.	0.0	0.4	1.1	1.7	2.2	1.9	2.3	3.0	2.1	0.9	0.1	0.	0.	0.	0.1	0.3	0.4	0.4
296	0.	0.1	0.4	1.1	1.6	2.2	1.9	2.3	3.1	2.2	1.0	0.1	0.	0.	0.	0.1	0.3	0.4	0.4
298	0.	0.1	0.4	1.1	1.6	2.2	1.9	2.4	3.2	2.3	1.1	0.1	0.	0.	0.	0.1	0.3	0.4	0.4
300	0.	0.1	0.4	1.1	1.7	2.2	2.0	2.4	3.4	2.5	1.2	0.2	0.	0.	0.	0.1	0.3	0.4	0.4
302	0.0	0.1	0.4	1.2	1.7	2.2	2.0	2.5	3.5	2.6	1.3	0.2	0.	0.	0.	0.1	0.3	0.3	0.4
304	0.0	0.1	0.5	1.2	1.7	2.2	2.0	2.7	3.7	2.7	1.4	0.2	0.	0.	0.	0.1	0.3	0.3	0.4
306	0.0	0.2	0.5	1.3	1.8	2.1	2.1	2.8	3.9	2.9	1.5	0.3	0.0	0.0	0.	0.1	0.2	0.3	0.4
308	0.0	0.2	0.5	1.3	1.8	2.1	2.1	2.8	4.1	3.1	1.6	0.3	0.1	0.1	0.	0.1	0.2	0.3	0.4
310	0.0	0.2	0.5	1.3	1.8	2.1	2.0	2.9	4.3	3.2	1.7	0.4	0.1	0.1	0.	0.1	0.2	0.3	0.4
312	0.0	0.2	0.5	1.3	1.8	2.0	1.9	2.8	4.5	3.4	1.8	0.4	0.1	0.2	0.	0.1	0.2	0.3	0.4
314	0.0	0.2	0.5	1.3	1.7	1.9	1.8	2.7	4.5	3.6	1.9	0.5	0.2	0.2	0.0	0.1	0.2	0.3	0.4
316	0.0	0.2	0.5	1.3	1.7	1.8	1.6	2.6	4.5	3.7	2.0	0.5	0.2	0.3	0.0	0.1	0.2	0.3	0.4
318	0.0	0.2	0.5	1.3	1.6	1.6	1.4	2.4	4.4	3.8	2.2	0.6	0.3	0.3	0.1	0.1	0.2	0.3	0.4
320	0.0	0.2	0.5	1.2	1.5	1.4	1.2	2.1	4.2	3.8	2.3	0.7	0.3	0.4	0.1	0.2	0.2	0.3	0.4
322	0.1	0.2	0.5	1.2	1.4	1.3	1.0	1.8	3.8	3.7	2.4	0.7	0.4	0.5	0.1	0.2	0.2	0.3	0.4
324	0.1	0.2	0.5	1.2	1.3	1.1	0.8	1.5	3.4	3.5	2.5	0.8	0.4	0.5	0.2	0.2	0.2	0.3	0.4
326	0.1	0.2	0.5	1.1	1.2	0.9	0.7	1.2	3.0	3.4	2.5	0.9	0.5	0.6	0.2	0.2	0.2	0.3	0.4
328	0.1	0.2	0.5	1.1	1.0	0.8	0.5	0.9	2.5	3.2	2.5	0.9	0.5	0.7	0.3	0.2	0.2	0.3	0.4
330	0.1	0.3	0.5	1.0	0.9	0.7	0.4	0.7	2.0	2.9	2.5	1.0	0.6	0.7	0.3	0.2	0.2	0.3	0.4
332	0.2	0.3	0.5	1.0	0.8	0.5	0.3	0.5	1.6	2.5	2.4	1.0	0.6	0.8	0.4	0.3	0.2	0.3	0.4
334	0.2	0.3	0.5	1.0	0.7	0.5	0.2	0.4	1.3	2.2	2.3	1.1	0.7	0.9	0.4	0.3	0.2	0.3	0.4
336	0.3	0.4	0.6	0.9	0.6	0.4	0.2	0.3	1.0	1.8	2.2	1.1	0.7	0.9	0.5	0.3	0.2	0.3	0.4
338	0.3	0.5	0.6	0.9	0.6	0.3	0.1	0.2	0.7	1.5	2.0	1.1	0.8	1.0	0.6	0.3	0.2	0.3	0.4
340	0.3	0.5	0.7	0.9	0.5	0.3	0.1	0.2	0.6	1.2	1.8	1.1	0.8	1.0	0.6	0.4	0.2	0.3	0.4
342	0.4	0.6	0.7	0.9	0.5	0.2	0.1	0.1	0.4	0.9	1.6	1.2	0.9	1.0	0.7	0.4	0.2	0.3	0.4
344	0.4	0.7	0.8	0.9	0.4	0.2	0.0	0.1	0.3	0.7	1.4	1.1	0.9	1.1	0.8	0.4	0.2	0.3	0.4
346	0.5	0.7	0.9	0.9	0.4	0.2	0.0	0.1	0.3	0.6	1.2	1.1	1.0	1.1	0.8	0.4	0.2	0.3	0.4
348	0.5	0.8	1.0	0.9	0.4	0.1	0.0	0.1	0.2	0.4	1.0	1.1	1.0	1.1	0.9	0.4	0.2	0.3	0.4
350	0.6	0.8	1.0	0.9	0.3	0.1	0.0	0.0	0.2	0.3	0.9	1.1	1.0	1.1	0.9	0.4	0.2	0.3	0.4
352	0.6	0.9	1.1	0.9	0.3	0.1	0.	0.0	0.2	0.3	0.7	1.1	1.1	1.1	1.0	0.4	0.2	0.3	0.4
354	0.7	0.9	1.1	0.9	0.3	0.1	0.	0.0	0.1	0.2	0.6	1.0	1.1	1.1	1.0	0.4	0.2	0.3	0.4
356	0.7	0.9	1.2	0.9	0.3	0.1	0.	0.0	0.1	0.2	0.6	1.0	1.1	1.1	1.1	0.4	0.2	0.3	0.4
358	0.7	0.9	1.2	0.9	0.3	0.1	0.	0.0	0.1	0.2	0.5	1.0	1.1	1.1	1.1	0.4	0.2	0.3	0.4
360	0.7	0.9	1.2	0.9	0.3	0.1	0.	0.0	0.2	0.2	0.5	1.0	1.1	1.1	1.1	0.4	0.2	0.3	0.4

APPENDIX B

LIST OF SYMBOLS

α	The angle used to define the radial position of a pole in a pole figure.
β	The angle used to define the azimuthal position of pole in a pole figure.
δ	A measure of the lack of parallelism of the major faces of a specimen.
ξ	The elastic displacement in the X_1 direction.
η	The elastic displacement in the X_2 direction.
ζ	The elastic displacement in the X_3 direction.
Θ	The strain energy function defined by equation (2.38).
Θ	The angle between the plane of polarization and the X axis.
θ	The angle of incidence of an x-ray beam on an (hkl) plane.
Λ	The wavelength of an elastic wave.
λ	The Lame constant.
μ	The rigidity modulus.
ν	The angle between the plane of vibration of a plane polarized wave and the X axis.
ρ	The density of an undeformed elastic medium.
ϕ	A cosine function defined by equation (3.1).
ϕ_o	The initial amplitude of a plane polarized cosine wave.
ϕ_x	The component of ϕ parallel to the X axis.

ϕ_y The component of ϕ parallel to the Y axis.

ϕ_R The resultant of ϕ_x and ϕ_y.

ψ The phase angle.

ω The angular frequency.

A
B
C The coefficients of a general equation of second degree.
D
E
F

A_1 The wave amplitude defined by equation (3.6).

A_2 The wave amplitude defined by equation (3.7).

c_{ij} The first order elastic constants.

c_{ijkl} The second order elastic constants.

D_{ij} The quantities defined by equations (2.19) and (2.26).

$\hat{e}$ The strain tensor.

e_{kl} The components of the strain tensor.

F The fraction of the crystallites in an aggregate which are oriented in the most preferential way.

f The linear frequency.

h The thickness of the elastic medium parallel to the direction of propagation.

K The ratio of the angular frequency to the wave velocity.

K_o The bulk modulus.

l
m The Murnaghan constants.
n

l_1
l_2 The direction cosines of the normal to the wave front.
l_3

P	The applied hydrostatic pressure.
p	The number of echoes to the nodal point in the pulse echo pattern.
S_{ij}	The elastic strains used in the definition of the strain energy function.
$\hat{T}$	The strain tensor.
T_{ij}	The components of the strain tensor.
t	Time.
t_1	The specimen transit time for a distortional wave polarized along the X_1 axis.
t_2	The specimen transit time for a distortional wave polarized along the X_2 axis.
U_j	The components of the displacement.
U_{jo}	The components of the displacement amplitude of a plane harmonic wave.
V	The velocity of a distortional wave in an isotropic medium.
V_1	The velocity of a distortional wave in a medium of oriented crystallites when the particle motion is parallel to the X_1 axis.
V_2	The velocity of a distortional wave in a medium of oriented crystallites when the particle motion is parallel to the X_2 axis.
V_L	The velocity of a longitudinal wave as defined by equation (2.39).
V_D	The velocity of a distortional wave as defined by equation (2.39).
$\frac{\Delta V}{V}$	The fractional velocity change associated with the double refraction of a distortional wave propagating in an anisotropic body.
v	The general velocity of a plane wave in an anisotropic body.
$\dot{X}_1$	The distortional wave velocity when the axis of polarization is parallel to the X_1 axis.

$\dot{X}_2$ The distortional wave velocity when the axis of polarization is parallel to the X_2 axis.

Z_0 The wave propagation distance required to produce a phase difference of 180°.

APPENDIX C

LIST OF MAJOR EQUIPMENT

Ultrasonic Attenuation Comparator--Manufacturer, Sperry Products Inc.

Y-Cut Quartz Crystals--10 Mc Resonant Frequency; Manufacturer, E. B. Lewis Company

Strain Indicator--Model 180; Manufacturer, Baldwin-Lima-Hamilton

Tensile Machine--Model TT-C; Manufacturer, Instron Corporation

VITA

Raymond Leon Gause

Candidate for the Degree of

Doctor of Philosophy

Thesis: INVESTIGATION OF ELASTIC DISTORTIONAL WAVE BIREFRINGENCE DUE TO CRYSTALLITE PREFERRED ORIENTATION AND STRESS IN ANISOTROPIC POLYCRYSTALLINE ALUMINUM

Major Field: General Engineering

Biographical:

Personal Data: Born in Cheyenne, Oklahoma, May 18, 1936, the son of Elmer L. and Gertie Ray Gause. Married to Barbara Janell Baxter, May 24, 1957. The father of a son Randy and a daughter Shari.

Education: Attended elementary and high school in Cheyenne, Oklahoma; graduated from Cheyenne High School in May, 1954. Received the Bachelor of Science Degree (Cum Laude) from Southwestern State College, Weatherford, Oklahoma, with a major in Physics, in August, 1957; completed the course work for the Master of Science degree in Engineering Mechanics at the University of Alabama in August, 1964; completed requirements for the Doctor of Philosophy Degree in December, 1966.

Professional Experience: Research Engineer with the Army Ballistic Missile Agency, 1957-58; Guided Missile Officer, U. S. Army, Rank of First Lieutenant, 1958-61; since 1961, except for a period of residence at the Oklahoma State University in 1964 and 1965, has been associated with the Marshall Space Flight Center (MSFC), National Aeronautics and Space Administration as a Research Physicist.

Organizations: Member of Sigma Pi Sigma and Alpha Phi Sigma.